UNCLASSIFIED

AD NUMBER
AD850142
LIMITATION CHANGES
TO: **Approved for public release; distribution is unlimited.**
FROM: **Distribution: Further dissemination only as directed by Air Force Space and Missile Systems Organization, SMSD, Los Angeles AFB, CA 90045, OCT 1968, or higher DoD authority.**
AUTHORITY
samso, usaf itr, 28 feb 1972

THIS PAGE IS UNCLASSIFIED

SAMSO TR-69-13 VOLUME II

AD850142

FINAL REPORT

ADVANCED PENETRATION PROBLEMS

WAKE STRUCTURE MEASUREMENTS

A. Demetriades

Space and Re-entry Systems

Division of Philco-Ford Corporation

October 1968

Advanced Research Projects Agency

Department of Defense

Washington, D. C.

This document may be further distributed by any holder only with specific approval of SAMSO (SMSD), ~~Norton AFB, California 92409~~ Los Angeles, A.F.S. Calif 90045

The distribution of this report is limited because it contains technology requiring strict approval of all disclosures by SAMSO.

DDC RECEIVED APR 11 1969 C

DISCLAIMER NOTICE

THIS DOCUMENT IS THE BEST QUALITY AVAILABLE.

COPY FURNISHED CONTAINED A SIGNIFICANT NUMBER OF PAGES WHICH DO NOT REPRODUCE LEGIBLY.

SAMSO TR-69-13 VOLUME II

FINAL REPORT

ADVANCED PENETRATION PROBLEMS

WAKE STRUCTURE MEASUREMENTS

A. Demetriades

Space and Re-entry Systems

Division of Philco-Ford Corporation

October 1968

Advanced Research Projects Agency

Department of Defense

Washington, D. C.

This document may be further distributed by any holder only with specific approval of SAMSO (SMSD), ~~Norton AFB, California 92409~~ Los Angeles AFS Calif 90045

The distribution of this report is limited because it contains technology requiring strict approval of all disclosures by SAMSO.

FOREWORD

This document describes work performed at Philco-Ford under Task 2, "Wake Structure Measurements" of Advanced Penetration Problems, ARPA Order 888, monitored by SAMSO under contract FO4701-68-C-0032, in the period 15 October 1967 to 15 October 1968. Certain subtasks of this work have, upon completion, been issued under separate cover as SAMSO technical reports for the purpose of documenting information in detail beyond that required contractually in monthly, semiannual, or final reports. These technical reports, already supplied to the appropriate SAMSO and ARPA personnel according to the pertinent distribution channels, are for brevity referred to frequently in the present document. They are:

(1) "Turbulent Front Structure of an Axisymmetric Compressible Wake", Philco-Ford Publication Number UG-4259, SAMSO TR 68-44, 15 November 1967.

(2) "Mean Flow Measurements in a Self-Preserving Turbulent Plasma Jet" SAMSO TR 68-166, February 1968.

(3) "Turbulent Mean-Flow Measurements in a Two-Dimensional Compressible Wake", Philco-Ford Publication Number UG-4431, SAMSO TR 68-369, October 1968.

This technical report has been reviewed and is approved.

R. W. Padfield, Lt., USAF
Advanced Penetration Problems
Project Officer

ABSTRACT

This report summarizes experimental work done in the period 15 October 1967 to 15 October 1968 on the structure of compressible turbulent wakes and turbulent plasmas. Detailed point measurements in the two dimensional wake, made very far from the body, have fully confirmed the predictions of the Dynamic Equilibrium Hypothesis regarding the asymptotic values of the velocity and temperature fluctuation and the statistics of the interface. For flight at angle of incidence radical changes in the wake structure have been observed, while heat transferred from the model to the flow was found to delay greatly the onset of transition to turbulence. In the plasma jet transition zone the remnants of the laminar fluid create a turbulent fluid of highly heterogeneous electron density with hitherto unexpected statistics. The longitudinal scales of the electrons are larger than those of the temperature but numerically not much different from low-speed turbulence scales. The electron density fluctuations always predominate the temperature fluctuations especially at the higher frequencies. Spectral decay obtains a (-5/3) range for the temperature but this behavior is not observed for the electrons.

Page iv Intentionally Left Blank

CONTENTS

CONTENTS (Continued)

ILLUSTRATIONS

ILLUSTRATIONS (Continued)

ILLUSTRATIONS (Continued)

ILLUSTRATIONS (Continued)

ILLUSTRATIONS (Continued)

ILLUSTRATIONS (Continued)

Page xiv Intentionally Left Blank

SECTION I

SUMMARY OF MAJOR ACCOMPLISHMENTS AND CONCLUSIONS

1.1 OBJECTIVES

The objectives of this work can be summarized as follows:

(1) The general objective is to predict the turbulence structure of the wake behind a vehicle moving in the atmosphere at hypersonic speeds.

(2) The specific objectives are (a) to measure experimentally the neutral gas dynamical features of turbulent compressible wakes such as the mean, intermittent, turbulent, and eddy magnitude distributions of velocity, density, and temperature and to map the statistical features of these variables, such as correlation and spectral functions; (b) to assess the importance, on these turbulence features, of reallistic reentry phenomena such as angle of attack and heat and mass transfer; (c) to measure the corresponding features of turbulent plasmas with the aim of establishing functional relationships between gasdynamical and electronic phenomena such as electron density, and gas velocity and temperature; and (d) to unify these results into laws not contradicting other available experimental results and to extend these scaling laws for hypersonic wake predictions through the basic flight parameters such as drag and altitude.

1.2 GUIDE TO THE PRESENT REPORT

This report covers work toward the cited objectives performed from 15 October 1967 to 15 October 1968, and discusses five major experiments at various stages of completion. In Section I, the status of these experiments is given in tabular form and major conclusions drawn from them are discussed as affecting hypersonic wake calculations.

Section II deals with turbulence measurements in a two-dimensional compressible wake without heat transfer or incidence effects (designated WED), and Section III with the intermittency properties of the same wake. The WED mean flow was measured in the 1966-1967 period, analyzed in the current period and reported in a separate SAMSO technical report (Reference 1). Since the latter report has been printed and distributed to SAMSO, Aerospace, and ARPA, it is referred to herein only in abstract form (Paragraph 1.3) for brevity.

Section IV discusses the turbulence and intermittency measurements in the plasma jet experiment (designated JEA). The JEA mean flow, measured in

the 1966-1967 period, was also analyzed in the current period and a SAMSO technical report (Reference 2) to this effect has been distributed as above. It is abstracted in Paragraph 1.3.

Section V discusses the wake at angle of attack (designated WEF) and Section VI the wake with heat transfer (WEG), and finally, Section VII presents recent developments in techniques and facilities devoted to this work and accounts for other such "logistics" of the project.

1.3 MAJOR ACCOMPLISHMENTS AND CONCLUSIONS

In the current period, the WED mean flow has well substantiated the earlier conclusions (Reference 3) that the mean axial velocity and the ambient wake temperatures are a Gaussian function of the wake radius. The abstract of Reference 1 states: "Excellent correlation of the lateral (radial) distribution of axial velocity is obtained when the lateral distance is divided by the transverse wake scale which is formed from the measured velocity defect. The latter is found to decay as the inverse square root of distance for the entire range of about 1850 virtual model thicknesses mapped; the transverse scale thus increases as the square root of distance. In the latter half of this range, the lateral distribution of static temperature also appears to correlate in the same lateral coordinate, and the temperature defect also decays as the inverse square root of distance. It is demonstrated that these results are accurately predictable from a basic similarity analysis beginning with Townsend's measured velocity decay on the axis; the turbulent Reynolds number of 13.0 agrees closely with Townsend's 12.5. The corresponding Prandtl number found lies in the range from 0.65 to 0.70." Implications of these statements are that the compressible wake is predictable, in the mean, on the basis of the <u>local</u> (inviscid) wake conditions and <u>independently of the body shape</u> (only the drag matters). The turbulent Reynolds number is now well settled, and for the axisymmetric wake the Prandtl number is, of course, higher than 0.70 (it is 0.83, according to Reference 3).

The expected properties of the turbulent front (boundary) have been abstracted in Reference 4: "Intermittency measurements have been performed within the first one hundred virtual diameters of an axisymmetric compressible wake. The primary measurements, performed with the hot-wire anemometer, concerned the intermittency factor and the frequency of zero occurrences. The intermittent flow covered most of the wake profile but for a narrow region about the axis, and was found to be normally distributed around the average front position. The latter, along with the extent of the front standard deviation, was found to agree numerically with expectations based on low speed wakes and to grow as the 1/3 power of axial distance. A week periodicity of the front was detected at a wavelength about nine times greater than the longitudinal scale of turbulent velocity fluctuations. This periodicity affects the turbulent spectra." In the two-dimensional wake experiments done in the current period, these conclusions were soundly reinforced (Section III) regardless of the characteristic growth (as the 1/2 power of distance) of the front scales for two-dimensional geometries.

Extremely important conclusions affecting the hypersonic wake turbulence were drawn in the current period from the WED turbulence studies detailed in Section II. The Dynamic Equilibrium Hypothesis had already been demonstrated to apply during the axisymmetric wake experiments (designated WEB) done in 1966-1967 (see References 5 and 6), and the same conclusion is now drawn from Section III. Specifically:

(1) The Strong Reynolds Analogy holds (i.e., given the velocity fluctuations one can compute the density or temperature fluctuations).

(2) The mass-flux and total temperature fluctuations are uncorrelated; the velocity and temperature are almost everywhere perfectly anti-correlated.

(3) On the axis, the velocity fluctuations become asymptotically 38 percent of the axis mean velocity; the temperature fluctuations become 45 percent of the temperature "deficit" across the wake.

There have also been phenomena observed differing substantially from previous expectations:

(1) The radial position of maximum velocity fluctuations (at a given distance behind the body) does <u>not</u> correspond to the maximum shear region (in contrast to WEB; see Reference 5).

(2) The radial distribution of the velocity fluctuation extends much farther out from the axis than the comparable low-speed fluctuations.

(3) It is possible to obtain fluctuation intensities which are larger in magnitude than the local velocity or density "deficits". The latter, therefore, do not indicate the absolute maximum attainable by the fluctuations as previously thought.

Although the angle-of-attack and heat-transfer data are not fully reduced, three important conclusions are drawn from Sections V and VI:

(1) Even small angles of attack at moderate Mach numbers make the wake resemble a shear layer and create severe departures from the above conclusions.

(2) The boundary (front) structure, measured by the local wake thickness, is unaffected by heat transfer.

(3) Heating the body stabilizes the wake and greatly displaces (downstream) the transition region. This fully verifies stability predictions (Reference 7) which also predict destabilization by cooling.

The conclusions drawn from work done in the current period with the turbulent plasma are now entering the phase of practical application. Reference 2 summarizes best the conclusions regarding, first, the mean flow of the reacting, highly heated flow: "Measurements of the temperature, density, axial velocity and electron density show that the overall gasdynamical jet structure attains the so-called self-preserving state within the region investigated. In the radial direction a similarity coordinate based on the Howarth-Dorodnitzyn radius correlates the distributions of temperature and axial velocity, and it is shown that the same coordinate should also correlate the relative concentration of electrons though not the absolute electron density. The measurements show that the electron relative concentration does not in fact become similar, and it is conjectured that the axial decay of electron density must be controlled by recombination reactions." Therefore, it is demonstrated that dynamical self-equilibration can occur independently of chemical relaxation if the ionization level is not too high. In Paragraph 4.2 it is further shown that the front structure is independent of the chemistry and, very significantly, the "electron intermittency" is indistinguishable from the regular intermittency. This applies even to the "weakly periodic" turbulent front whose wavelength scales are the same as for the compressible wake.

From the host of turbulent plasma phenomena observed and measured (Section IV), the following conclusions are drawn:

(1) Two distinct phases of turbulence exist in the jet: A heterogeneous portion apparently associated with transition and a homogeneous portion resembling the familiar turbulence phenomenon.

(2) Nearer the heterogeneous region the gas temperature spectra have a very clear -5/3 slope which change into a much faster spectral decay (with frequency) in the homogeneous region. The electrons <u>never</u> attain the -5/3 slope, and in the homogeneous region they decay about as the -4.6 power of frequency.

(3) In the homogeneous region the off-axis maxima in the <u>electron density</u> fluctuations occur where the flow <u>shear</u> is a maximum.

(4) In the heterogeneous portion, abnormally high "spike" electron fluctuations make the rms electron density much higher (by a factor of 5) than the mean. These spikes do not exist in the temperature and are unrelated to intermittency, which also makes $\Delta n/n$ very high near the jet edge.

(5) Agreement of the gas velocity and temperature fluctuations, scale magnitudes, etc., with values obtained with non-plasma jets in other laboratories is generally very good. Specifically, the longitudinal integral

scale Λ_T of the temperature seems to bear the same relation to the so-called "transverse scale" ($\Lambda_T = 0.75L$) that it does in other jets and wakes.

(6) The longitudinal integral scale Λ_e of electrons is related to Λ_T as follows: $\Lambda_e = 0.6\ \Lambda_T$.

(7) The frequency-integrated, normalized electron density fluctuation $\Delta n/n$ is greater everywhere than the corresponding temperature fluctuation $\Delta T/T$. At each point, it is also greater than $\Delta T/T$ across the spectrum.

1.4 PRESENT STATUS

The present status of the work is shown on Table I.

TABLE I. STATUS OF EXPERIMENTAL WORK IN SUPERSONIC WIND-TUNNEL

Experiment	Experiment Design	Hardware Construction	Measurements	Data Reduction	Data Analysis	Report
A/S Wake Mean Flow	C	C	C	C	C	C
A/S Wake Intermittency	C	C	C	C	C	C
A/S Wake Turbulence	C	C	C	C	C	C
2-D Wake Mean Flow	C	C	C	C	C	C
2-D Wake Intermittency	C	IP	IP	-	-	-
2-D Wake Turbulence	C	C	C	IP	IP	IP
Incidence (10 Degrees) Mean Flow	C	C	C	IP	-	-
Incidence (10 Degrees) Intermittency	C	IP	-	-	-	-
Incidence (10 Degrees) Turbulence	C	C	IP	-	-	-
Incidence (20 Degrees) Mean Flow	C	C	C	IP	-	-
Incidence (20 Degrees) Intermittency	C	IP	-	-	-	-
Incidence (20 Degrees) Turbulence	C	C	IP	-	-	-
Heat Transfer Mean Flow	C	C	C	IP	-	-
Heat Transfer Intermittency	C	IP	-	-	-	-
Heat Transfer Turbulence	C	C	IP	-	-	-
Jet Mean Flow	C	C	C	C	C	C
Jet Intermittency	C	C	C	C	C	IP
Jet Turbulence (Temperature)	C	C	C	C	IP	-
Jet Turbulence (Electrons)	C	C	C	C	IP	-
Jet Eddy Properties	C	IP	-	-	-	-

NOTE: C: Completed
IP: In Progress

SECTION II

TURBULENCE MEASUREMENTS IN A TWO-DIMENSIONAL COMPRESSIBLE WAKE

2.1 INTRODUCTION

The simplicity of the two-dimensional model geometry makes it ideal for turbulence measurements at large distances from the body. Until a few years ago the bulk of all knowledge on turbulent wakes came from experiments with two-dimensional models immersed in low-speed flows. A number of investigators reported detailed work in the far wake of cylinders placed normal to the stream; prominent among such work is that of A. A. Townsend (Reference 8). In the present series of experiments detailed compressible turbulence information has been obtained with an axisymmetric wake (Reference 5) where data were taken to about 100 (virtual) diameters from the model. All evidence collected in the experiment showed that the turbulence quantities attained self-preservation within that distance, but the significance of the results warranted confirmation and extension to greater distances behind the model. A logical next step, therefore, was the measurement of compressible turbulence behavior with a two-dimensional model, where such distances could be easily attained.

As with the mean-flow results, some important differences exist between turbulence behavior in a two-dimensional and in an axisymmetric wake. For example, the rms axis fluctuation level decreases in the former case as $\bar{X}^{-1/2}$, whereas in the latter it decreases as $\bar{X}^{-2/3}$. However by normalizing with the mean properties these fluctuations are each constant (i.e., independent of $\bar{X}$) and, in fact, as anticipated by Townsend and already shown on Reference 5, are about equal to each other. Two-dimensional studies of turbulence, therefore, not only greatly accelerate the fundamental knowledge on turbulent wakes, but contribute directly to the needed practical rules for predicting the axisymmetric behavior typical of engineering applications.

The turbulence measurements described in this section were performed with the two-dimensional model whose wake mean flow is reported in detail in Reference 1. Reference 1 should be consulted for information on the tunnel facility and the characteristics of the model; only a very brief repetition of this information will be given for completeness. Later in this discussion use will also be made of the results of Reference 1 with no commentary on their method of acquisition.

2.2 FLOW FACILITY AND MODEL

The work was done in the Mach 3.0 wind tunnel in continuous flow at a stagnation pressure of 730 mm Hg absolute and a stagnation temperature of 38°C. The model was a 0.004 inch thick, 0.116 inch wide stainless steel ribbon stretched at zero angle of attack across the test section. The leading edge was beveled to a half-angle of about 27 degrees and the trailing

edge was square (i.e., the base was flat). No heat was exchanged between the model and flow, i.e., the experiment was adiabatic. The relevant Reynolds numbers were as follows:

(1) The Reynolds number

$$Re_{\infty} \equiv \frac{U_{\infty} C_D h}{\nu_{\infty}} = 632 \qquad (1)$$

is based on conditions external to the wake (see Reference 1) and the equivalent ribbon "base height" $C_D h$ was in reality the wake momentum thickness and was measured by integrating the measured momentum flux in the wake.

(2) The Reynolds number

$$Re_{w} = \frac{(U_{\infty} - U(0))L}{\nu_{\infty}} = 158 \qquad (2)$$

is based on the velocity deficit $U_{\infty} - U(0)$ between the axis and external velocities U_{∞} and $U(0)$, respectively, and on the so-called transverse scale L.

These and further findings of the mean flow field will be discussed later.

2.3 INSTRUMENTATION

The turbulence measurements were performed with a single hot-wire anemometer probe which could be traversed continuously in the wake and could thus sense changes in the turbulence properties over distances much smaller than the wake thickness. An elaborate description of the technique, which is in many respects classical, is provided in Reference 5; only a few points of general importance will therefore be mentioned here. The hot-wire is operated at a number of predetermined electric heating currents (constant current operation) and thus provides, at each point, a corresponding number of fluctuating voltage outputs. The latter are then inserted as forcing functions into an over-determined system of linear algebraic equations in which the coefficients of the unknowns are numerically fixed by the local mean flow properties (measured earlier and reported already in Reference 1). Invoking the constant-pressure assumption, the system is solved by the least-squares method for the local fluctuations in the flow velocity, density (or temperature), and the temperature-velocity correlation coefficient. This procedure is normally performed first for a very wide frequency band within which the total (integrated) rms is obtained. Afterwards, a combined spectral-modal analysis is performed by which the contribution of each fluctuation mode is obtained at each point in the spectrum.

The characteristics of the hot-wire, the calibrations performed, and a detailed journal of its usage are discussed in pages 61 and 62 of Reference 6.

2.4 GENERAL FEATURES OF THE WAKE FLOW FIELD

The two-dimensional wake of the ribbon grew in a regular manner behind the model for a distance of about 1850 virtual body diameters. It is worthwhile to summarize here some general features of this wake before the turbulence measurements are detailed:

(1) The uniformity of the wake along its span is quite satisfactory.

(2) No shock waves or other disturbances emanating from the model intersect or distort the wake. The bow shock system affects the wake only beyond (downstream of) the region studied.

(3) It was demonstrated conclusively that the angles of attack and twist were sufficiently close to zero.

(4) Measurements of transition, fluctuation intensity, spectral density, and intermittency demonstrated that the wake was indeed turbulent.

(5) Transition to turbulence occurred within the first few X-Stations along the wake (details will be furnished when the fluctuation measurements are described).

(6) Day-to-day reproducibility of the wake flow field was excellent.

A summary is given below of the mean-flow results for the turbulent wake at hand. These experimental results are shown correlated into simple algebraic formulas which, at the same time, are the general scaling laws for two-dimensional compressible wakes. The nomenclature has the usual aerodynamic connotation.

(1) Proper axial coordinate:

$$\bar{X} \equiv \frac{X-X_o}{\sqrt{C_{Dh}}} \quad (X_o \text{ is virtual origin}) \tag{3}$$

(2) Velocity defect:

$$W \equiv \frac{U_\infty - U(0)}{U_\infty} = \sqrt{\frac{R_T}{10\,\bar{X}}} \qquad (R_T = 13.0) \tag{4}$$

(3) Transverse scale:

$$L = \frac{\sqrt{C_{Dh}}}{4W} = 0.22\sqrt{\bar{X}} \tag{5}$$

(4) Lateral coordinate:

$$\tilde{Y} \equiv \int_0^y \frac{\rho}{\rho_\infty} dY \quad \text{(The Howarth-Donodnitzyn radius)} \tag{6}$$

(5) Proper non-dimensional lateral variable:

$$\eta \equiv \tilde{Y}/L \tag{7}$$

(6) Lateral variation of axial velocity:

$$\tilde{U} \equiv \frac{U_\infty - U}{U_\infty - U(0)} = e^{-0.69\eta^2} \tag{8}$$

(7) Lateral variation of static temperature:

$$\tilde{T} \equiv \frac{T - T_\infty}{T(0) - T_\infty} = e^{-0.45\eta^2} \tag{9}$$

(8) Axial variation of temperature defect:

$$\theta \equiv \frac{T(0) - T_\infty}{T_\infty} = \sqrt{\sigma}(\gamma - 1) M_{\infty w}^2 = 0.336 M_{\infty w}^2 \tag{10}$$

These laws, which will be used frequently to understand the turbulence behavior at each point in the wake, are applicable primarily in its self-preserving portion so that they are only approximate in the first 20 percent of the wake length studied, and exact thereafter.

The pertinent Reynolds numbers which are relevant to this wake are shown in Paragraph 2.2. The quality and behavior of turbulence can be prejudged on the basis of two more Reynolds numbers, added to those indicated above. First, consider the Reynolds number of turbulence:

$$Re_T \equiv \frac{\Delta u \cdot \Lambda}{\nu} \tag{11}$$

where Δu is the rms velocity fluctuation, Λ the integral scale of turbulence, and ν the local kinematic viscosity of the gas. Now, asymptotically Δu is about $0.4(U_\infty - U(0))$ (on the axis) whereas Λ is of the order of the transverse scale L and ν is, far in the wake, of the order of the free-stream kinematic viscosity ν_∞. Therefore, Re_T is about $0.4\ Re_W$ where the latter is the wake Reynolds number, already noted in Paragraph 2.2, to be constant at about 160; thus, $Re_T = 64$. Secondly, consider the dissipation time for the very small eddies which Kovasznay (Reference 9) has computed in typical wind tunnel situations. On the basis of his computation, a corresponding limit for the Reynolds number of the dissipating eddies has been derived in Reference 6; assuming that the smallest eddy is that which dissipates over a convected distance equal to its size, then this Reynolds number (called Re_λ) is 40.

These computations put bounds on the expected structure of turbulence because they imply that the macroscale and the microscale are about equal. This wake is therefore coarse-grained in the sense that no eddies smaller than the integral scale are expected. Also, Reference 1 has already shown that the mean flow in this wake is in all respects almost exactly analogous to those obtained at a much higher Reynolds number. The important additional conclusion is drawn that the arrangement of the mean (average) properties, and therefore the important mixing processes, result from the action of the larger eddies alone. It remains to see what the power spectrum of this coarse-grained wake is.

2.5 EXPERIMENTAL TECHNIQUE AND PROCEDURE

2.5.1 PURPOSE OF THE INSTRUMENTATION

The hot-wire anemometer was used to measure the following statistical properties of the turbulent wake: (1) the root-mean-square fluctuation of the axial component of fluid velocity (where "axial" will henceforth refer to a direction parallel to that of the tunnel stream) resulting from all active Fourier components, i.e., integrated across a very broad frequency band; (2) the root-mean-square fluctuations in the static temperature similarly integrated across the spectrum; (3) the spectral "density" of the above-mentioned velocity fluctuation; (4) the spectral density of the temperature fluctuation; (5) the integral scale (correlation length) of the velocity fluctuations in the axial direction; (6) the integral scale of temperature fluctuations; (7) the "Taylor microscale" of velocity fluctuations; and (8) the same microscale of the temperature fluctuations. It was furthermore desired to map these quantities at each point in the turbulent flow.

Some points should be stressed regarding these objectives. First, certain combinations of the sought-after parameters (such as the mass-flux and total temperature fluctuation) are also directly obtainable by the hot-wire. Secondly, certain assumptions justified by earlier experiments are needed in reducing the data. For example, it is necessary to have no pressure fluctuations (sound waves) in order to extract the velocity fluctuations from the data. Third, there is no need to resort to questionable assumptions (e.g., isotropy or homogeneity) in order to obtain these results.

2.5.2 CRITERIA FOR RESOLUTION AND STATISTICAL ACCURACY

A number of criteria must be satisfied so that the measurement will be valid. Some of these involve a precise knowledge of the measured quantities and thus, can be checked only a posteriori. However, with a precise knowledge of the electronic circuits and a fair estimate of the turbulence properties drawn from the mean measurements (Reference 1) and exploratory work, the criteria were also checked a priori.

a. Space Resolution. In the direction of flow (x direction), the 0.00005-inch diameter of the wire assures excellent resolution.* Taking a typical wake width of 0.100 inch and estimating a typical small eddy size of 0.010 inch, one obtains a resolving power of 1 to 200, applying equally to the x- and the y-direction (i.e., the lateral direction). However, in the z-direction the hot-wire length is 0.010 inch, that is equal to the estimated eddy size. Resolution in this direction is therefore not as good.

b. Time Resolution. Even if adequate space resolution in the x-direction is assured, the question arises whether the hot-wire and its circuits are capable of exploiting this resolution. The frequency, f, corresponding to an eddy of size d = 0.01 inch = 0.025 cm and its convection velocity u = 60,000 cm/sec past the probe is f = u/d = 2,400,000 Hz. Formally, this is the estimated maximum frequency to which the turbulence spectrum extends. The hot-wire system must therefore operate properly at these frequencies. Now the hot-wire employed in this work has a time-constant of about 0.15 msec, that is, an intrinsic "cutoff" at 7000 Hz; this is much lower than needed. To bridge the gap between the required and the available frequency limits, two supplementary techniques were used, one based on real-time electronic compensation of the high frequency response, and the other on computer corrections during the reduction of data. These two schemes have been described in Paragraph 2.6 of Reference 5, so that only a brief review will be given here.

The constant-current amplifier used includes an adjustable RC network which has a gain of unity at low frequencies and amplifies preferentially the higher frequencies. The transfer function of this network is of the type

$$\frac{e_{out}}{e_{in}} \simeq \left(1 + t_I^2 \omega^2\right)^{1/2} \qquad (12)$$

where ω is the circular frequency and e_{out} and e_{in} are the rms voltage out of and into this network, respectively, in a narrow passband about ω. The circuit time constant t_I is fully adjustable at the front panel to an accuracy of 1 microsecond. The advantage of this transfer function is that, of course, it is algebraically inverse to that of the hot wire itself where

$$\frac{e'_{out}}{e_{in}} = \left(1 + t^2\omega^2\right)^{-1/2} \qquad (13)$$

with t being the time constant of the wire arising from thermal lag. Just prior to each measurement, t is measured and t_I is set equal to it. Then

---

*The wire is actually not stretched taut between the needle supports but with a curvature which is of order 20 percent of its length, i.e., about 0.002 inch. Thus, for eddy sizes of order 0.010 inch, one still obtains good resolution.

the compensator output e_{out} is equal to the "flow" input e'_{in} into the hot wire (by multiplying Equation (12) with (13)) as would be expected of an ideal system.

The upper frequency at which Equation (12) applies also marks the upper frequency limit where the compensation just indicated applies. This limit depends on t_I. To find the exact form of Equation (12), the amplifier is calibrated before each experiment. In the WED experiment the calibration was least-squares fitted by a trivariate function and used in the WEB-II program:

$$C\left(\frac{e_{out}}{e_{in}},\ \omega,\ t_I\right) = 0 \tag{14}$$

The departure of Equation (12) from the desired behavior (Equation (14)) is such that at $t_I = 0.1$ msec the upper compensating frequency is 800 kHz and at $t_I = 0.2$ msec, it is 400 kHz, which appears to greatly improve the 7 kHz intrinsic limit of the wire itself.

Unfortunately, there are other transfer functions in the circuit to consider, and another limitation arises from the "straight" amplifier itself. For the WED experiment, the transfer function of the latter was calibrated and curve-fitted into:

$$\frac{e_{out}}{e_{in}} = 1 + 6.144 \times 10^{-4}F - 7.718 \times 10^{-6}F^2 + 1.085 \times 10^{-8}F^3 - 4.610 \times 10^{-12}F^4 \tag{15}$$

(with F in kHz) which indicates a roll-off frequency beginning at about 80 kHz and an attenuation of $e_{out}/e_{in} = 0.43$ at 500 kHz. Thus, the straight amplifier response is generally inferior to that of a perfectly-matched ($t = t_I$) wire-compensator system. It is estimated that the complete system begins degenerating severely around 300 kHz.

To extend this range further to the 2 MHz estimated range of turbulence, the "response restoration" technique described in pages 13 to 29 of Reference 5 was used. This is based on the spectrum of a signal being obtained with a non-ideal system (i.e., a system with a non-flat response), then the correct spectrum can be reconstructed provided that the frequency response of the entire system (i.e., its transfer function) is known accurately. To do this, the frequency response of the chain of experimental equipment is obtained component-by-component so that the so-called "overall transfer function" of the system is known at each point in the wake. Also, at each point, the spectrum of each admitted signal is measured, and a computer program is then used to restore the latter spectrum to the form it would have if detected by an ideal electromechanical system.

The response-restoration technique is obviously limited by the electronic noise present. In this experiment, spectra were taken to 1.2 MHz so that slightly more than half the presumed range of turbulence activity is

covered. However, it should be considered that the majority of the turbulence signal at the hot-wire arises at the lower frequencies. The a priori conclusion was that with the present system, it should be possible to measure the rms velocity and temperature fluctuations integrated over the entire band of turbulence activity, but that perhaps the details of the spectrum above 1 MHz are elusive. Further discussion of these points will be made during the presentation of experimental results.

c. Statistical Accuracy. A statistical measurement can become very inaccurate if the domain of measurement is not much larger than the size of eddies lying within it. Otherwise stated, the hot-wire must remain at the point of measurement for a time which is so long that a large number of eddies of all sizes go by it. In the course of earlier experiments (the WEB), it was seen that the integral scale, for example, was only 4 times smaller than the statistical wake diameter. Using the integral scale as a useful measure of the larger eddies, and a local wake velocity of order 6×10^4 cm/sec, the time of passage of such an eddy past a point is estimated typically as 2 microseconds. For proper statistics, the residence time of the probe at a point should be long enough to record the passage of, perhaps, 1000 such eddies; this time should then be 2 milliseconds. For the continuous-flow tunnel used here, this time is safely exceeded by orders of magnitude. Even with the method of traversing the probe continuously through the jet the residence-time requirement is fulfilled easily, since it takes several seconds for the probe to traverse a lateral distance equal to one correlation length.

2.5.3 FULFILLMENT OF THE "FROZEN TURBULENCE" CRITERION

Another criterion to be fulfilled for these measurements to be valid is the so-called "frozen turbulence" criterion, i.e., the Taylor hypothesis. This states that in a locally uniform convection, the time and space coordinates can be interchanged provided that the time needed to change the turbulence structure is not shorter than the averaging time of the signal. Otherwise stated, the eddies must remain unchanging as they are being counted by the probe. Estimates usually made of the validity of Taylor's hypothesis are limited to changes made in the fine (small-eddy) structure of turbulence by viscosity. Kovasznay (Reference 9) estimates the viscous decay time, t_ν, for small eddies to be of order $(\nu k^2)^{-1}$, where ν is the molecular kinematic viscosity and k is the eddy wake number, $k = 2\pi/\lambda$ (where λ is the eddy diameter). Obviously, if the "life distance" $d = ut_\nu$ of such an eddy is much larger than its own size, the Taylor hypothesis is valid; this criterion (see also Reference 6, page 123) can be expressed by the following alternate forms:

$$ut_\nu \gg \lambda, \quad Re_\nu = \frac{u\lambda}{\nu} \gg 40, \quad \lambda \gg \frac{40\nu}{u} \qquad (15)$$

Since the wake conditions will be close to ambient over most of the wake, the freestream unit Reynolds number U_∞/ν_∞ = 80,000 per cm (at the conditions used) can be substituted in the latter inequality. The result is that the minimum eddy size which can be measured in the framework of Taylor's hypothesis is 40/80,000 = 0.0005 cm in size. This rough estimate thus

shows that the space-time transformation is very reasonable for the 0.025 cm eddies estimated to make up the fine structure of the wake at hand.

2.5.4 EXPERIMENTAL PROCEDURE

The hot-wire was positioned parallel to the z axis (Figure 1) at the center-span ($z = 0$) plane.* Twenty-four positions along the x-axis (called "X-Stations") were chosen and designated X-Station 0, 1, 2 .....23. The corresponding distance behind the body, for each x-station, is shown on Table II. At each position the wire was traversed continuously across the wake in the Y direction and its output versus position was plotted on a function plotter.

The circuit block diagram is shown in Figure 2. The hot-wire is connected to a Transmetrics Model 6401 constant-current anemometer set which includes a heating circuit, ac amplifier, and square-wave generator for checking the wire time-constant, characteristics of the amplifier can be found in Appendix A of Reference 5. For measurements of spectral density, a Hewlett-Packard wave analyzer Model 310A was used, with a mechnical sweep drive; for the integrated rms measurements a Ballantine Model 320A wideband true-rms voltmeter was employed. Assorted oscilloscopes, display analyzers, etc., complemented this system. All data was in dc form and was plotted by a Moseley Model 7001A function plotter.

2.5.5 MEAN VOLTAGE MEASUREMENTS

Since all data is handled and utilized in dimensionless form, the mean (average) wire resistance variation across the wake was needed. The work was done at fifteen different settings of the dc current through the wire, so that an accurate least-squares determination of the results could be made. These currents are shown in Table III. At each current and at each X-Station the "reference voltage" of wire No. 6-7/1 was first measured just outside the wake and then the probe was moved at constant speed through the wake, producing a voltage versus distance trace. A typical traverse was completed in about 30 seconds and produced a maximum deflection of about 500 millivolts dc. A representative set of fifteen such traces is shown in Figure 3.

2.5.6 FLUCTUATING VOLTAGE MEASUREMENTS

Another set of fifteen traverses at each X-Station was made by again setting the dc current at the levels of Table III. In this instance the ac signal was amplified by a factor of 47 and high-passed above 1000 Hz to eliminate stray signals (such as chance 60-cycle line ripple or mechanical vibrations) which might arise at low frequencies. (Strain gage vibrations had been eliminated in the process of calibration.) The wire was again

---

*No detailed measurements were taken at $z \neq 0$; however, the good quality of the flow at $z = +0.5$ and $z = -0.5$ was confirmed by preliminary tests.

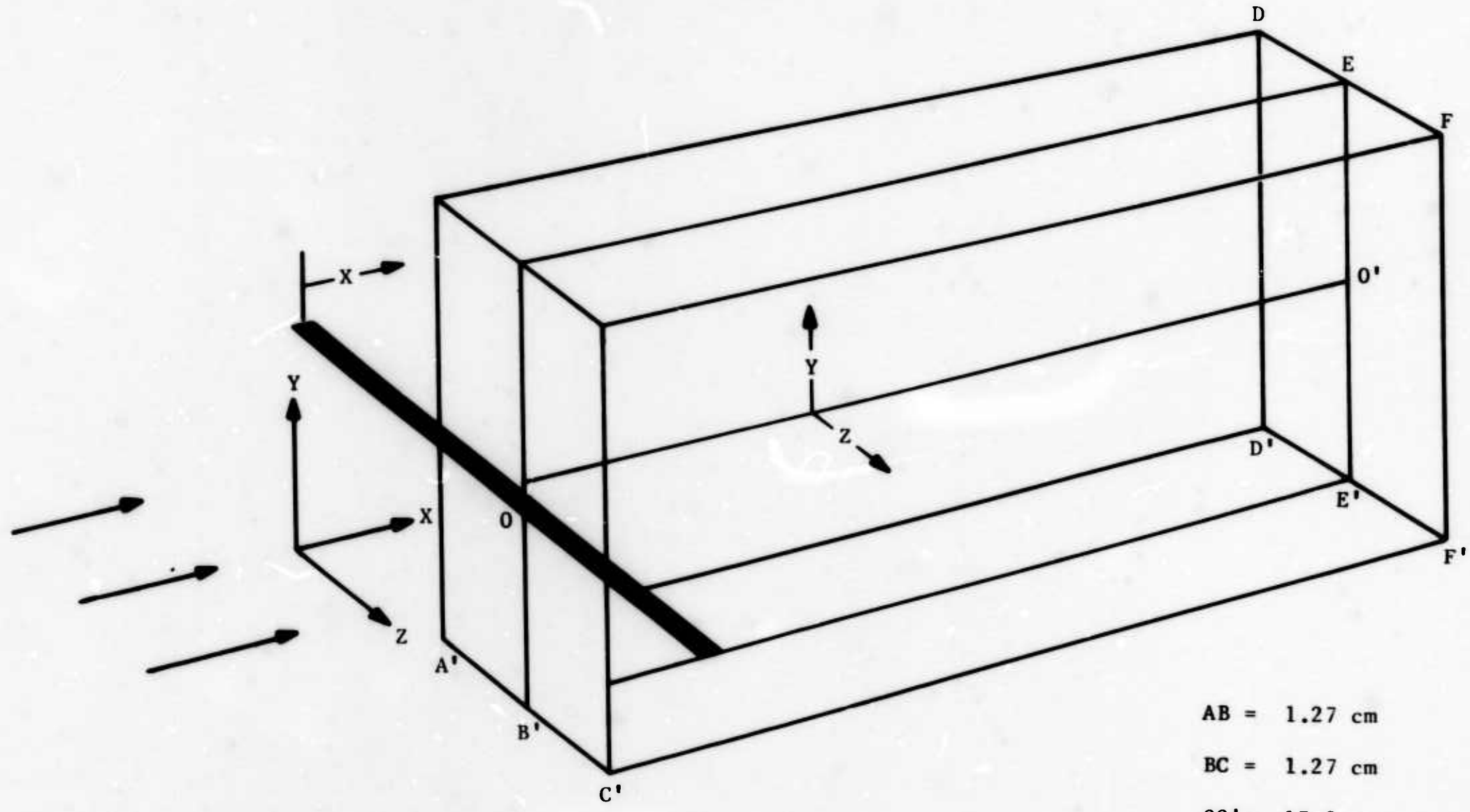

AB = 1.27 cm

BC = 1.27 cm

OO'= 17.8 cm

F12121 U

FIGURE 1. SCHEMATIC OF WED EXPERIMENT GEOMETRY SHOWING COORDINATE NOMENCLATURE. MEASUREMENTS WERE MADE WITHIN THE RECTANGULAR PARALLELEPIPED SHOWN.

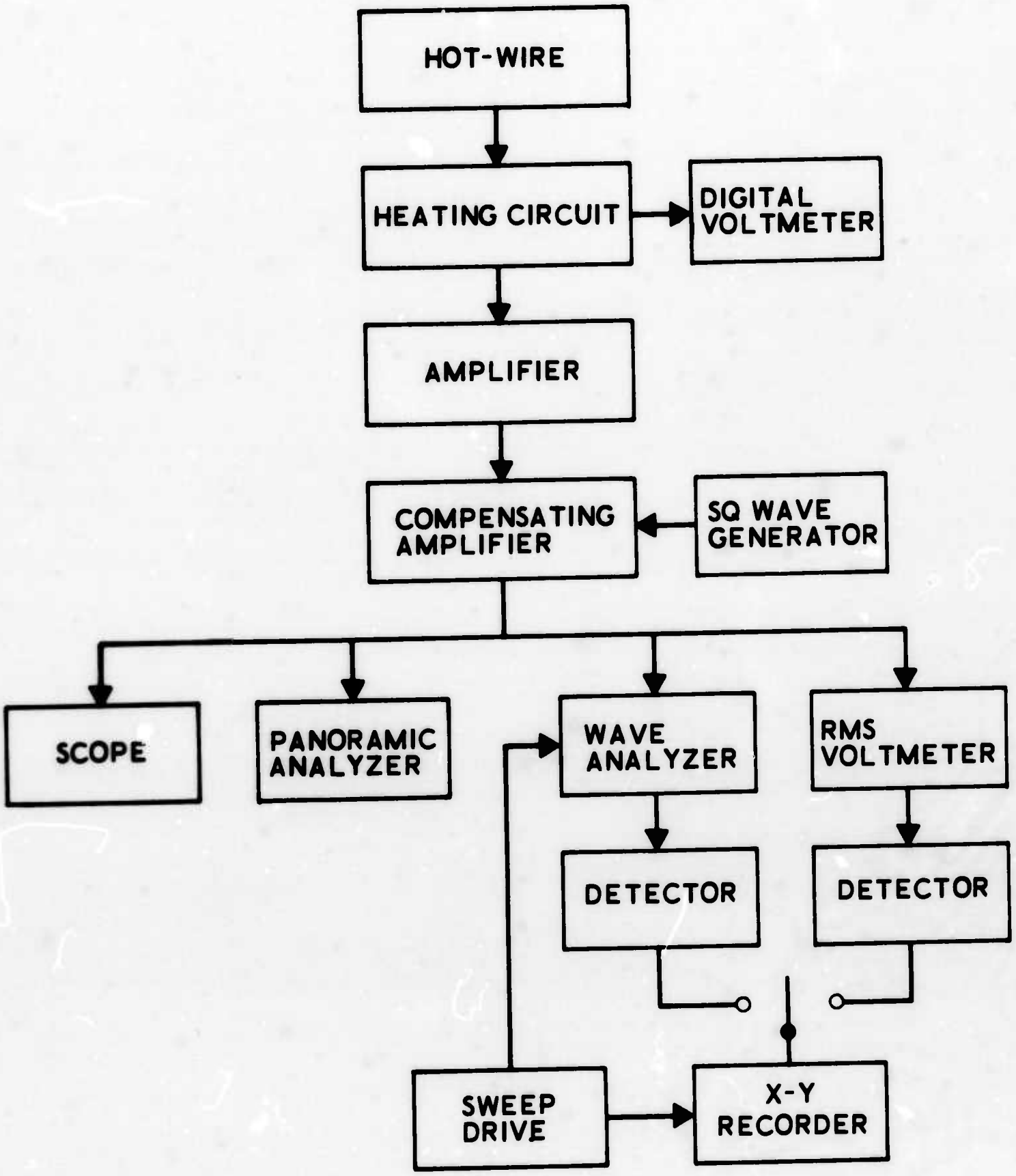

F09813 U

FIGURE 2. ELECTRONIC CIRCUIT USED FOR THE WED TURBULENCE MEASUREMENTS

TABLE II. AXIS VALUES OF MEASURED TURBULENCE PROPERTIES

X-Station	$\bar{X}$	$\frac{\Lambda_{\rho u}}{\rho u}$	$\frac{\Lambda T_o}{T_o}$	$\frac{\Lambda_u}{u}$	$\frac{\Lambda_\rho}{\rho}$	r_{mt}	$r_{\sigma r}$
0	--	0.0477	0.0624	0.0117	0.0357	-1.23	-1.09
1	0	0.519	--	0.0038	0.0469	--	-3.94
2	84	0.131	--	0.0525	0.0962	--	-0.95
3	168	0.200	0.0758	0.0668	0.121	0.65	-0.88
4	251	0.152	0.0459	0.0436	0.1035	0.38	-0.83
5	335	0.122	0.0338	0.031	0.0926	-0.05	-0.76
6	419	0.121	0.0307	0.0268	0.0957	-0.25	-0.80
7	503	0.119	0.0367	0.0214	0.0933	-0.08	-0.84
8	587	0.113	0.0293	0.0057	0.0860	-0.09	--
9	670	0.103	0.035	0.0155	0.0776	0.14	-0.81
10	754	0.091	0.0281	0.0149	0.0702	0.03	-0.82
11	838	0.081	0.0241	0.0145	0.0626	0.01	-0.83
12	922	0.077	0.0219	0.017	0.0581	0.08	-0.77
13	1006	0.068	0.024	0.012	0.0522	0.13	-0.74
14	1089	0.068	0.020	0.014	0.052	0.09	-0.76
15	1173	0.064	0.019	0.015	0.048	0.18	-0.76
16	1257	0.059	0.014	0.013	0.046	-0.08	-0.79
17	1341	0.056	0.016	0.013	0.044	-0.08	-0.71
18	1425	0.051	0.013	0.0066*	0.043	-0.41	-0.92
19	1508	0.051	0.013	0.0091*	0.041	-0.26	-0.80
20	1592	0.045	0.012	0.0056*	0.038	-0.46	-0.98
21	1676	0.047	0.014	0.0049*	0.038	-0.20	-1.09
22	1760	0.045	0.013	0.0056*	0.037	-0.32	-0.86

*Uncorrected

TABLE III. HOT-WIRE HEATING CURRENTS FOR TURBULENCE MEASUREMENTS

High Range (ma)	Medium Range (ma)	Low Range (ma)
7.404	6.437	5.320
7.192	6.273	4.892
6.988	6.115	4.292
6.795	5.825	3.650
6.614	5.562	3.176

TABLE IV. CHARACTERISTICS OF HOT-WIRES USED IN THE WED EXPERIMENT

Wire No.	Measuring Properties	R(^{o}C)	α (per ^{o}C)	ℓ (inch)	ℓ/d
6-7/1	Turbulence (all X-Stations)	39.10	0.0162	0.011	220
6-7/1	Spectra X-Station	39.10	0.00162	0.011	220
7-12/1	Spectra X-Station 3-9	37.43	0.00158	0.0105	210
7-19/1	Spectra X-Station 11-21	36.37	0.00160	0.102	204

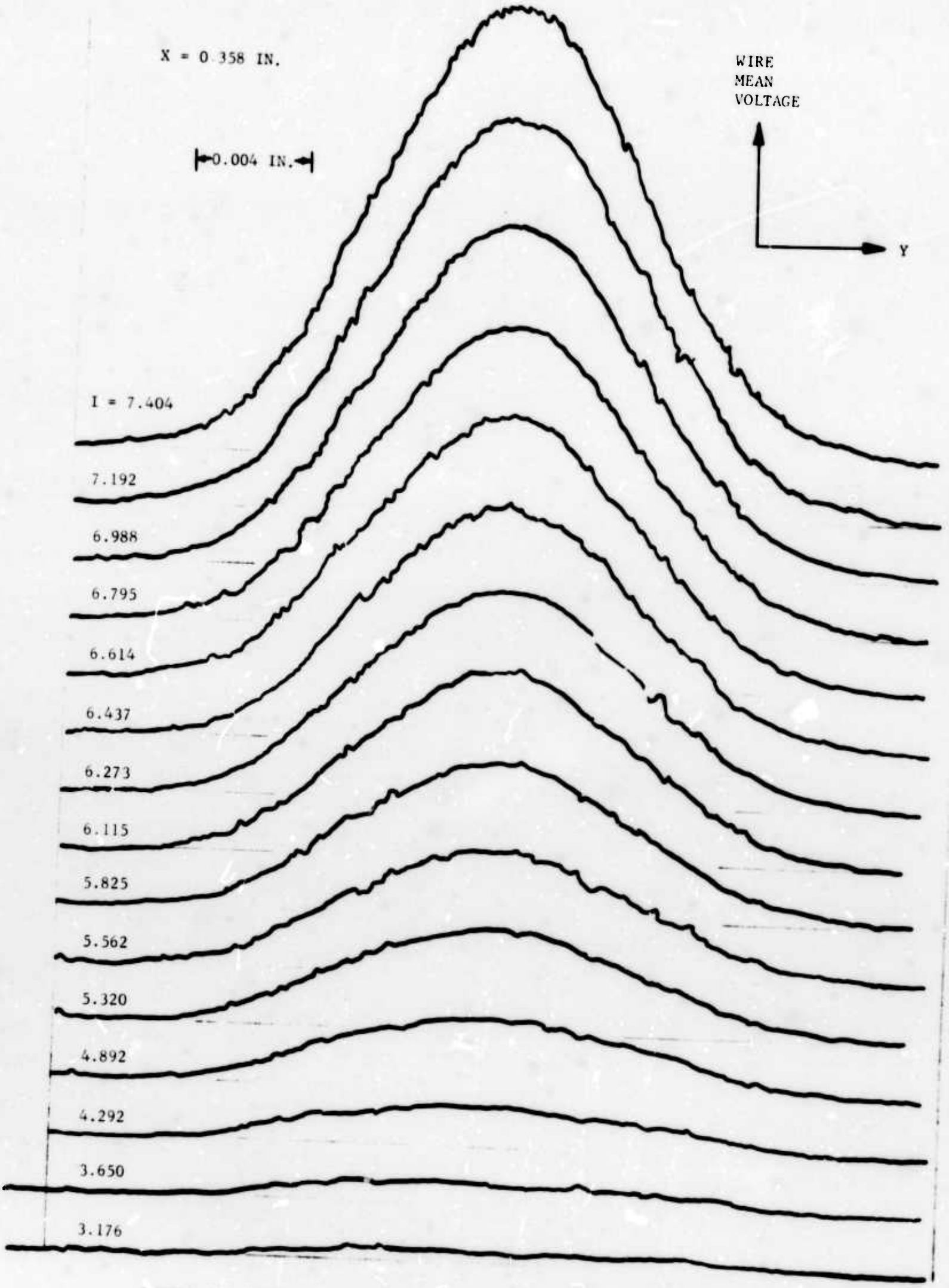

FIGURE 3. TYPICAL PROFILES OF MEAN HOT-WIRE VOLTAGE ACROSS TWO-DIMENSIONAL WAKE AT CONSTANT DISTANCE BEHIND THE BODY. FOR EACH CURVE THE WIRE CURRENT IS CONSTANT

F12129 U

first positioned just outside the wake; its time constant was read and the compensator dial was set at that level. Typical time constants at each point varied from 150 to 110 microseconds, depending upon dc current. The reference (ambient) turbulence level and electronic noise level (independent of Y) were also recorded at this point. Then, for each current, the wire was traversed through the wake at a compensation setting equal to the free-stream value corresponding to that current. During this traverse the ac signal is continuously converted to dc by the circuit of the rms meter proportional to the mean-square of the ac level. Finally this dc voltage is plotted versus position. Five of a typical set of fifteen such "turbulence" traces are shown in Figure 4.

2.5.7 MEASUREMENTS OF THE SPECTRA

In the previous paragraphs it was shown that a total of 15 + 15 = 30 traces were taken at each X-Station; for the total of 24 stations involved, this adds up to 720 traces. These, in principle, contain all the information necessary to deduce the turbulent fluctuations. As already noted, however, the insufficient frequency response of the system made it necessary to also measure the spectra of turbulence signals (at each wire current and point in the flow). Now, it will be recalled (Reference 5, page 28), that the objective of the spectra, besides yielding the spectral density function, is to provide an "error ratio" J which is used to multiply the fluctuation intensity discussed in Paragraph 2.5.6; this brings up the latter to the correct value if recorded by an ideal system. This would, in turn, require that spectra are taken at closely spaced points for each wire current. Since this is clearly impractical* the following was done: spectra were taken for each of 6 currents at each of 10 radial points at alternate X-Stations, beginning with X-Station 1, for a total of 720 spectra. Extensions of these J's so obtained to other currents and points could be later made by interpolation. The electric currents used spanned the range of those used for the "turbulence" measurements (see Table III), and were 3.174, 4.891, 5.820, 6.432, 6.981, and 7.401 milliamperes. Wire No. 6-7/1 had, by this time, failed and other wires closely resembling it were used for the spectral measurements. Their characteristics are shown in Table IV.

Each wire was first positioned outside the wake where its time-constant was measured and compensated for. The wire was then lowered to the desired point in the wake, and with the compensation unchanged from the stream value (for that particular current), the spectrum was taken. Amplifier gain was 650, the passband was from 1 to 320 kHz, and the wave analyzer was set at 1 volt range, normal mode at -10 dB input. A 3-kHz analyzer bandwidth was used and was swept across the spectrum at a speed of about 7 to 8 kHz/sec by means of the mechanical sweep drive. The signal in the 3 kHz bandwidth

---

*For example, if 20 radial points were chosen for the 24 x-stations and 15 currents, one would require 7200 spectra - the equivalent of about 1000 hours of testing.

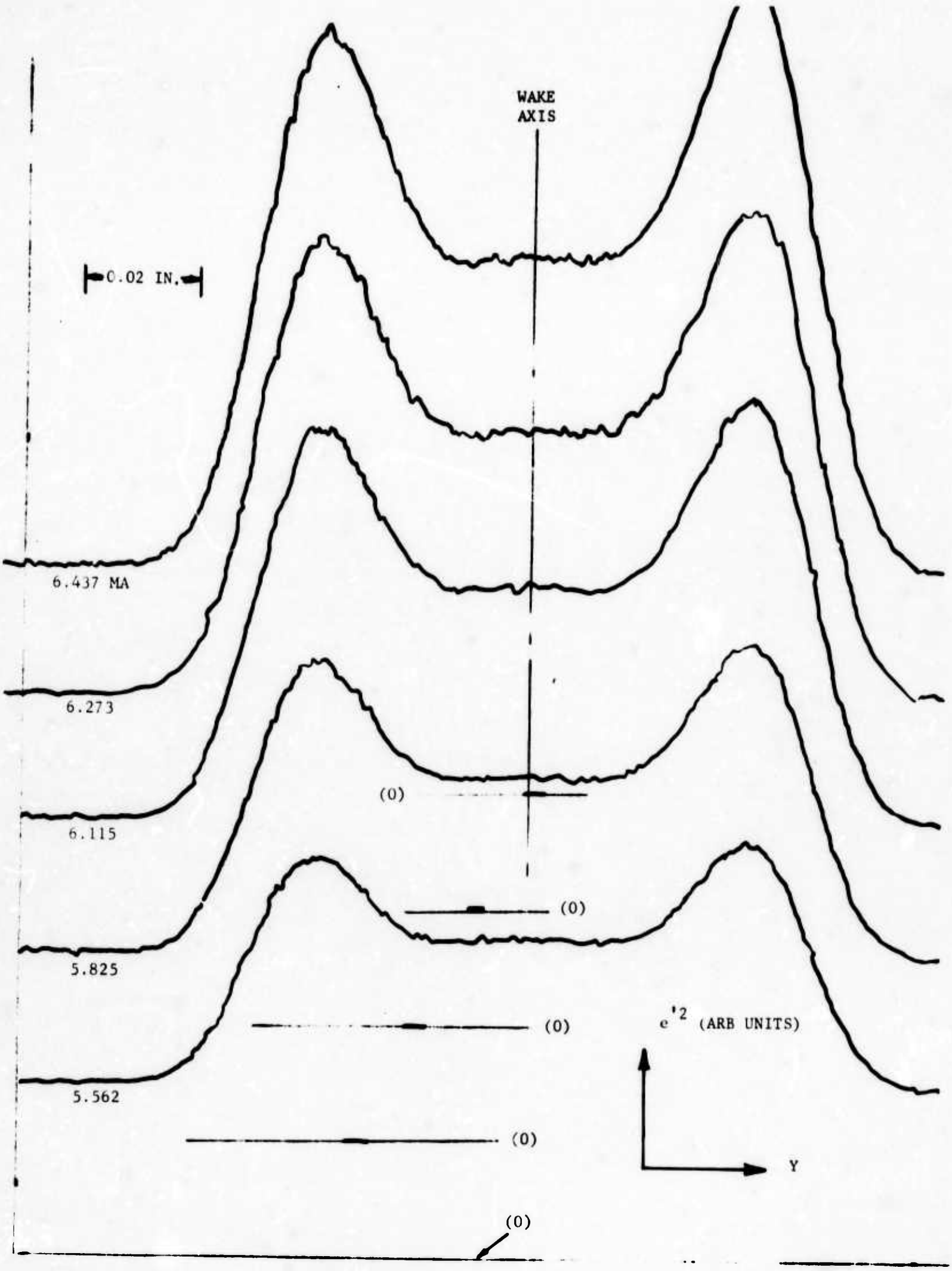

F12130 U

FIGURE 4. TYPICAL PROFILES OF RMS WIRE OUTPUT ACROSS TWO-DIMENSIONAL WAKE

was converted into dc across a 1000 ohm resistor and fed into the Y axis of the Moseley plotter. The sweep drive also produced a dc voltage proportional to frequency, which drove the other (x) axis of the plotter. A typical spectrum is shown in Figure 5. Since it is necessary to know the spectral distribution of electronic noise, that spectra of the noise were also taken.

2.6 RESULTS

2.6.1 RESPONSE RESTORATION AND SYSTEM PERFORMANCE

Data reduction began with the restoration of the frequency response of the system, accomplished by feeding the spectra information (Paragraph 2.5.7) into the WEB-II program (SRS No. 0073). The main objective here was to extract the error ratio, J, at each point in the wake.

The frequency response of the main system components is shown, for a typical situation, in Figure 6. The ordinate of this plot denotes the logarithm of "gain squared", that is, of the mean-square voltage coming out of each component divided by the mean-square voltage input. The graph shows results at a single point in the wake (X-Station 1, x = 0, Y = 0) and for one particular current (7.401 ma). Note, first, the rapid deterioration of the hot-wire itself, the attenuation (in the square) being about a million at 600 kHz. The compensator has a time-constant setting not quite adequate because of mismatched time-constants, and its gain never exceeds 100,000. The amplifier* also deteriorates, and its frequency response together with that of the hot-wire and compensator, produce the curve labeled "overall transfer fuction" (OTF) which is seen to produce an attenuation of about 100,000 at 1 MHz. The computer program is thus set up to multiply the wire output by 1/OTF and thus bring it to the level it would have ideally.

The hot-wire response is, of course, controlled by its time constant. Figure 7 shows the axial and lateral variation of the hot-wire time constant at the two extremes of current employed: 3.17 and 7.40 ma. For orientation, it should be recalled that the zero-current time constant limit for the type of wire employed is about 0.09 millisecond which is consistent with the data of Figure 7. More importantly, note that data are displayed from three different wires. Except at the lowest overheats (currents) it is evident that the time constant variation is small from one wire to another. It is also evident that the variation of time constant with x and Y becomes quite small, as it should, at far distances although it depends strongly, of course, on the heating current value.

A crucial test of the effect of using different wires (unavoidable because of wire breakage) insofar as the error ratio J is concerned is shown in Figure 8. Here can be seen the very large "corrections" necessary to bring

---

*The zero-frequency gain of the amplifier is not shown.

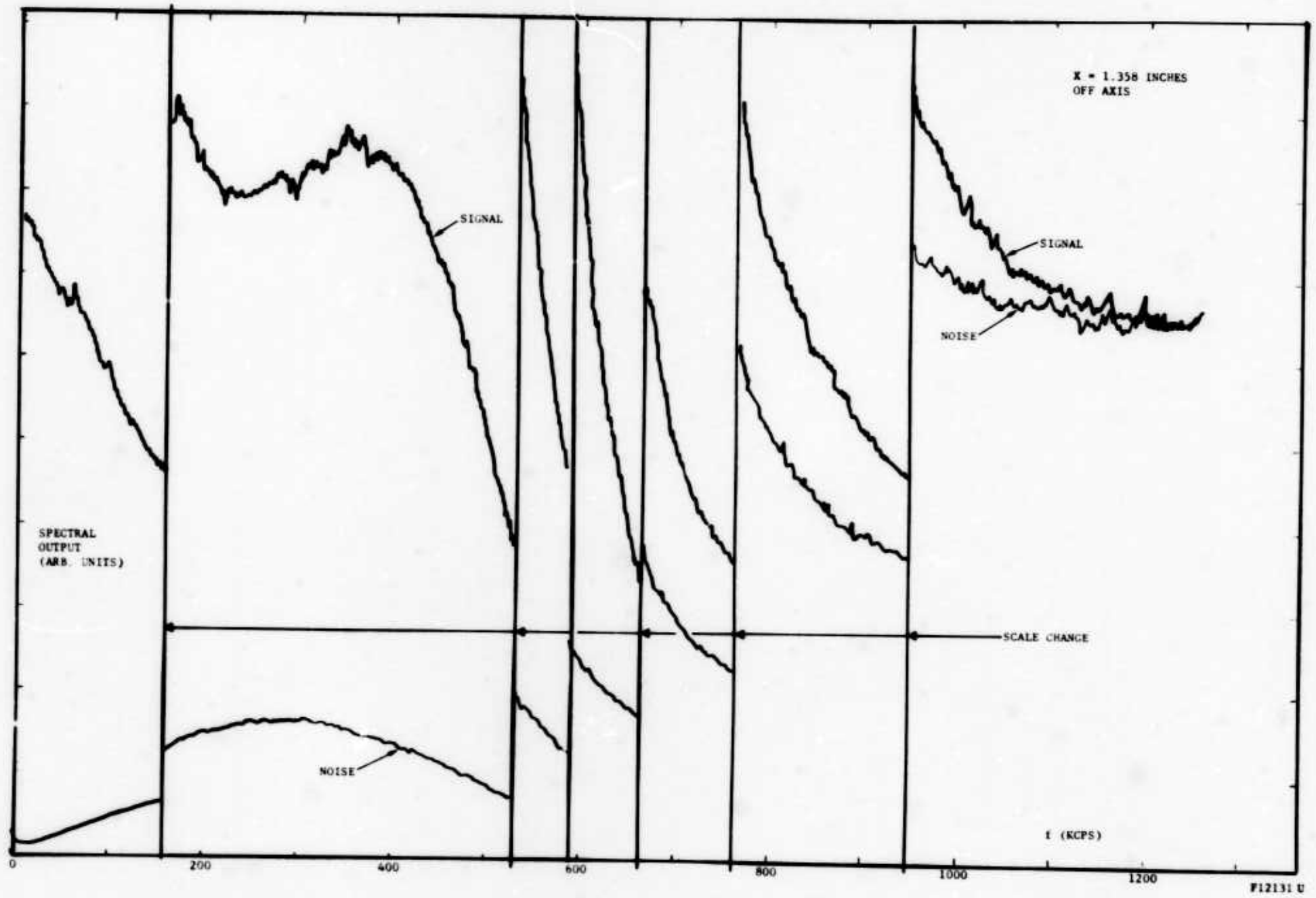

FIGURE 5. TYPICAL WIRE OUTPUT SPECTRUM. VERTICAL LINES MARK SCALE CHANGES

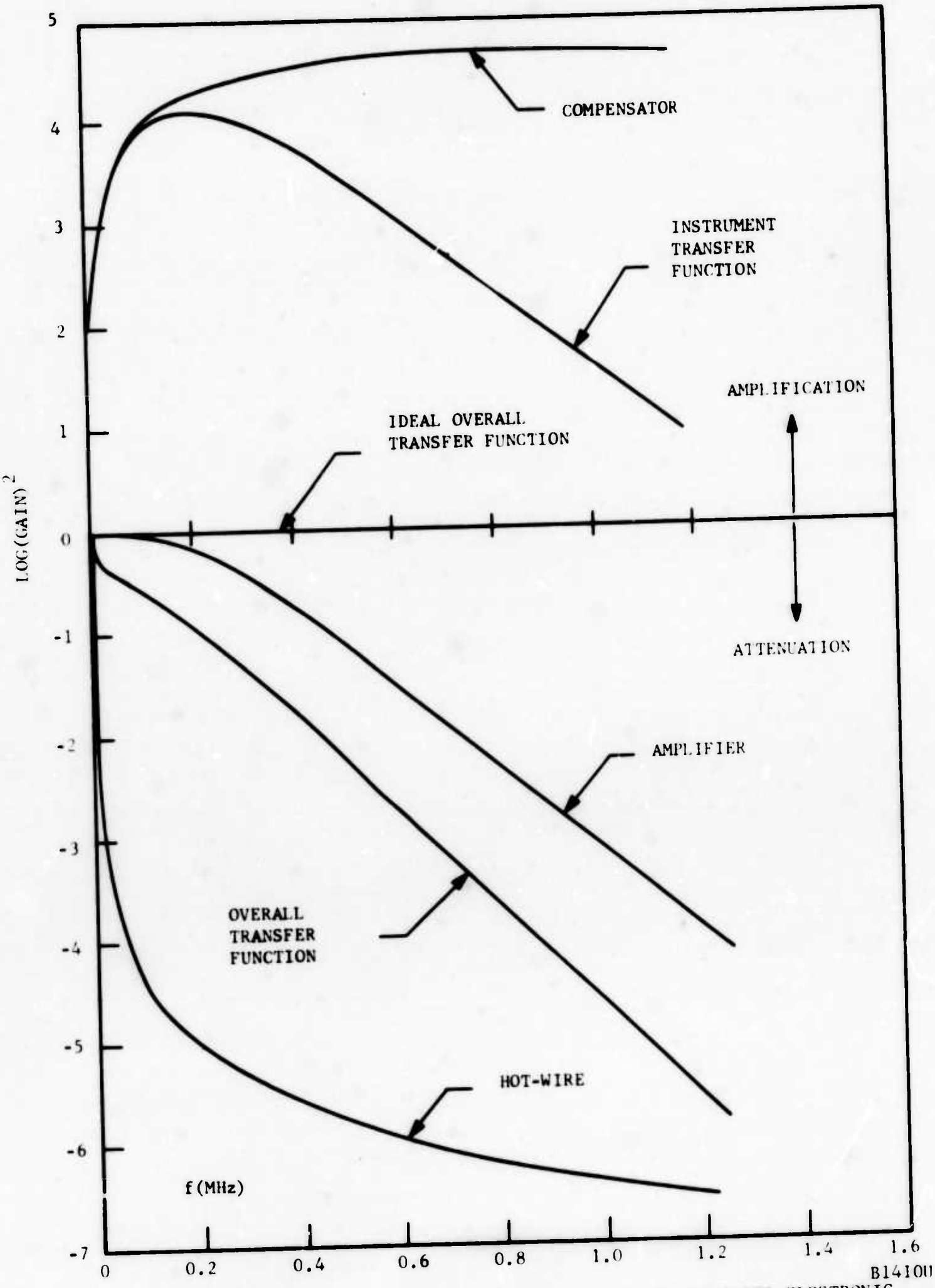

FIGURE 6. FREQUENCY RESPONSE OF EACH COMPONENT, OF THE COMPLETE ELECTRONIC EQUIPMENT ("INSTRUMENT TRANSFER FUNCTION") AND OF THE ENTIRE SYSTEM ("OVERALL TRANSFER FUNCTION")

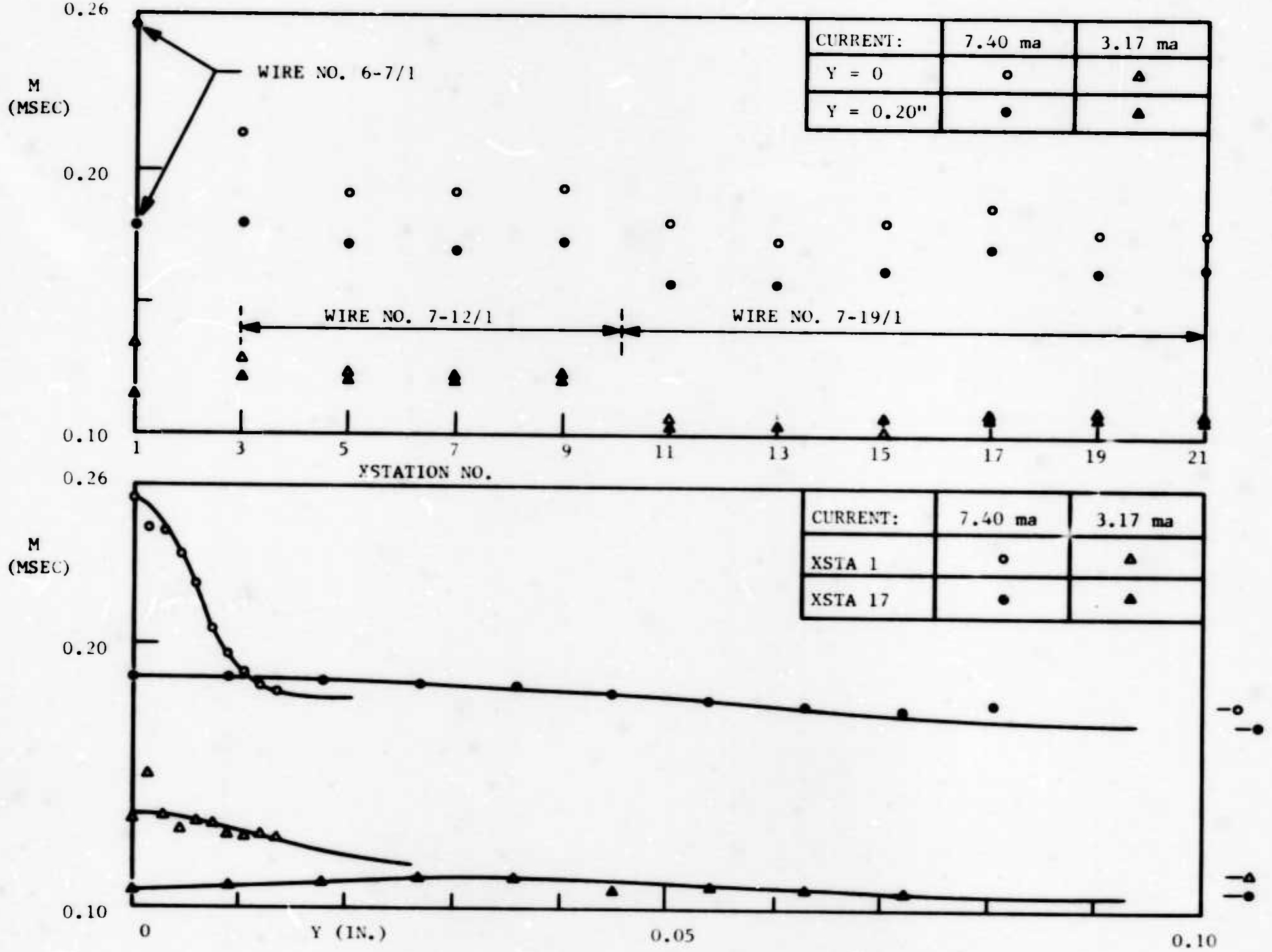

FIGURE 7. VARIATION OF MEASURED HOT-WIRE TIME CONSTANT WITH AXIAL (ABOVE) AND LATERAL (BELOW) DISTANCE

B1411U

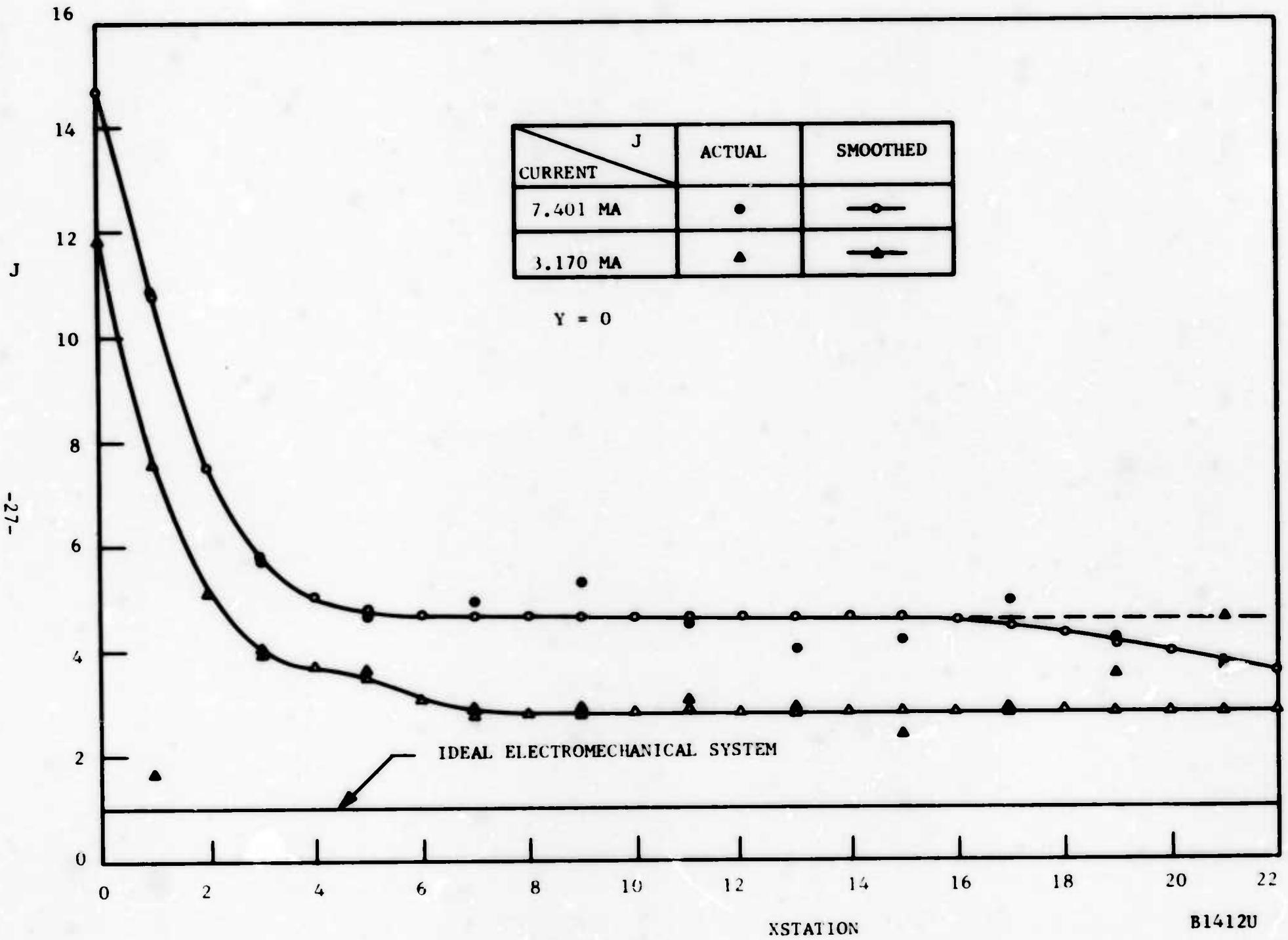

FIGURE 8. VARIATION OF ERROR RATIO J ALONG WAKE AXIS. DASHED LINE ALTERNATE SMOOTHING (FOR I = 7.401) WHICH WOULD ELIMINATE OBSERVED ANOMALIES BEYOND X-STATION 17.

the data to the level produced by a hypothetical ideal system. The J is as high as 15 on the axis very near the body and at the higher currents. By X-Station 6, J has attained asymptotically a constant value bracketed between 4.7 (at high currents) and 2.8 at the lowest current. The curves marked "smoothed" are an empirical attempt to reduce the data scatter (in the WEB-IV and WEB-VII outputs) by reducing the scatter in the J. As will be seen later, the break in the high-current curve occuring around X-Station 16 is significant. Equally significant is the rather gross departure, at the lowest current, between the actual and the smoothed J's past the same point. In the meantime, it is clear that there is no obvious break in the curves around X-Station 10 where the change from wire 7-12/1 to 7-19/1 occured. As is seen from Table IV, these two wires are structurally similar; the conclusion is that, with this similarity, uniform J's are obtainable.

The lateral variation of J for I = 7.401 ma is shown in Figure 9 for various X-Stations. It is noteworthy that off-axis J reaches values even larger than the axis values. Finally, Figure 10 shows the variation of J with current for two lateral positions in the wake. In all these figures, the disconcerting fact is noted that J does not attain the low values (about 1.5) in the free-stream which it attained in the axisymmetric wake (WEB) experiment (see Reference 5, page 19). At this juncture, the most likely explanation is that there is much more high-frequency content in the freestream turbulence of this experiment than in the WEB experiment.* However, no turbulence spectra were taken in the free-stream.

With the large J's shown on Figures 8 and 10 and the deteriorated frequency response of the system shown in Figure 6, it is clear that the output spectrum of the measuring system will be severely distorted at each current and flow point. The printed output of WEB-II lists both these actual (distorted) spectra and the "ideal" spectra; these are of course voltage output spectra, at this point still unresolved modally (i.e., not indicating the velocity and density spectral densities separately). A comparison of actual and ideal spectra are typically shown in Figure 11. They differ greatly, as they should. The differences lie not only at the high frequencies where the actual spectra are greatly attenuated, but also in shape. The latter very important point will be discussed further in Paragraph 2.6.4.

A final important point regarding the output of WEB-II concerns the two alternate methods of measuring the (integrated) flunctuations intensity. This is formally measured by the wide-band Ballantine voltmeter (see Paragraph 2.5.4), but is also independently available from the spectral measurements (Paragraph 2.5.7) since the total rms intensity is, after all, the integral of the spectral density. The latter integral is listed in WEB-II as VTVM2 (in units of volts squared) while a total rms measurement

*The WEB experiment was done at P_o = 508 mm Hg where the tunnel side-wall boundary-layer capable of radiating onto the wake was laminar. In WED (P_o = 730 mm Hg) the layer was turbulent, with possible enhancement of the stream turbulence by radiation.

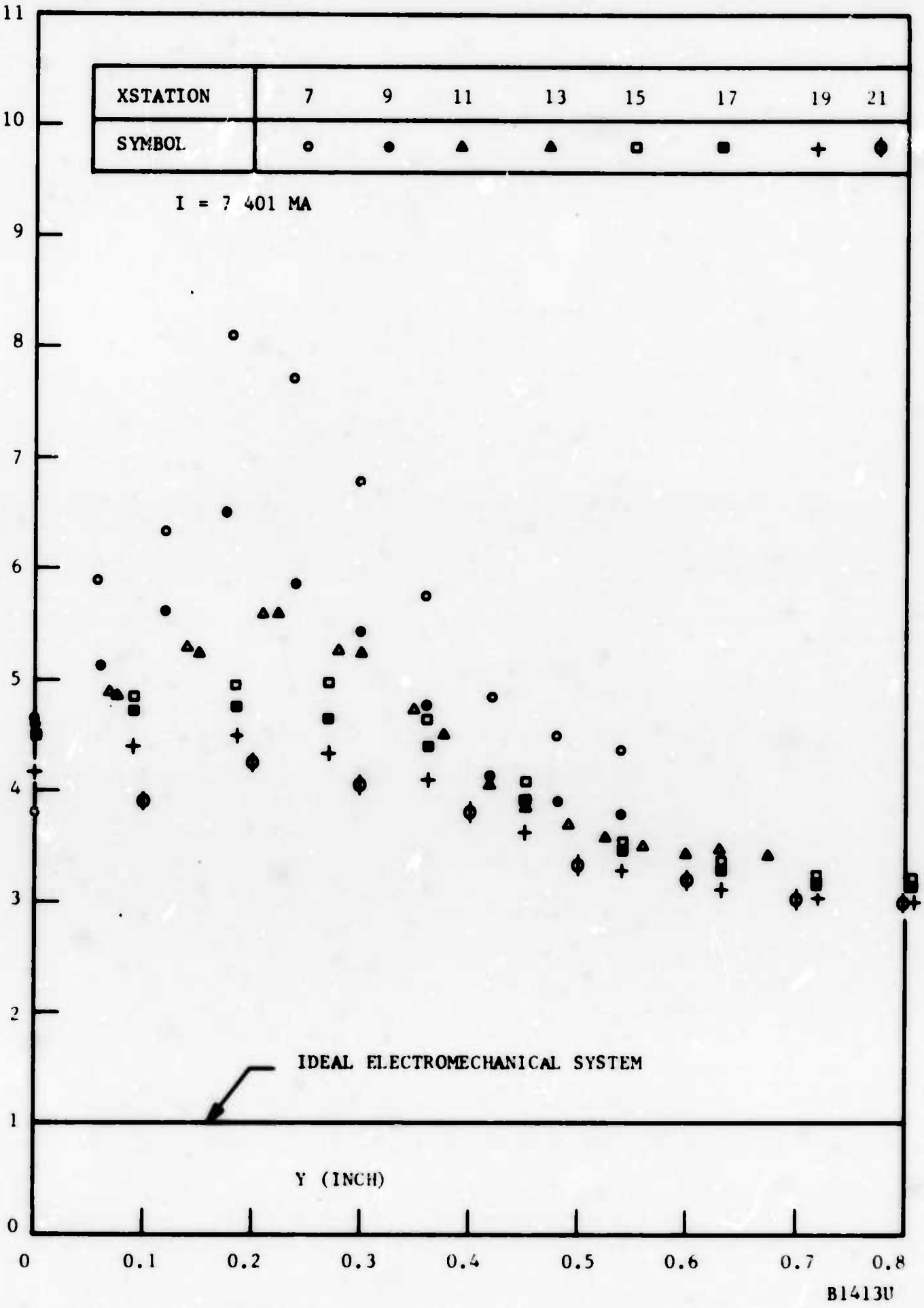

FIGURE 9. LATERAL VARIATION OF J FOR CONSTANT X

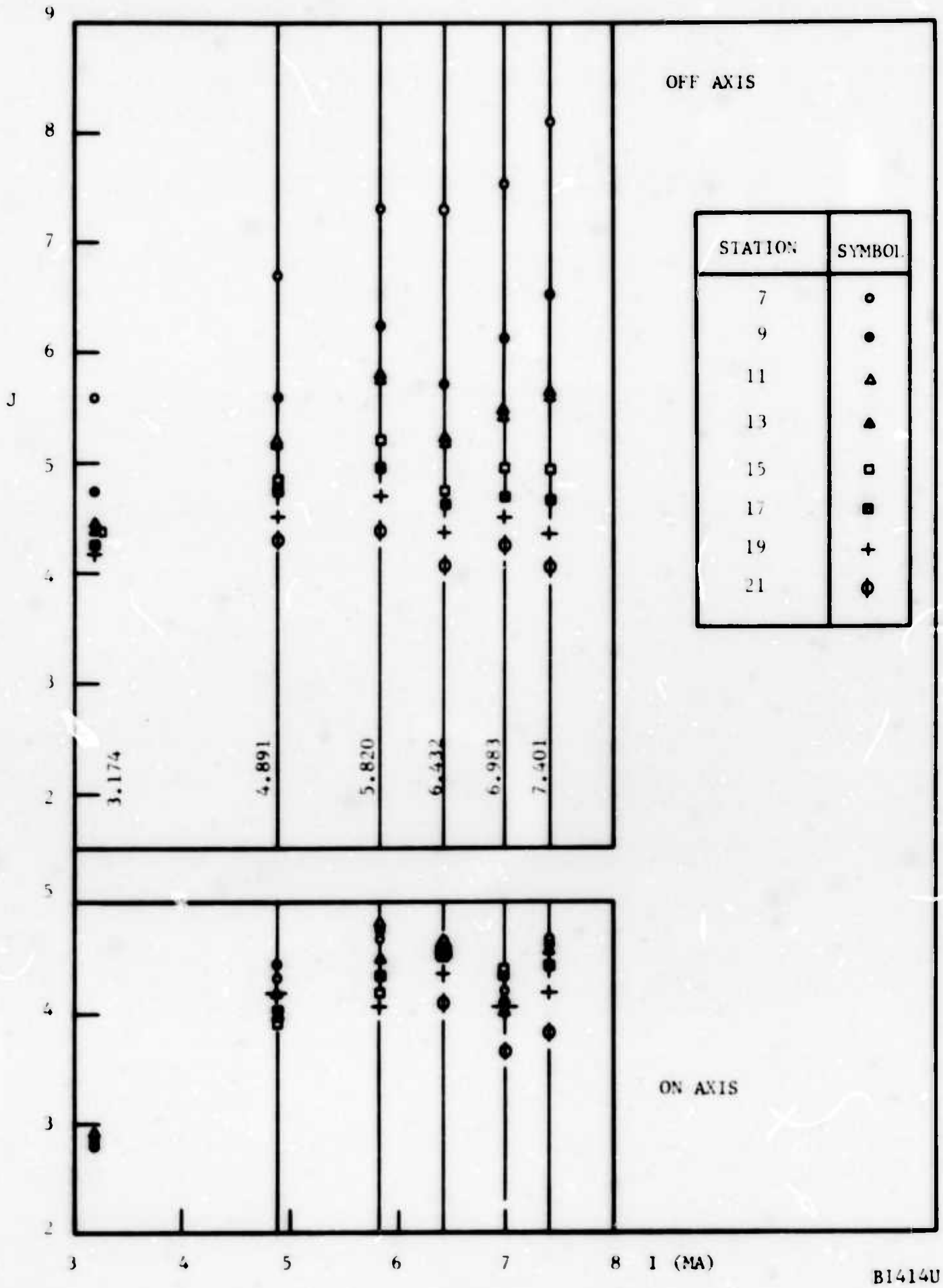

FIGURE 10. VARIATION OF J WITH HEATING CURRENT FOR TWO LATERAL POSITIONS

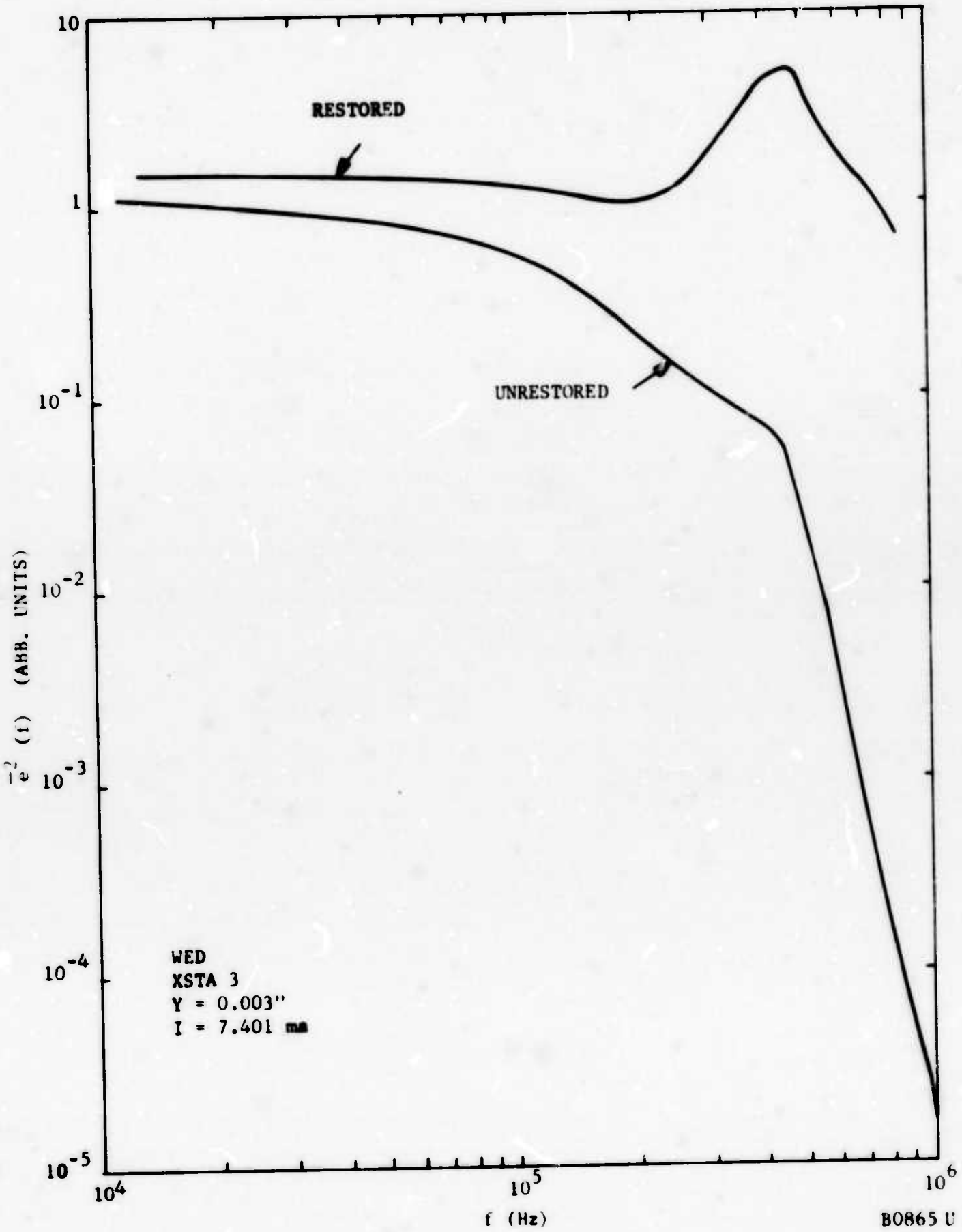

FIGURE 11. EFFECT OF COMPUTER-AIDED RESPONSE RESTORATION ON THE MODALLY UNRESOLVED TURBULENCE SPECTRA (WED EXPERIMENT)

made in conjunction with the spectra is labeled E02. Representative values for the ratio E02/VTVM2 are shown in Figures 12 and 13. This ratio should be unity for perfect correspondence, but it is in fact almost everywhere constant near 1.5 (i.e., a difference of about 20 percent in the root-mean-square) meaning that the directly measured output is always higher than that reconstructed by integrating the spectrum. Because of the multitude of operations necessary to the latter, the 20 percent difference is actually much better than expected and is in fact an endorsement of the accuracy of the measurement.

2.6.2 THE WEB-III PROGRAM

The next step in the data reduction process combines the J values from the WEB-II output and the turbulence data (Paragraph 2.5.6) into the WEB-III program (SRS Program 0083) from which the integrated rms wire voltage is obtained at each point of the wake, and for each heating current, free from frequency-response limitations of the system.

Turbulence information was obtained from 22 equidistant points spaced 0.004 inch apart, beginning at the axis and extending laterally to Y = 0.084 inch. The total points involved, therefore were (22 Y's) x (15 currents) x (23 X-Stations) = 7590, since the 24th X-Station, that numbered 23, was not used. At the WEB-II output the number of J's available were (10 Y's) x (6 currents) x (12 X-Stations) = 720, since the spectra were taken sparsely to save time. The required J's were then obtained from those available by interpolation. In the latter process a certain amount of smoothing of the data was performed in order to decrease experimental scatter in the final outcome. An indication of this type of smoothing is already shown in Figure 8. Certain parts of this process are thought to have caused artificial perturbations of the final data, a point which will be discussed further.

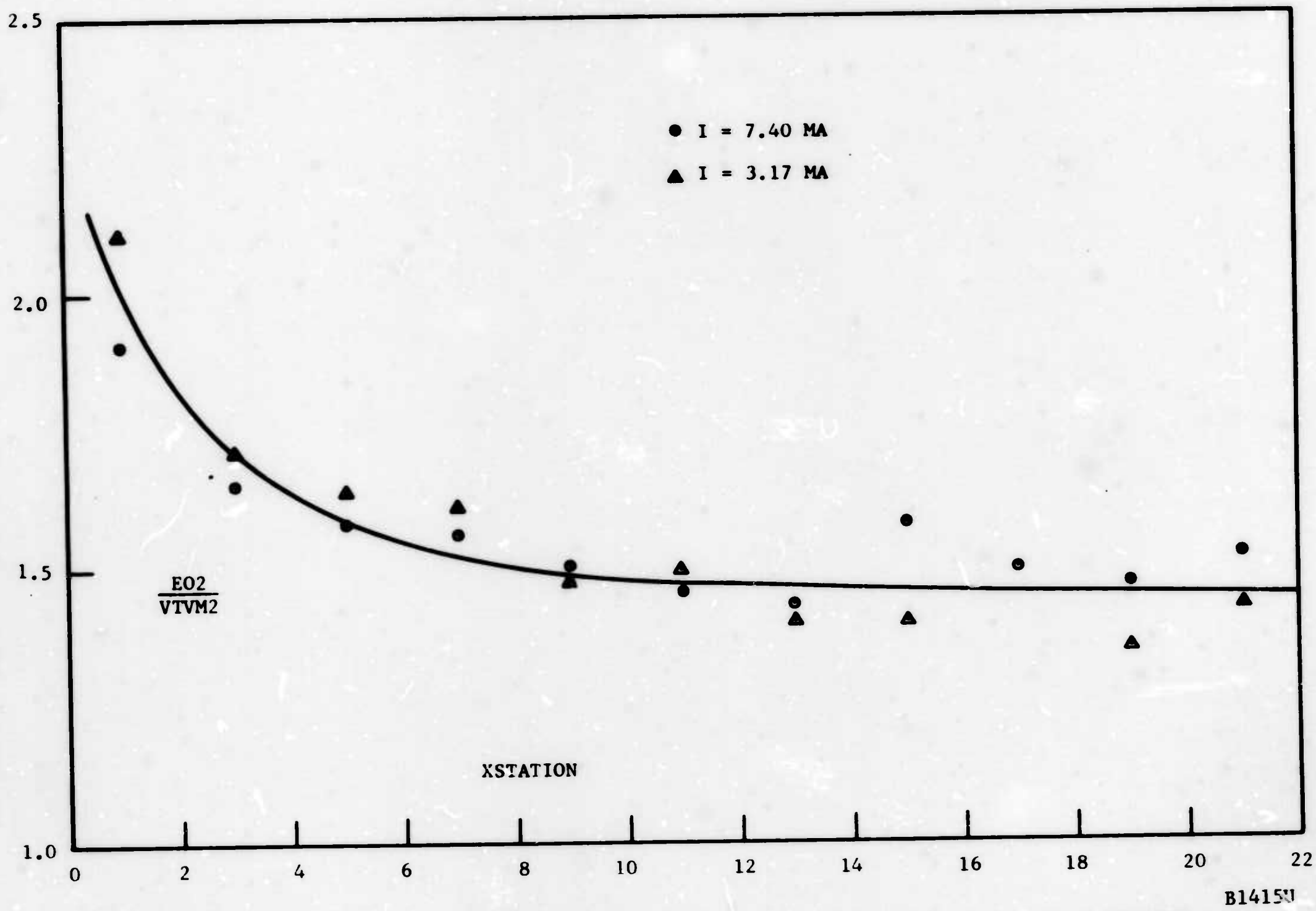

FIGURE 12. CONSISTENCY CHECK WITHIN THE WEB-II PROGRAM: AXIAL VARIATION

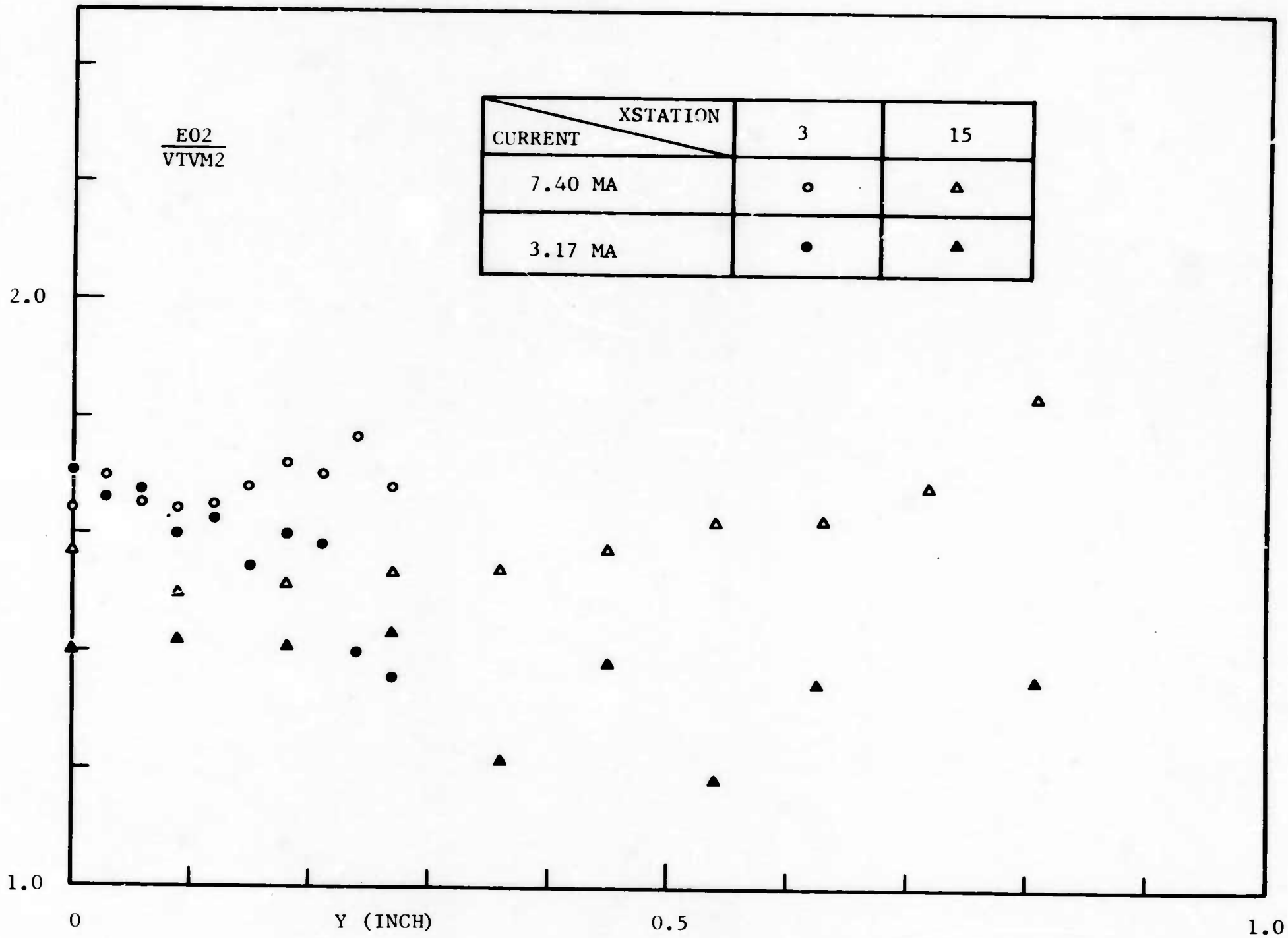

FIGURE 13. CONSISTENCY CHECK WITHIN THE WEB-II PROGRAM: LATERAL VARIATION

2.6.3 EXPERIMENTAL RESULTS IN THE FLUCTUATION INTENSITY

The WEB-IV program gives the intensity of turbulent fluctuations at each of the 22 lateral positions and the 23 X-Stations (X-Station 0 through 22). This paragraph discusses the nomenclature, method of analyzing the data, and the results themselves. The latter deal only with the so-called modal analysis, i.e., the fluctuation intensity; the spectra, as well as the scaling rules by which the results are applicable to high speeds, are discussed in subsequent paragraphs.

In the text and figures found below, the following nomenclature is used:

(1) $\Delta u/u$ is the local root-mean-square fluctuation in the axial velocity u, normalized by the local mean (average) axial velocity, and integrated over all frequencies.*

(2) $\Delta\rho/\rho$ is analogous to (1), above, for the local gas density.

(3) $\Delta T/T$ is analogous to (1) for the local static temperature. Note $\Delta T/T = \Delta\rho/\rho$ for constant pressure.

(4) $\Delta\rho u/\rho u$ and $\Delta T_o/T_o$ are analogous to (1) for the local mass-flux ρu and total temperature T_o.

(5) $$r_{mt} = \frac{\overline{(\Delta\rho u/\rho u)\ (\Delta T_o/T_o)}}{(\Delta\rho u/\rho u)\ (\Delta T_o/T_o)} \qquad (17)$$

is the cross-correlation coefficient, at the same point, between ρu and T_o fluctuation (the barred numerator obviously is the averaged product of the instantaneous counterparts of $\Delta\rho u/\rho u$ and $\Delta T_o/T_o$).

(6) $$r_{\sigma T} = \frac{\overline{(\Delta u/u)\ (\Delta T/T)}}{(\Delta u/u)\ (\Delta T/T)} \qquad (18)$$

is the cross-correlation coefficient, at the same point, between u and T fluctuations. Note that although

$$\frac{\Delta\rho}{\rho} = \frac{\Delta T}{T} \qquad \text{(rms sense)} \qquad (19)$$

instantaneously

$$\left(\frac{\Delta\rho}{\rho}\right)_{INST.} = -\left(\frac{\Delta T}{T}\right)_{INST.} \qquad (20)$$

* In this work, and in Reference 5, Δ is used as a root-mean-square operator.

so that the following relation exists between the velocity-density and the velocity-temperature correlations:

$$\frac{\overline{(\Delta\rho/\rho)(\Delta u/u)}}{(\Delta\rho/\rho)(\Delta u/u)} = -\frac{\overline{(\Delta T/T)(\Delta u/u)}}{(\Delta T/T)(\Delta u/u)} = -r_{\sigma\tau} \tag{21}$$

(7) In the WEB-IV output the following alternate designations are used:

$$M \equiv \Delta\rho u/\rho u \tag{22}$$

$$T \equiv \Delta T_o/T_o \tag{23}$$

$$RMT = r_{mt} \tag{24}$$

$$\sigma = \text{Sigma} \equiv \Delta\rho/\rho = \Delta T/T \tag{25}$$

$$\tau \equiv \text{Tau} \equiv \Delta u/u \tag{26}$$

$$RSTAU = r_{\delta\tau} \tag{27}$$

$$U\ PRIME \equiv \Delta u/\left(u_\infty - u(o)\right) \tag{28}$$

$$RHO\ PRIME \equiv \Delta\rho/\left(\rho_\infty - \rho(o)\right) \tag{29}$$

where in the latter two cases, ∞ and (0) refer to conditions outside of and on the axis of the wake, respectively, and where Δu and $\Delta\rho$ retain their rms meanings.

(8) Eta, or η, is the normalized radial distance (see Equation (7)).

The equation relating the fluctuation intensities to the local rms voltage output e of the hot-wire can be written in the following alternate ways:

$$e^2 = e_m^2 M^2 + e_\tau^2 T^2 - 2\,MT\,e_m e_\tau r_{m\tau} \tag{30}$$

$$e^2 = e_\tau^2 \tau^2 + e_\sigma^2 \sigma^2 + 2\,t\sigma\ e\sigma\ e_\tau r_{\sigma\tau} \tag{31}$$

with the symbols as given above and with e_m, e_τ and e_σ being the appropriate "sensitivity coefficient" to the various fluctuation modes. These coefficients are in principle functions only of the local mean flow properties, which were measured earlier (see Paragraph 2.4 and Reference 1) and of the wire characteristics, provided by the wire calibration and inputed into WEB-IV. Equation (30) is exact, but Equation (31) is approximate in that contributions to e^2 due to

sound waves are assumed ni.* Either equation may be used, depending on which of the unknowns are to be obtained. Separate computations are performed in WEB-IV, one for each of Equations (30) and (31).

In the present program, Kovasrzay's original suggestion (Reference 9) is followed reducing these two formulas into convenient second-degree equations with unknown coefficients. For example, Equation (31) is written:

$$\frac{e^2}{e_\sigma^2} = \tau^2 + \left(\frac{e_\tau}{e_\sigma}\right)^2 \sigma^2 + 2\tau\sigma\left(\frac{e_\tau}{e_\sigma}\right) r_{\sigma\tau} \qquad (32)$$

which is of the second degree in the known and controllable parameter (e_τ/e_σ). Since at each heating current setting a pair of number (e_τ/e_σ) and $e^2/a^2\sigma$ are measured, three such settings result in a system of three Equations (31) in the three unknown τ, σ and $r_{\sigma\tau}$. The accuracy is much improved in the present system: fifteen settings are used and the computer least-squares fits a second-degree curve to the fifteen points.

a. Sensitivity Coefficients. Figure 14 shows typical variation of the hot-wire sensitivity coefficients at a point in the wake. The true indication of wire sensitivity is its so-called "overheat" A_w' (which is roughly proportional to the percentage increase of wire resistance over its equilibrium unheated value). A range of A_w' from perhaps 0.05 to 0.5 is desired usually in order to maintain measurement accuracy, the wire melts around $A_w' = 0.6$. In Figure 14, A_w' varies from 0.02 to 0.40. In the example shown, note that $A_w' = 0.335$ (corresponding to I = 6.7 ma) the hot-wire sensitivity to velocity fluctuations is nil, and the wire is therefore sensitive to density fluctuations only.

b. Mass-Flux-Total-Temperature Correlation. Figure 15 shows the axial (along Y = 0) and Figure 16 a typical lateral variation of r_{mt}, the cross-correlation coefficient between ρu and T_o. No correlation was found in either direction, as also was noticed in the axisymmetric wake (Reference 5, page 52).

c. Mass-Flux and Total Temperature Fluxtuation. Typical lateral variations of $\Lambda\rho u/\rho u$ and $\Lambda T_o/T_o$ appear in Figures 17 and 18, and their axial variation (along Y = 0) in Figure 19. The $\Lambda T_o/T_o$ fluctuations are always much smaller than $\Lambda\rho u/\rho u$ by a factor varying from 3 to 6.

The small size of $\Lambda T_o/T_o$ is caused by the fact that the flow is adiabatic, and it should be zero if the effective Prandtl number of the wake was unity. As will be seen later, with very small ΛT_o the so-called "Strong Reynolds Analogy" holds and enables one to predict the temperature (or density) fluctuations from known velocity fluctuations.

*Formally, inclusion of sound waves introduces three more terms in Equation (31) and three more unknowns: The pressure fluctuation and the pressure-velocity and pressure-density correlations. It should be also noted that both Equations (30) and (31) are linearized, that is, applicable for small magnitudes of the unknowns, M, T, σ and τ.

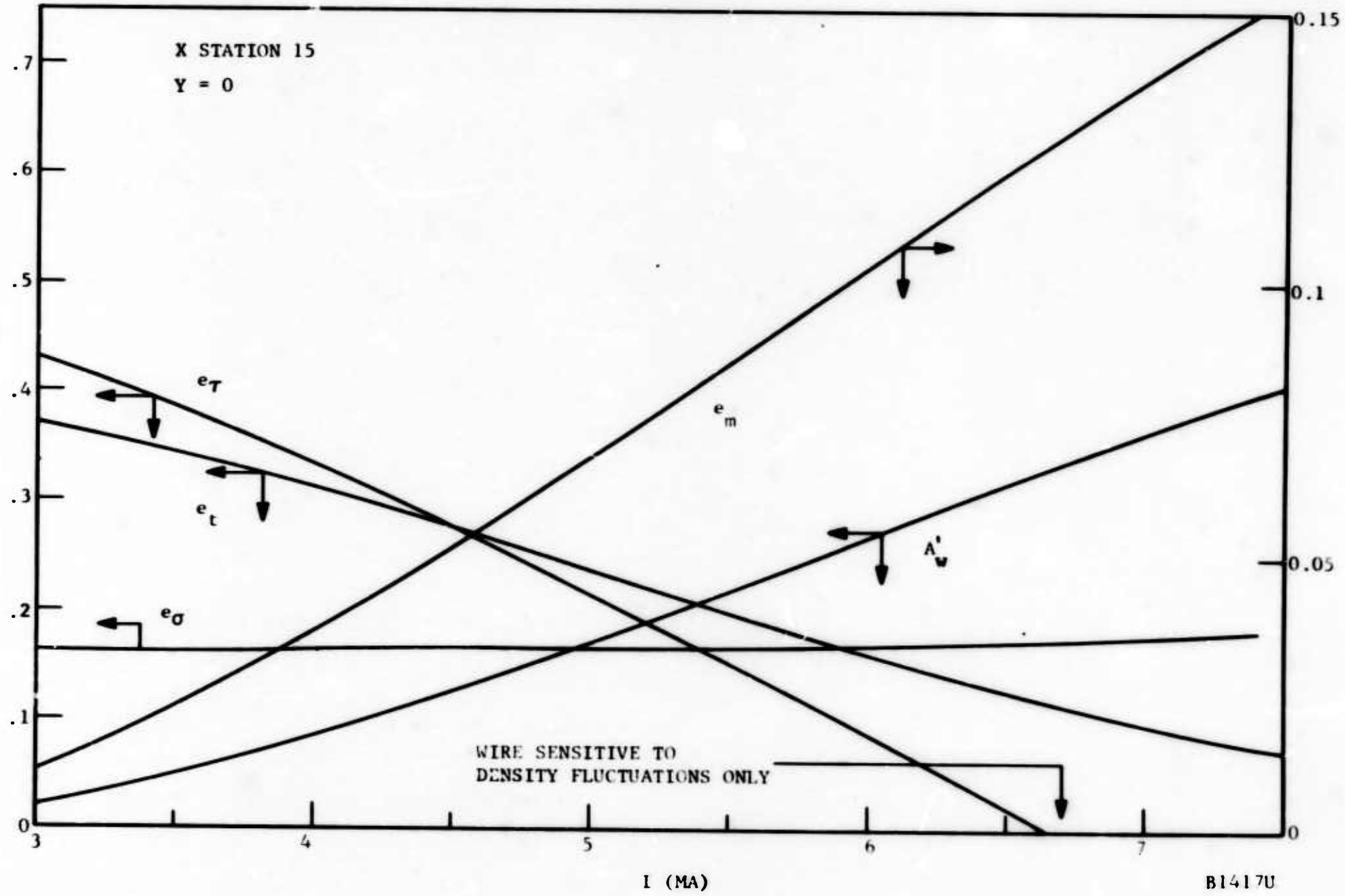

FIGURE 14. EFFECT OF HEATING CURRENT (AT A FIXED POINT IN THE WAKE) ON VARIOUS SENSITIVITY COEFFICIENTS OF THE HOT WIRE

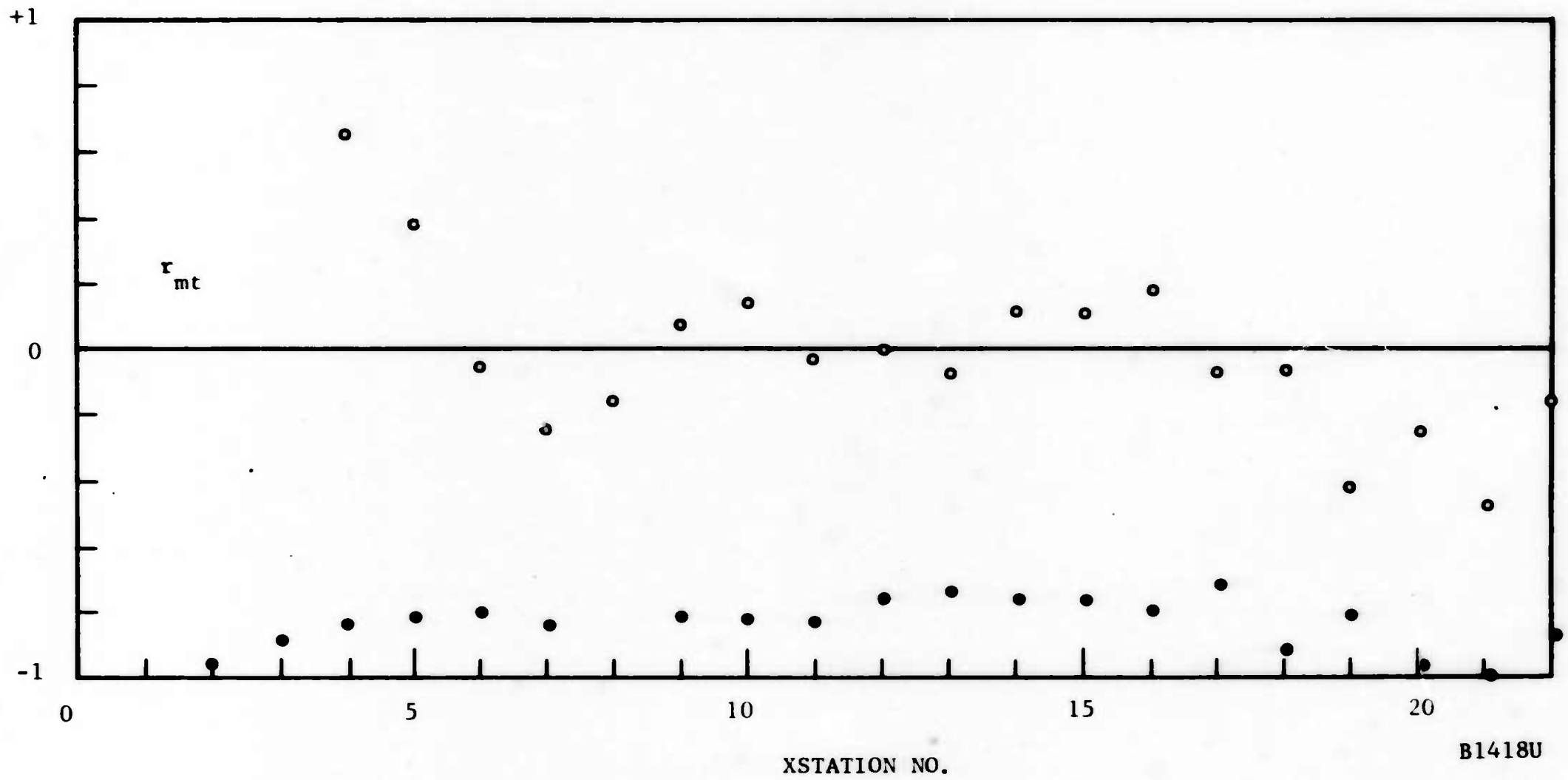

FIGURE 15. VARIATION OF THE MASS-FLUX AND TOTAL-TEMPERATURE CROSS-CORRELATION COEFFICIENT ALONG THE WAKE AXIS

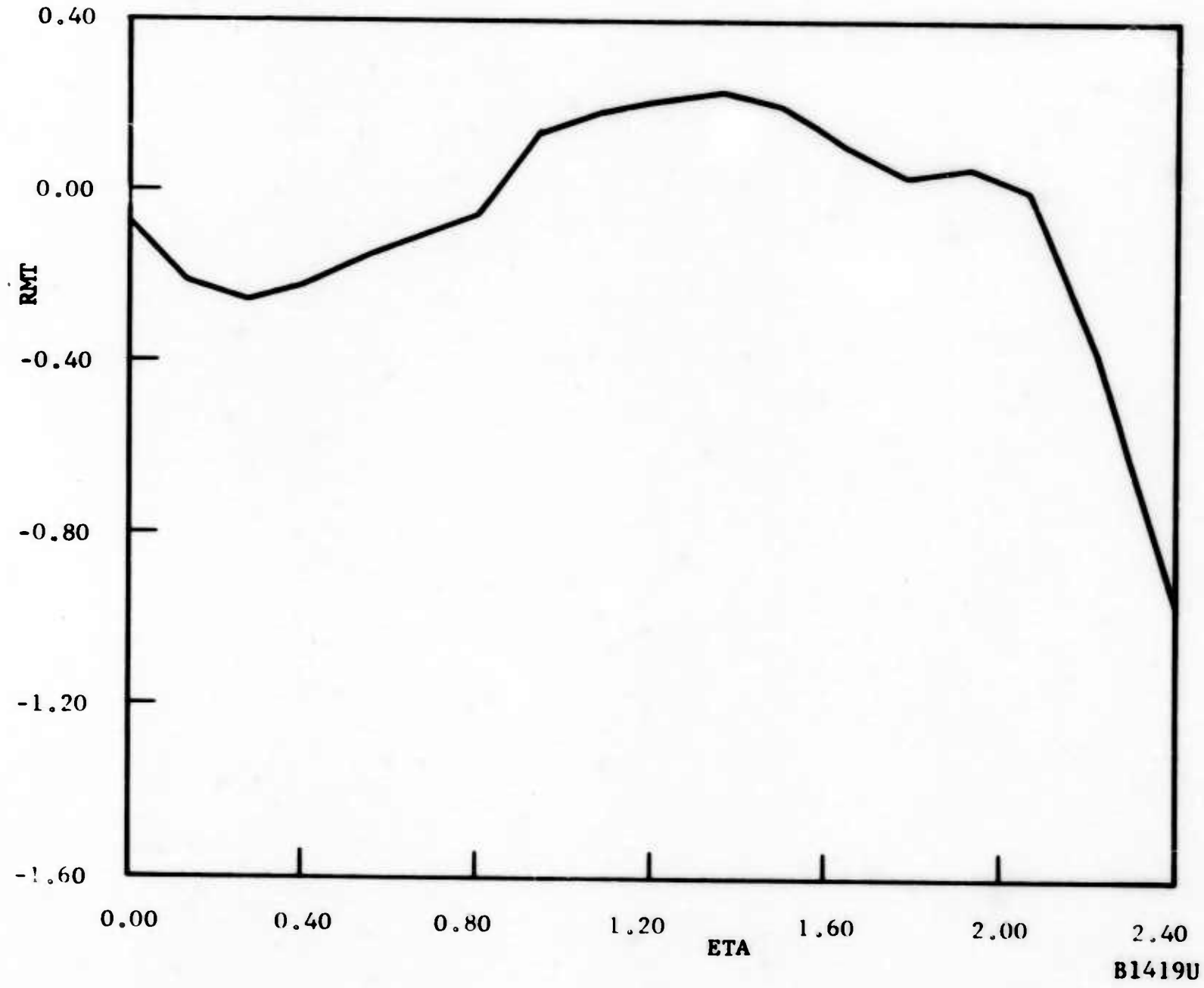

FIGURE 16. VARIATION OF THE MASS-FLUX AND TOTAL-TEMPERATURE CROSS-CORRELATION COEFFICIENT IN THE LATERAL DIRECTION (FIXED X)

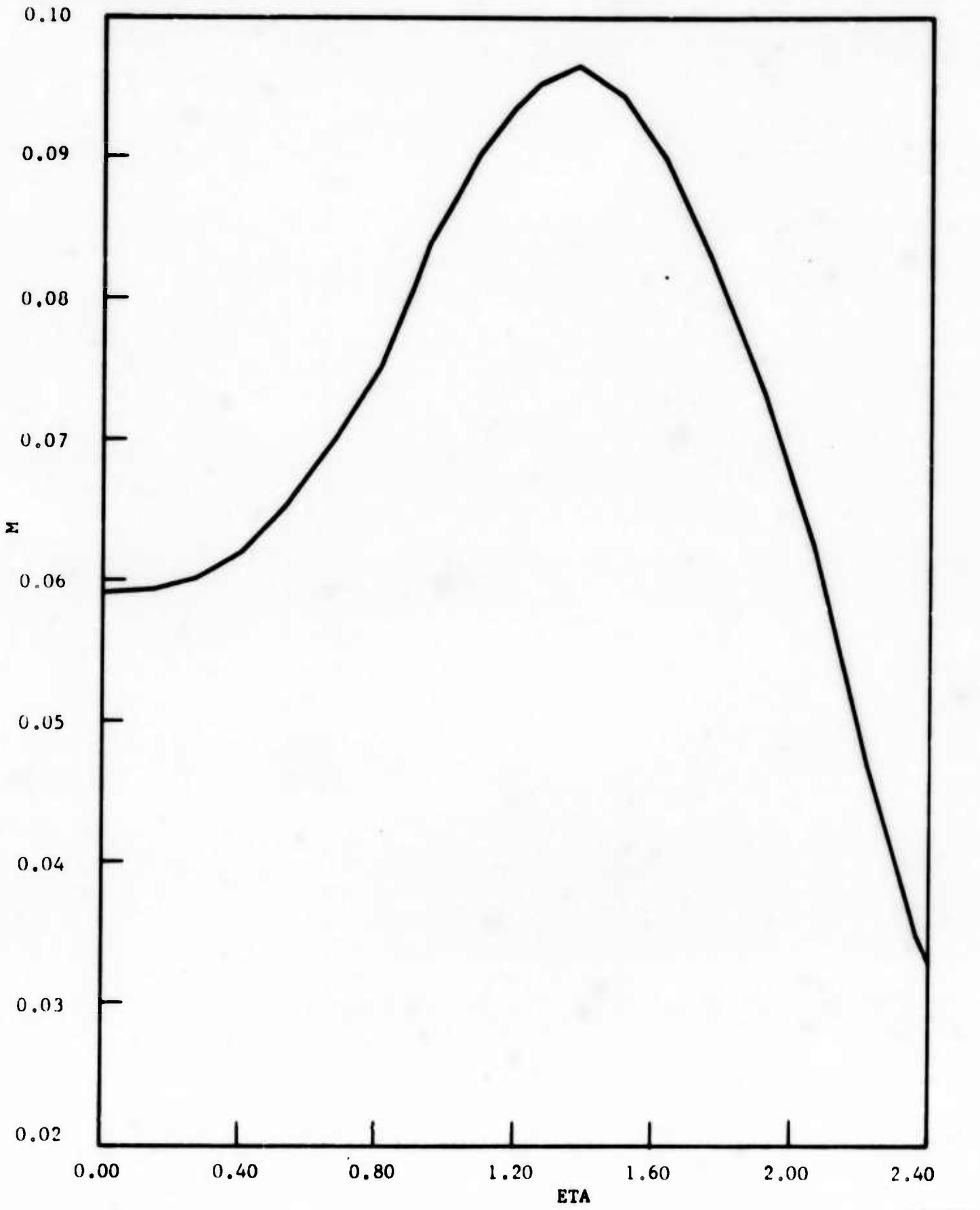

FIGURE 17. TYPICAL VARIATION OF THE RMS MASS-FLUX FLUCTUATION (NORMALIZED WITH ITS LOCAL MEAN) IN THE LATERAL DIRECTION

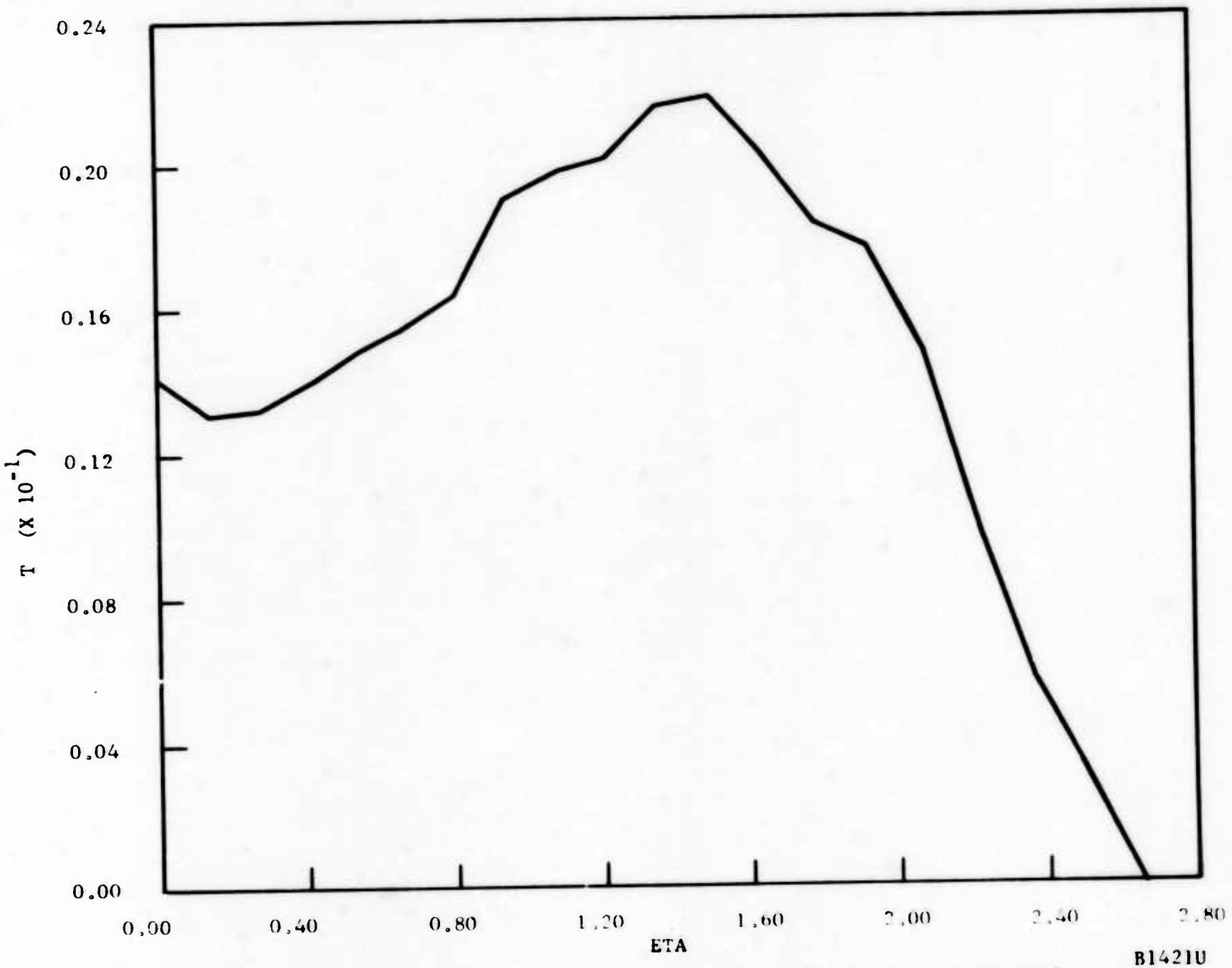

FIGURE 18. TYPICAL VARIATION OF THE RMS TOTAL TEMPERATURE FLUCTUATION (NORMALIZED WITH ITS LOCAL MEAN) IN THE LATERAL DIRECTION

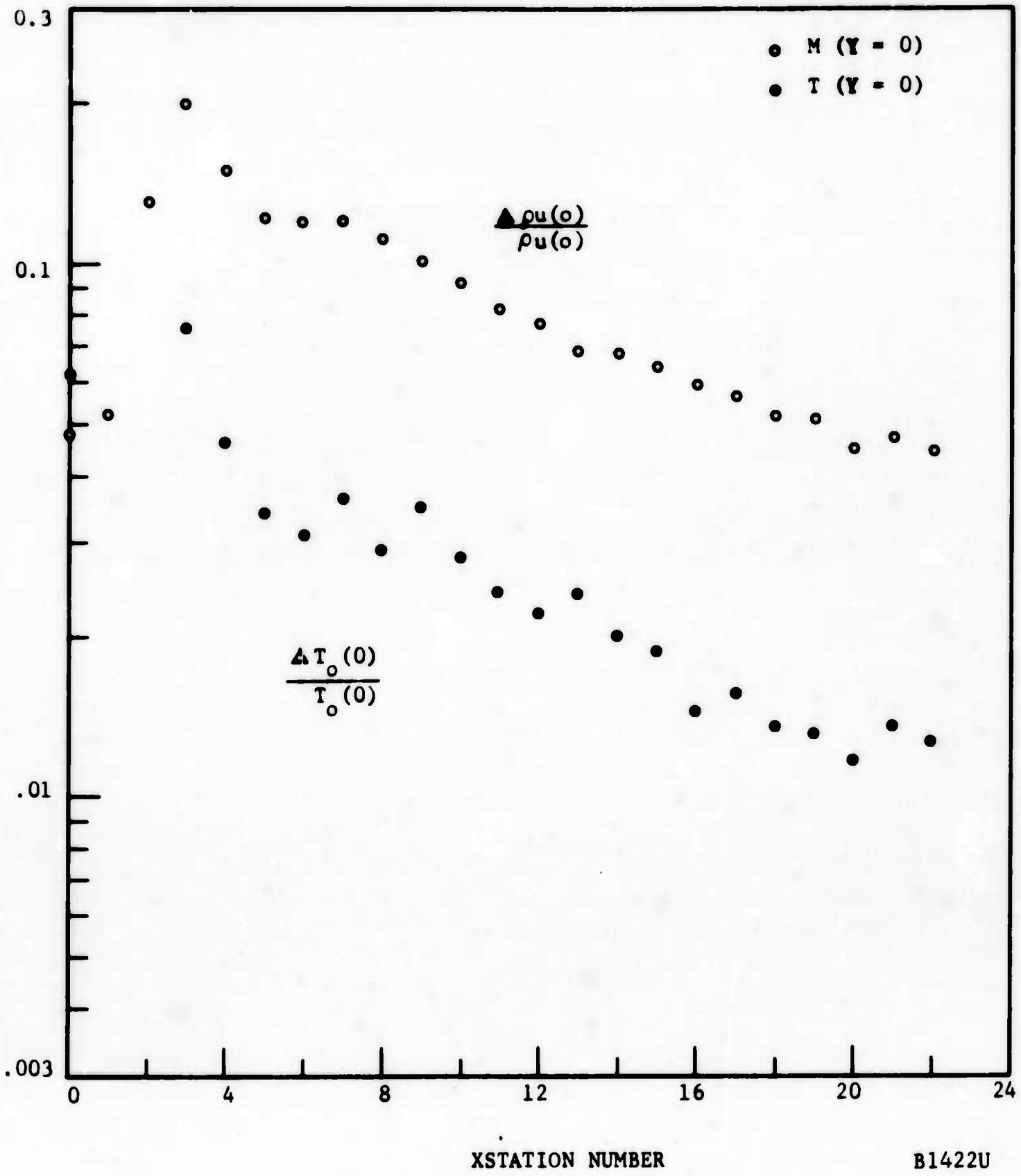

FIGURE 19. VARIATION OF THE NORMALIZED MASS-FLUX AND TOTAL TEMPERATURE FLUCTUATIONS ALONG THE WAKE AXIS

Laterally both types of fluctuations show the off-axis maximum characteristics of symmetric free turbulent flows; this will be discussed later.

d. Velocity Fluctuations. The axial variation of velocity fluctuations $\lambda u/u$ is shown in Figure 20. As with the axial behavior of $\lambda T_o/T_o$ and $\lambda \rho u/\rho u$, the fluctuations in velocity initially increase until they reach a value of about 0.06 at a distance of approximately 200 diameters from the body and thereafter decrease. In the end of the range probed (beyond X-Station 17) the fluctuations become quite anomalous. It is conjectured that this rather abrupt change is due to incorrect smoothing of the J factors, that is, to the artifically decreasing J shown beyond that distance on Figure 8. To test this conjecture the following test was performed: the J values (for each heating current) at X-Station 21, Y = 0 were taken as inputted into WEB-IV program but prior to the change noted around X-Station 17. Actually, the J values at X-Station 15, Y = 0 were used. The results were as follows:

Using J from X-Station 21:

$\tau = \lambda u/u = 0.0049$

$\sigma = \lambda \rho/\rho = 0.038$

Using J from X-Station 15:

$\tau = 0.0113$

$\sigma = 0.039$

Two very important conclusions are drawn from this computation: (1) if the J's used in the "anomalous" region (X-Station 17 to 22) are made identical to those prior to that region, then the λu fluctuation levels come back on what seems to be the level properly expected; (2) the density fluctuation $\lambda \rho$ are almost completely unaffected by changing J. In changing J, λu changes by about 250 percent, whereas $\lambda \rho$ by about 3 percent only. The explanation of this behavior is as follows: In the computational method used (which) finds the fluctuations from the shape parameters of a curve fitting experimental points), the velocity fluctuations result from the slope of a curve (specifically, the e^2/e_σ^2 versus (e_τ/e_σ) curve of Equation (32)), whereas the temperature fluctuations result from the intercept of this curve with the e_τ/e_σ axis. It turns out that the slope of the curve is very sensitive to J, whereas the intercept is not. At this juncture, the anomaly in J is studied so that its cause can be located.

Lateral distributions of the velocity fluctuations are typically shown on Figure 21. This lateral profile follows the general trend of the fluctuations in $\lambda \rho u/\rho u$ and $\lambda T_o/T_o$: a region of relatively low turbulence on the axis, with a considerable increase off axis and the natural decline toward zero at the wake edge. Note that the maximum in the fluctuation intensity occurs at η definitely higher than 1.0. This maximum is heretofore considered to mark the lateral location in the wake where turbulence production, shear,

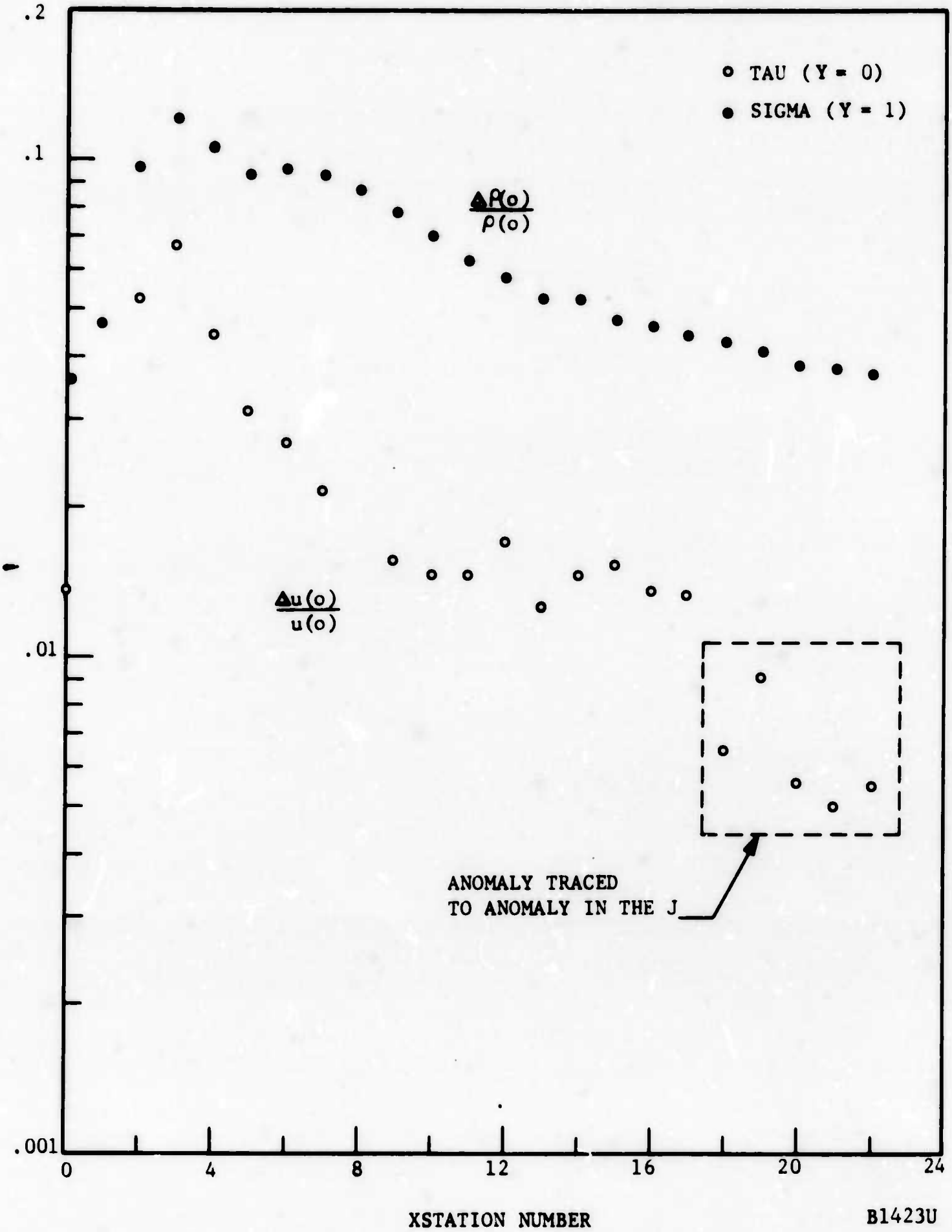

FIGURE 20. VARIATION OF THE NORMALIZED VELOCITY AND DENSITY (TEMPERATURE) FLUCTUATIONS ALONG THE WAKE AXIS

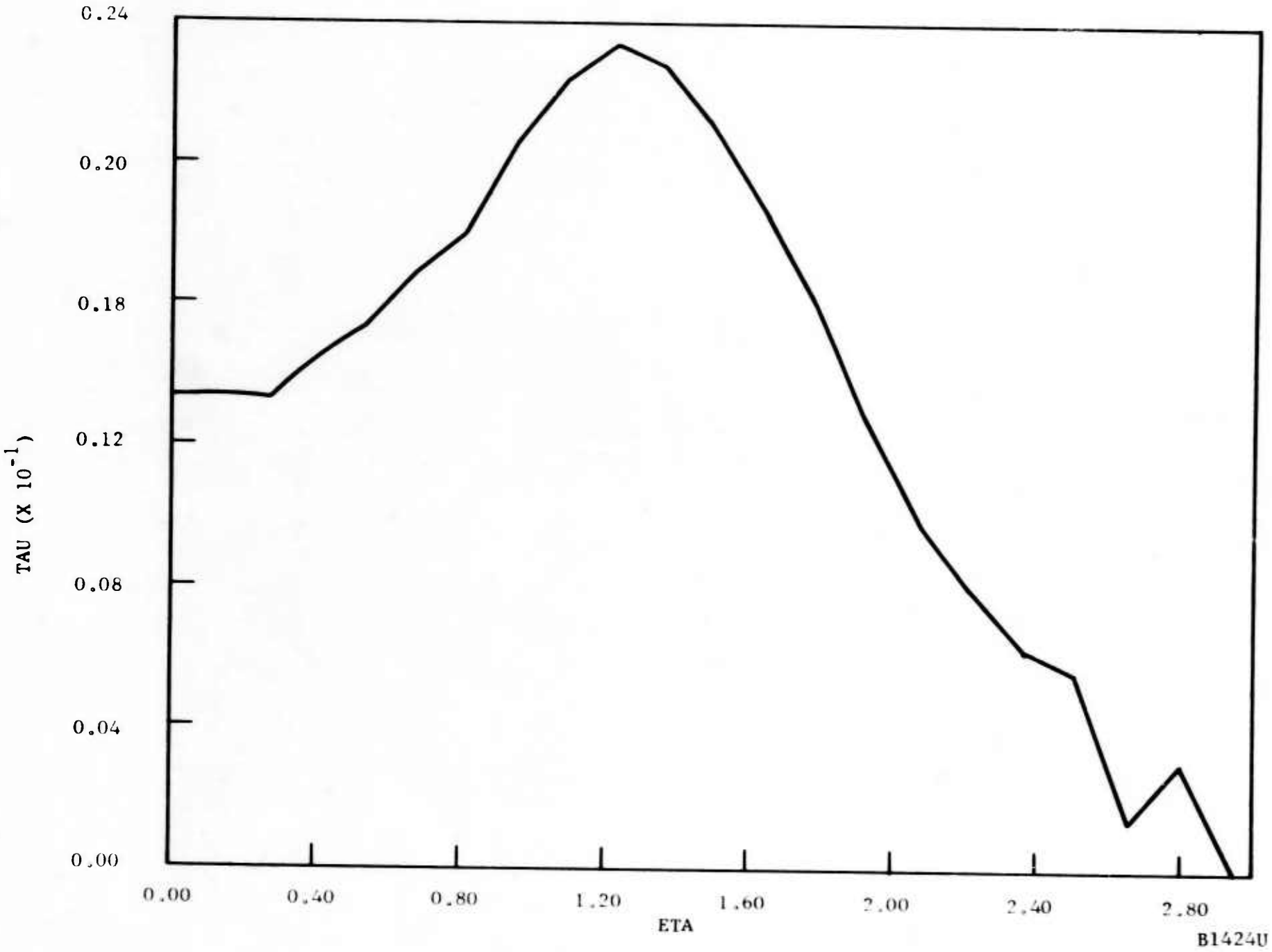

FIGURE 21. TYPICAL LATERAL VARIATION OF THE NORMALIZED VELOCITY FLUCTUATION.

is also the greatest. However, the mean-flow experiments described in Reference 1 indicate that the region of maximum shear lies nearer the point η - 0.85. At this stage the conclusion is, therefore, that turbulence production alone cannot account for the maximum in $\sqrt{u}/u$.

e. Density (Temperature) Fluctuations. The axis value of the fluctuation $\Delta\rho/\rho$ in the density is shown in Figure 21, while Figure 22 shows a typical lateral distribution. Because of the insensitivity of this type of fluctuation to J, there is no abnormal scatter in this data. It is significant that this fluctuation is higher everywhere than $\Delta u/u$, and this difference will later be explained on the basis of the "Strong Reynolds Analogy" for an adiabatic body.

2.6.4 THE FLUCTUATION SPECTRA

In addition to the resolution of the fluctuations into the different modes (e.g., velocity and temperature), it is necessary to carry out a spectral analysis for each mode separately. This analysis is done by the WEB-VII computer program, which supplies additional information for each point in the wake such as the longitudinal integral scales of velocity and temperature. These computations are not completed as yet. In what follows, the analysis of spectra is performed (from the WEB-IV output) on the modally unresolved hot-wire output.

Figure 23 compares restored spectra of the signal at three different positions along the wake. The absolute level of these spectra is irrelevant at this point, but the other features shown are significant beyond the context of the present experiment.

First, observe the intense peak (energy concentration) for the spectra at 168 and 670 diameters behind the model. This peak is quite unnatural for longitudinal (i.e., one-dimensional) spectra of turbulence, which should in fact, resemble the spectrum shown at 1676 diameters. Secondly, note that the peak frequency decreases with increasing X; finally, the peak intensity also decreases with increasing X. The interpretation of this phenomenon is as follows: The turbulent front is arranged, geometrically, into a weakly-periodic manner so that "waves" of a distinct wavelength are formed by it. To a stationary observer a fixed distance way from the axis this "waviness" appears as periodic in time. If the front was strongly periodic then the periodicity in time (i.e., a peak in the spectrum) would be sharp and intense. In fact, by "weakly" periodic it is meant that the stationary variable representing the front has a random spectrum (probably much like that of turbulence) with a superimposed peak. This is called the "intermittency" spectrum. In reality the hot-wire responds to a superposition of this spectrum and the actual turbulence spectrum, and it is apparent that the peak persists in this superposed phenomenon. This interpretation thus states simply that the peak is due to the intermittency, and thus implies that it should be absent on the wake axis and at its edge, and prominent in between where the intermittency is most intense. Figure 24 shows five typically restored spectra taken at the same X position and wire current. On the axis and at the edge of the wake (Y = 0 and 0.048, respectively) the peak is hardly discernible, but indeed becomes very prominent in the intervening region.

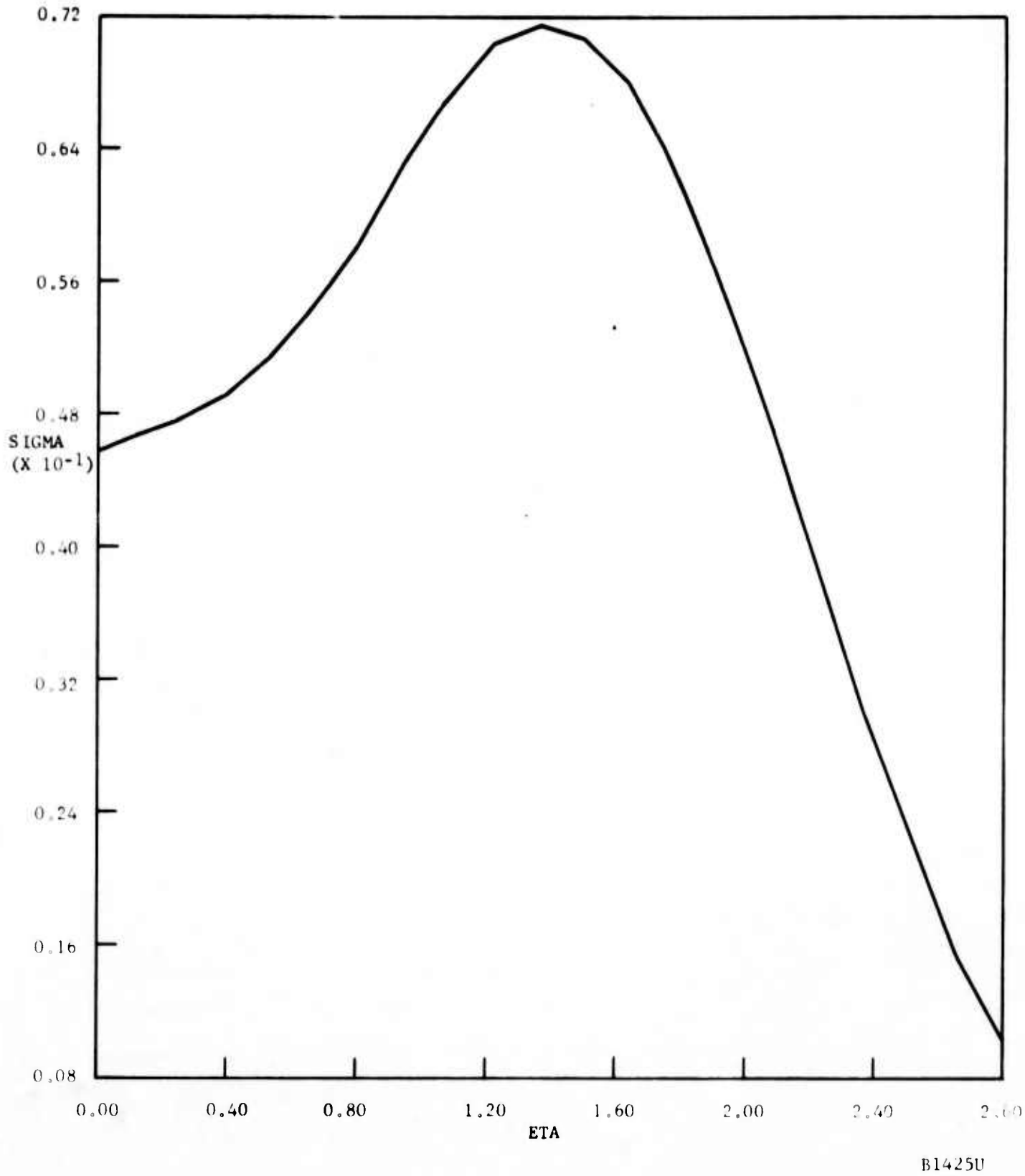

FIGURE 22. TYPICAL LATERAL VARIATION OF THE NORMALIZED DENSITY FLUCTUATION

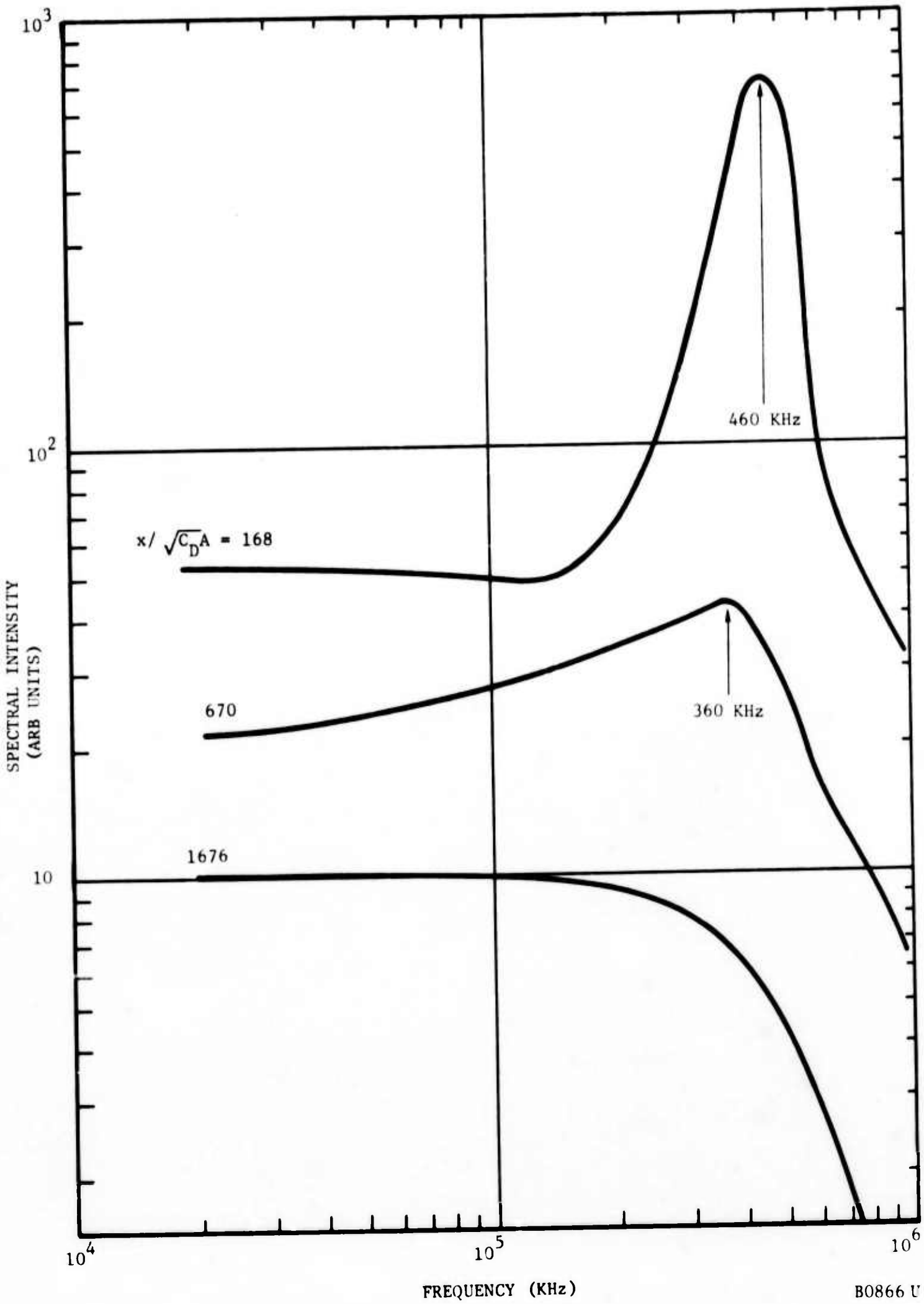

FIGURE 23. EVOLUTION OF THE HOT-WIRE MEAN-SQUARE VOLTAGE OUTPUT SPECTRUM ALONG THE WAKE AXIS

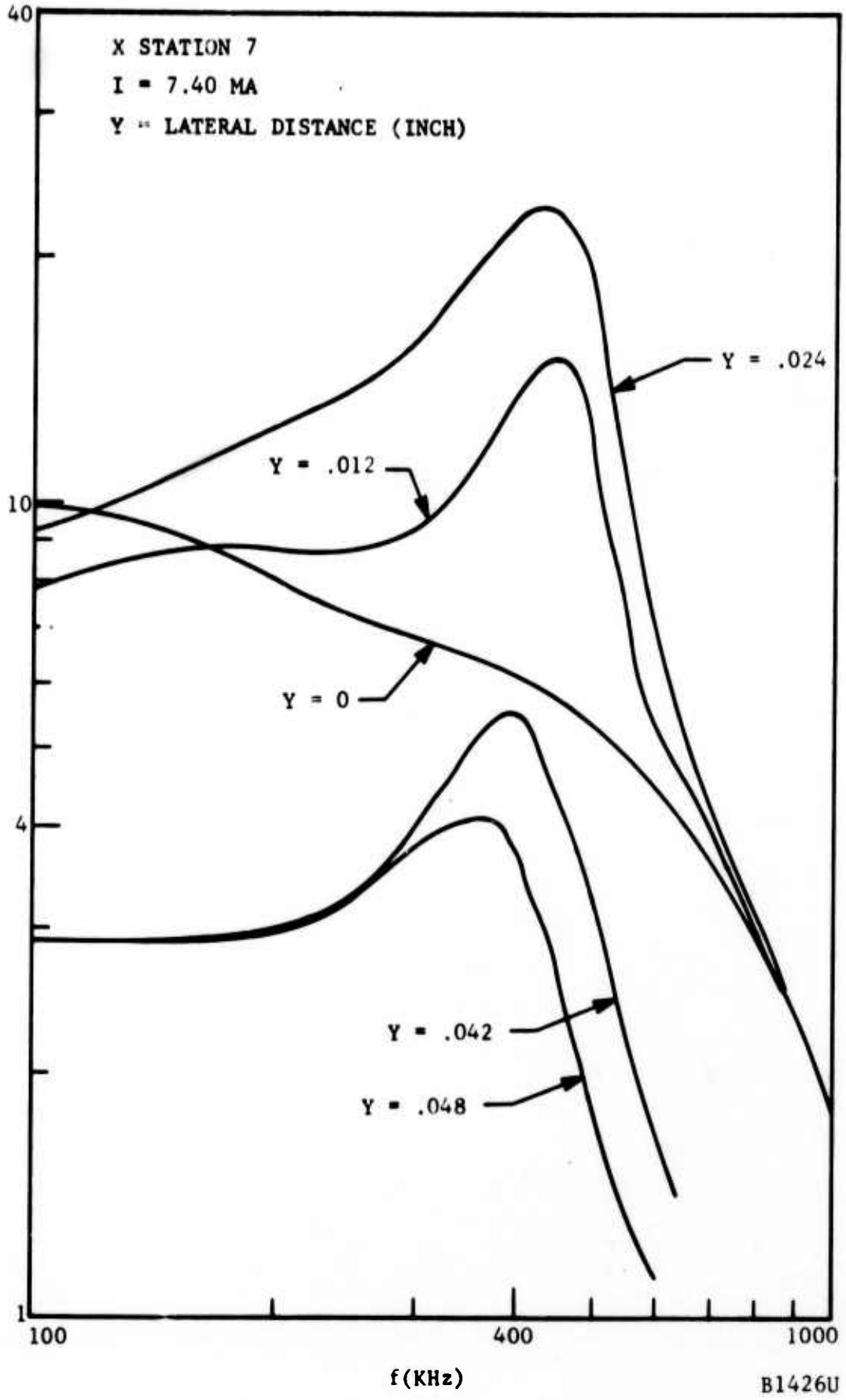

FIGURE 24. TYPICAL LATERAL EVOLUTION OF THE HOT-WIRE MEAN-SQUARE VOLTAGE OUTPUT SPECTRUM

This interpretation was first thought likely in the axisymmetric wake work (see References 4 and 5) and was in fact used to compute the front wavelength, Λ_F, in that experiment, giving $\Lambda_F \simeq 9L \simeq 2d$; here L is the transverse scale and d the approximate wake diameter. The interpretation can be further strengthened if a closely similar Λ_F is found for the present experiment. Using a peak frequency of 360 kHz and a stream velocity of 600 meters/sec, a wavelength Λ_F = 1/6 cm = 0.17 cm is computed. Furthermore, d, as defined above, is twice the distance from the axis to the root-mean-square position of the turbulent front, represented by Y_{FT} and shown versus x on Figure 47, page 91 of Reference 6. At X-Station 7, $Y_{FT}^2 = 0.4 \times 10^{-3}(\text{inch})^2$ and $Y_{FT} = 2 \times 10^{-2}$. Therefore, $d = 2Y_{FT}$ = 0.04 inch = 0.1 cm, so that $\Lambda_F/d = 0.17/0.1 = 1.7$, whereas the axisymmetric wake $\Lambda_F/d = 2$ as noted above. Although exact identity is not expected, it is clear that the ratio of the front wavelength to the wake diameter is nearly independent of geometry, as expected.

2.7 SCALING LAWS AND SIMILARITY

It remains to show how the present turbulence results can be used to derive or support scaling laws which are useful in predicting hypersonic wake properties. In the absence of a theory of turbulence, the present results can be used to test and support the most, if not the only, reasonable empirical scaling laws grouped under the title "Dynamic Equilibrium Hypothesis" (DEH). The DEH emerged from the original work of Townsend (Reference 8); its credentials include a satisfactory demonstration of its applicability to compressible flows by Morkovin (Reference 10) and equally satisfactory prediction of the results of the only detailed compressible wake experiment to date (Reference 5). In the absence of heat transfer or sound waves these scaling law detailed in the latter reference, give the following prediction for the self-preserving compressible wake:

$$\frac{\rho}{\rho(0)} \frac{\Lambda u}{\Lambda u(0)} = f(\eta) \tag{33}$$

$$\frac{\rho(0)}{\rho}^3 \left(\frac{u(0)}{u}\right)^2 \left(\frac{\Lambda \rho}{\Lambda \rho(0)}\right)^2 = f(\eta) \tag{34}$$

$$\frac{\Lambda T}{T} = (\gamma - 1)\, M^2 \frac{\Lambda u}{u} \tag{35}$$

$$r_{\sigma T} = -1 \tag{36}$$

$$\frac{\Lambda u(0)}{u_\infty - u(0)} = \left[g(0) \frac{\rho_\infty}{\rho(0)} \right]^{1/2} \tag{37}$$

$$\frac{\Lambda \rho\ (0)}{\rho_\infty - \rho(0)} = \left[g(0) \frac{\rho(0)}{\rho_\infty} \right]^{1/2} \frac{1 - w}{S} \tag{38}$$

$$\frac{\Delta\rho(0)}{\rho_\infty - \rho(0)} \quad \frac{u_\infty - u(0)}{\Delta u(0)} = \frac{(1-r)\ (1-w)}{S} \tag{39}$$

If the mean flow properties are know as a function of x, the above formulas can describe fully the fluctuation magnitudes and their variation from point to point in the compressible wake. Since the physical quantities represented by the above symbols are now known (for example r, w, ρ, etc., are known from the mean measurements of Reference 1 and the turbulence properties are presented in Paragraph 2.6) the objective of this paragraph will be to see if these formulas indeed hold. Note that S has been determined to be 0.84 for the present wake, while the DEH gives the value of g(0) as 0.14.

Program WEB-VII gives the measured turbulence properties in a form exactly as shown above. Since the WEB-VII output is not available yet, this comparison will not be made as complete as desired. Thus, in Figures 25 and 26 the lateral distributions shown are in the form $\Delta u/(u\rho-u(0))$ and $\Delta\rho/(\rho_\infty-\rho(0))$ rather than the form suggested by Equations (33) and (34) which account for the compressibility; the rationalization here is that at these far distances $\rho(0)/\rho_\infty$ is very close to unity anyway. Note, first that the scaling with η is poor until about X-Station 11. Beyond that station the data collapse on well-defined curves; lateral similarity is thus obviously attained both for the velocity and the density fluctuation, as predicted by Equations (33) and (34). The shape of the correlating curves will be discussed later.

The all-important constant g(0) can be checked by plotting $\Delta u(0)/(u_\infty - u(0))$ and $\Delta\rho(0)/(\rho_\infty - \rho(0))$ versus x. In Figure 27 the asymptotic values of these normalized fluctuations, drawn in solid lines, are obtained from Equations (37) and (38) in the limit $\rho_\infty = \rho(0)$ and $\omega = 0$, that is, in the far wake:

$$\lim_{x\to\infty} \frac{\Delta u(0)}{u_\infty - u(0)} = \sqrt{g(0)} = \sqrt{0.14} = 0.38 \tag{40}$$

$$\lim_{x\to\infty} \frac{\Delta\rho(0)}{\rho_\infty - \rho(0)} = \frac{\sqrt{g(0)}}{S} = \frac{0.375}{0.84} = 0.45 \tag{41}$$

The data show remarkably good agreement with the value of g(0) used above, the slight deviation implying a g(0) a little greater than 0.14. In this figure three distinct regions are distinguished: Up to about X-Station 3 the transition process is still continuing; from there to about X-Station 8 for the velocity and X-Station 12 for the density the fluctuations deviate considerably from the DEH-predicted asymptotic value, which sets in beyond those stations. The disparity in the approach to equilibrium between the two fluctuation modes is, of course, predictable because of the generally slower decay of temperature in high-speed wakes. What is interesting is that from work done earlier the initial (relaxation) values of $\Delta u(0)/(u_\infty - u(0))$ were predicted to be higher than the asymptotic value, as indeed verified in Figure 27 but the density fluctuations, predicted to be small until they reach the asymptote, actually overshoot the latter, reaching a level of about 0.75 at about X-Station 6.

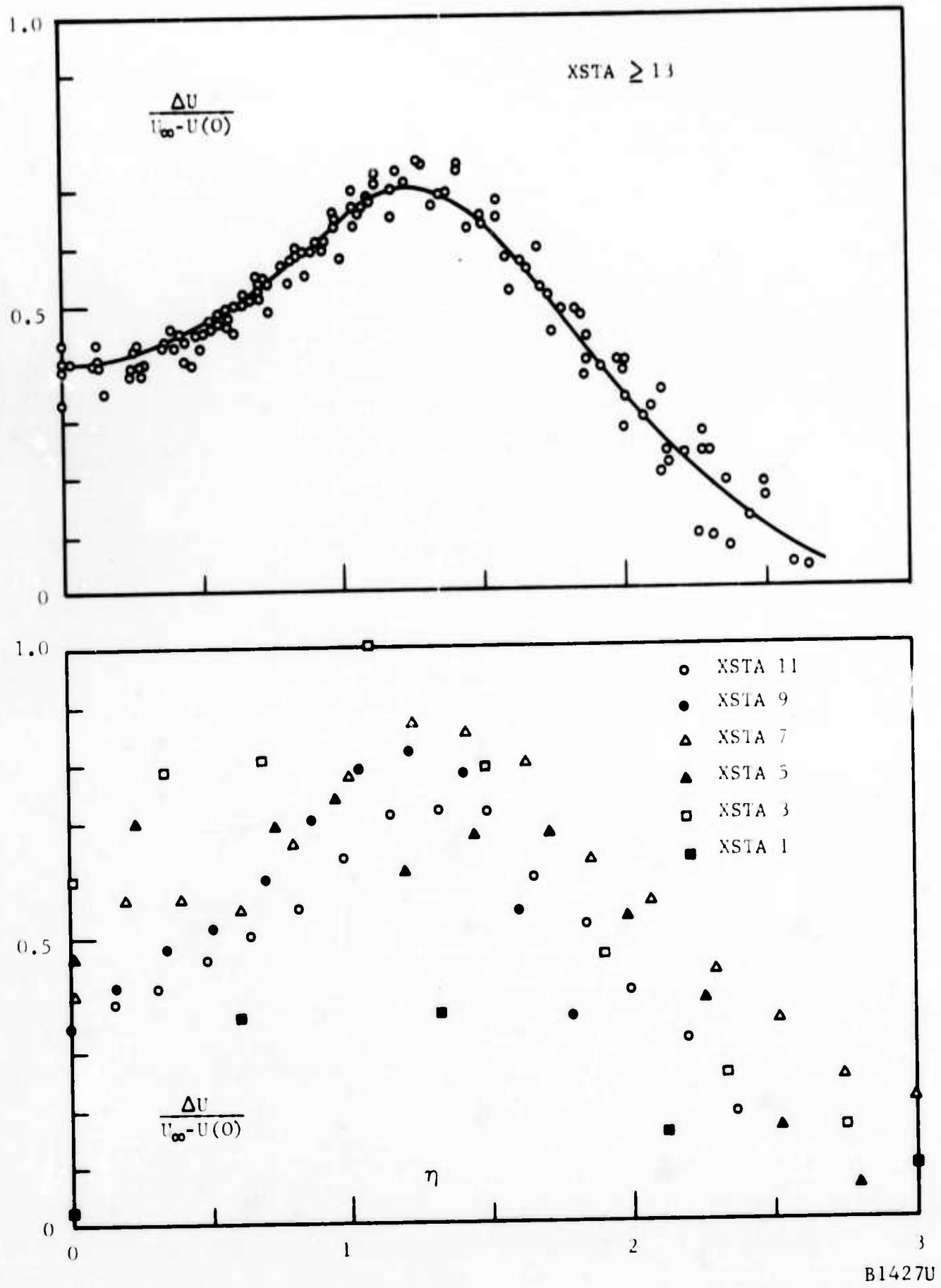

FIGURE 25. LATERAL VARIATION OF THE AXIAL VELOCITY FLUCTUATIONS NORMALIZED WITH THE LOCAL WAKE VELOCITY DEFICIT. ABOVE: SELF-PRESERVING FLUCTUATIONS (FAR WAKE). BELOW: NEAR (RELAXING) WAKE.

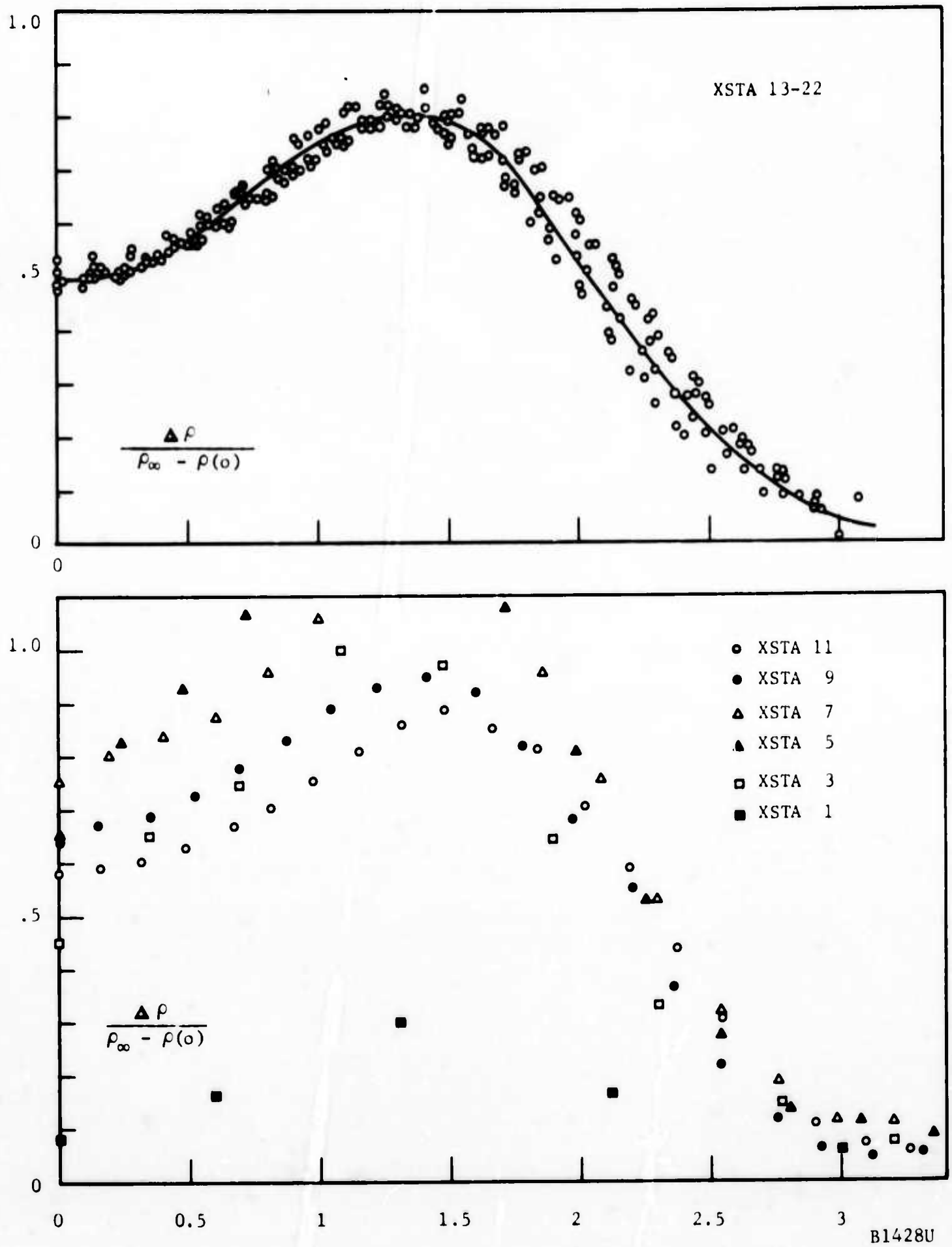

FIGURE 26. LATERAL VARIATION OF THE DENSITY FLUCTUATIONS NORMALIZED WITH THE LOCAL WAKE DENSITY DEFICIT. ABOVE: SELF-PRESERVING FLUCTUATIONS (FAR WAKE). BELOW: NEAR (RELAXING) WAKE.

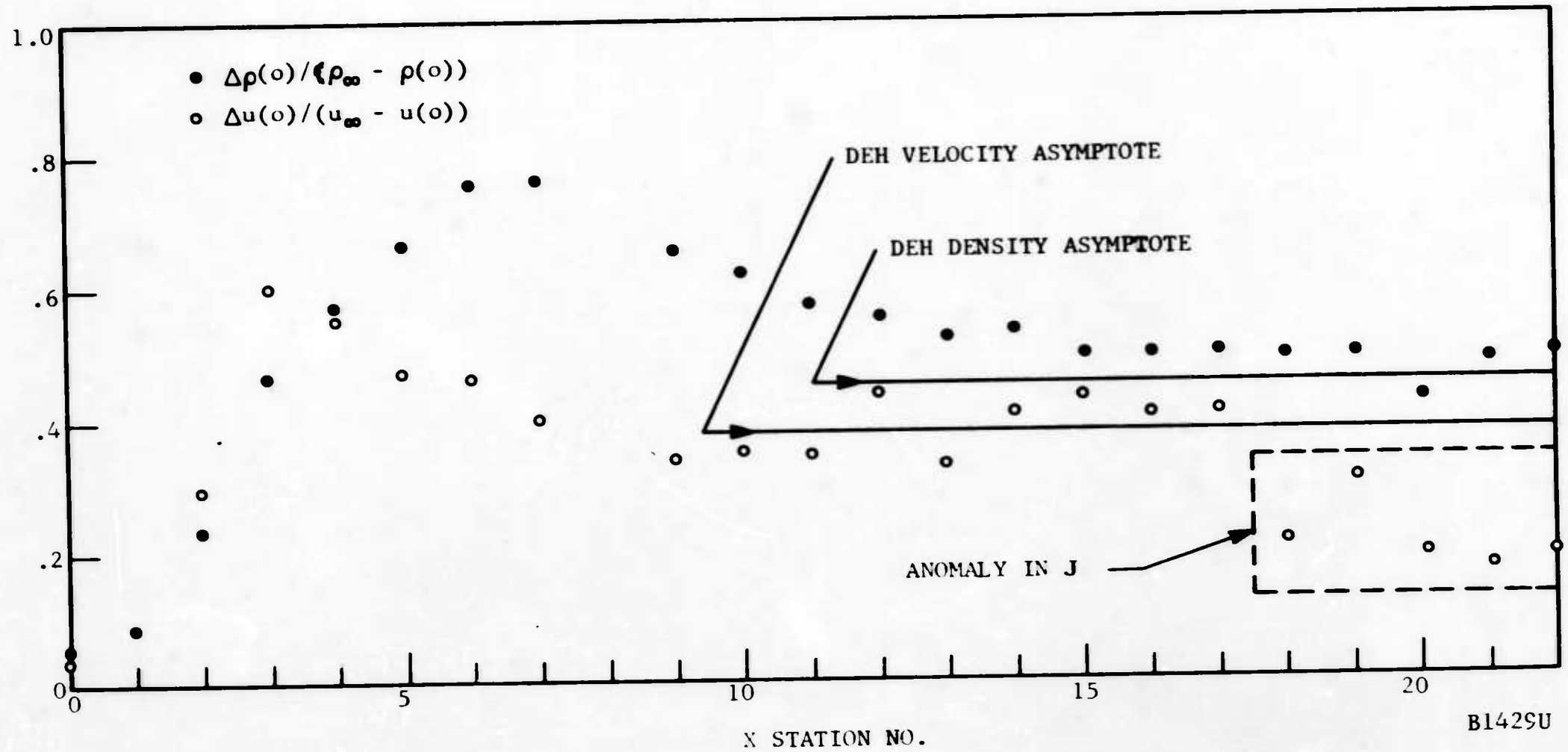

FIGURE 27. AXIAL VARIATION OF THE AXIS VELOCITY AND DENSITY FLUCTUATIONS SCALED TO THE LOCAL WAKE DEFICITS

From a dimensional standpoint, the velocity "scale" at any distance behind the body is, of course, the local difference $u_\infty - u(0)$; that is why Equation (37) asymtotically connects Λu and $u_\infty - u(0)$. The question arises whether Λu can ever exceed $u_\infty - u(0)$. In Figure 28, the maximum values of the fluctuations $\Lambda u/u_\infty - u(0)$ and $\Lambda\rho/(\rho_\infty - \rho(0))$ are plotted as obtained from the off-axis maxima of Figures 25 and 26. Asymptotically these reach values of 0.70 and 0.80, respectively. In the relaxing region, however, $\Lambda u/(u_\infty - u(0))$ reaches a value equal to one, and near X-Station 6 the density fluctuations reach 125 percent of the mean density difference across the wake. The precise physical rationale allowing such large fluctuations is not clear.

Since g(0) controls both the velocity and the density fluctuations far from the body, a simple check of the DEH is suggested by Equation (39). Figure 29 plots the left-hand-side of this equation as measured directly, and independently the right-hand-side (by a solid curve) with the w, r, and S supplied from the mean measurements. As expected, the agreement is poor in the relaxing portion of the wake, but beyond 900 diameters the data are close to the expected behavior. In fact the data beyond 1400 diameters, if corrected for the difficulties met in computing J, continue in very good agreement with the "theoretical" prediction.

The relative magnitude of density (temperature) and velocity fluctuations with respect to the stationary hot-wire, are given by Equation (39). Figure 30 shows that the expectations are met (especially with data corrected for J as discussed above) in the self-preserving wake. In the latter, in fact, the Strong Reynolds Analogy is closely followed by the data in the lateral coordinate except very near the wake edge. Here the temperature fluctuations are uncommonly large, as was also observed in the axisymmetric wake (Figure 35, page 78, Reference 5). This is explained as occurring due to intermittency, implying that the temperature "jumps" across the turbulent front are much larger than the corresponding velocity jumps.

It should be added that the Dynamic Equilibrium Hypothesis predicts that for adiabatic wakes $\Lambda T_0 = 0$ and $r_{\sigma T} = -1$. Both of these predictions, and especially the latter, are fully borne out in the present experiment, as shown by Figures 15 and 30. The result is that, once the velocity fluctuation in an adiabatic wake is known, the temperature (density) fluctuations can be predicted. In fact, the ratio of density to velocity fluctuations is a simple function of the Mach number. This is well borne out in Figures 31 and 32.

A final point concerns the rather high velocity fluctuations measured in the wake. Figure 33 compares these measurements with data taken by Townsend (Reference 8) at low speeds. It should be noted that Townsend's mean-velocity measurements are correlated in the following empirical formula (Reference 8, page 162):

$$\tilde{u} = \frac{u_\infty - u}{u_\infty - u(0)} = e^{-14.4a^2}\left[1 + \frac{1}{3}\left(\frac{a}{.35}\right)\right]^4 \qquad (42)$$

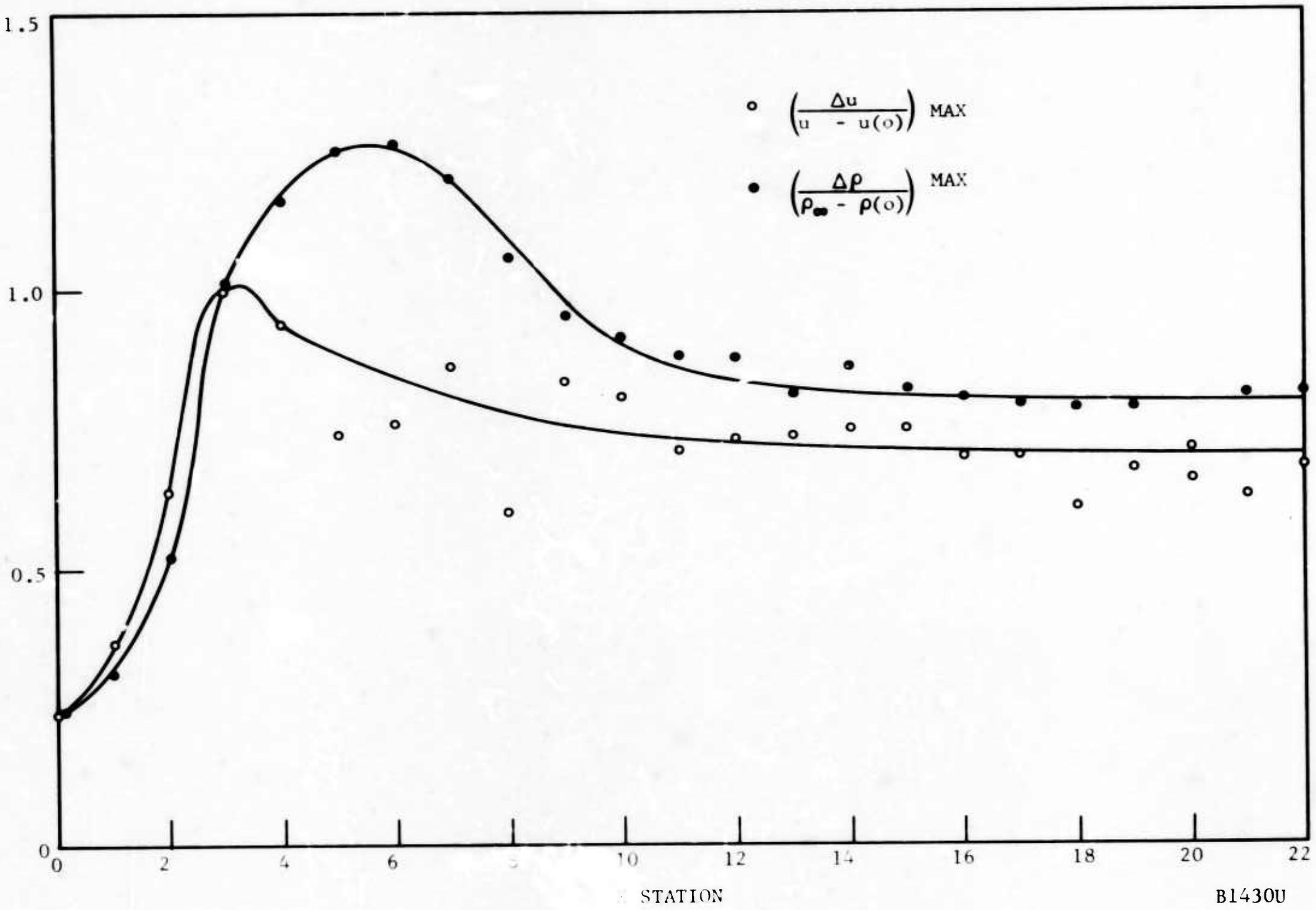

FIGURE 28. AXIAL DEVELOPMENT OF THE MAXIMUM (AT EACH X) OF THE VELOCITY AND DENSITY FLUCTUATIONS SCALED TO THE LOCAL WAKE DEFICITS

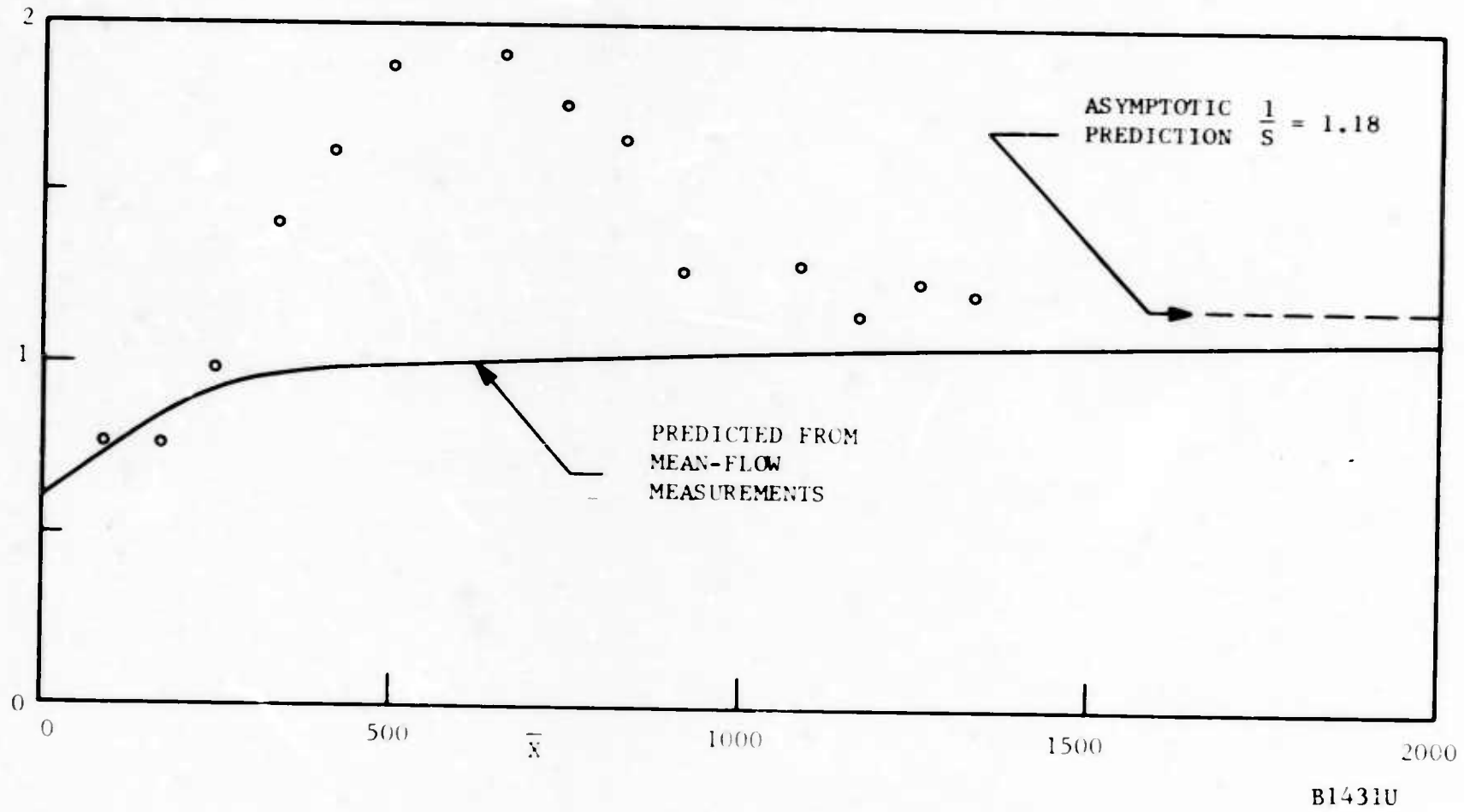

FIGURE 29. AXIAL VARIATION OF THE RATIO OF THE DENSITY TO THE VELOCITY FLUCTUATIONS COMPARED TO PREDICTIONS OF THE DYNAMIC EQUILIBRIUM HYPOTHESIS

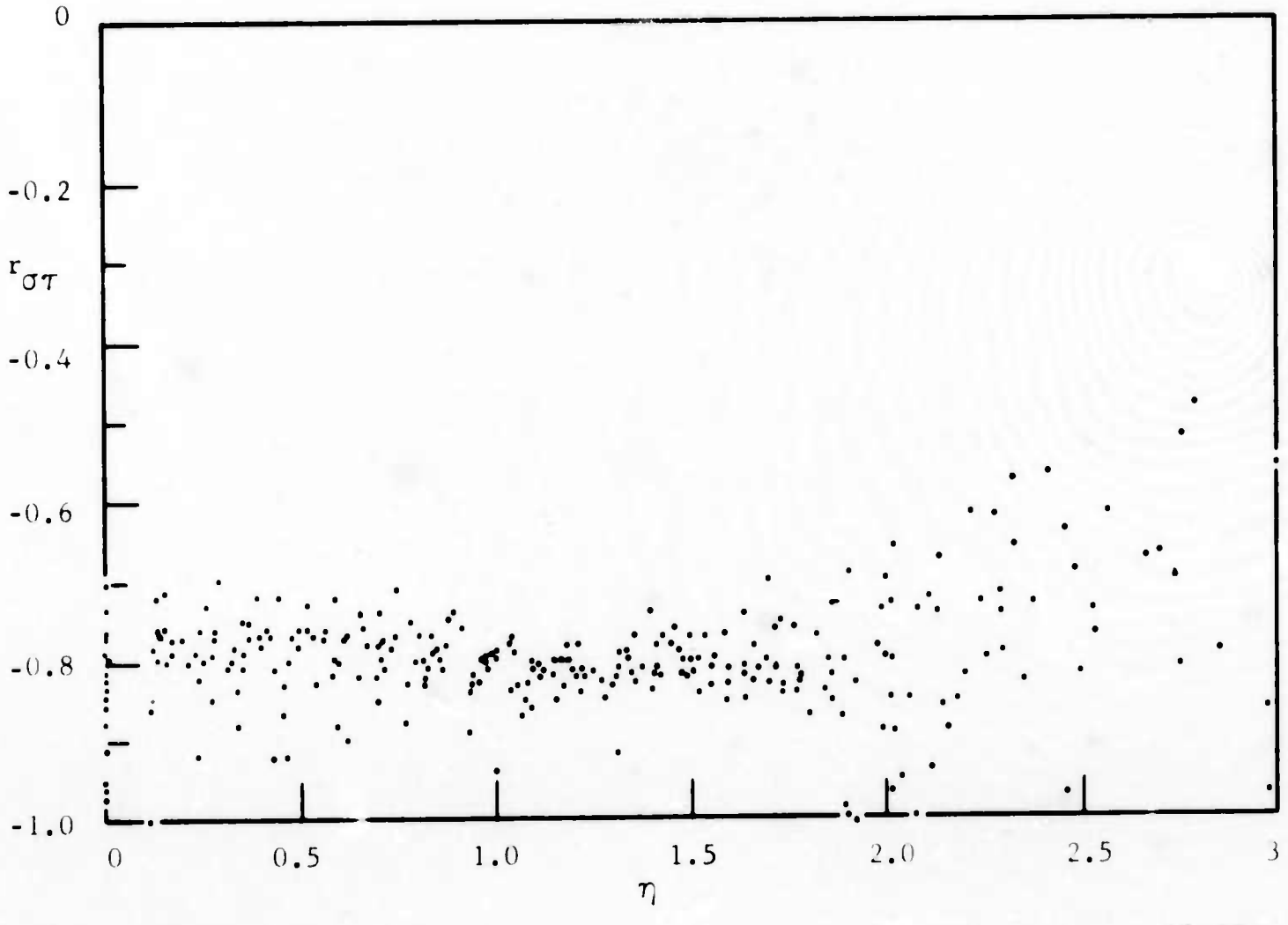

B1432U

FIGURE 30. LATERAL VARIATIONS OF THE VELOCITY-TEMPERATURE CROSS-CORRELATION COEFFICIENT

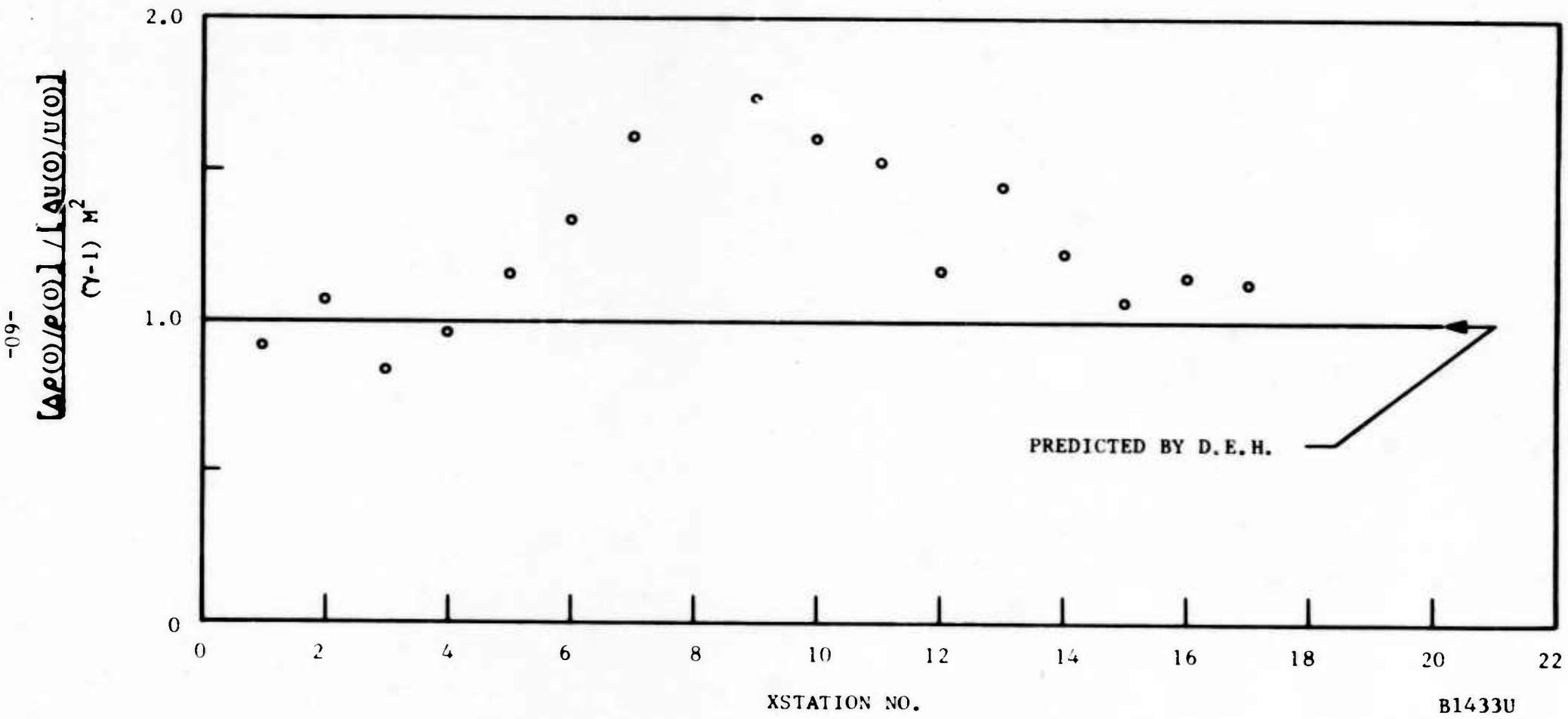

FIGURE 31. TEST OF THE STRONG REYNOLDS ANALOGY ALONG THE WAKE AXIS

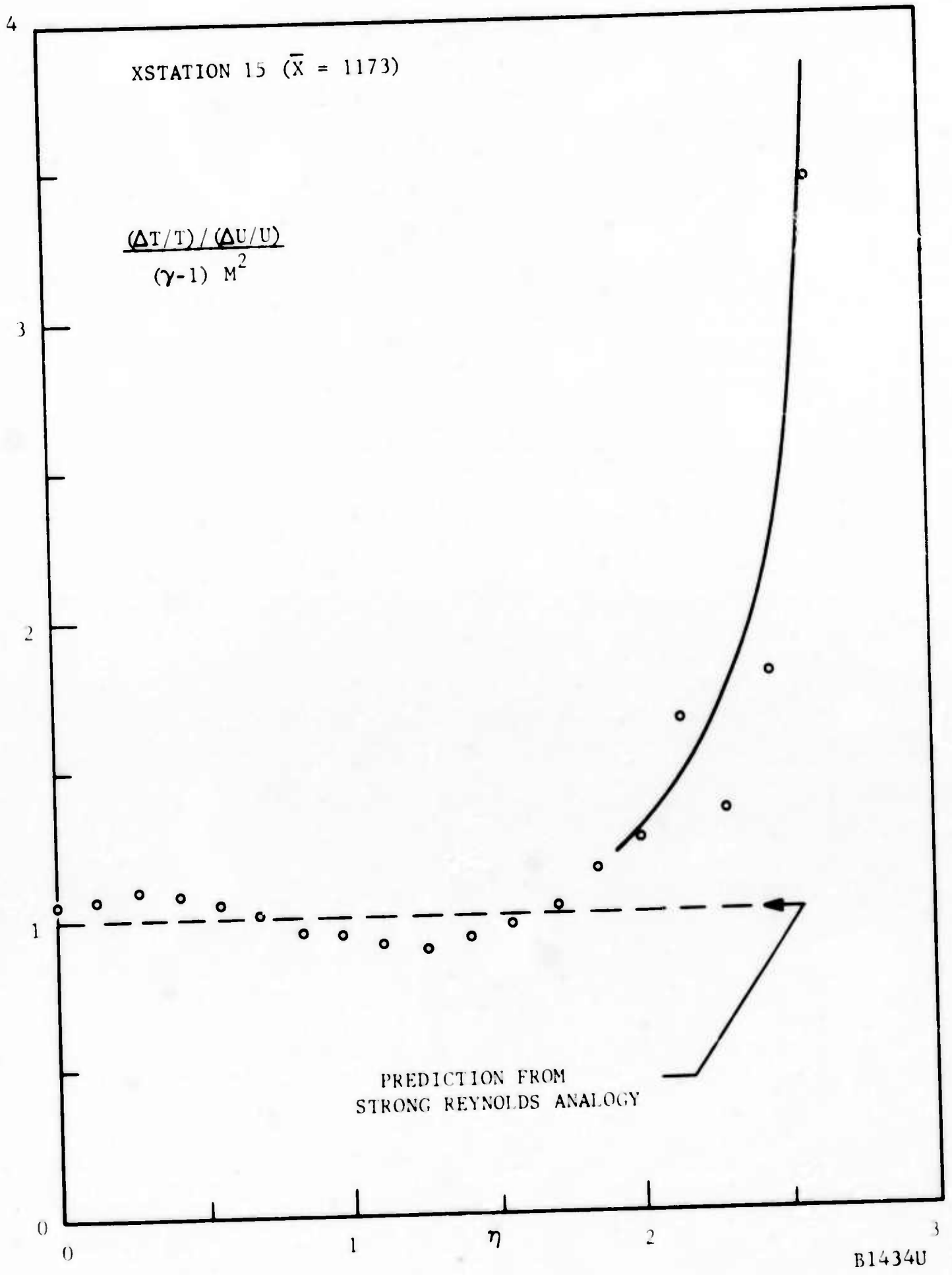

FIGURE 32. TEST OF THE STRONG REYNOLDS ANALOGY IN THE LATERAL DIRECTION AT CONSTANT X

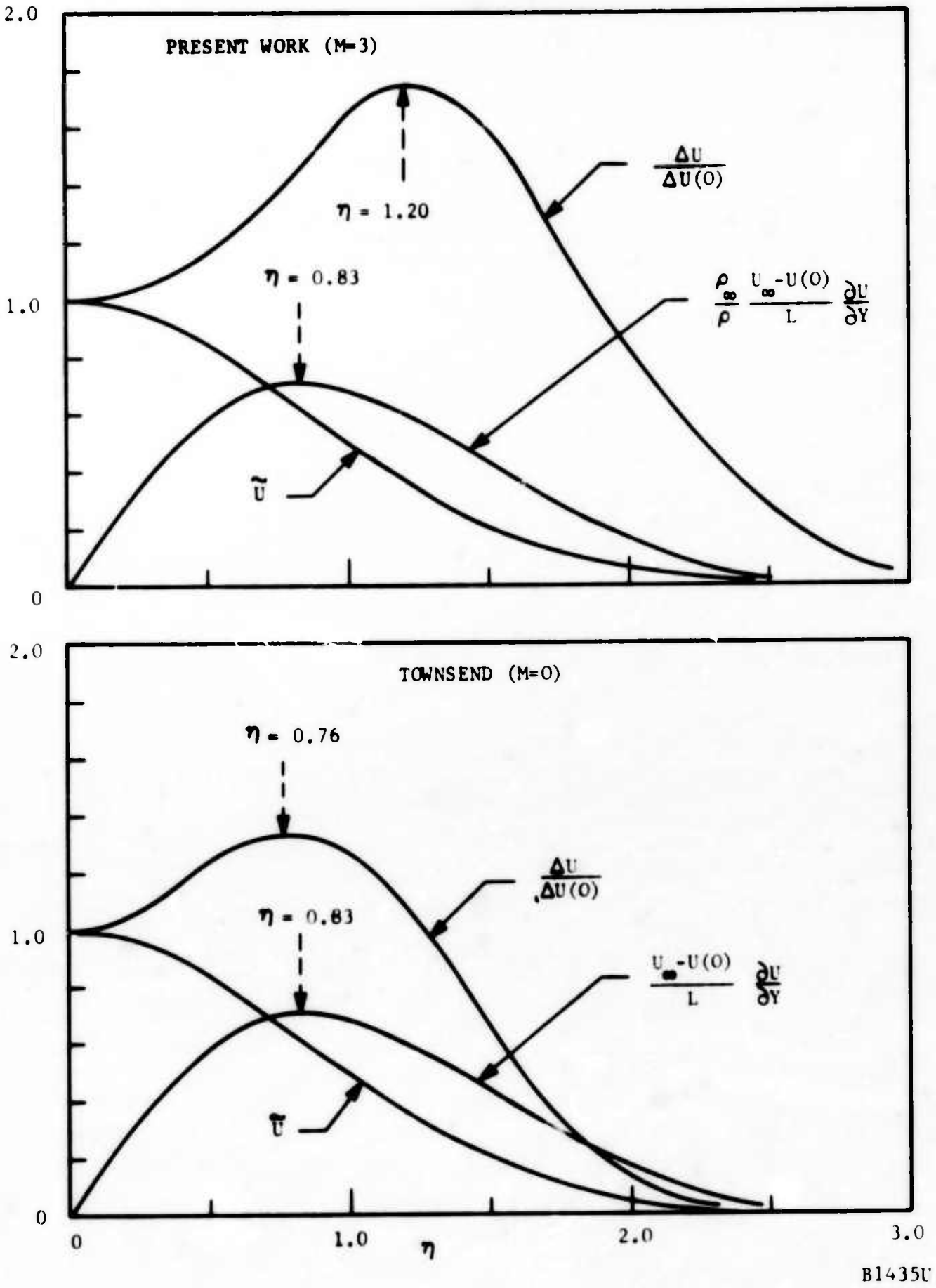

FIGURE 33. VELOCITY, SHEAR, AND VELOCITY FLUCTUATION PROFILES (ABOVE) COMPARED WITH SIMILAR PROPERTIES OF LOW-SPEED WAKES (BELOW)

where

$$a \equiv \frac{Y}{\left[(x-x_o)\ d\right]^{1/2}} \tag{43}$$

and d is the cylinder diameter. This lateral coordinate a can be related to the η used herein since for cylinder the drag coefficient $C_D = 1$ and since, in the present experiment

$$Y \simeq \tilde{Y}$$

$$L = \sqrt{\frac{C_D h}{4\omega}}$$

$$\omega = \frac{1.14}{\left[(x-x_o)/\sqrt{C_D h}\right]^{1/2}}$$

Since in Townsend's case one obtains

$$\left[C_D h\right]^{1/2} = [h]^{1/2} = \sqrt{d}$$

The result becomes

$$L = \frac{\left[(x - x_o)d\right]^{1/2}}{4.56} \tag{44}$$

and

$$a = \frac{Y}{[(x-x_o)d]^{1/2}} = \frac{Y}{4.56L} \simeq \frac{\tilde{Y}}{4.56L} = \frac{\eta}{4.56} \tag{45}$$

With this transformation from a to η, Equation (42) becomes

$$\tilde{u} = e^{-0.69\eta^2}\ (1 + 0.051\eta^4 \tag{46}$$

which is in good agreement with the mean-velocity distribution found in the present work:

$$\tilde{u} = e^{-0.69\eta^2}$$

In Figure 33 the u curves are thus identical, as are the corresponding distribution of shear $\partial u/\partial Y$. The significance of the latter is that its maximum should correspond with the maximum of the fluctuations. This is verified for Townsend's results but not obtained in the present experiment. Another unexpected occurrence is that the fluctuation maximum, reaching 135 percent the axis value in the low-speed wake reaches above 170 percent in the present wake. The net result is that the fluctuation thickness of

the present wake is considerably thicker than at low speeds. No explanation of this phenomenon can be offered at this time.

2.8 CONCLUSIONS

The following conclusions can be drawn from the present work on two-dimensional wake turbulence:

(1) General Conclusion: The data obtained support firmly the empirical body of predictions known as the Dynamic Equilibrium Hypothesis.

(2) The axis values of temperature and longitudinal velocity fluctuations reach asymptotically the same percentage of the mean axis values as encountered in previous experiments, including those at low speeds.

(3) The wake total temperature fluctuations are relatively insignificant when no heat is exchanged between the flow and the body.

(4) The local velocity in the wake is almost perfectly anti-correlated with the local temperature; there is no correlation between total temperature and mass-flux fluctuations.

(5) For adiabatic wakes, the temperature (density) fluctuations can be obtained, by the Strong Reynolds Analogy, from a knowledge of the distribution of mean Mach number and velocity fluctuations.

(6) Near the wake edge the Reynolds Analogy fails; it is conjectured that the front corrugations of the wake can be thought of as "jumps" in the mean properties, especially the temperature.

(7) Similarity in the distribution of fluctuation occurs long after the mean properties themselves become self-similar.

(8) By comparing almost all measured mean and turbulent properties with their low-speed counterparts, it is shown that the proper scaling length is not the body diameter but rather the appropriate momentum thickness of the wake.

(9) A notable exception shows in the lateral distribution of velocity fluctuations; the maximum of these occurs farther from the axis and is higher than its counterpart at low speeds.

SECTION III

INTERMITTENCY OF THE TWO-DIMENSIONAL COMPRESSIBLE WAKE

3.1 PURPOSE

In addition to the mean-flow investiagation of the two-dimensional wake (Reference 1) and of its turbulence field (Section II), its intermittency characteristics have also been measured and will be reported in this Section.

The intermittent flow plays an extremely important role in the characteristics of the hypersonic wake as viewed by a ground observer. In the work with the axisymmetric compressible wake (Reference 4) the intermittency measurements gave the rms location $\bar{Y}$ of the turbulent front and its standard deviation σ. These quantities were found to bear numerically the same relationship to the transverse scale L as in the two-dimensional wake of Townsend's (see Reference 5 , page 42). This important finding, implying that neither the geometry of the body nor compressibility affects $\bar{Y}/L$ and σ/L, would so greatly simplify hypersonic wake calculations that it merited additional study; hence the intermittency measurements with the present two-dimensional wake were made.

3.2 TECHNIQUE AND PROCEDURE

The technique necessary for this type of measurement is described in great detail in Reference 5. Briefly, the hot-wire anemometer is held at various lateral positions Y and at each X-Station. The heating current of the element is increased to the maximum sensitivity possible and its ac signal is processed through the intermittency meter built especially for such work at Aeronutronic. Through a series of rectifying and clipping actions this instrument distinguishes between the time the wire is immersed in dc turbulence and the time it is not; its output in a fraction of one volt ac then gives the "intermittency factor" $0 < \gamma < 1$ which is the fraction of turbulence immersion time to the total time. In a fully turbulent fluid $\gamma = 1$, whereas whenever the sensor is so far from the axis that it never encounters turbulence, $\gamma = 0$. If $\gamma(Y,x)$ is known then $\bar{Y}(x)$ and $\sigma(x)$ can be calculated by statistical methods (Reference 11, page 10).

In addition to γ, the average wavelength of the front is important. A measurement of the so-called null frequencies, N sec^{-1}, can give this sort of wavelength in the form of statistical scale of the front if the latter is truly random. For the axisymmetric wake and also from work with the jet (Section IV), it appears that although the front is truly random in amplitude it may not be truly random in time and the existence, if any, of its wavelength (rather than the purely statistical scale) became another objectives of this work.

Hot-wire No. 8-2/1 was used for measuring the two-dimensional wake intermittency. Data were taken, beginning at Station 2, for all X-Stations used during the mean and turbulence measurements.

3.3 RESULTS

Figure 34 shows the front lateral radius $\overline{Y}$ and its standard deviation σ, normalized with the transverse scale L, plotted along the wake. It is quite evident that the ratios Y/L and σ/L are constant within the scatter (Note that L increases by a factor of 3 in the range $200 < \bar{x} < 1800$). For $\overline{Y}$/L this constant value is about 1.96, which is only 7 percent lower than the value expected on the basis of the known behavior of wake flows (see Table III, Reference 4). The findings of the WEB experiment are therefore further substantiated.

The value of σ/L however, shown on Figure 34 to be about 0.38, is considerably lower than expected, by a factor of 2 or more. This is shown in another manner on Figure 35, where the lateral distribution of γ is shown for all XSTATIONS. The data are scattered, so much so that a distinction between "near-wake" and "far-wake" behavior is made. What is important, however, is that the region of intermittent activity is much shorter (and the extent of fully turbulent fluid much greater) than Townsend found at low speeds; this means that σ should be also much smaller, as Figure 35 already showed. In the mean-time, the distribution of intermittent activity around $\overline{Y}$ is fairly symmetric; this is also illustrated on Figure 36. That $\overline{Y}$ grows as $x^{1/2}$ is also well illustrated in Figure 37, where the Y corresponds to the maximum of the probability distribution $d\gamma/dY$.

To explain these findings, two alternatives seem likely: (1) there is a substantial difference between this wake and Townsend; (2) there were inadequacies and errors in the experimental method. At this stage, the second alternative appears more likely. Since the corrections applied by computer to compensate for the hot-wire frequency response are applicable to the rms sense only, there is much of the intermittency behavior which the wire does not see. The turbulence caused by the front its, in fact, proportional to $\gamma(1-\gamma)$ and thus is maximum at $\gamma = 1/2$, where $\overline{Y}$ is located. Near the wake axis ($\gamma = 1$) and at the edge ($\gamma = 0$) this turbulence is small and the wire does not sense that it is crossing into and out of the front. Under these circumstances the location of $\overline{Y}$ will be given correctly but σ will be greatly underestimated, as indeed found.

The conclusion then, is as follows: the position $\overline{Y}$ of the turbulent front is found with fair accuracy for WED, but the standard deviation is underestimated due to inadequacies in the technique. Improvements in the hot-wire anemometer, presently under way, will enable a more accurate repetition of this measurement.

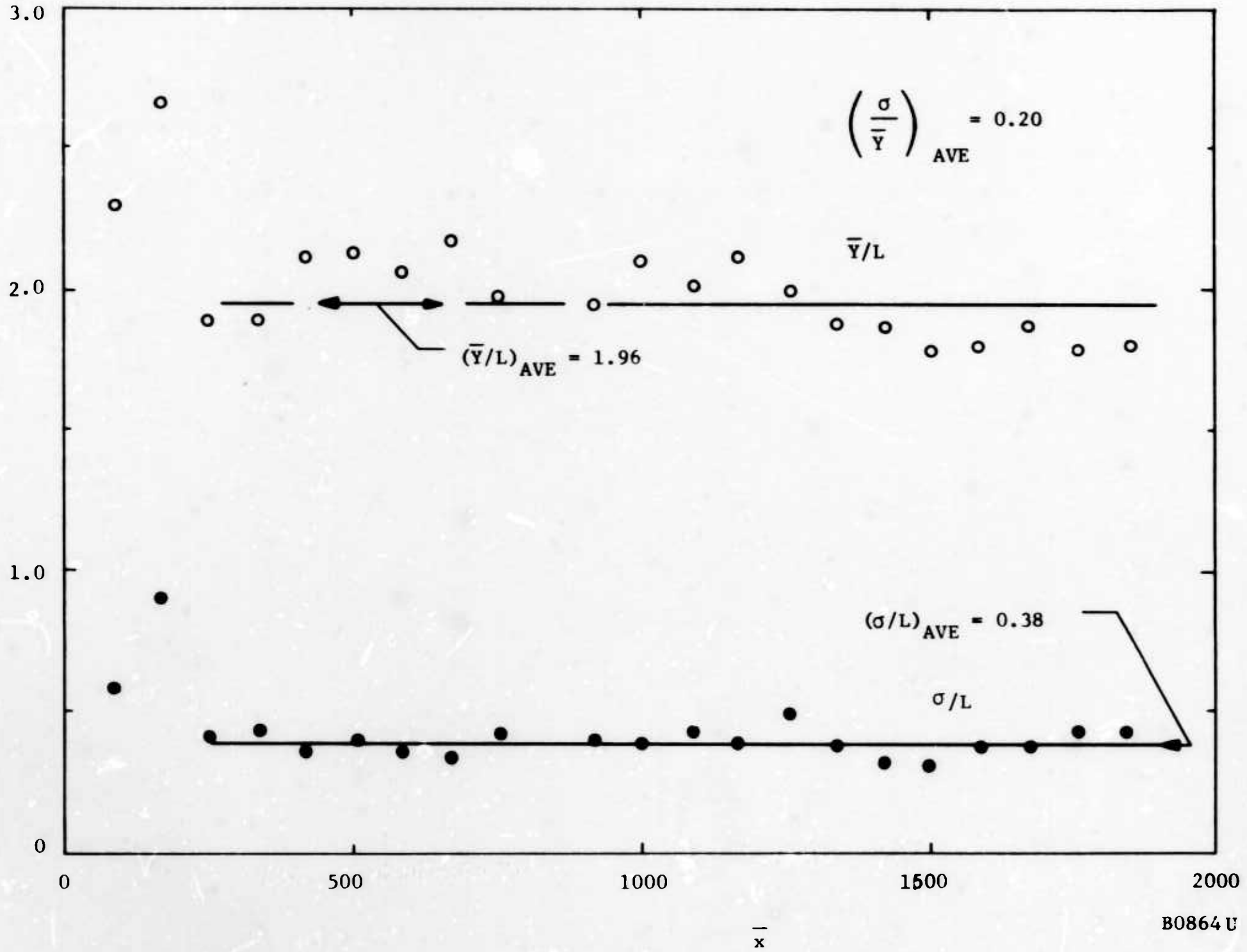

FIGURE 34. AXIAL VARIATIONS OF THE TURBULENT FRONT POSITION AND ITS STANDARD DEVIATION NORMALIZED WITH THE WED TRANSVERSE SCALE

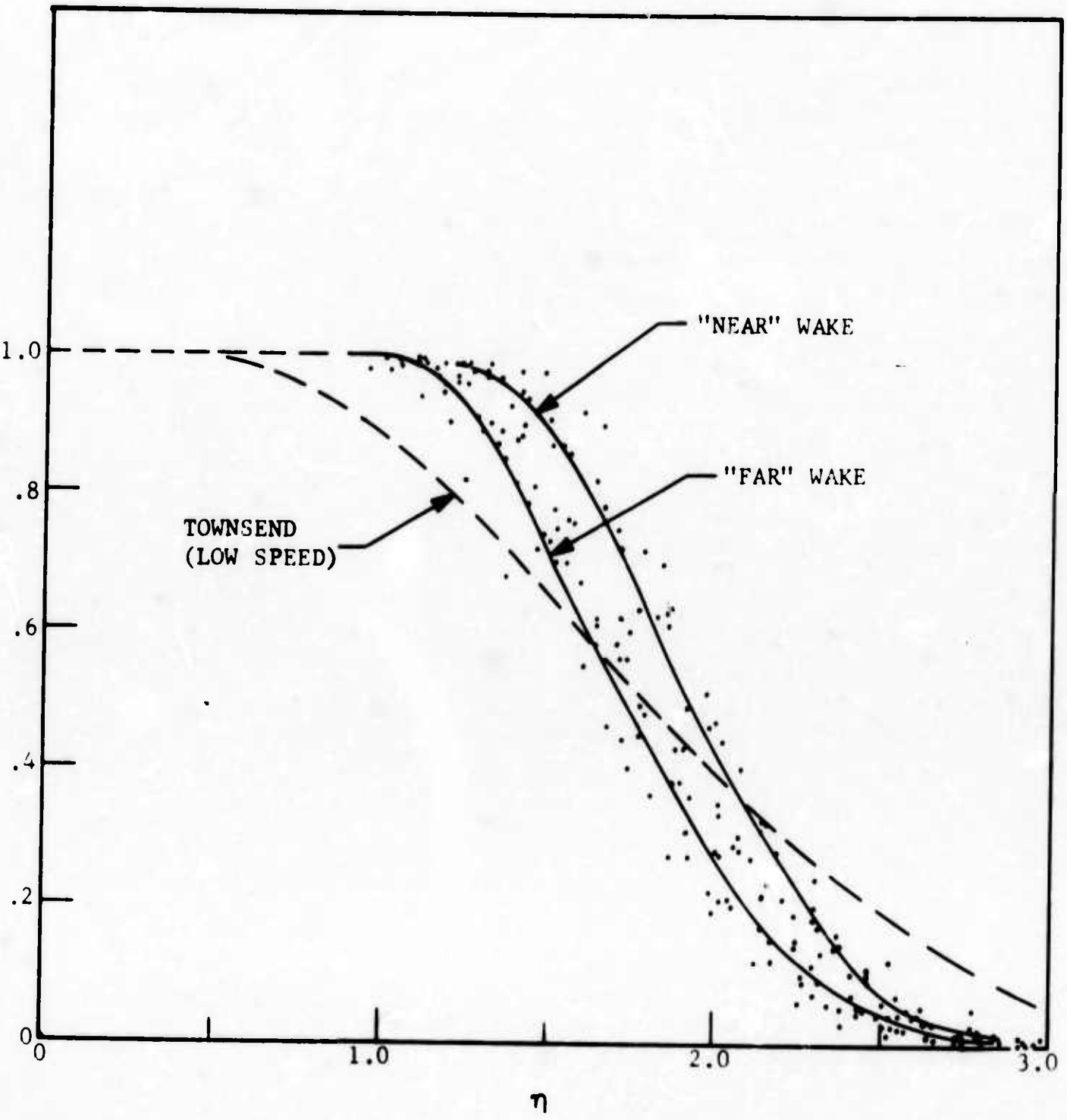

FIGURE 35. DISTRIBUTION OF INTERMITTENCY FACTOR IN WED COMPARED WITH LOW-SPEED RESULTS

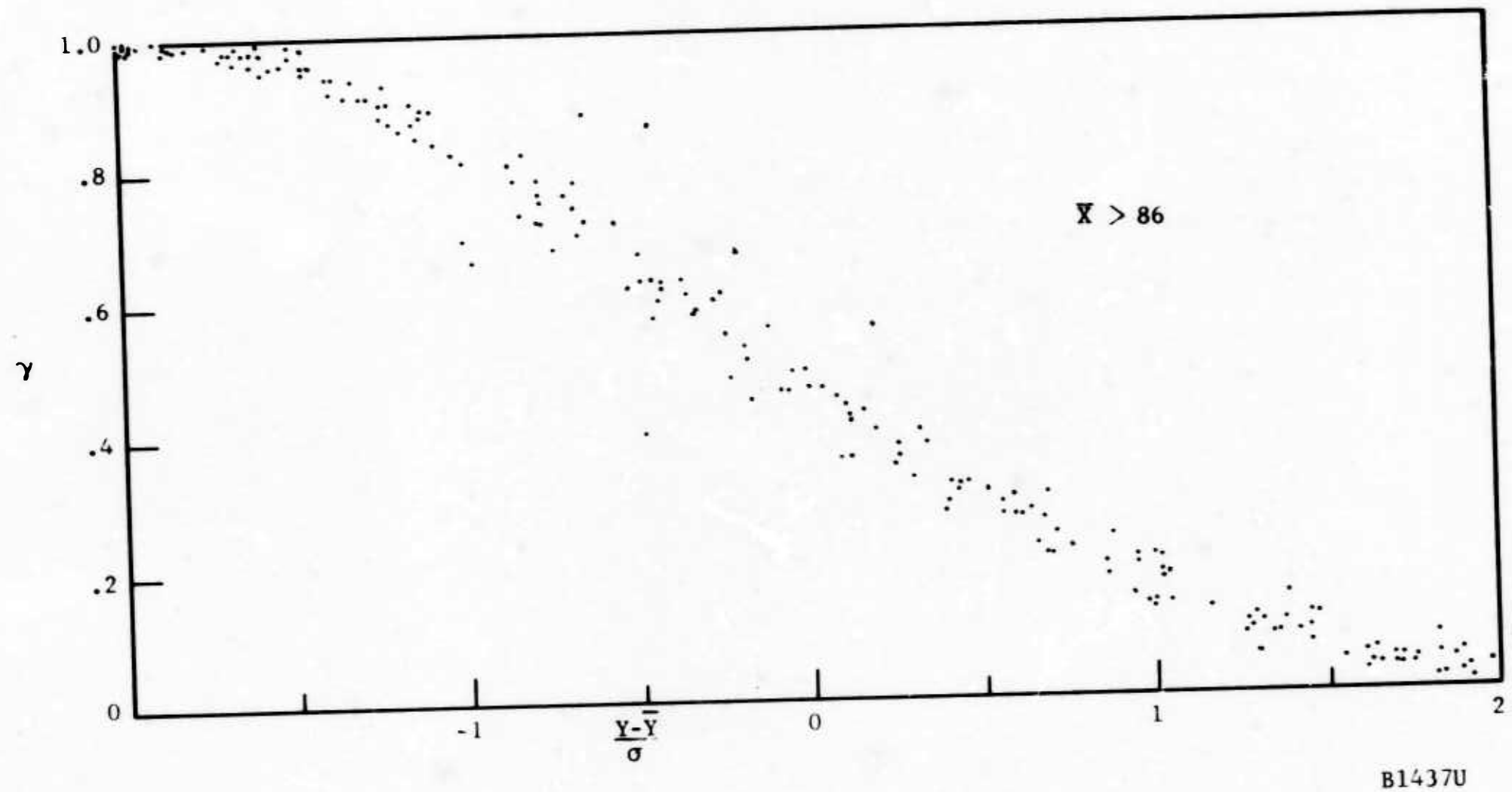

FIGURE 36. DISTRIBUTION OF THE INTERMITTENCY FACTOR ABOUT THE FRONT POSITION, IN UNITS OF THE STANDARD DEVIATION

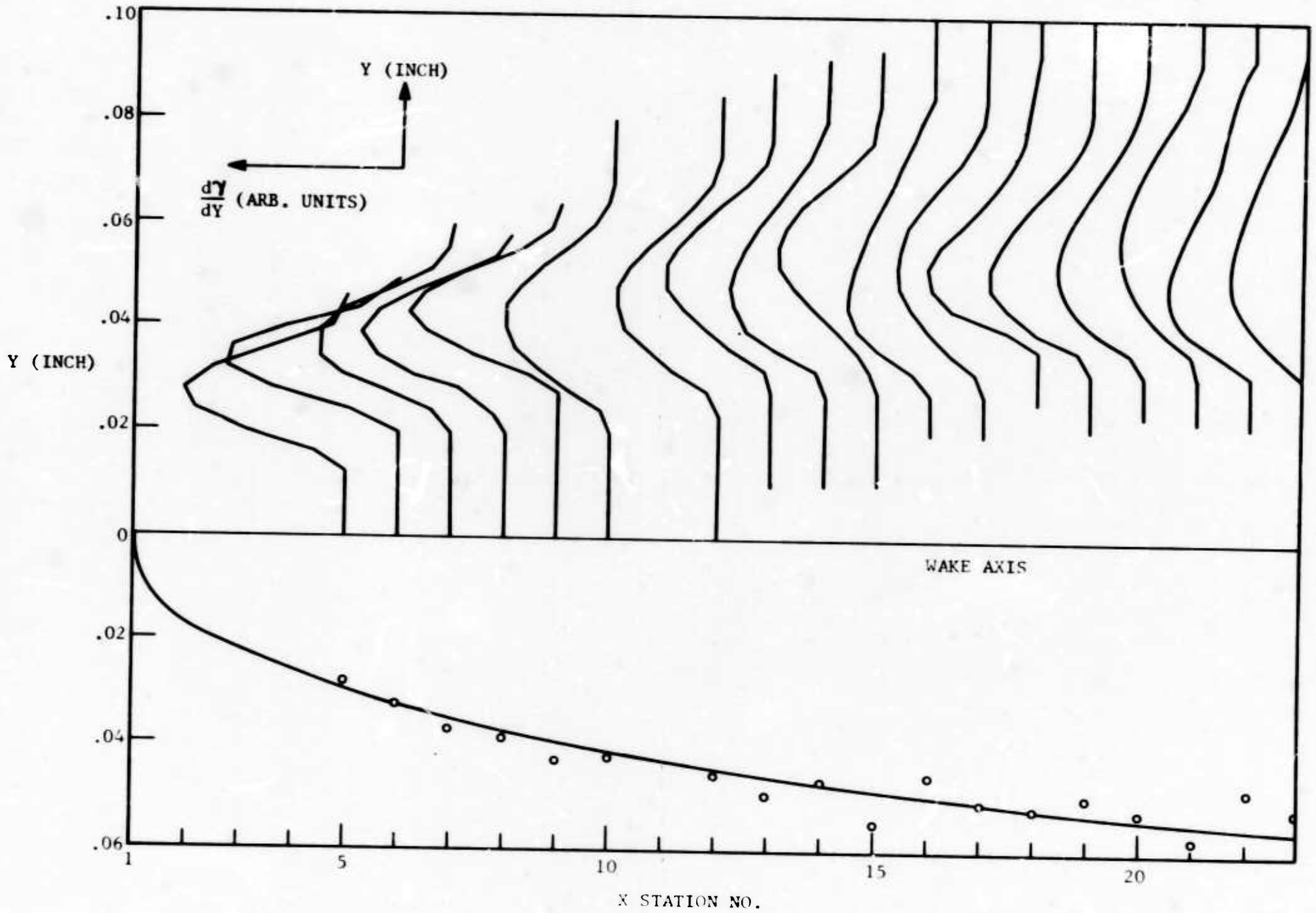

FIGURE 37. LATERAL DISTRIBUTION OF THE FRONT LOCATION PROBABILITY (ABOVE). BELOW, POINTS DENOTE THE MOST PROBABLE FRONT LOCATION.

SECTION IV

TURBULENCE BEHAVIOR OF THE PLASMA JET

4.1 CRITIQUE OF CURRENT TURBULENT PLASMA RESEARCH

The work described so far deals exclusively with perfect-gas wakes devoid of chemical effects, and from which geometric, mechanical, and to some extent thermal features of wake turbulence can be extracted. A second area of effort, described in this Section, deals with free turbulence in which the wake feature is discarded in favor of producing hyperthermal and electronic phenomena. The turbulent plasma jet, such as employed here, is a unique and inexpensive tool for producing such phenomena.

It is fair to say that, in view of the present shortage of and demand for information on electron behavior in turbulent plasmas,* accurate and well-resolved data obtained from laboratory plasmas are significant regardless of their direct applicability to the hypersonic wake problem. Thus, the data already obtained under the present contract (Reference 6) as well as those of Guthart (Reference 12), Granatstein (Reference 13), and Johnson (Reference 14) have for the first time yielded information on the electron density fluctuation intensity and spectra, the correlation scales, etc. Phenomena peculiar to electron benavior (contrasted to ordinary turbulence) have also been observed and are reported in Paragraph 4.3 below.

For these data to be useful for the present purpose, they should be compiled into scaling laws. Presently these scaling laws appear very difficult to obtain theoretically. Even in the case where they are obtainable experimentally in a jet, their simple transposition to the case of the wake is not straightforward. If the consensus of References 6, 12, 13, and 14 was, for example, that the turbulence scale of electrons is a constant fraction of the local jet radius, there is still no assurance that the same relation applies to the wake. Even for totally inert chemistry, as another example, the laws of axial electron density decay assume different forms depending on compressibility (high or low speeds) geometry (two-dimensional or axisymmetric) and type of flow (jet or wake).

It appears that the major usefulness of the jet experiments is to find an empirical connection between the electron turbulence behavior and the turbulence behavior of the overall gas. For instance, if a unique relation between the electron and the temperature integral scales is found, then the application to the wake would only require knowledge of the temperature scales in the wake - knowledge which is now being accumulated under this contract (Sections I through III). It is therefore necessary to measure

---

*A substantial body of knowledge exists on the so-called "plasma turbulence" which, however, involves phenomena on the atomic scale with electric and magnetic fields and is of no consequence here.

the fluid-dynamical turbulence in the jet, as well as the electron turbulence; this has been done in the past year under this contract. The next crucial problem is to fine the one or more variables on which this empirical connection depends. This has already been done (and, in fact, the problem solved) for the two extremes in chemistry: equilibrium flow (References 15 and 16) and frozen flow (Reference 15). For the present, the choice of parameter controlling the connection between gasdynamic and electron fluctuations is unclear, as the discussion of turbulence results will show.

There is one phenomenon which does not depend overtly on the chemistry: that is, turbulence intermittency. Intermittency data in the plasma jet were taken during the previous contract period (Reference 6, pages 176-180). In the present contract period these data were reduced and interpreted and will be discussed first prior to the turbulence results, in the following paragraphs.

4.2 INTERMITTENCY IN THE PLASMA JET

The intermittency properties of wake flows have already been obtained and discussed in Reference 4 for the axisymmetric wake and in Section III of this report for the two-dimensional wake. Scaling laws have been given (Reference 4, page 47) by which the geometric structure of the hypersonic wake front can be predicted. The question now arises: will these scaling laws appear identical to a "temperature" and an "electron" observer? In other words, does the front surface, which is known to abruptly separate gases of dissimilar temperature also separate the electron-rich from the electron-poor gas?

4.2.1 PROCEDURE

In the present experiment the front properties were measured with the hot-wire anemometer and the Langmuir probe. The signal from the hot-wire amplifier (or the ac amplifier connected across the load of the Langmuir probe) was fed to an intermittency circuit; this circuit, described in Reference 4 is not unlike similar devices used by Bradbury (Reference 17) and others, and supplied the intermittency factor as a fraction of one volt dc. The factor γ was recorded at each of about 20 radial positions Y at each x. The rms front position $\overline{Y}$ and its standard deviation σ were then obtained from the usual formulas:

$$\overline{Y} \equiv \int_0^\infty Y \frac{d\gamma}{dY}\, dY \tag{47}$$

$$\sigma \equiv \left[\int_0^\infty (Y-\overline{Y})^2 \frac{d\gamma}{dY}\, d(Y-\overline{Y}) \right]^{1/2} \tag{48}$$

In these formulas computational convenience requires that γ is expressed as a function of Y. This was done by polynomial-fitting the experimental points with the computer.

In addition to $\bar{Y}$ and σ the autocorrelation scale of the front is of some interest. If the front behaves like a stationary random variable it is possible to find this scale from a measurement of the so-called null-crossings (or null frequencies) of the front, that is by the frequency $N_o \equiv N(\bar{Y})$ at which a sensor, located at $Y = \bar{Y}$, enters the front. To this end the distribution of null frequencies $N(Y)$ with radius were recorded by electronically counting the rectangular pulses at the Schmidt-trigger output of the intermittency circuit. These distributions, which of course peak at or near $\bar{Y}$, were also computer-fitted by polynomials. The microscale of the front is given by

$$\lambda_F = \frac{\sqrt{2}}{\pi} \frac{u(\bar{Y})}{N_o} \tag{49}$$

where $u(\bar{Y})$ is the jet velocity at $\bar{Y}$. An alternate and possibly more meaningful front "wavelength" is simply

$$\Lambda_F = \frac{u(\bar{Y})}{N_o} \tag{50}$$

4.2.2 RESULTS AND DISCUSSION

Figure 38 shows a typical comparison of the distributions, with radius, of the intermittency factor, the temperature, and the electron density. As expected, the fluid is strongly intermittent at distances from the axis at which the mean temperatures is very close to the ambient. Also from Figure 38, observe that the corresponding relation between electron density and the intermittency factor is analogous but highly inconsistent from one x to another: at a fixed value of $\gamma = 0.5$, for example, $\tilde{n}$ varies considerably in the x-range investigated.

Important questions to be settled in analyzing the intermittency data include the randomness of the interface, the coincidence between electron- and temperature-interface and the comparison of the front geometry and behavior to that of low-speed jets. The growth of the front "radius" $\bar{Y}$ is shown dimensionally in Figure 39 and non-dimensionally as $\bar{Y}/L$, together with the standard deviation σ/L, in Figure 40. There is little doubt that these two quantities grow linearly and scale with L, and that they certainly are independent of the method of measurement. With $\bar{Y}$ and σ so computed it is possible to make a test of the randomness of the front such as is shown in Figure 41; we see that the Gaussian distribution of the intermittency factor about the front position, that is with $(Y-\bar{Y})/\sigma$, again obtains in the fashion characteristic of stationary random variables. In the same figure further evidence of randomness is supplied by the distribution of the normalized crossing frequencies N/N_{max} about the radial location $Y_{max} = Y(N_{max})$. The scatter is appreciable, but enough data points are available to illustrate the Gaussian behavior of N/N_{max} characteristic of randomness. As before, there is no systematic difference between data taken with the hot-wire and data taken with the Langmuir probe.

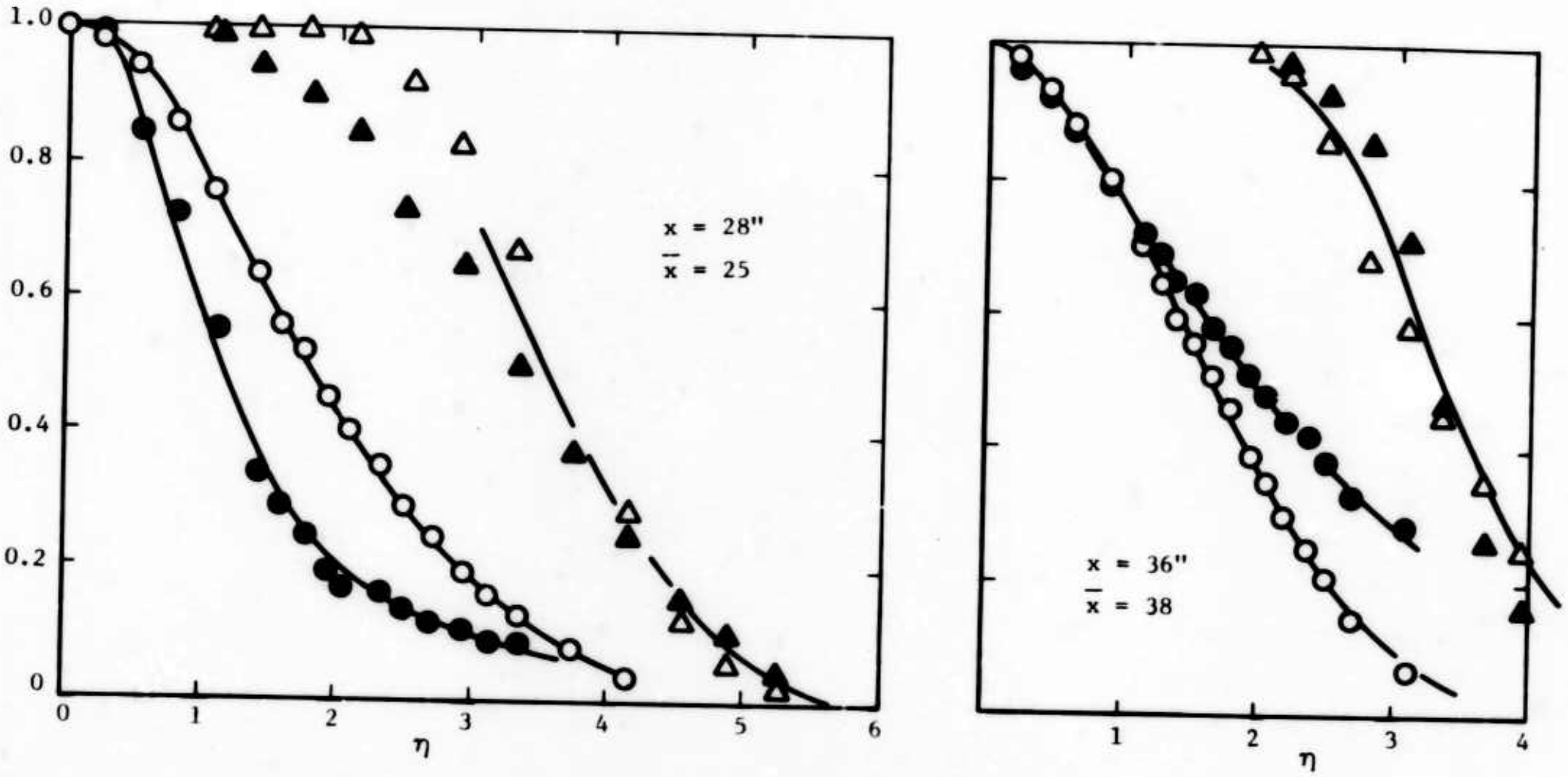

B0867 U

FIGURE 38. TYPICAL RADIAL DISTRIBUTIONS OF MEAN ELECTRON DENSITY, MEAN GAS TEMPERATURE AND INTERMITTENCY FACTOR IN THE JET

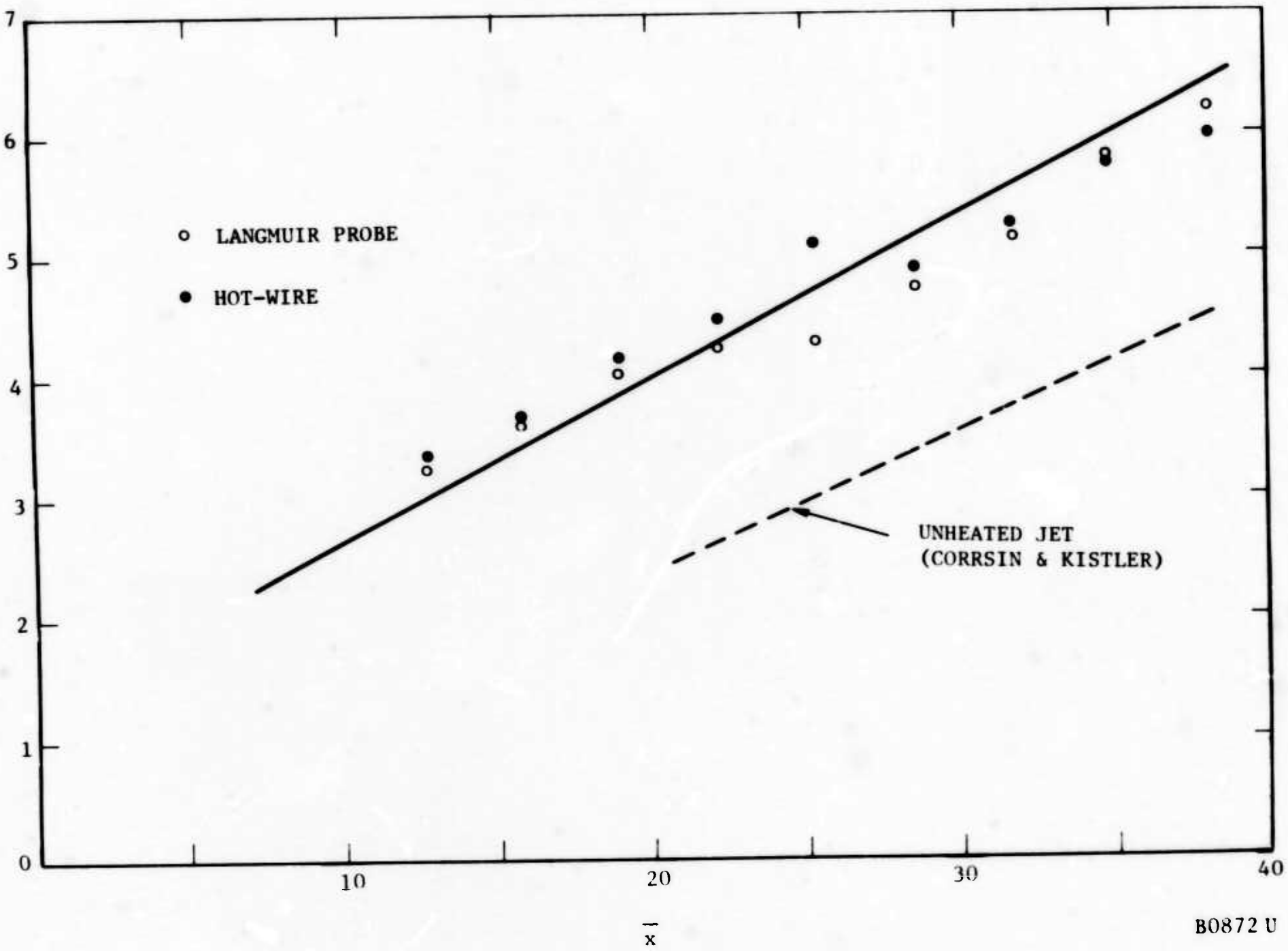

FIGURE 39. MOST PROBABLE TURBULENT FRONT POSITION IN THE JET

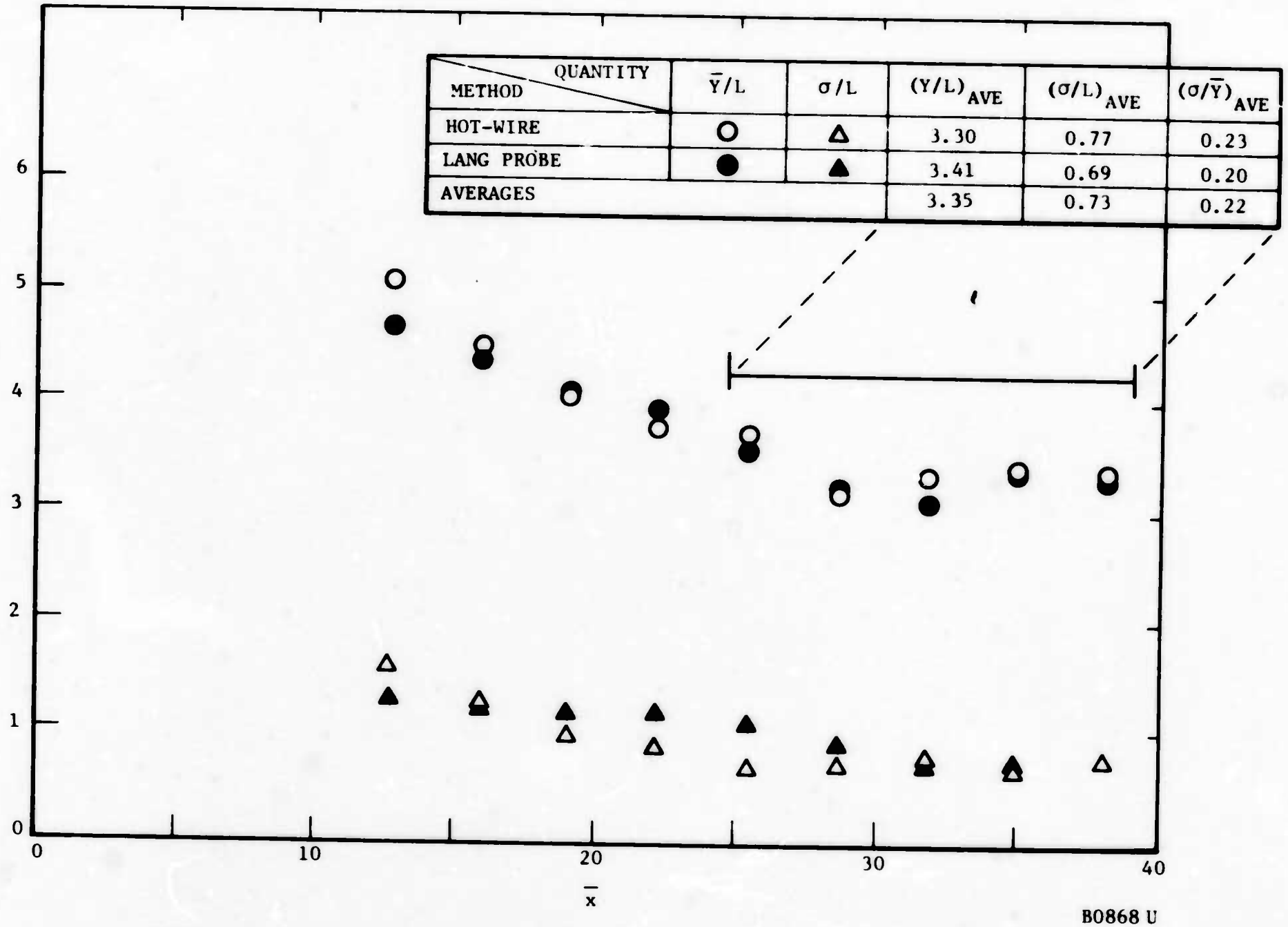

FIGURE 40. AXIAL VARIATION OF THE TURBULENT FRONT POSITION AND ITS STANDARD DEVIATION IN THE JET, NORMALIZED WITH THE TRANSVERSE SCALE

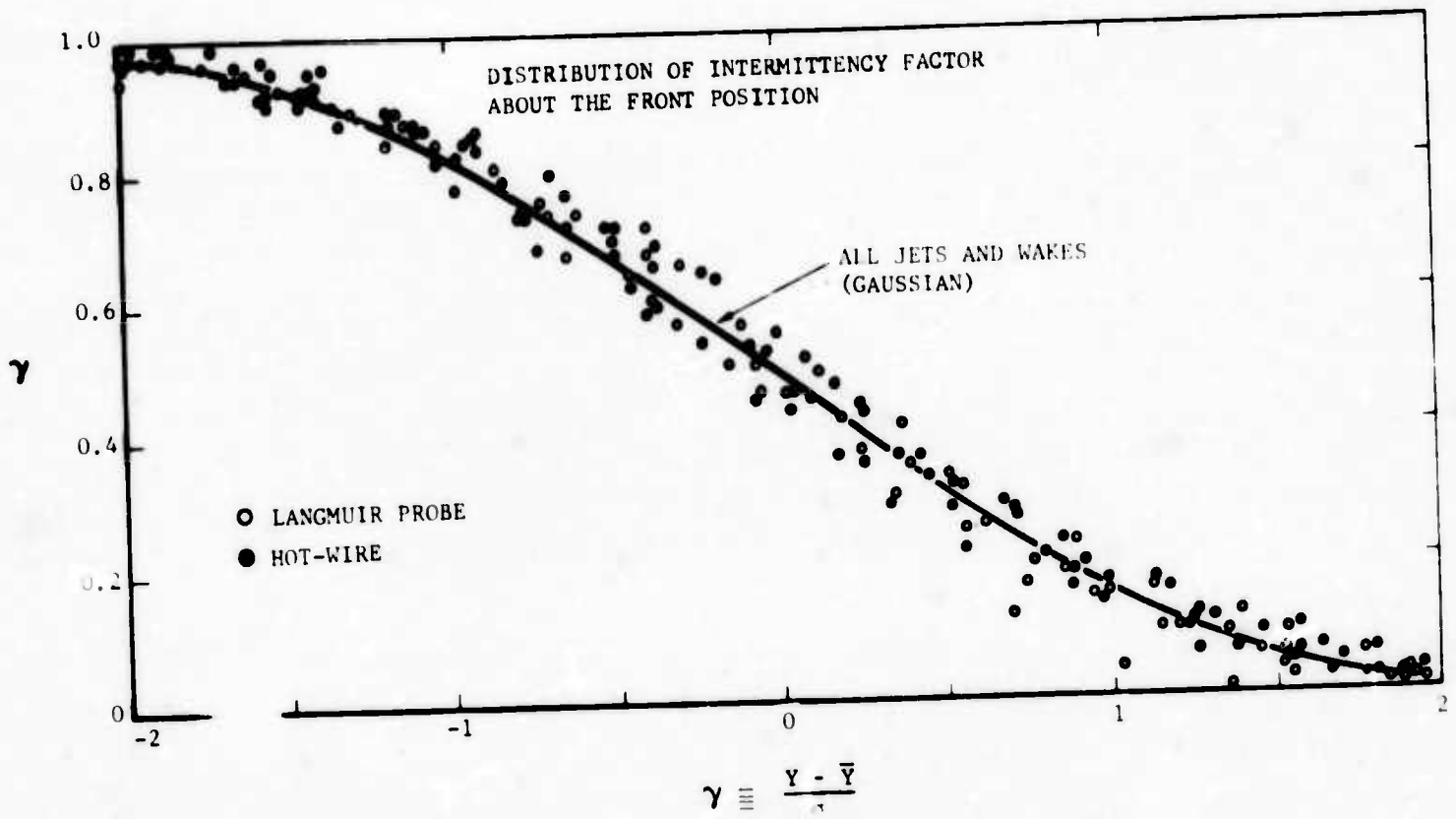

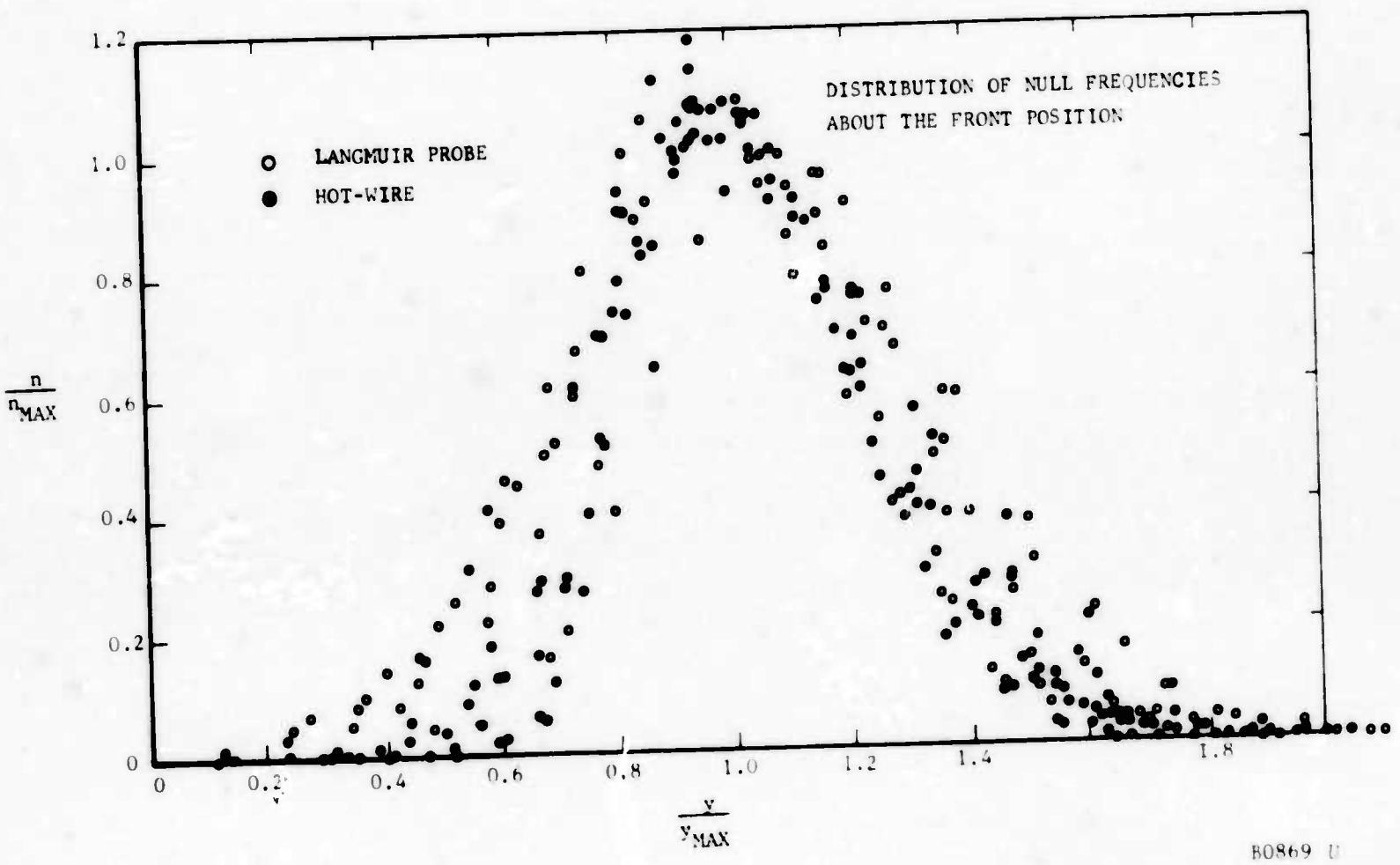

FIGURE 41. RADIAL DISTRIBUTION OF CROSSING FREQUENCIES AND INTERMITTENCY FACTOR IN THE JET

The null frequencies N_o, defined as the crossing frequencies measured at the position of the interface, were found to be very close to the maximum frequency N_{max} measured (at each x) at Y_{max}; thus, $N_o \equiv N(Y_{max}) = N(\bar{Y}) = N_{max}$ as expected. Figure 42 shows the variation of N_o with x; again, the frequencies measured with the hot-wire and the Langmuir probe are about the same at each $\bar{x}$. The decrease of N_o shown in this figure immediately suggests the lengthening of the front scale λ_F (or Λ_F) expected as the turbulent flow widens with distance. However, the computation of these scales from Equations (49) and (50) cannot be performed with the velocity data shown so far; these latter are mean velocities, whereas what is of course needed is the velocity of the front itself or at least the mean velocity within the front - the so-called eddy velocity.

Measurement of eddy velocities within "corrugations" in the jet boundary were made with the double Langmuir probe (two-wire correlation probe) mentioned previously and pictured on page 126 of Reference 6. Eddy velocities with such a probe can best be measured from the cross-correlation function of the probe signals; in the present work the more primitive method was adopted of obtaining a finite number of dual-trace oscillograms, of the turbulence pattern as it was convected by the wires. From these samples a rudimentary statistical distribution of the local eddy velocity was constructed at each point from which the mean velocity (and its fluctuation) could be extracted. The (mean) eddy velocity at $\bar{Y}$ was then used in place of u in Equations (49) and (50).

Reference 4 describes experiments done on the intermittency features of compressible wakes and advises the use of the "front wavelength" Λ_F (rather than λ_F) as a more significant measure of the front geometry. In doing so, evidence is drawn from observations (Reference 5) of the turbulence spectra (near the front position $\bar{Y}$) that the front itself may not be truly random, but rather weakly periodic at a wavelength Λ_F. The asymptotic form $\Lambda_F/L = u/N_oL$ of this wavelength for the axisymmetric wake is drawn in Figure 43 in which the jet front wavelengths, obtained per the previous paragraph, are also presented. The agreement between these two independent experiments is quite revealing. The wavelength of the jet front appears to bear the same relation to L (about $\Lambda_F/L \simeq 9$) that it does for the wake.

It should be noted that the physical dimensions of the front are given here in physical coordinates, and this should be accounted for comparing the present results with other experiments. In the latter the radius is usually normalized with the so-called half-radius $r^{1/2}$. Thus, Becker et al (Reference 18) gives $\bar{Y}/r_{1/2} = 1.78$, Bradbury (Reference 19) 1.73 and Corrsin and Kistler (Reference 11) values ranging from 1.65 to 2.00. From the present experiment (see Figure 40), we obtain $\bar{Y}/L = 3.35$ on the average, and in terms of the half-radius we get $\bar{Y}/r_{1/2} = 2.0$. It therefore appears that quite a few jet experiments generally agree as to $\bar{Y}/r_{1/2}$. It should be remembered, however, that heating the fluid generally increases the jet radius; the end result, shown on Figure 39, is that our $\bar{Y}$ extends farther out, by about 30 percent, than Corrsin's $\bar{Y}$ for example.

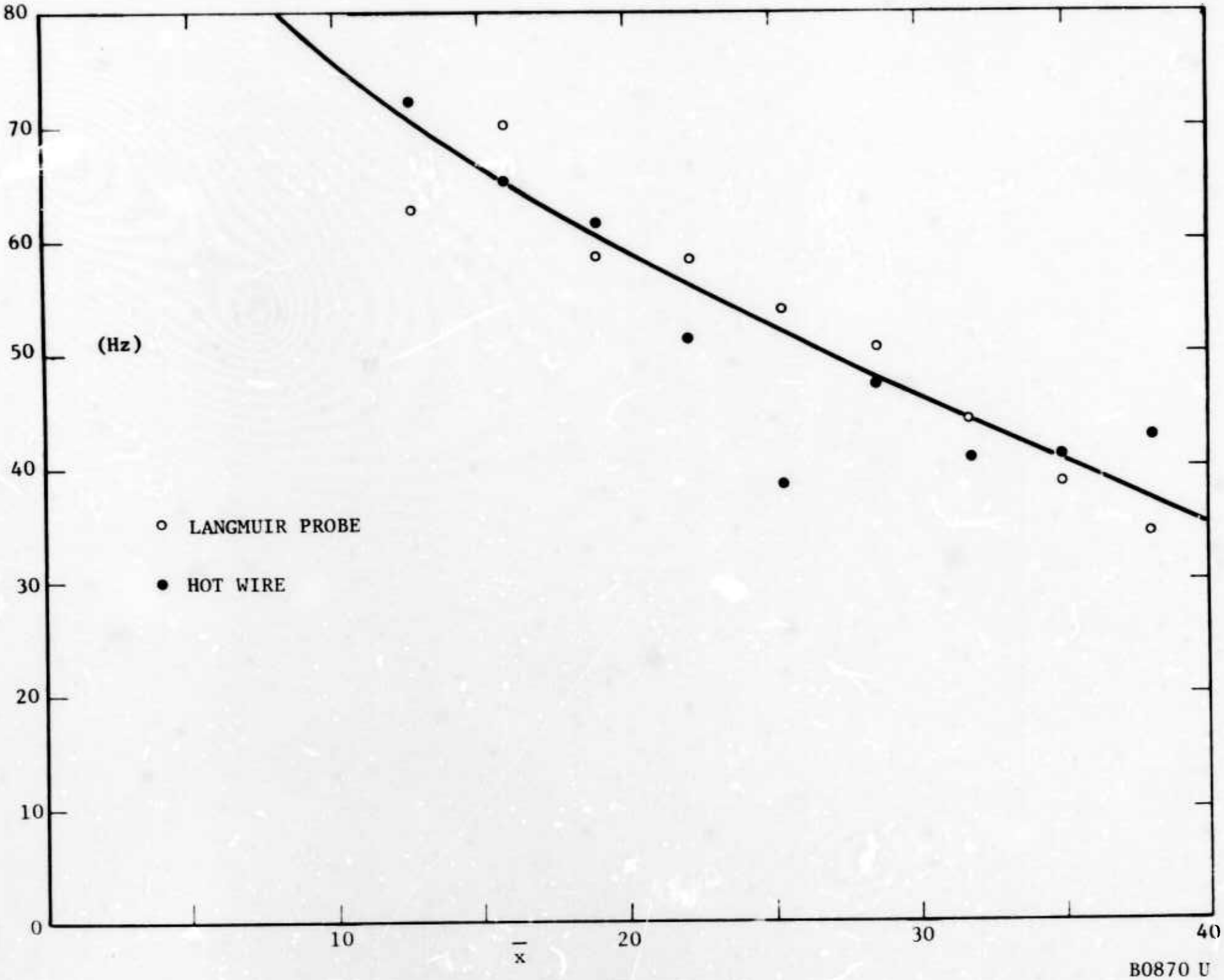

FIGURE 42. AXIAL DISTRIBUTION OF MAXIMUM CROSSING FREQUENCY IN THE JET

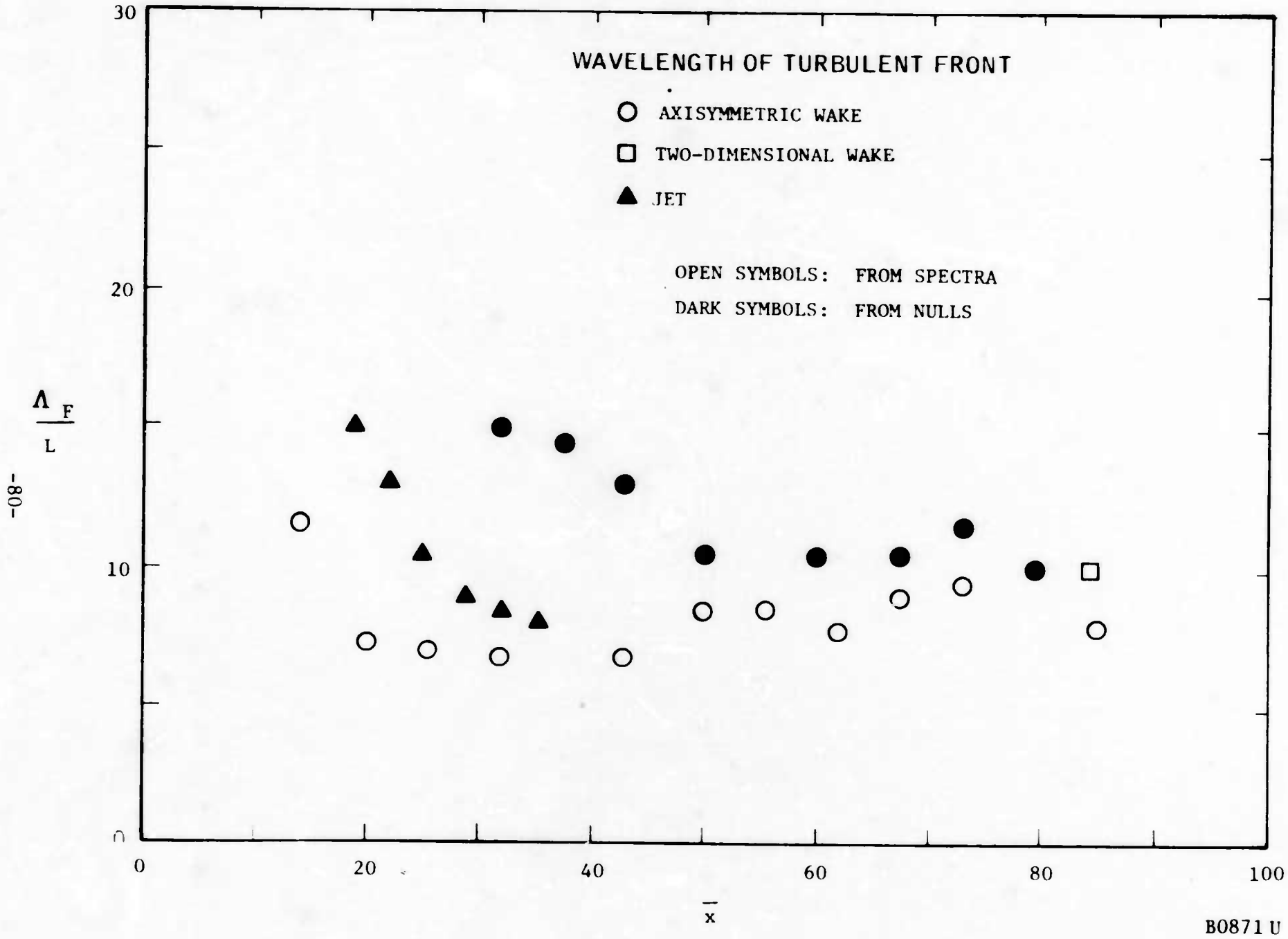

FIGURE 43. FRONT WAVELENGTH FOR JETS AND WAKES NORMALIZED WITH THE TRANSVERSE SCALE FOR EACH FLOW

The value of σ/Y obtained here is 0.23, not far from Bradbury's value of 0.22 or Corrsin's range of 0.23 to 0.29. However, Becker et al obtained $\sigma/Y = 0.16$. This might be interpreted as a difference in intermittent properties between an inert contaminant and the temperature field, but it is more likely that Becker's method of measurement and perhaps differences in the turbulent Reynolds number are responsible. Becker and his co-workers have at any rate obtained a unique relation between the intermittency factor and the contaminant density distribution with radius. In the reacting jet employed here the electrons are distributed radially in an irregular manner because of reactions (see Figure 38) and this relation does not materialize.

4.2.3 CONCLUSIONS

The main question posed in this section has been answered: the front characteristics are identical for the electron-sensitive and the temperature-sensitive probe. The implication is that the intermittency characteristics of the hypersonic wake, as predicted from gasdynamical studies alone, are also the intermittency characteristics relevant to the radar.

4.3 ELECTRON DENSITY FLUCTUATIONS

Data reduction has been completed on the magnitude of the electron density fluctuations in the plasma jet, raw data on which were presented in last year's report (Reference 6). The final data reduction was accompanied by further experimental measurements needed to "fill in" portions of interesting electron behavior. In this section, the following is discussed: (1) Theoretical calculations on the validity of the Langmuir probe technique, (2) the final form of the rms electron density fluctuation magnitude as distributed axially and radially, (3) data-reduction of the electron density spectra, and (4) studies and interpretations of the very large fluctuations observed in the transition region. Comparison with other measurements will also be given.

4.3.1 LANGMUIR PROBE SHEATH CALCULATIONS

The radius of the electrostatic sheath surrounding the Langmuir probe used in this work is crucial to the validity of the data. Specifically, the sheath ra'ius

$$a \ll \lambda_e \tag{51}$$

where λ_e is the electron mean-free-path. The earliest computations of a, under this contract, were based on a combination of the Langmuir-Mott-Smith and Langmuir-Blodgett theories (Reference 20). More recently this computation was replaced by one performed by Bettinger and Walker (Reference 21) whose attractiveness rests of its use of integral and conservation laws. Sutton (Reference 22) has proposed that the sheath is computed on the basis

of work done by Laframboise which is basically an extension of original work by Langmuir. To compare these choices for computing a, the following formulas were plotted:

(1) Langmuir, Mott-Smith and Blodgett:

$$\frac{a}{r} = 2.8\left(\frac{h}{r}\right)^{3/2} \eta^{1/2} \tag{52}$$

(2) Bettinger and Walker:

$$\left(\frac{a}{r} - 1\right) \ln\left(\frac{a}{r} - 1\right) = 1.66 \left(\frac{h}{r}\right) \eta^{3/4} \tag{53}$$

(3) Laframboise:

$$\frac{a}{r} = 1.63 \left(\frac{h}{r}\right)^{0.6} \eta^{1/2} \tag{54}$$

where r and h are the probe and Debye radius, respectively, and η the non-dimensional probe voltage $\eta \equiv q\nu/kT$. The former two equations are valid for $h/r > 1$, whereas the latter presumably for $0.1 < h/r < 2$.

These relations have been plotted on Figure 44. They indicate that the Langmuir-Mott-Smith-Blodgett approach gives sheaths which are in agreement with the other theories for $h/r = 1$, but much higher than the latter for $h/r >> 1$. Because this theory is also the least sophisticated (and presumably least accurate) of the others, it is concluded that the original estimates of a were unduly pessimistic; the results on electron fluctuations discussed in this report are thus more valid than originally thought.

4.3.2 MAGNITUDE OF ELECTRON DENSITY FLUCTUATIONS

Figures 45 and 46 summarize the final results of the electron fluctuation magnitude in the turbulent plasma. From these two figures, it is clear that the electron fluctuations undergo two phases: up to about 24 inches from the nozzle the fluctuations are extremely large on the axis (about 5 times the mean) whereas beyond that distance they decrease to a small percentage of the mean and develop off-axis peaks. The former will be called "transitional" or "heterogeneous" fluctuations whereas the latter will be called "asymptotic" or "homogeneous".

Perhaps the single most interesting phenomenon observed during the turbulence measurements was the very large magnitudes of the electron density fluctuation. It is statistically possible for the standard deviation of a stationary variable to exceed the mean value of the variable when the amplitude distribution of the latter is extremely skew. Such situations exist in the intermittent zones of ordinary turbulent jets for any flow variable Q which fluctuates between nil in the ambient ("irrotational") environment and some mean level within the turbulent front. If the latter does not decrease

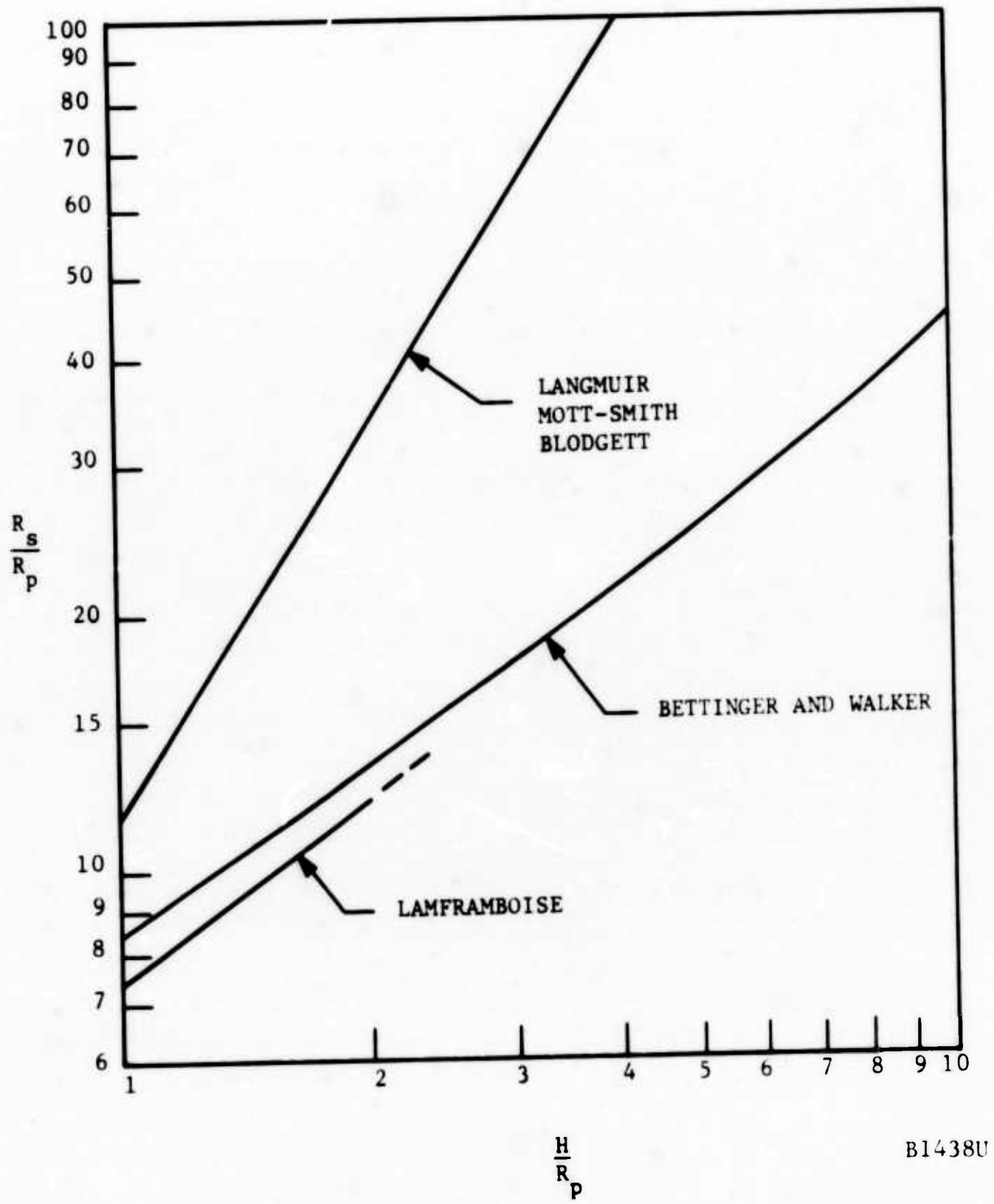

FIGURE 44. COMPARISON OF THREE THEORETICAL PREDICTIONS OF THE SHEATH RADIUS R_s IN TERMS OF THE PROBE RADIUS R_p AND DEBYE DISTANCE H.

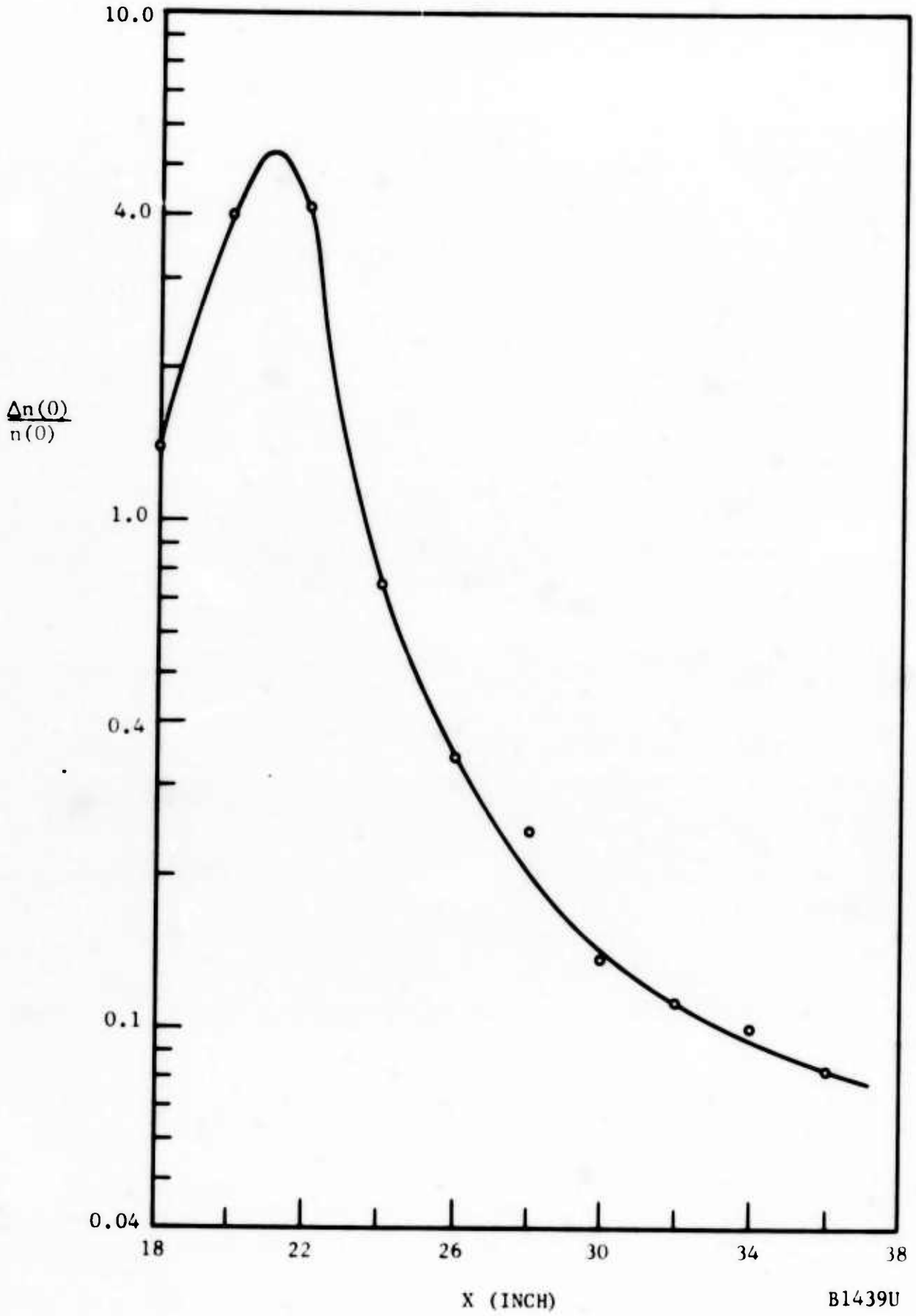

FIGURE 45. AXIAL VARIATION OF THE RMS ELECTRON DENSITY FLUCTUATIONS, NORMALIZED WITH THE LOCAL ELECTRON DENSITY, ON THE JET AXIS

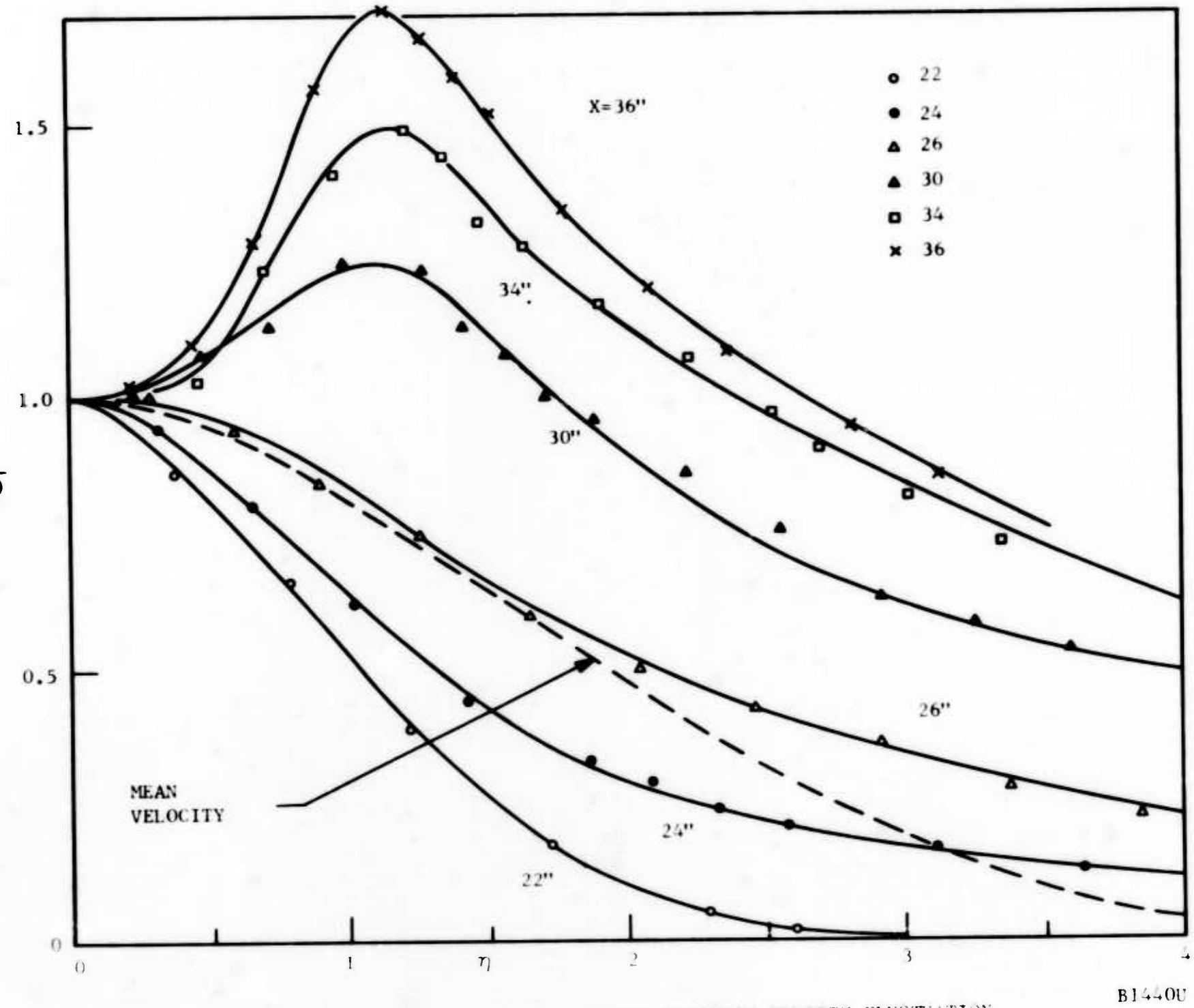

FIGURE 46. RADIAL VARIATION OF RMS ELECTRON DENSITY FLUCTUATION NORMALIZED WITH THE AXIS VALUE

too fast with increasing radius then it is well known that $\Delta Q/Q$ can diverge with radial distance. In fact Becker, Hottel and Williams (Reference 18) have observed this divergence by utilizing an inert contaminant concentration for an observable.

The possibility that the large fluctuations on the axis pictured on Figure 45 are caused by the intermittency is excluded by the simple fact that the flow on the axis is fully turbulent as already demonstrated. From the results thus far shown in fact, it appears that we have here a fully turbulent fluid with normal temperature fluctuation but with highly-skewed electron fluctuations. An oscilloscopic study of the turbulent jet immediately showed large "spikes" in the electron density time history at a point; these spikes are indeed what statistics would require to produce the large $\Delta n/n$ of Figure 45. Figure 47 shows a comparative oscilloscope study of the Langmuir probe and hot-wire output at various radial positions but at the same distance from the jet nozzle. By properly adjusting the scope gain it is possible to show conclusively, first, the differences between intermittent and fully turbulent flow and, secondly, the differences between Langmuir-probe and hot-wire output in the fully turbulent region. Attention is drawn to the large spikes in the Langmuir probe traces which are clearly absent from the hot-wire traces.

The appearance of the large spikes persisted for several inches in the upstream end of the turbulent zone studied, but decayed and eventually vanished as the probe was moved downstream; the fluctuation level $\Delta n/n$ also decayed below unity as Figure 45 shows. To complete the picture, an investigation of the laminar and transitional portions of the jet was made using a Langmuir probe thicker than described previously in this paper, so that it could withstand the much higher heat fluxes in the laminar jet. For obvious reasons the output of this probe was not quantitatively interpretable, but it made possible to piece together a reasonable description of the events leading to the generation of the large fluctuations.

Figure 48 shows this picture. The Langmuir probe observation made is typified by an instantaneous "snapshot" of the electron density on the jet axis from the nozzle exit well into the turbulent zone. In the laminar jet the mean electron density is high with an unsteady component consisting of the rectifier-driven 360 Hz modulation whose rms magnitude is about 10 percent of the mean. At the flow velocities prevalent here the wavelength of this sinusoidal fluctuation is actually very much larger than the length of the laminar jet (about 10 feet compared to about 1 foot). In the transition region the breakdown process mixes ambient fluid with the ionized fluid; the former is electron-poor so that large "negative" pulses (if one thinks of the electron current as producing a positive displacement of the scope beam) appear as shown on Figure 48: the signal is thus "negatively one-sided". The mean electron density thus decreases below the maximum level, which also decreases because of recombinations. Farther downstream the spikes widen (but do not necessarily deepen), and still farther the signal begins reversing itself, i.e., becoming "positively one-sided". In this latter case the mean electron density drops considerably below the tops of the spikes, the fluctuation distribution is very skew and the rms fluctuation level is considerably higher than the mean level. It is at this stage that the oscillograms shown on Figure 47 were taken.

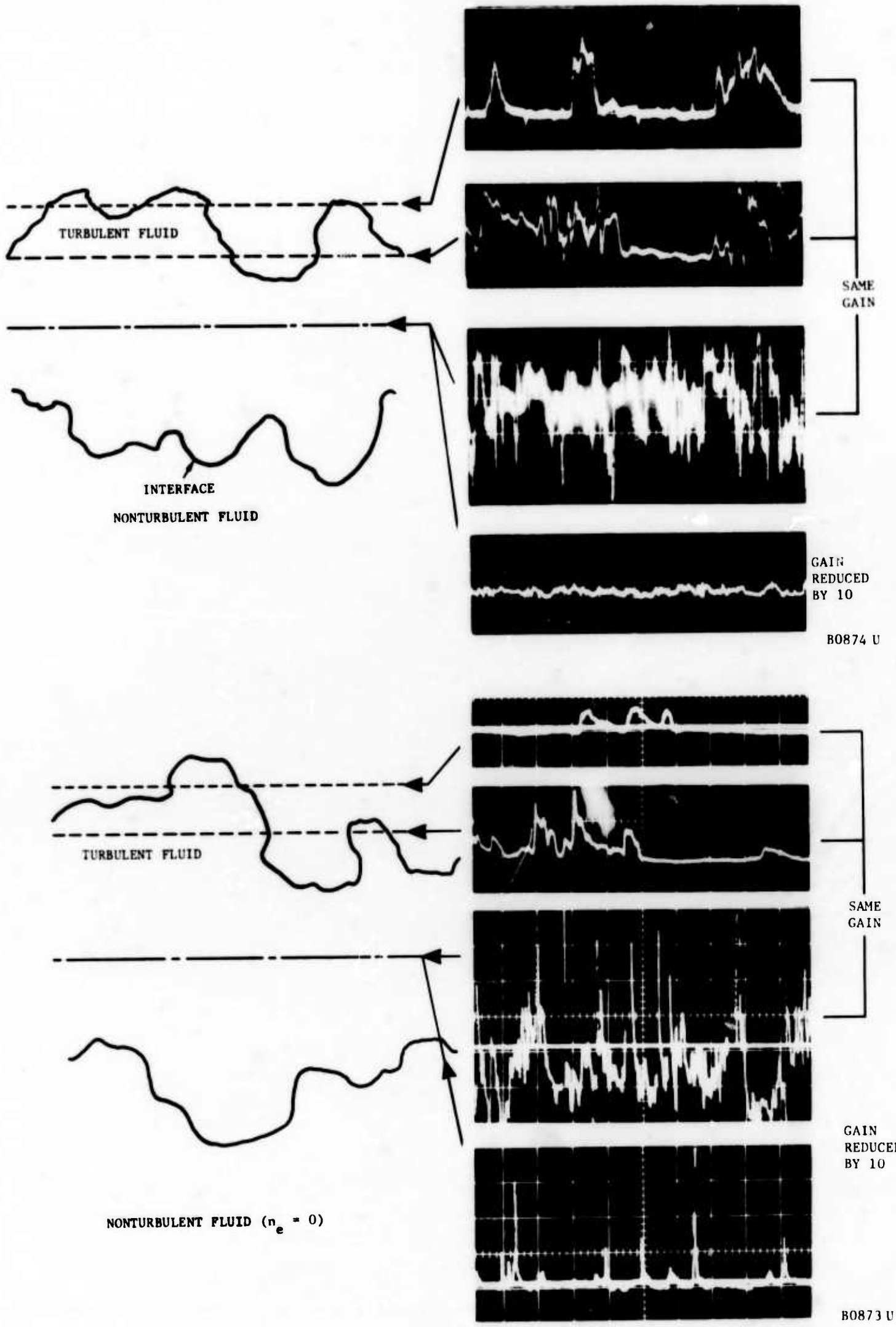

FIGURE 47. OSCILLOSCOPIC STUDY OF TEMPERATURE AND ELECTRON DENSITY FLUCTUATIONS

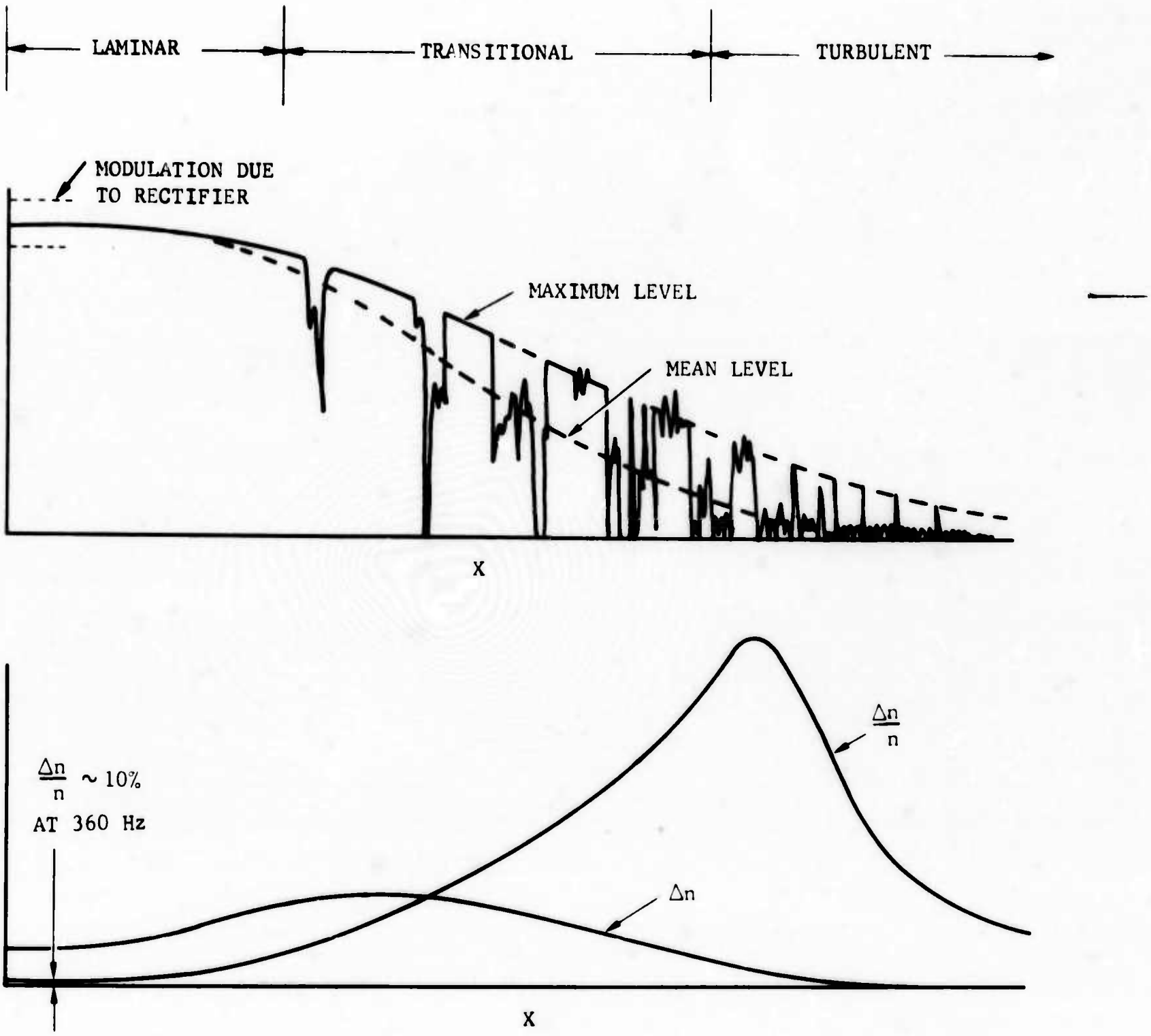

FIGURE 48. SCHEMATIC OF TYPICAL INSTANTANEOUS ELECTRON DENSITY DISTRIBUTION ALONG THE JET AXIS AS INFERRED FROM PROBE MEASUREMENTS

It should again be emphasized that at this stage the fluid is fully turbulent from the standpoint of intermittency, and that turbulent fluctuations in the electron density, of order 20 to 40 percent of the mean, exist in addition to the large electron density spikes. The latter are obviously the remnants of the laminar flow upstream of the transition zone, in which the electron density level is very high when compared to the level in the turbulent fluid itself. Eventually these spikes also disappear and, as Figure 45 shows, the ratio $\Delta n/n$ settles to values of order 10 percent in the far jet.

In Figure 48 it is schematically shown that the maximum of the normalized fluctuations is attained where the mean electron level is much below the maximum level n_m, that is, the locus of the spike maxima. If the spikes are truly the results of the process of engulfment of the ambient, electron-poor fluid by the electron-rich fluid of the jet, and if the electron density of the former is n_c, then

$$\left(\frac{\Delta n}{n}\right)^2 (x) = \frac{\left(n_m/n_c - 1\right)^2 (P/\dot{m} - 1)}{\left(n_m/n_c - 1\right) + P/\dot{m}^2} \qquad (55)$$

where $P/\dot{m}$ is the ratio of the total mass to the jet mass. Here it has been assumed that both fluid components are laminar so that the signal can locally oscillate between n_m and n_c only, in the manner suggested some time ago by Feldman and Proudian (Reference 23) and Lin (Reference 24). The type of fluctuations of Equation (55) are nil before entrainment begins ($P/\dot{m} = 1$) and also when $P/\dot{m}$ tends to infinity in the far jet, and they peak in between with a magnitude depending on n_m/n_c. For equilibrium chemistry, when n_m and n_c are directly obtainable from the corresponding temperatures T_m and T_c, it is shown by Reference 15 that $\Delta n/n$ of order 10^6 or higher can obtain for practical values of T_m/T_c. For finite reaction rates the ratio $\Delta n/n$ becomes extremely sensitive to the chemistry.

Nevertheless the simplicity of the jet flow brought about by gasdynamical self-preservation allows certain broad tests of Equation (55) to be made easily. For example the entrainment rate is given theoretically and has also been measured directly. For recombination reactions the n_m might also be obtained as a function of x. The normalized electron density fluctuations of Equation (55) thus become dependent only on the ratio n_{m_o} (of the maximum electron density in the laminar flow) to the "ambient" value n_c. The former is actually obtainable from the experiment but the latter is not, since the electron density at the base of the spikes was detected to be turbulent and of a mean value much higher than that outside the jet. Computations made with Equation (55) using estimated values of n_c gave reasonable numerical agreement with the measured axial variation of $\Delta n/n$ shown on Figure 45.

Equation (55) thus appears to be a reasonable descriptor of the physical mechanism giving rise to the large electron density fluctuations - on the strength of the mixing model it describes. It does not necessarily endorse the "laminar mixing" ideas of References (23) and (24) since the participating lumps of fluid (whether electron-rich or electron-poor) are turbulent

in character. At this time it also appears to affect the transitional zone more so than the turbulent activity in the far jet; in the present experiment this zone is only a few jet thicknesses long.

Once beyond the region of very high level, the electron density fluctuations decrease, according to Figure 45, to values more typical of homogeneous mixing. The following points are significant: first, the axis values of $\sqrt{n}/n$ do not appear to attain an asymptote. This may be attributed either to the fact that the overall jet fluctuations themselves have not relaxed to the self-preserving state; or, which is more likely, that no self-preservation of the electron fluctuations attains where all other types of fluctuations have become self-preserving (e.g., constant fractions of the mean values). Secondly, the off-axis maxima of these fluctuations (see Figure 46) occur in the general vicinity of $\eta = 1.3$. By comparison, the region of maximum shear in the jet occurs at

$$\eta = \eta \left(\frac{d\tilde{u}}{d\eta} = 0 \right) \tag{56}$$

which, using the self-preserving velocity distribution

$$\tilde{u} = e^{-0.24\eta^2} \tag{57}$$

is seen to occur at

$$\eta = \left[\frac{1}{0.48} \right]^{1/2} \doteq 1.45 \tag{58}$$

It thus seems that the maximum of electron density fluctuation occurs at or near the same radial position in the jet occupied by the maximum shear region. This is an important finding with obvious applications to the hypersonic wake problem.

At radial positions beyond $\eta = 1.45$, the fluctuation level does not decay as rapidly as expected. In fact it appears that from the standpoint of fluctuations the jet is much wider than evidenced by the mean-flow measurements. There is presently no explanation of this phenomenon available other than the effect of intermittency. As is already shown in Paragraph 4.2, the intermittent electron flow extends considerably farther from the axis than the distribution of electron density. For example, at x = 30 inches, the flow is intermittent still at $\eta = 5.5$, whereas the electron density has reached ambient (zero) value by $\eta = 4.5$. Now in intermittent zones the "turbulent" signal is made up of a combination of real turbulence and intermittency in a way given functionally by Corrsin and Kistler (Reference 11). In the example cited the intermittency contribution should be prevalent in the outer region, say in $4 < \eta < 6$. To test this, Figure 49 plots the $\sqrt{n}/n$ distribution at x = 30. Also plotted is the signal expected if it consisted of the intermittency contribution alone, as given by the formulas developed in Appendix B of Reference 4:

$$\frac{\sqrt{n}}{n} = \left(\frac{1}{\gamma} - 1 \right)^{1/2} \tag{59}$$

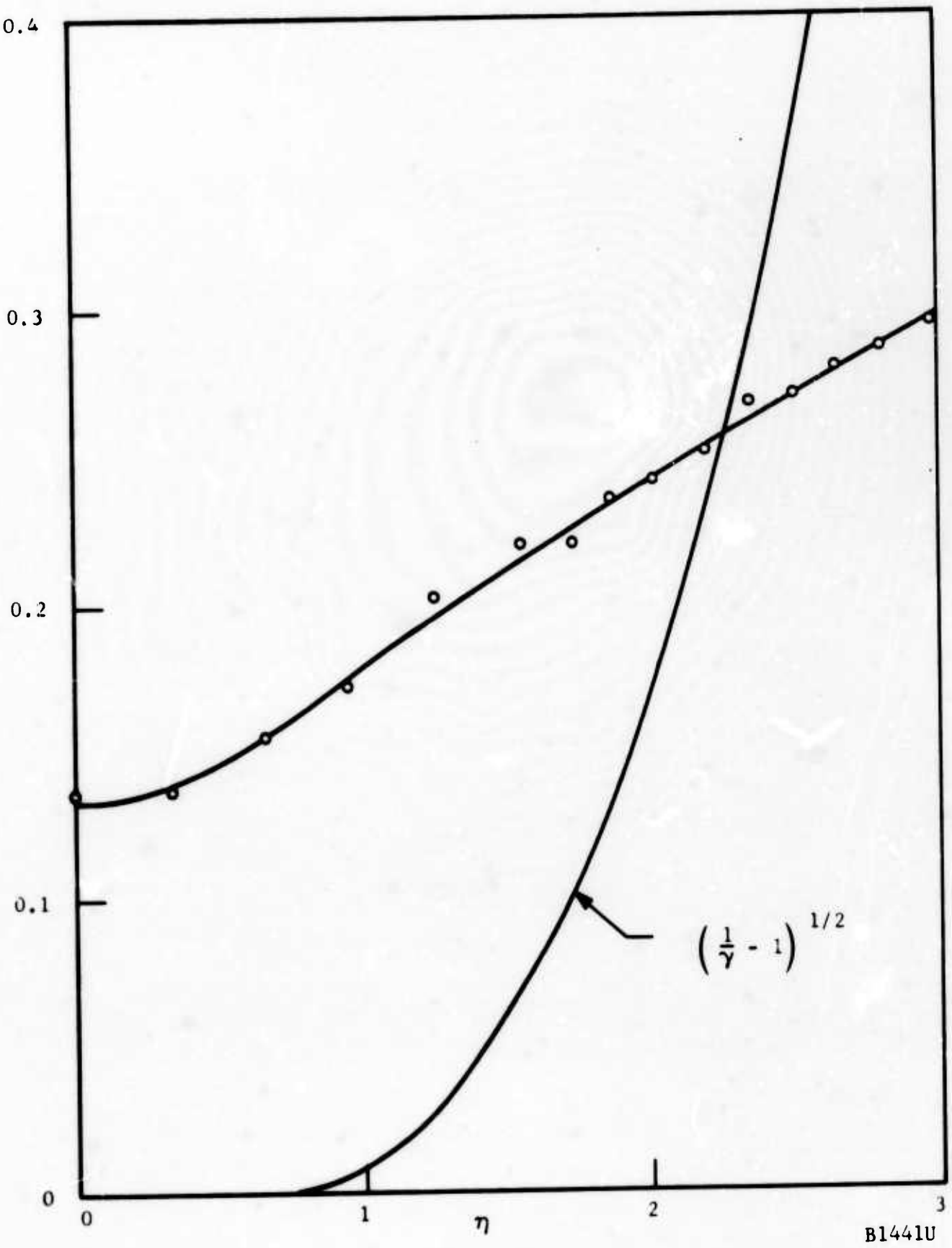

FIGURE 49. TYPICAL RADIAL VARIATION OF NORMALIZED RMS ELECTRON DENSITY FLUCTUATIONS ALSO SHOWING THE SUSPECTED CONTRIBUTION OF INTERMITTENCY

where γ is the intermittency factor. Near the axis, where $\gamma = 1$ the signal is obviously all due to turbulence, but the curves cross around $\eta = 2.3$. This is surprising since it says that near the jet edge the signal is smaller than the minimum expected. The question is open at this juncture. A likely explanation is that Equation (59) is oversimplified because it assumes: (1) no electrons outside the jet, (2) an intermittency signal idealized by "flat top" distribution, and (3) a jump in electron density across the front which, at a point fixed near the jet edge, is constant in time.

4.3.3 SPECTRA OF ELECTRON DENSITY FLUCTUATIONS

In the previous reporting period, spectra of the electron density fluctuations were taken at all x and Y positions with a wave analyzer whose minimum bandwidth was 200 Hz. These data, reduced during the current period, showed two deficiencies connected with the very-low frequency range. First, many of the spectra were recorded with an x-Y recorder gain such that the low-frequency spectral density went off scale. Secondly, it was evident that the spectral density dropped off rapidly in the first few hundred cycles, so that measurements in that region were inaccurate due to the 200 Hz bandwidth. Thus, the data could only be considered useful above a certain frequency, which was set at 2 kHz.

To fill the low-frequency gap in each spectrum, all spectra were re-taken in the 0-2 kHz range using the setup of Figure 50. A Hewlett-Packard Model No. 302A Wave Analyzer was used with a range of 50 kHz and bandwidth fixed at 7 Hz. This bandwidth could resolve the spectral density at much lower frequencies than before, but it also introduced the classic output unsteadiness typical of sharply filtered low-frequency spectral analysis. To damp this out, a vacuum thermocouple was interposed between the wave analyzer dc output and the plotter. Figure 51 shows the transfer function of the thermocouple which was used in the computerized data reduction process to connect the dc appearing at the plotter input to the filtered output of the wave analyzer. With this equipment spectra were recorded from 0 to 2 kHz. Each of these spectra was then joined with its corresponding predecessor (taken with the previous arrangement) at the 2 kHz point. In the process, account was taken of the fact that the preceding spectra were in terms of the root-mean-square, while the most recent ones in terms of the mean-square spectra.

The data were reduced by the JEA-II (SRS 0024) computer program which is described in Appendix A. This program gives an independent check of the total rms fluctuation by integrating the area under each spectrum. After the data was first reduced it developed that this cross-check did not conform with expectations. It was found that the Runge-Kutta integration scheme used was not accurate for functions changing rapidly between adjacent frequencies. The data were therefore processed again through the program using a Simpson-type integration.

The electron density fluctuation spectra are shown on Figures 52 through 58. The first two figures show the spectra on the axis; the remainder show

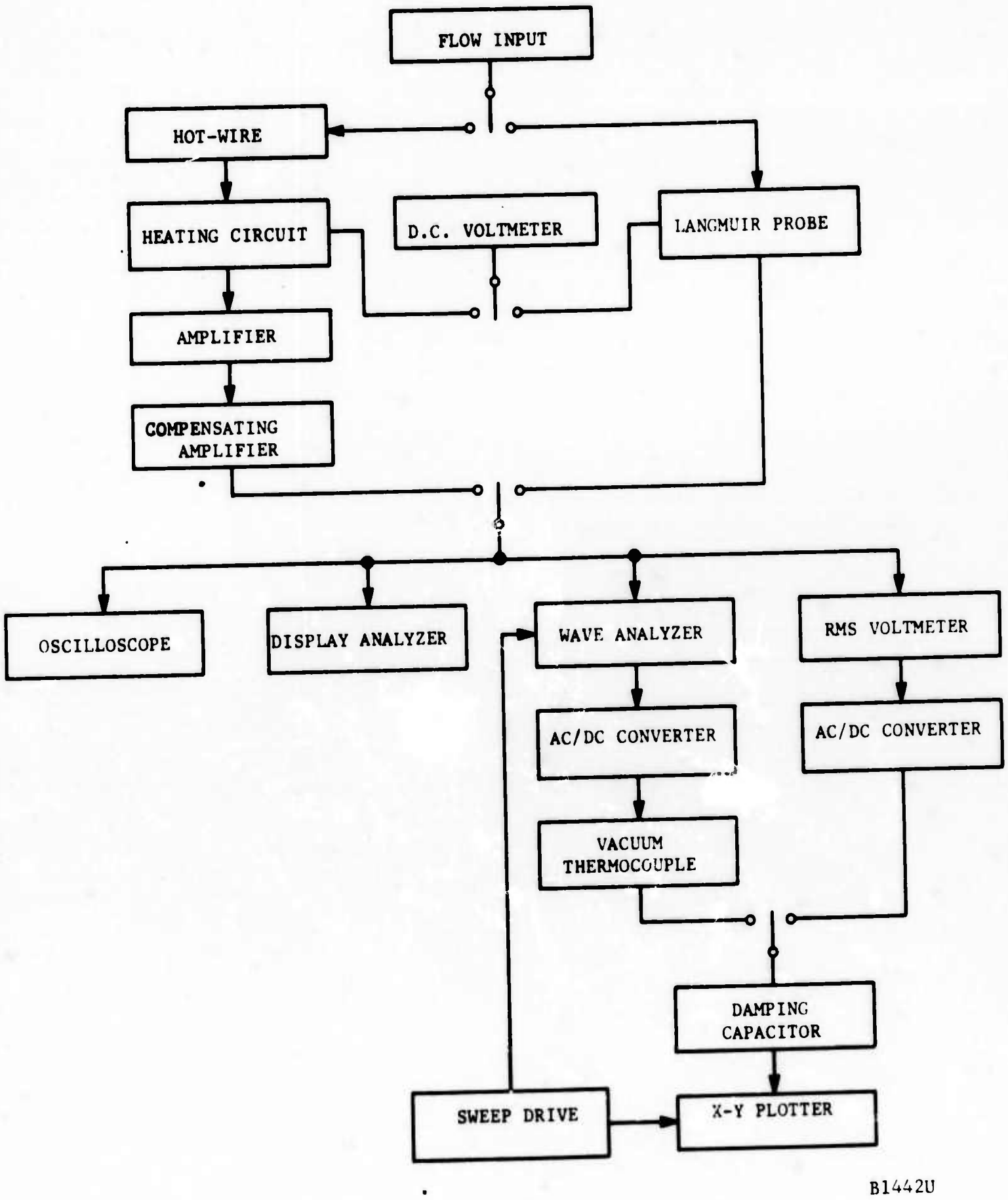

FIGURE 50. BLOCK DIAGRAM OF THE JET TURBULENCE ELECTRONICS

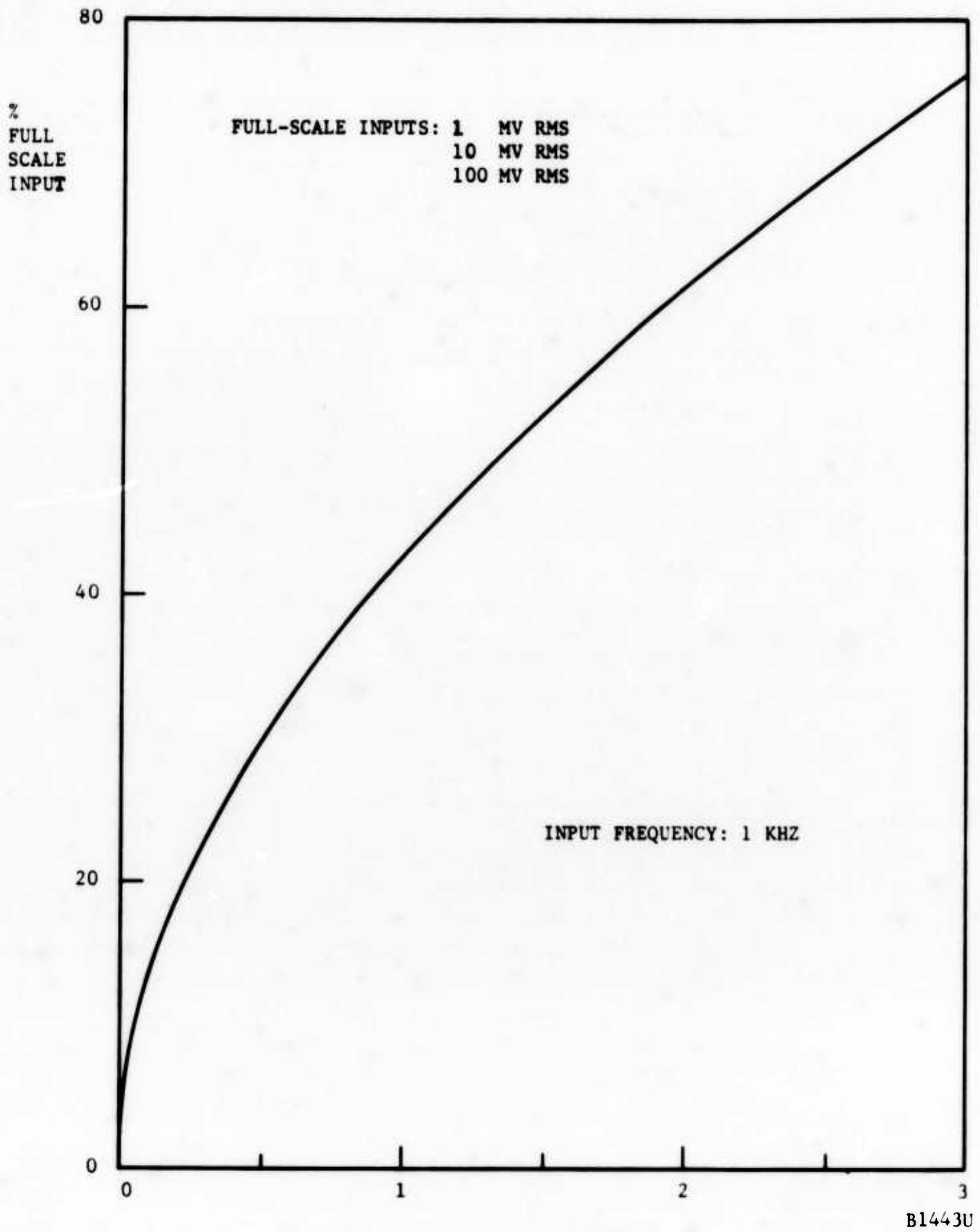

FIGURE 51. TRANSFER FUNCTION OF VACUUM THERMOCOUPLE USED TO CONVERT THE SPECTRAL DENSITY SIGNAL INTO DC VOLTAGE

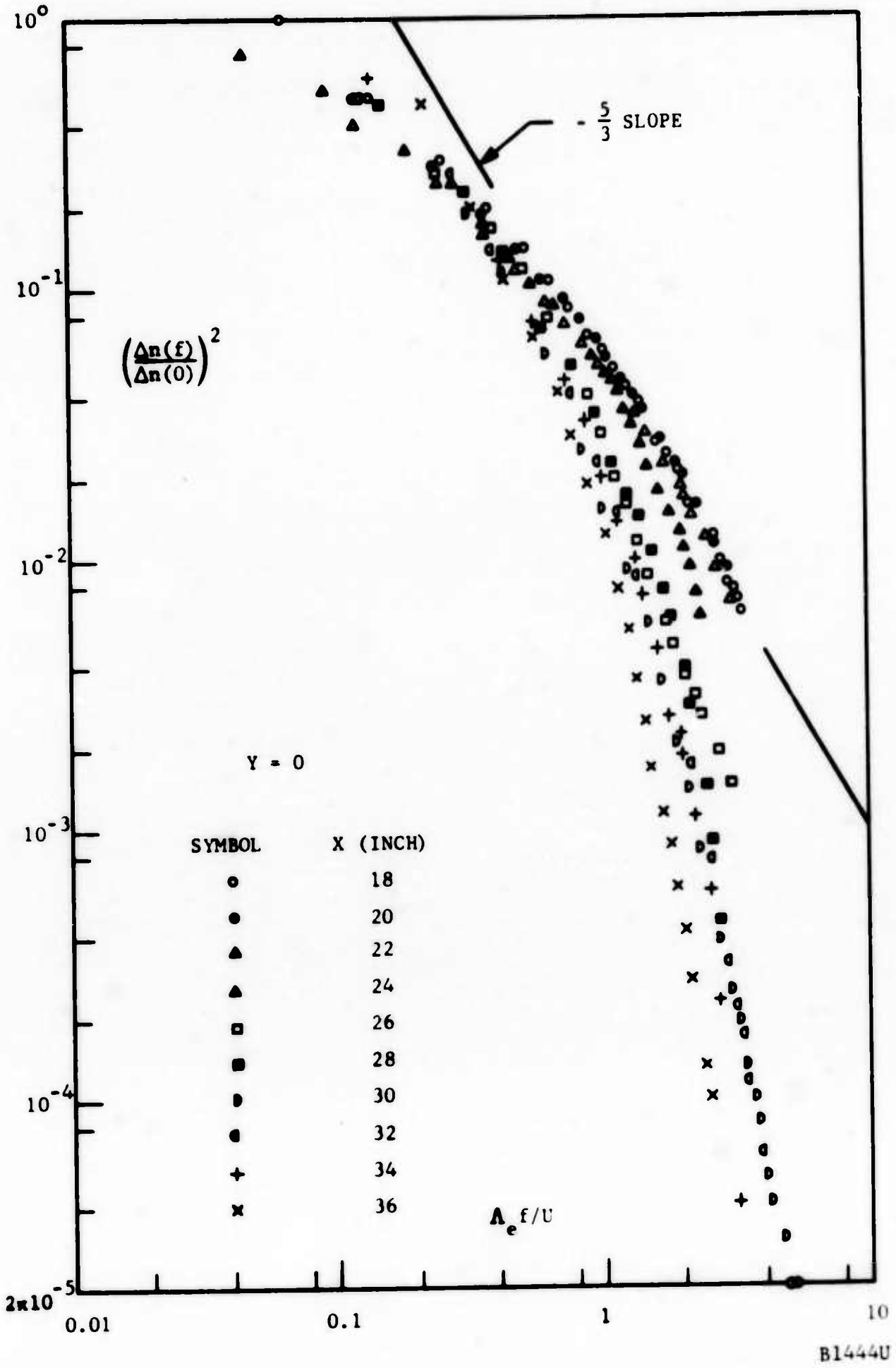

FIGURE 52. NORMALIZED SPECTRAL DENSITY OF ELECTRON FLUCTUATIONS ALONG THE JET AXIS

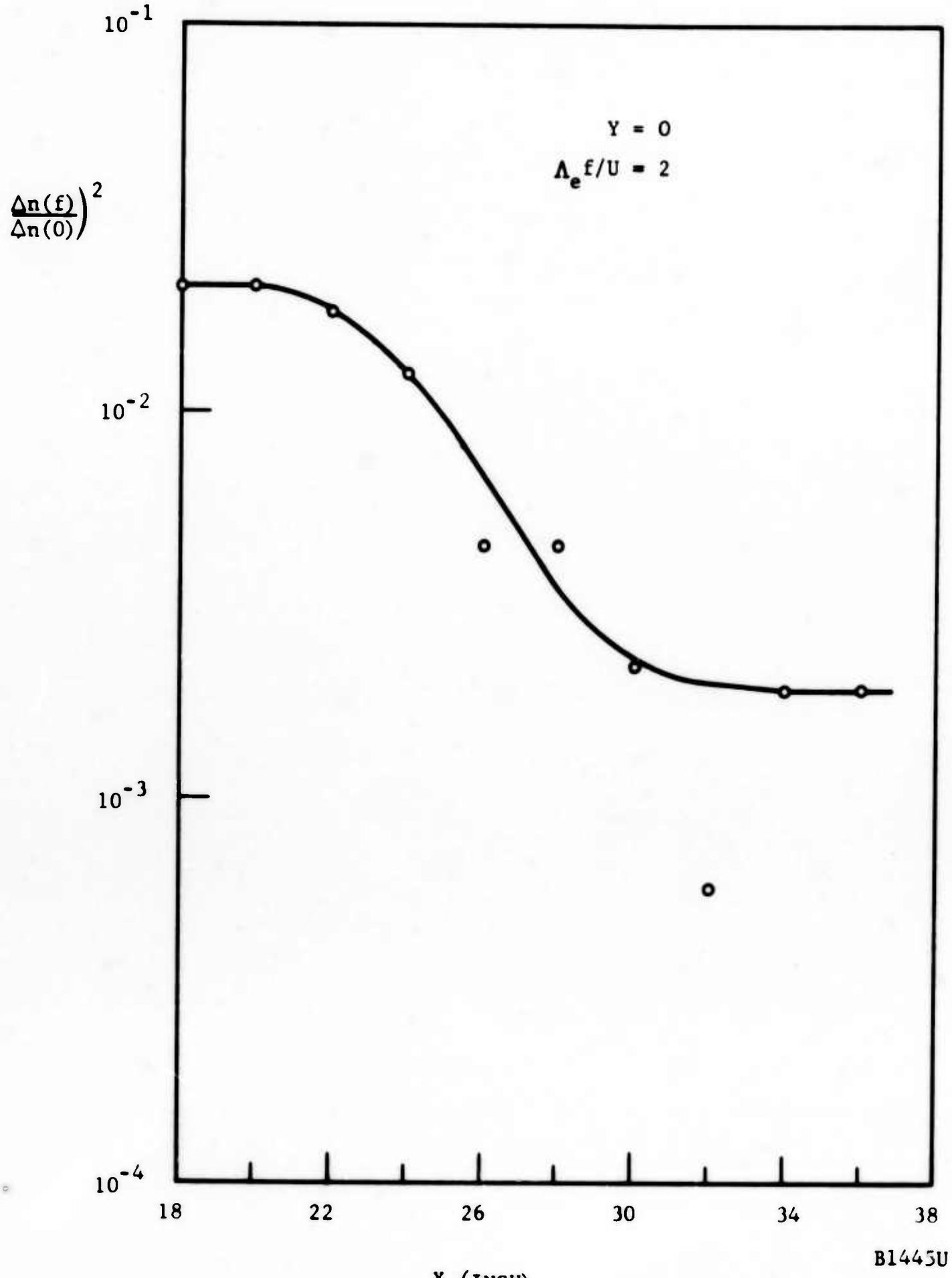

FIGURE 53. AXIAL VARIATION OF ELECTRON SPECTRAL DENSITY FOR EDDIES HALF THE MACROSCALE SIZE, SHOWING THE DECREASING IMPORTANCE OF SUCH EDDIES FAR FROM THE NOZZLE

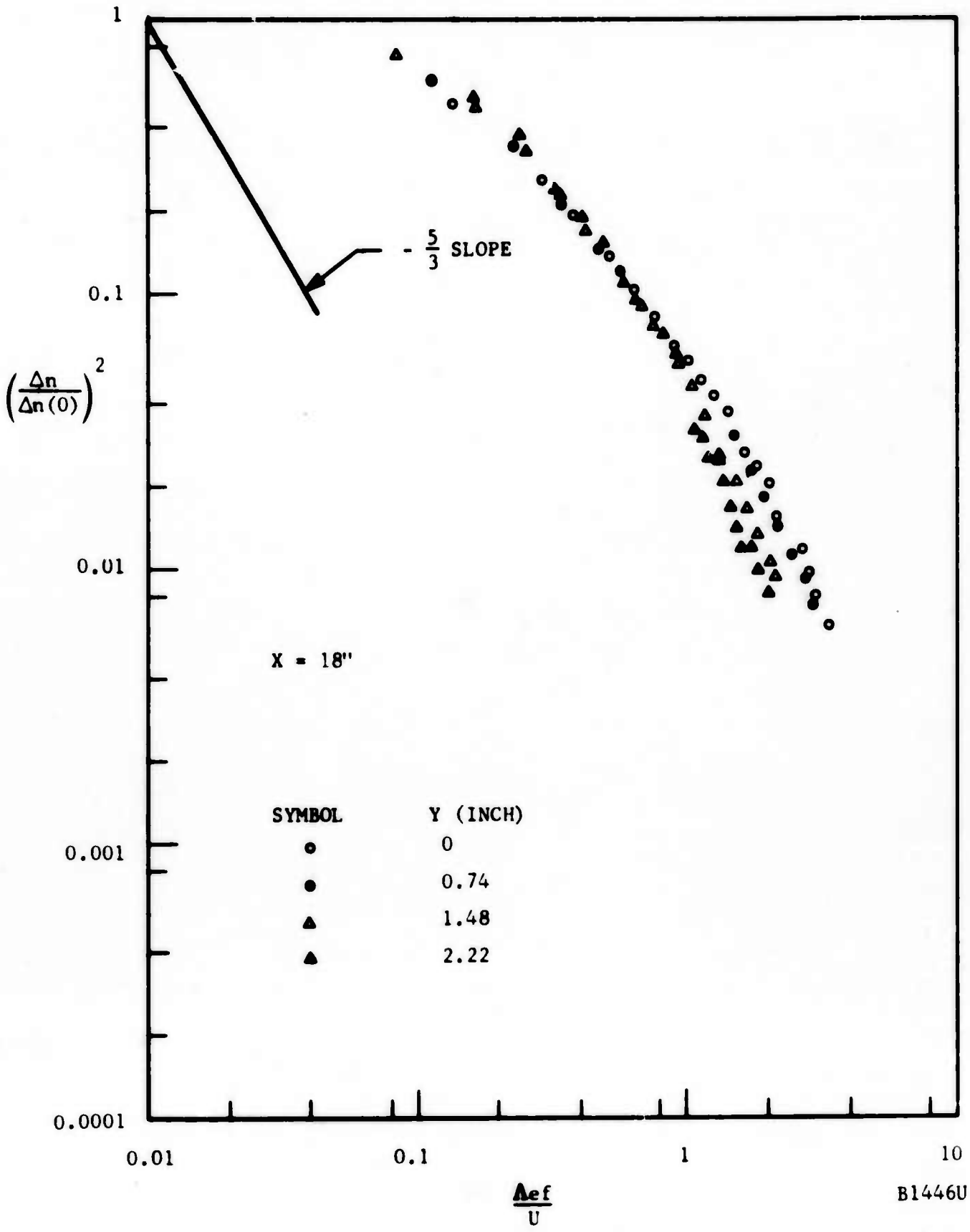

FIGURE 54. NORMALIZED SPECTRAL DENSITY OF ELECTRON FLUCTUATIONS AT 18 INCHES FROM THE NOZZLE

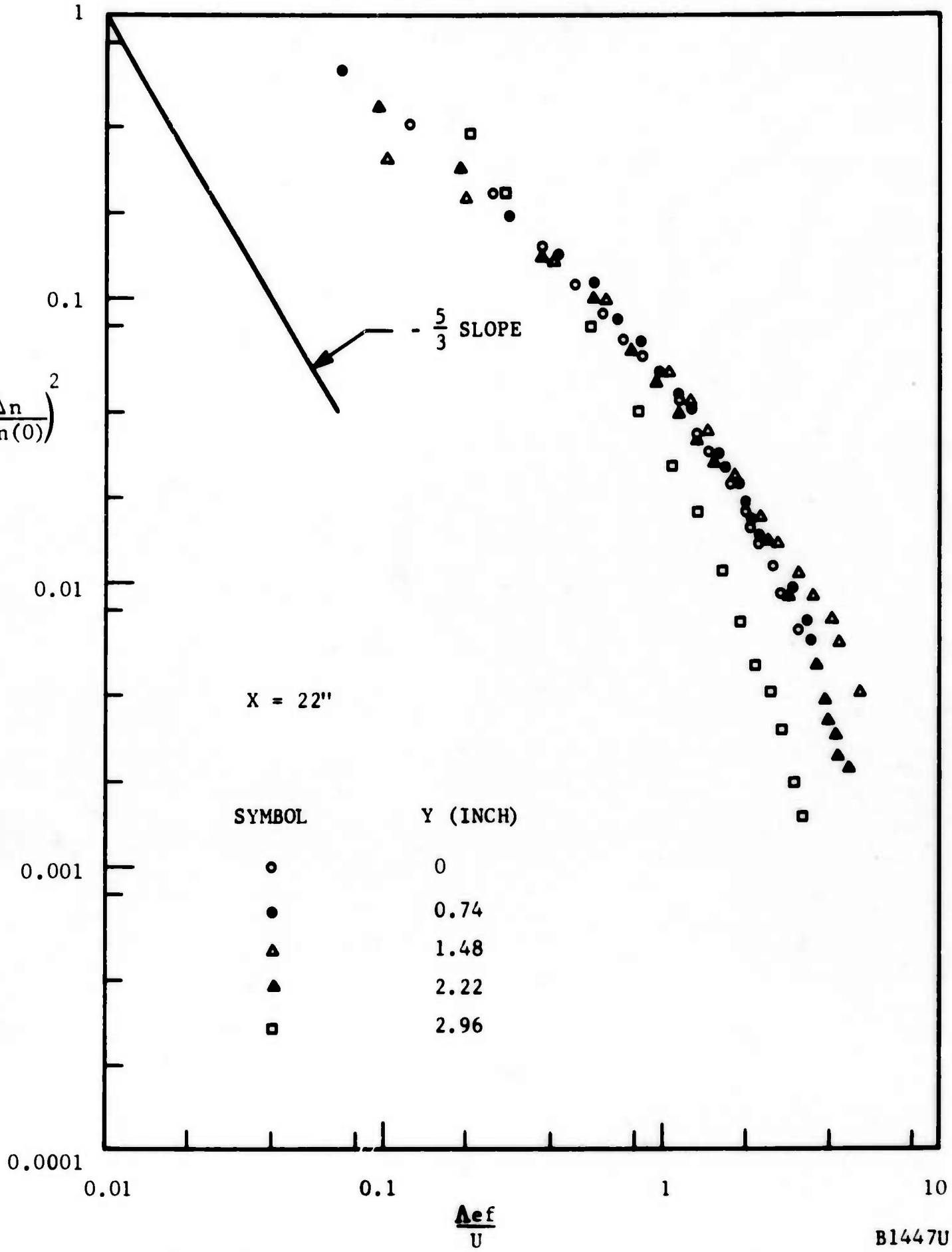

FIGURE 55. NORMALIZED SPECTRAL DENSITY OF ELECTRON FLUCTUATIONS AT 22 INCHES FROM THE NOZZLE

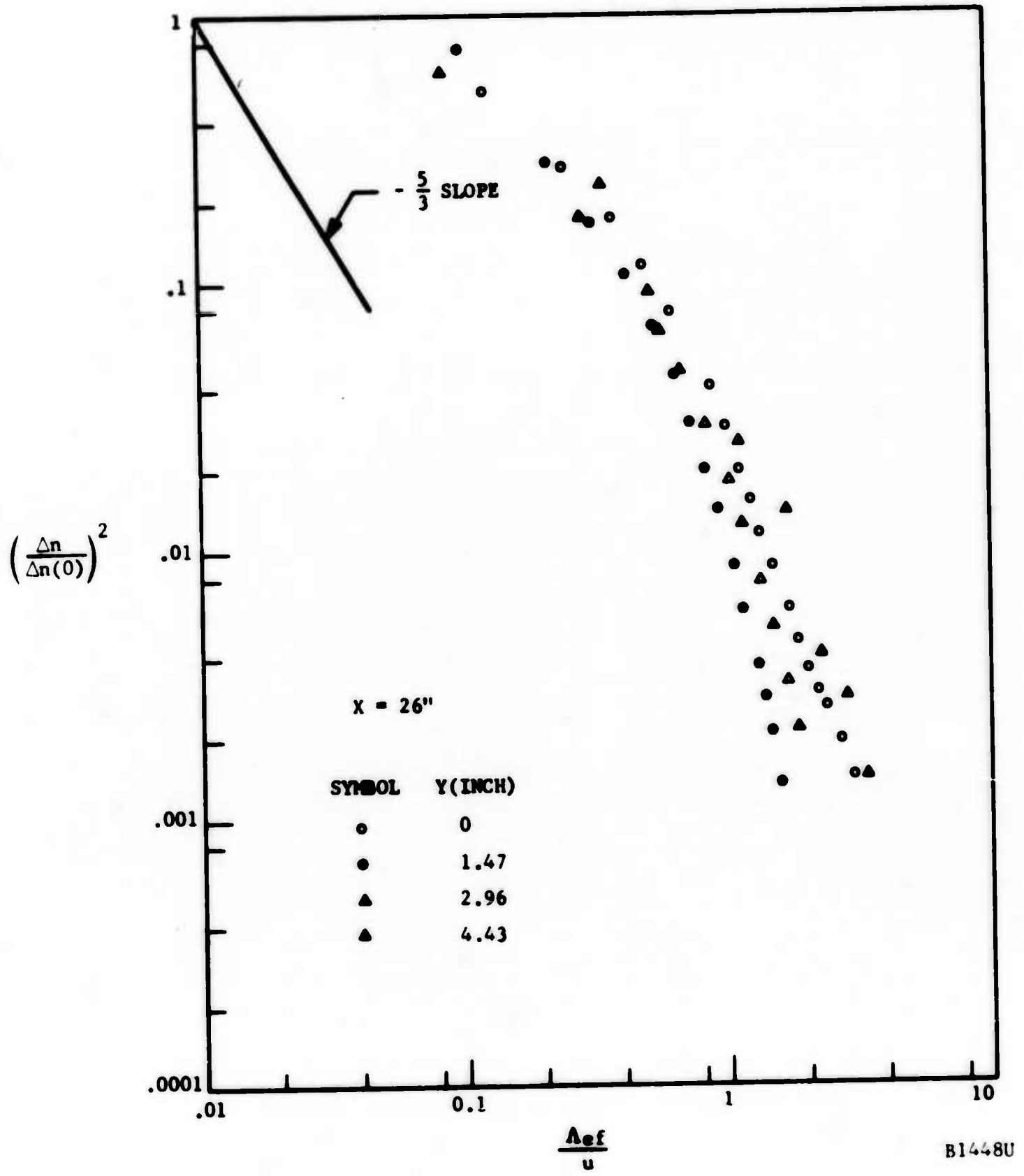

FIGURE 56. NORMALIZED SPECTRAL DENSITY OF ELECTRON FLUCTUATIONS AT 26 INCHES FROM THE NOZZLE

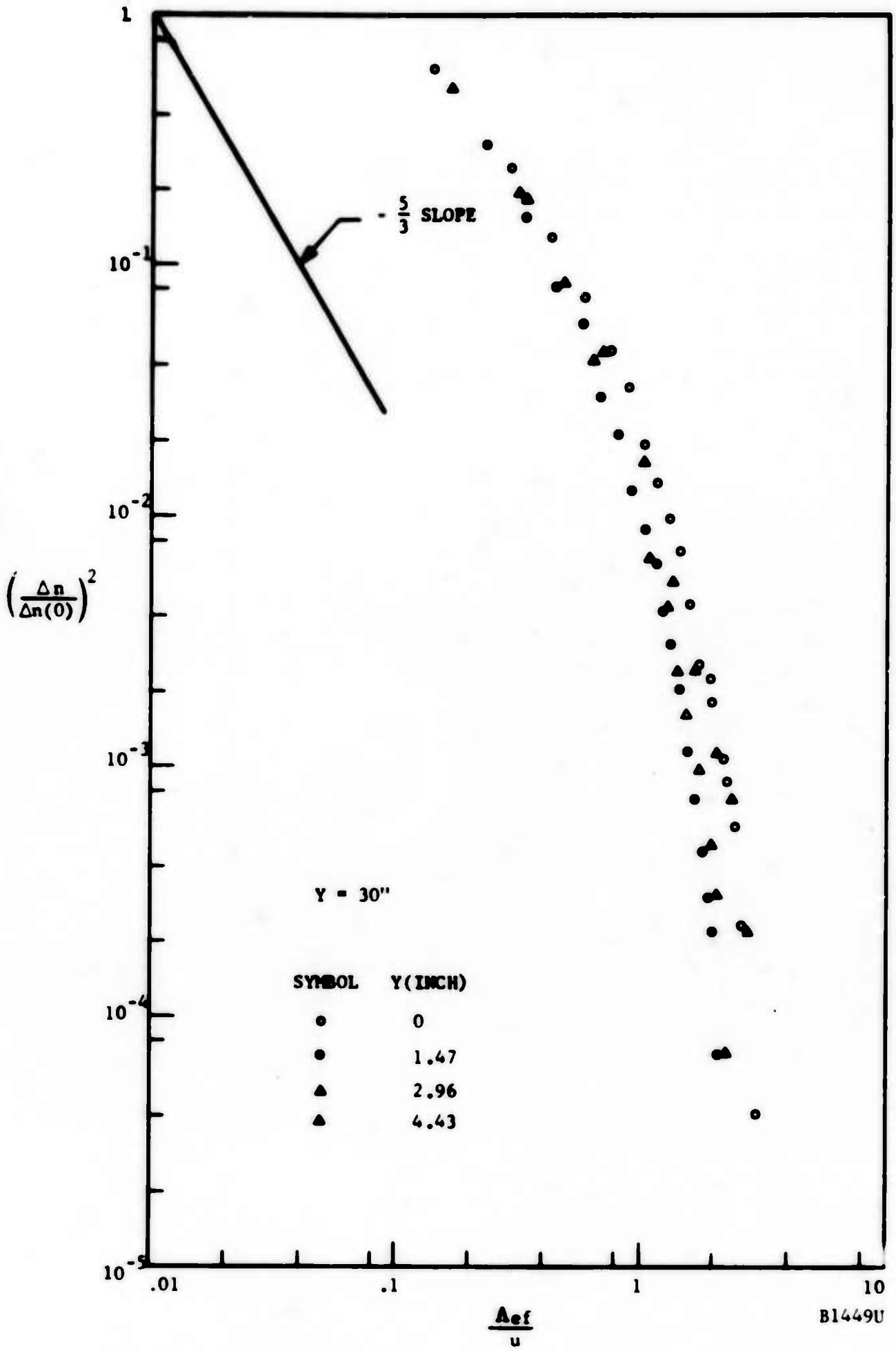

FIGURE 57. NORMALIZED SPECTRAL DENSITY OF ELECTRON FLUCTUATIONS AT 30 INCHES FROM THE NOZZLE

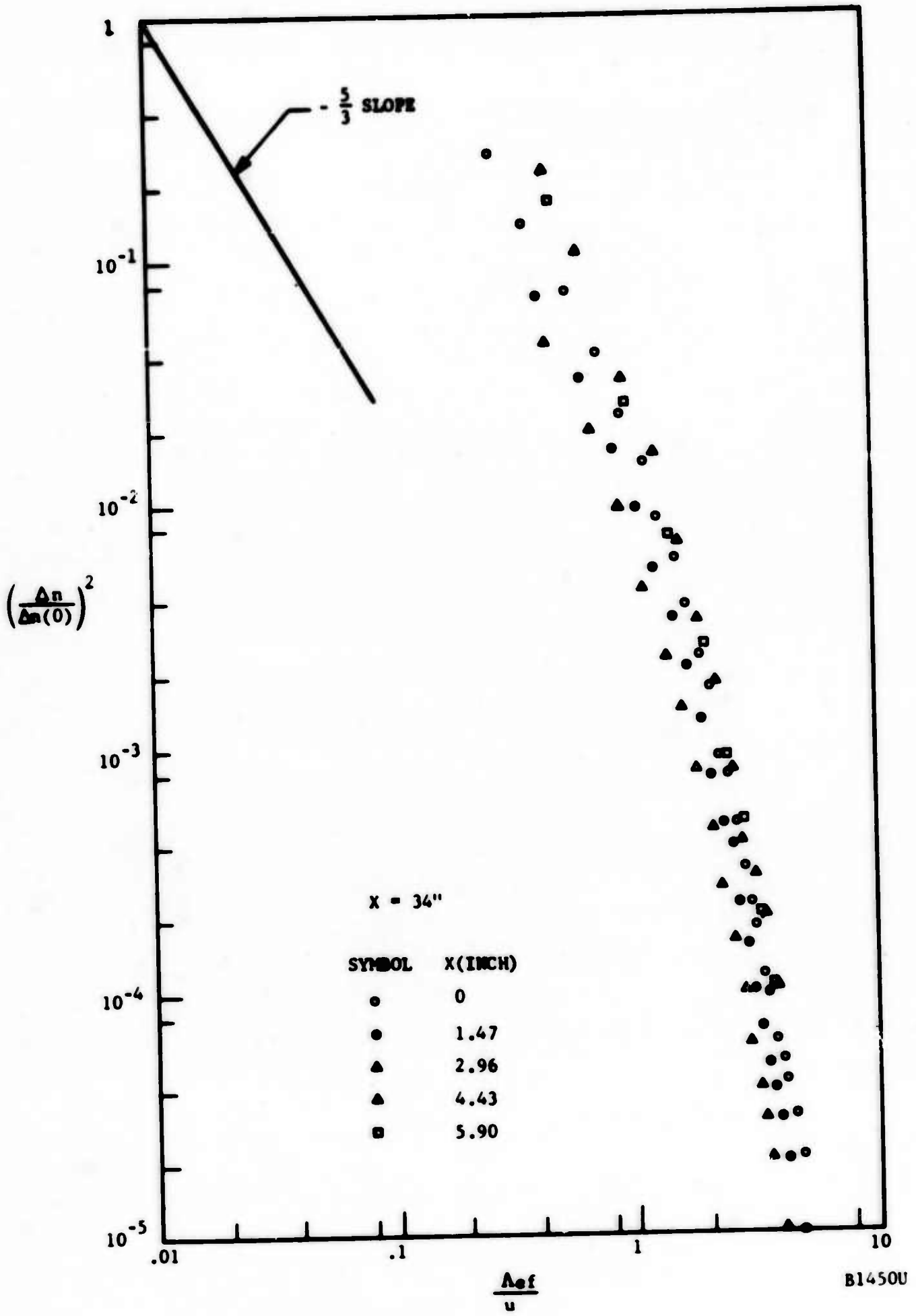

FIGURE 58. NORMALIZED SPECTRAL DENSITY OF ELECTRON FLUCTUATIONS AT 34 INCHES FROM THE NOZZLE

representative spectra at off-axis positions. The ordinate in these graphs is in the square of the electron fluctuation spectral density and is normalized to the asymptotic value at zero frequency. The abscissa $f_N = f\Lambda_e/u$ is the frequency made dimensionless with the local integral scale of electrons Λ_e and the local velocity* u. For example, $f_N = 0.1$ refers to an eddy size ten times larger than the integral scale.

The axis spectra evolve along a characteristic pattern. According to Figure 52, nearer the nozzle the decline of spectral density with frequency is quite gradual, but becomes most precipitous at the four XSTATIONS. At the latter, the spectra appear to become "locked" to an invariant shape, for which

$$\left(\frac{\Delta n}{\Delta n(0)}\right)^2 \sim f^{-4.6}$$

beyond $f_N > 1$. It is further demonstrated by Figure 53 that the change in the spectral shapes occurs mainly between x = 24 inch and x = 28 inch, that is, in the region where the transition from "heterogeneous" to "homogeneous" turbulence occurs.

In the radial direction the change in spectral shapes is generally gradual and small, especially at large X. In the "heterogeneous" portion, the spectral density tends to decrease at the higher frequencies as one moves away from the axis. At larger X a slight but repeatable reversal occurs, so that the higher frequencies are more prominent on the axis and again near the jet edge and less so in between.

It will be noted that in all graphs shown there is no portion of any spectrum where the spectral density decays with the (-5/3) power of frequency as expected for an inertial subrange. This matter will be discussed in detail in Paragraph 4.5.

The longitudinal scales (macroscales) of electron fluctuations are derived in the JEA-II program from the measured spectra by the usual formula:

$$\Lambda_e \equiv \frac{u}{4} \frac{(\Delta n(0))^2}{(\Delta n)^2} \tag{60}$$

Here u is the local velocity and $(\Delta n)^2$ is the total (frequency-integrated) mean-square fluctuation in units of cm^{-6}. The $(\Delta n(0))^2$ is the contribution to $(\Delta n)^2$ which comes from a one-cps-wide passband at f = 0; it has the units $(cm^{-6}) \times (cps)^{-1} = (cm^{-6})\,(sec^{-1})^{-1} = (cm^{-6})\,(sec)$, and has been obtained from the spectral density. Thus, Λ_e has the units of length, as it should. To double-check the validity of $(\Delta n(0))^2$, the program performs the following integration from the measured spectrum $(\Delta n(f))^2$ versus f at each point:

$$EINT = \int_0^\infty (\Delta n(f))^2 \frac{df}{f_B} \tag{61}$$

---

*Since Λ_e is proportional to u also, this nondimensional frequency is independent of u.

where fB is the filter bandwidth (f_B = 200 Hz and 7 Hz, respectively, in the two sets of data obtained). There is generally good agreement between EINT and the mean-square electron fluctuation measured with a voltmeter and shown on Figure 45.

The scales so measured are shown, on the jet axis, on Figure 59. The following observations are made: (1) the data are quite scattered, (2) initially the scale is high in the heterogeneous region, decreases abruptly and increases slowly in the homogeneous region. Because of the scatter a cross-check was performed after the spectral measurements, where $(\Delta n)^2$ and $(n(0))^2$ were recorded separately. The cross-check data (filled-in symbols on Figure 59), gave generally higher values, somewhat less-scattered, than the spectral data. It turns out that the average of both measurements has still lower scatter. Taking the last six XSTATIONS and the point ($x = 0$, $\Lambda_e = 0$) the following straight line was fitted by least squares:

$$\Lambda_e = 0.034\ x \tag{62}$$

and the following proportionality between Λ_e and the transverse scale L of the jet was found:

$$\Lambda_e = 0.47\ L \tag{63}$$

As will be seen below, these formulas come very close to the scale magnitude for jets in the absence of reactions. Nevertheless the scatter, typical of the technique rather than the experiment (see Reference 25), is much worse than expected from, say, two-point correlation measurements.

Radial distributions of electron scales, already shown in last year's report (Reference 6) are deferred until eddy velocity measurements are complete.

4.4 THE GAS TEMPERATURE FLUCTUATIONS

4.4.1 FLUCTUATION MAGNITUDES

The frequency-integrated magnitudes of the temperature fluctuation, together with a discussion of the hot-wire technique, appear in Reference 6, page 181. In the present period additional data were taken to corroborate the earlier results, the latter were analyzed and compared with earlier measurements in other laboratories, and certain improvements in technique were made.

The temperature fluctuations are shown on Figures 60 and 61. On the axis these decrease in a rate nearly proportional to the decrease of the mean temperature "deficit" $T(o)-T_\infty$. In the radial direction the familiar off-axis increase in fluctuation intensity is noted, to a degree dependent

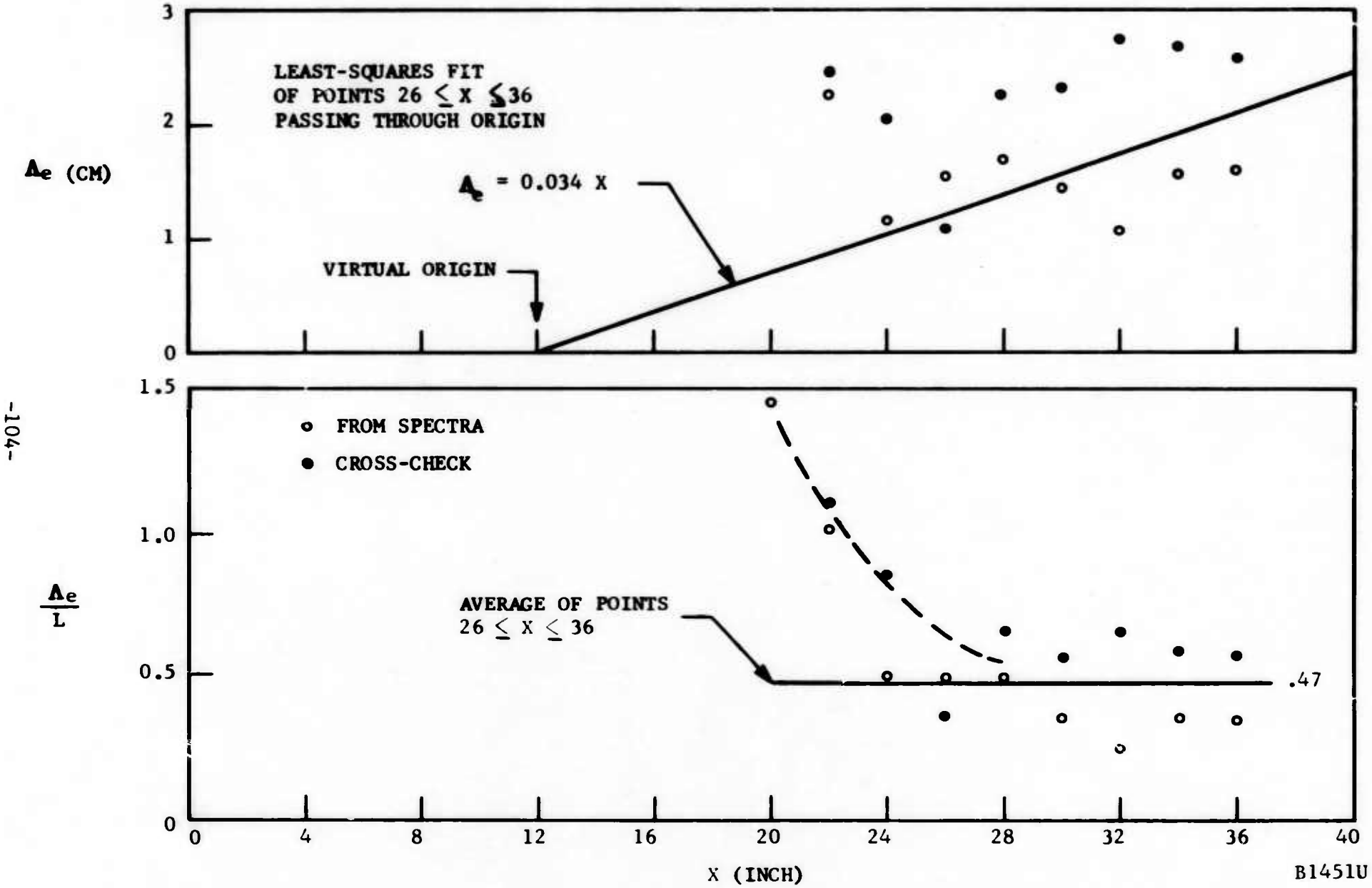

FIGURE 59. AXIAL VARIATIONS OF LONGITUDINAL INTEGRAL SCALE OF ELECTRON DENSITY FLUCTUATIONS GIVEN DIMENSIONALLY (ABOVE) AND NORMALIZED WITH THE TRANSVERSE SCALE (BELOW)

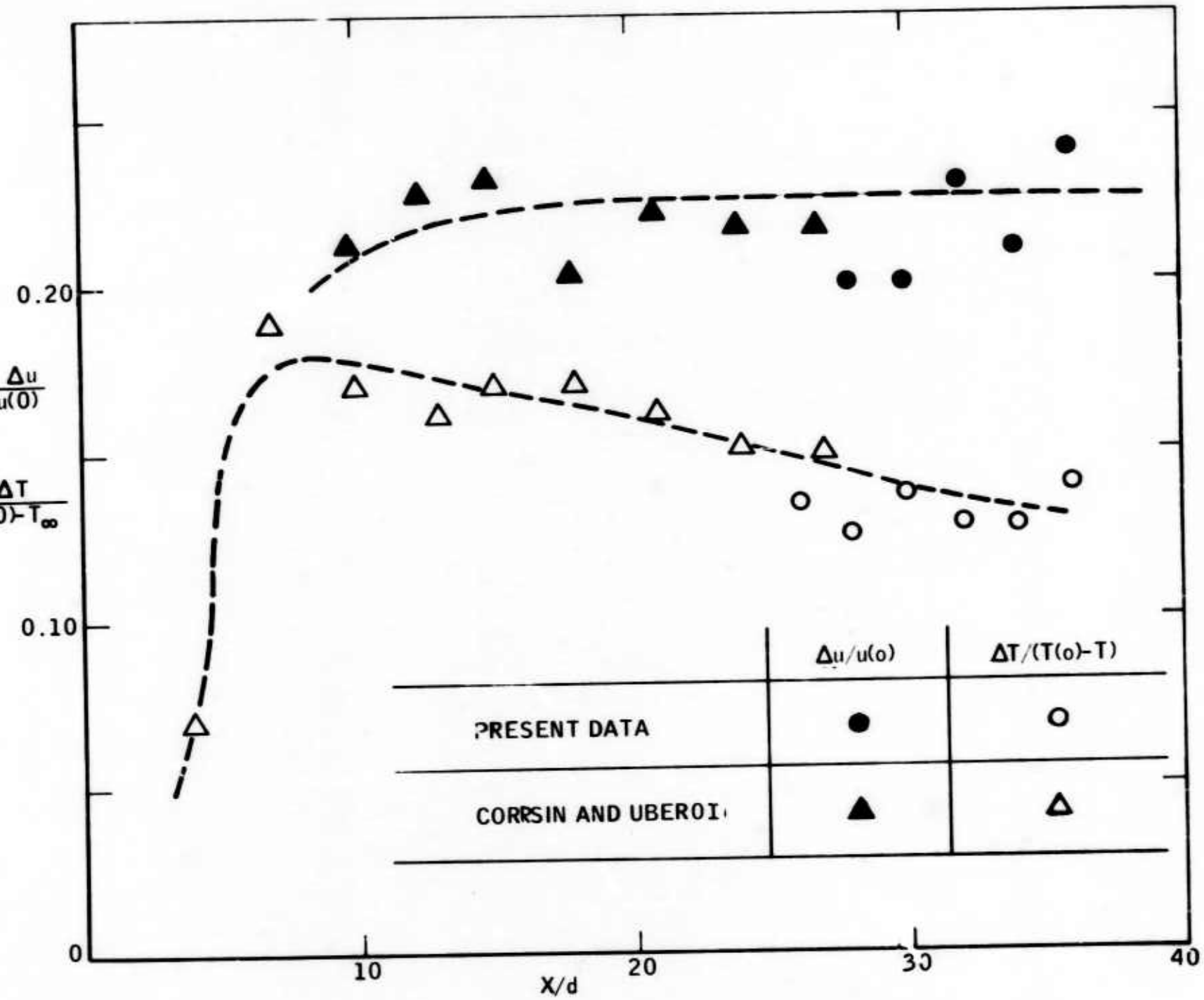

FIGURE 60. AXIAL VARIATION OF VELOCITY AND GAS TEMPERATURE FLUCTUATIONS NORMALIZED WITH THEIR CORRESPONDING AXIS "DEFICITS"

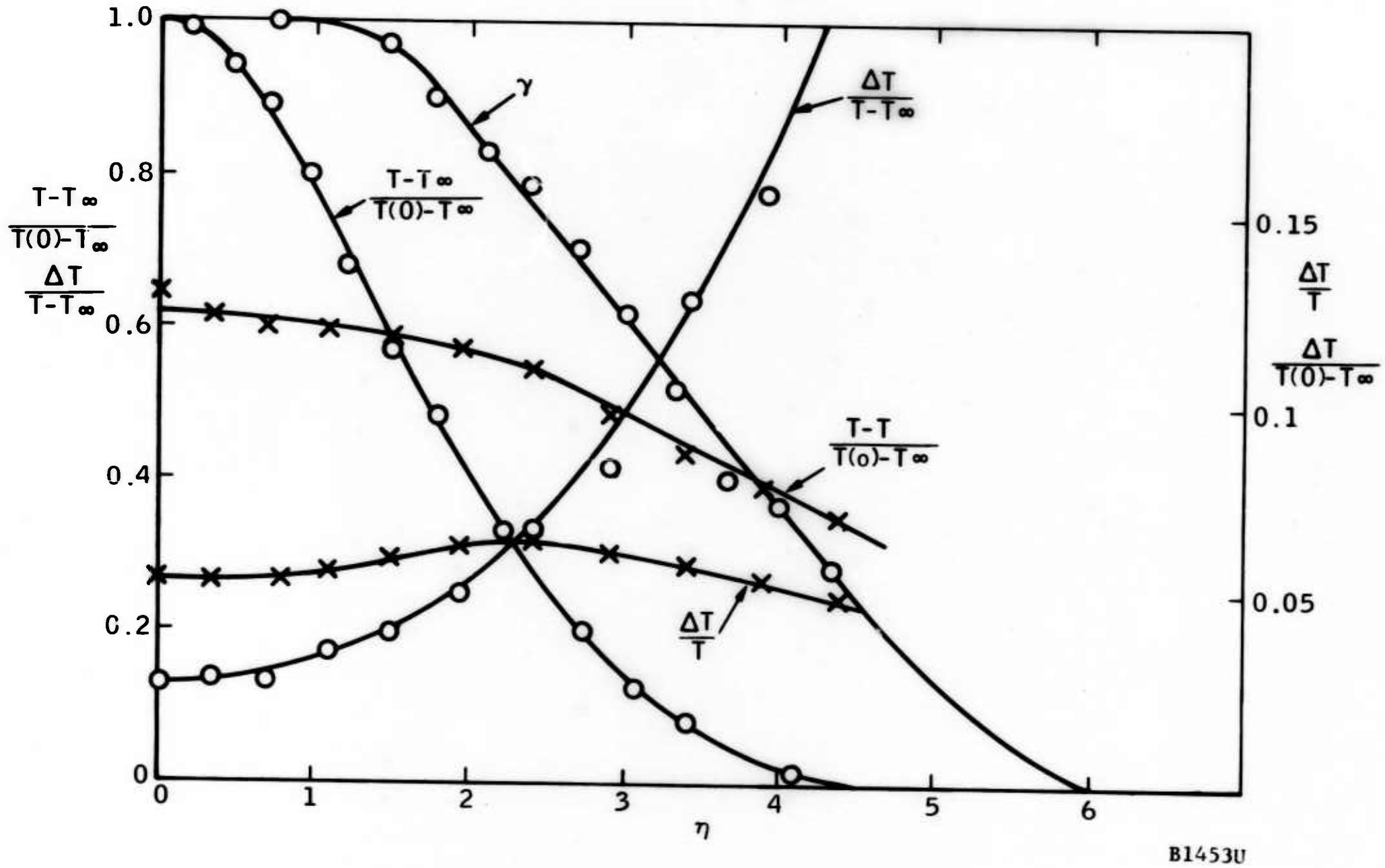

FIGURE 61. TYPICAL RADIAL VARIATIONS OF GAS TEMPERATURE PROPERTIES: MEAN TEMPERATURE, TEMPERATURE INTERMITTENCY, AND TEMPERATURE FLUCTUATIONS

strongly on the manner by which ΔT is normalized.* There are expected similarities between these results and those of Corrsin and Uberoi especially in the ratio $\Delta T/(T-T\infty)$ which attain a value of about 0.15 far from the nozzle. The velocity fluctuations measured with the double (correlation) probe are also shown on Figure 60. These peaks originally, but eventually seem to level out to a value proportional to the axis velocity u(o). Note the close correspondence between our data and the data of Corrsin and Uberoi. However, it should also be added that from a comparison of Corrsin's data with their own, Wygnanski and Fielder (Reference 25) conclude that true self-preservation of the turbulent jet properties occurs quite late - probably in the range from 50 to 100 nozzle diameters.

4.4.2 THE TEMPERATURE FLUCTUATION SPECTRA

During the current period, repeated measurements of the temperature fluctuation spectra were made. In these measurements, as well as in interpreting previous data (see Reference 6, page 183) the main problem encountered dealt with the hot-wire time constant, that is, with the change of time constant as the constant-current wire is traversed through the jet. Because of the changing thermal lag, this time-constant distorts the transfer function (frequency response) of the detecting equipment in a way difficult to detect and compensate for. In practice the probe is first moved outside the jet, the thermal lag measured by the oscilloscope and the compensating amplifier switched on to the proper value of the time constant. After traversing through the jet with this constant setting of compensation, deviations of the time constant from setting could be computed a posteriori and used to correct the readi (this procedure is identical to that used in the supersonic wind-tunnel, (see Paragraph 2.5). This computation is, in turn, made from knowledge of the variation of wire resistance through the jet.

In contrast to results obtained with the wake, the technique is not easy to use in the jet.** For the 0.00014-inch-diameter wire used, a time-constant of 4.5 milliseconds was measured outside the jet. Initially the data showed this value to increase to nearly 7 milliseconds in the flow. Additional data showed that the increase inside the flow was not higher than about 5 milliseconds, and that there was no increase at x = 30, 32, 34 and 36 inches. Anomalies at x = 28 inches were noted and these data are not discussed herein.

The temperature spectra were recorded in two groups. In the frequency band 2-20 kHz, a Hewlett-Packard Model No. 310A Wave Analyzer was used, with its recorder output signal in a 200 Hz band channeled directly into the X-Y plotter. In the range from 0 to 2 kHz, the signal was filtered

---

**The difficulties arise in the problems of heat transfer from cylinders at extremely small Mach and Reynolds numbers (typically) 0.01 and 0.001, respectively). A technical report on this problem is contemplated.

outside the 7 Hz band of a 302A Wave Analyzer, whose restored output is channeled to a vacuum thermocouple and from there to the plotter. Capacitor damping at the plotter input was used for stabilizing the signal further. The circuit is shown in Figure 50.

As with the electron spectra, spectra were recorded every two inches along the jet axis from x = 24 inches to x = 36 inches. The forward limit, x = 24 inches, was chosen for fear that closer to the nozzle the hot-wire would melt. At each XSTATION, spectra were recorded at radial distances spaced about 0.75 inch apart. The data were reduced with the aid of the SPECTR program written for the General Electric Time-Sharing System. An access terminal to this computer is available on an almost full-time basis for this work. Details of the program appear on Appendix B.

A summary of the temperature spectral results appear on Figures 62 through 65. As with the electron spectra, the ordinate in these graphs is normalized with the spectral density at zero frequency. The frequency has been non-dimensionalized with the integral scale Λ_T (which will be discussed later) and the local axial velocity u. Figure 62 shows the evolution of these spectra on the axis, while the other figures show their radial development at selected XSTATIONS. The spectra are remarkably similar to each other and not too different from expectations. They seem to fall into three broad categories:

> Type I: Nearer the nozzle and close to the axis the high-frequency content is intense. The spectrum goes as $f_N^{-5/3}$ where $f_N = \Lambda_T f/u$.
>
> Type II: Over the rest of the entire jet but not too close to the edge the data collapse into a behavior showing a gradual decrease of the spectral density without any distinct regions where it follows the (-5/3) slope. Typically at $f_N = 4$, the spectral content is down a factor of 10 below the Type I spectra.
>
> Type III: At the edge of the jet, the high-frequency content is still lower and the spectral decay somewhat steeper.

The evolution of the spectra from one type into another is best illustrated on Figure 63. It is very clear that on and near the axis one obtains the (-5/3) slope. At Y = 1.47, the "break" away from this behavior (Type I) occurs at earlier frequencies. Also, the departure of the data at the jet edge (Y = 6.64) from the Type II data is obvious. Tentatively, the following conclusion is reached that Type I spectra are associated with the "heterogeneous" jet, where the large electron density fluctuations also occur. Type II are apparently connected with the "homogeneous" jet, where the electron spectra also assume a constant shape.

An attempt was made to compare these data with spectra taken in other jets. Of the latter there is only the data by Corrsin and Uberori (Reference 26).

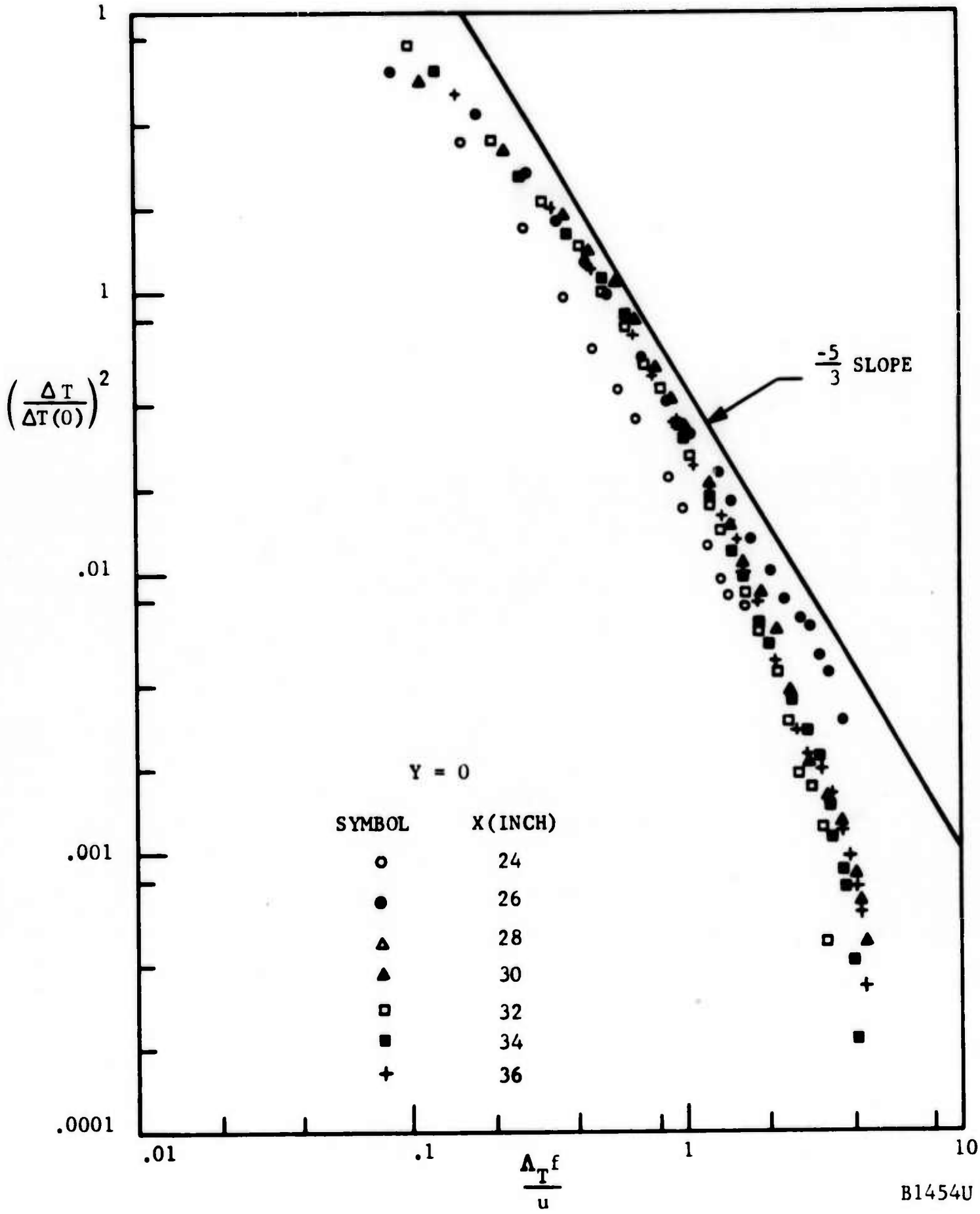

FIGURE 62. NORMALIZED SPECTRAL DENSITY OF THE GAS TEMPERATURE FLUCTUATIONS ALONG THE JET AXIS

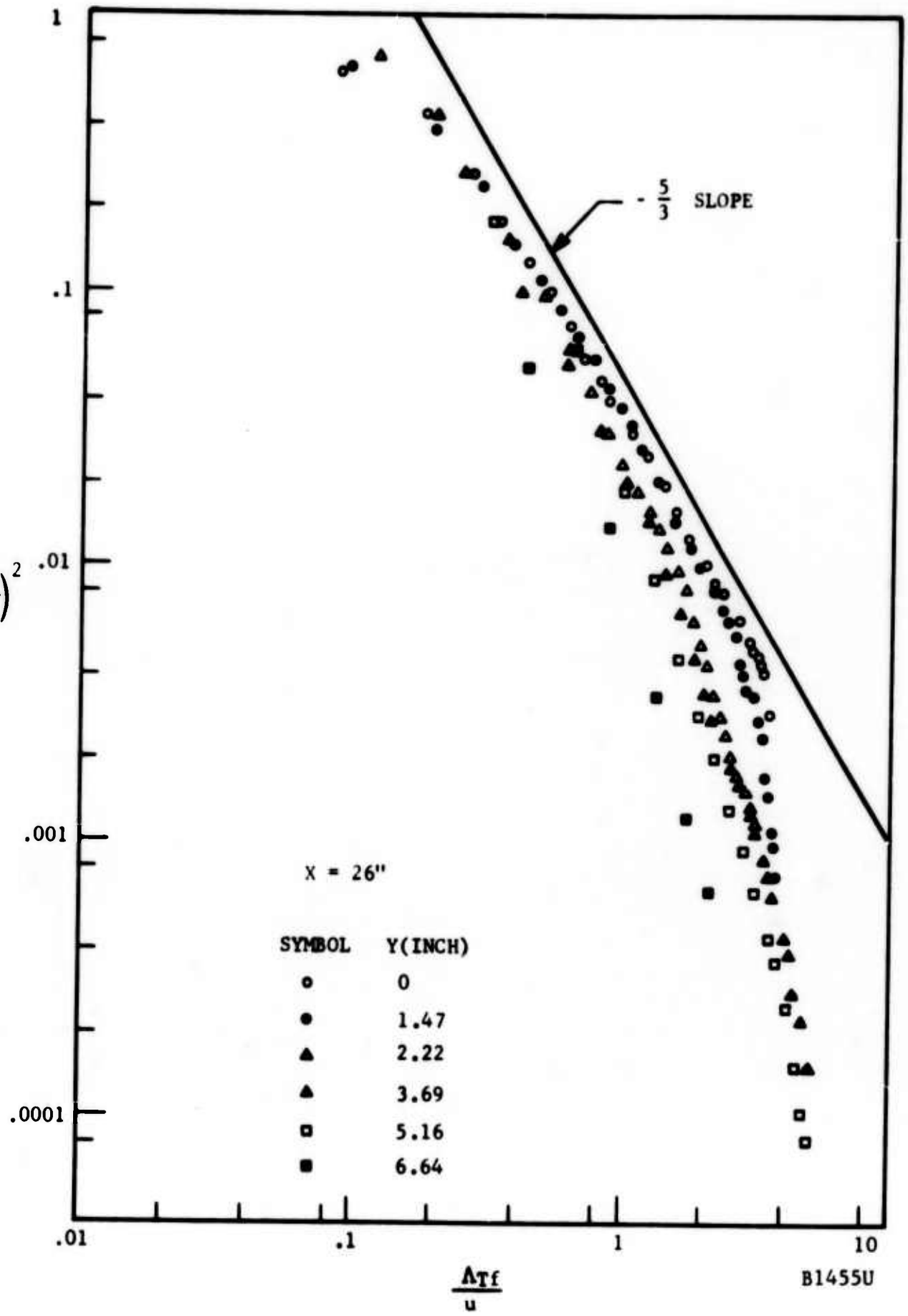

FIGURE 63. NORMALIZED SPECTRAL DENSITY OF THE TEMPERATURE FLUCTUATIONS AT 26 INCHES FROM THE NOZZLE

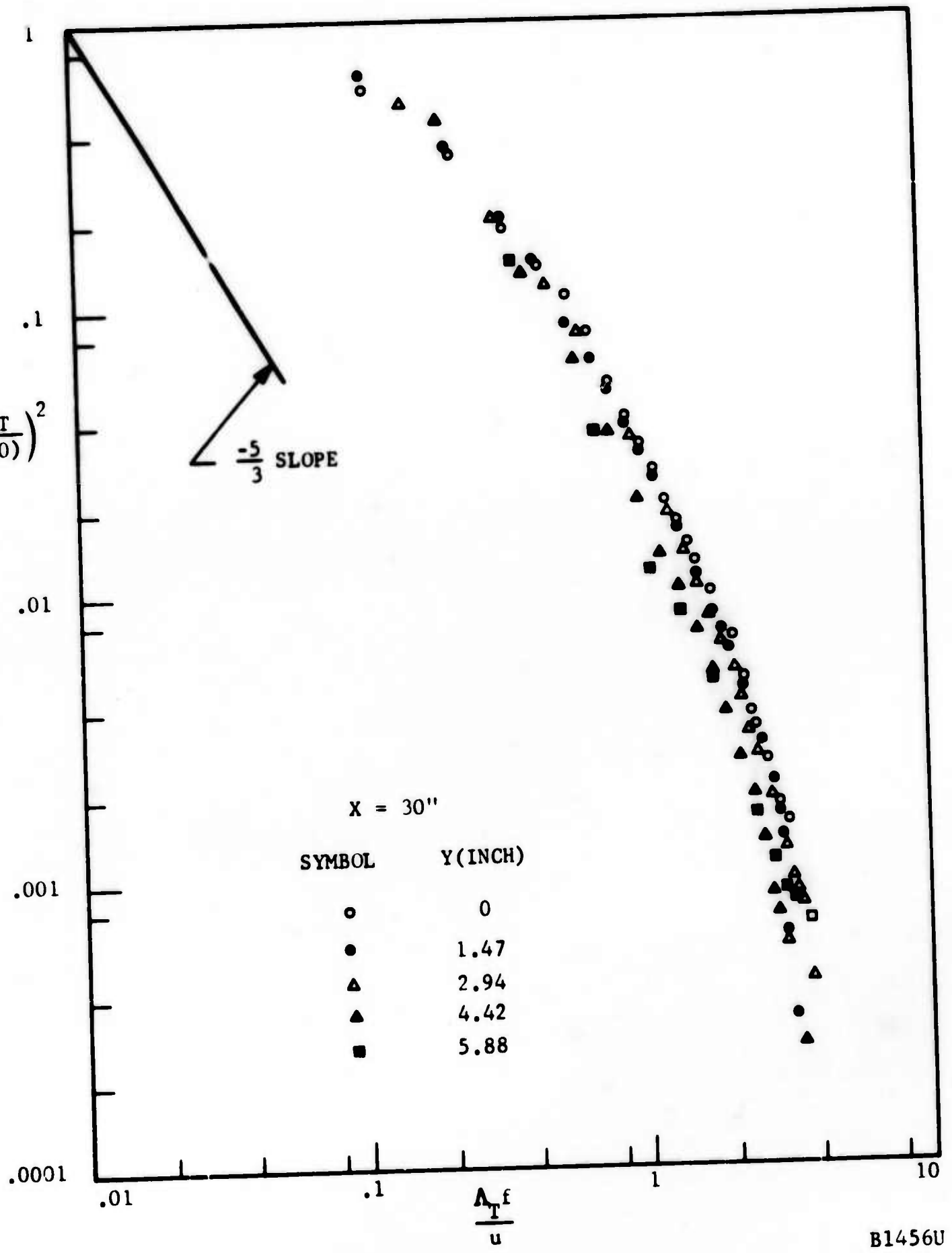

FIGURE 64. NORMALIZED SPECTRAL DENSITY OF THE TEMPERATURE FLUCTUATIONS AT 30 INCHES FROM THE NOZZLE

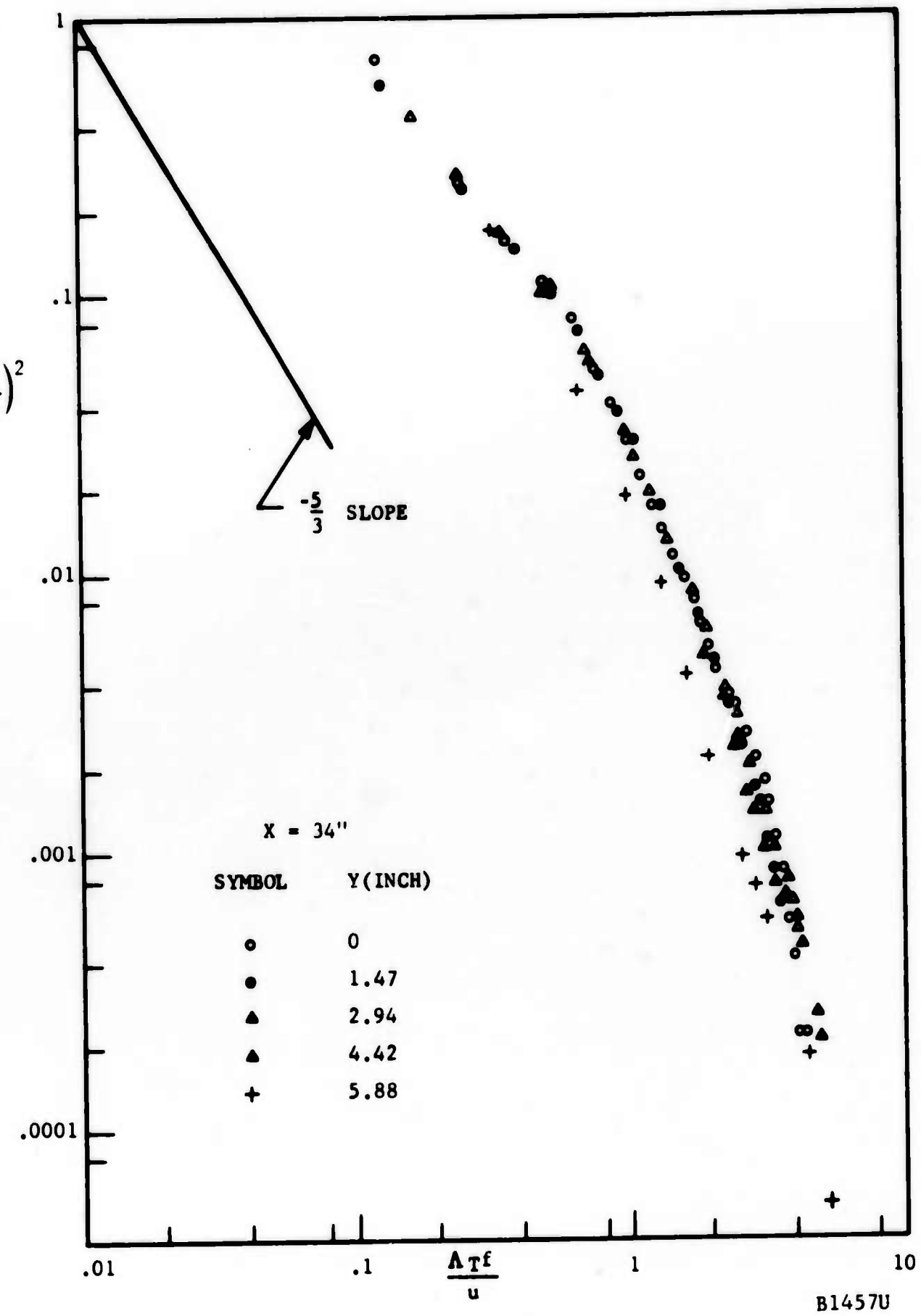

FIGURE 65. NORMALIZED SPECTRAL DENSITY OF THE TEMPERATURE FLUCTUATIONS AT 34 INCHES FROM THE NOZZLE

In Figures 66 and 67, the data are instead compared with more general turbulent flows from which some conclusion about the present data can be drawn. It is seen that the Type I spectra are comparable with high-Reynolds number flows where isotropy is expected. At lower Reynolds numbers grid turbulence compares well with Type II spectra. The interpolation formula giving a dependence f_N^{-2} does not correlate well either type of data.

The longitudinal integral scale of the temperature fluctuations is shown on Figure 68. As with the electron scales the method of measurement, which utilizes the spectra, results in rather large scatter. The scales are supposed to grow linearly with distance, and the least-squares fit by the straight line shown has been forced to go through the virtual origin of the jet (x = 12 inches). The linear growth is actually supported in fact by the near-proportionality of Λ_T with the transverse scale L also shown in Figure 68. The following relations emerge:

$$\Lambda_T = 0.079\ x \tag{64}$$

$$\Lambda_T = 0.79\ L \tag{65}$$

It should be noted that these two relations imply that L = 0.076 x, which is not far from the result found for this jet in Reference 2, page 78:

$$L = 0.079x \tag{66}$$

A comparison of this result with previous experiments is also shown on Figure 68. The excellent experiments of Wygnanski and Fielder (Reference 25) at Boeing, have been chosen for the purpose. These data are chosen because of their clear superiority in measuring technique and abundance of points, and also because they were obtained in the far jet where self-preservation has been attained. The velocity scale growth observed by Wygnanski and Fielder is summarized as follows:

$$L = 0.053\ x \tag{67}$$

$$\Lambda_u = 0.0385\ x \tag{68}$$

In comparing the present scale growth, Equation (64) with the Boeing result, Equation (68), it should be stressed that the present jet is highly heated, whereas the Boeing jet was cold (isothermal). Also, Λ_T is the temperature, whereas Λ_u is the velocity scale. These two differences easily explain the apparent and contrast of Figure 68. First, the present jet is thicker because of the initially very high temperature, an effect predicted and observed by Corrsin and Uberoi (Reference 26) and analyzed by Laufer (Reference 27) and also immediately apparent from Equation (66) and (67). If "corrected" for the temperature effect the scale Λ_u obtained by Boeing would move up by a factor of 0.079/0.053, from Equations (66) and (67):

$$\Lambda = \frac{0.079}{0.053}\ 0.0385\ x = 0.057\ x \tag{69}$$

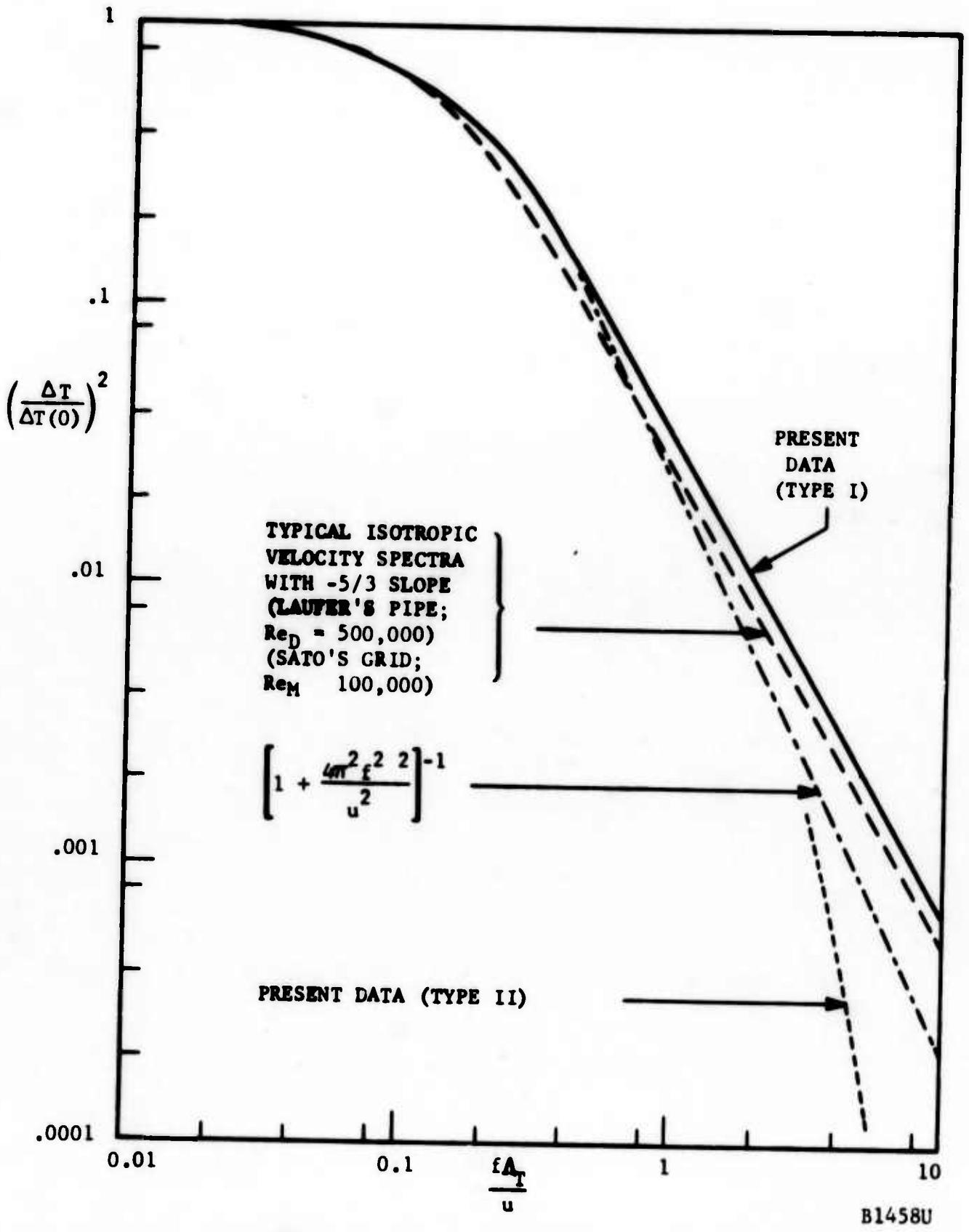

FIGURE 66. COMPARISON OF TYPE I TEMPERATURE SPECTRA WITH HIGH-REYNOLDS-NUMBER ISOTROPIC VELOCITY SPECTRA AND THE KARMAN INTERPOLATION SPECTRUM.

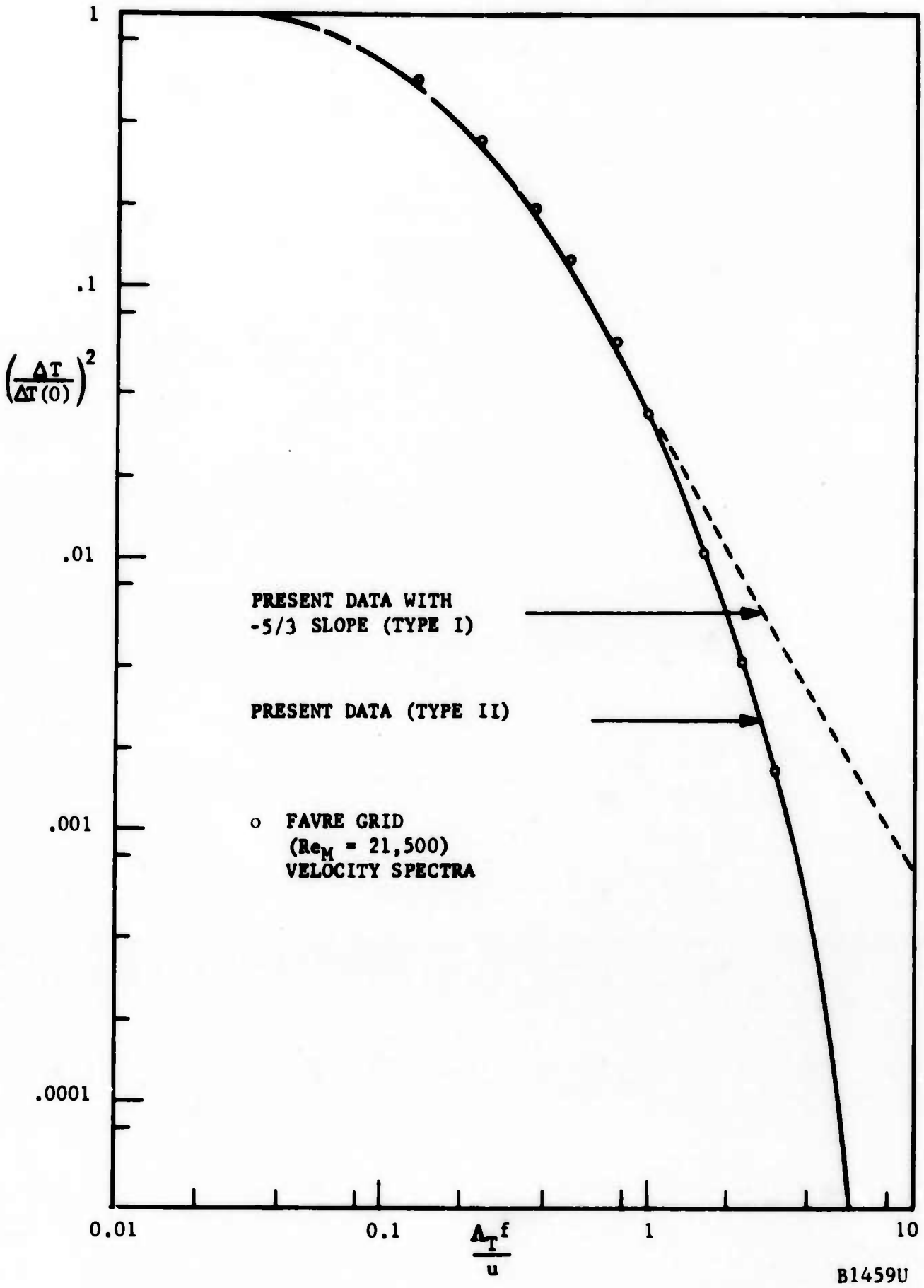

FIGURE 67. COMPARISON OF TYPE II TEMPERATURE SPECTRA WITH TYPICAL LOW-REYNOLDS-NUMBER VELOCITY SPECTRUM

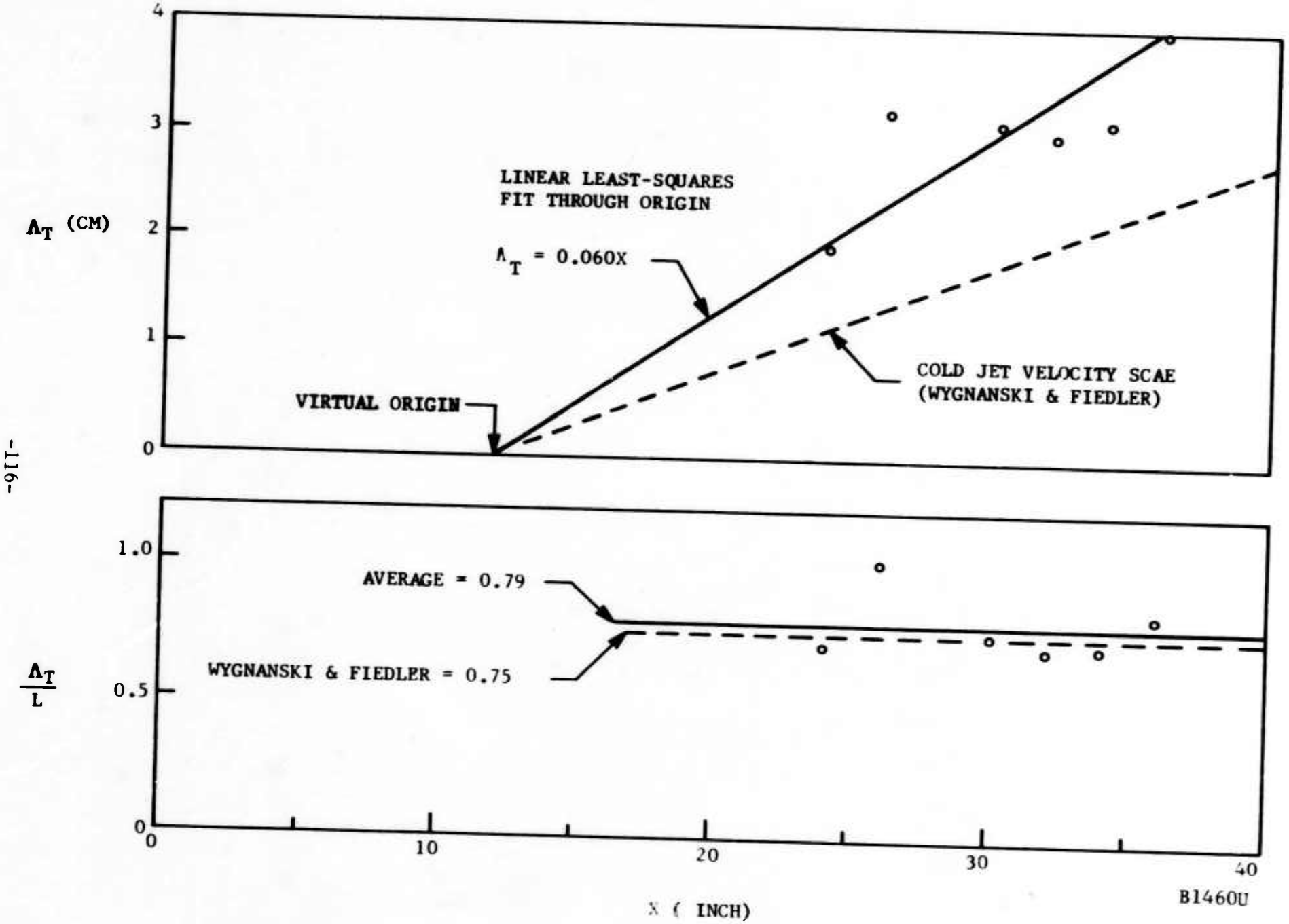

FIGURE 68. AXIAL VARIATIONS OF LONGITUDINAL INTEGRAL SCALES OF THE TEMPERATURE FLUCTUATIONS IN DIMENSIONAL FORM (ABOVE) AND AS NON-DIMENSIONALIZED WITH THE TRANSVERSE SCALE (BELOW)

In the second place, however, it is known (Reference 26) that the temperature scale is smaller than the velocity scale, so that value would again decrease somewhat. In any way, the agreement with the Boeing results is good in view of the scatter in the present data and the possibility that the present jet has not yet become self-preserving.

Two features of Figure 68 are important to the present problem: in both the Boeing and the present jet, Λ/L is about constant at 0.75; in other words, the longitudinal integral scale appears to be a constant fraction of the jet width. Secondly, this ratio is apparently nearly the same in jets and wakes: note that about the same ratio Λ/L was obtained for the WEB experiment (Reference 4, page 42).

4.5 COMPARISON OF ELECTRON AND TEMPERATURE FLUCTUATIONS

As it was noted in the introduction to this section (Paragraph 4.1), the ultimate aim of this task is to establish a connection between electron and temperature fluctuations in a turbulent plasma. Certain results in this direction are now available and are summarized in Figures 69 through 72.

On Figure 69, the ratio $(\Delta n/n)/(\Delta T/T)$ is shown on the jet axis beyond $x = 26$ inch, that is, in the region in which temperature fluctuation data are available. The electron density fluctuation here predominates, especially nearer the nozzle, where ratios as high as 5 are found. Note that at $x = 26$ inches, the jet flow is already beyond the so-called "heterogeneous" stage, implying that ratios much higher than 5 are probable in the range $18 \text{ inch} < x < 26$ inch. Toward the farthest point of the axis ($x = 36$ inch), the ratio approaches unity. Near the jet edge, as Figure 70 shows, the ratio is as high as 10 or so.

Figures 71 and 72 plot the ratio of electron-to-temperature fluctuations resolved according to wave number. Physically, these graphs indicate the desired ratio separately for each eddy size. The two temperature spectral types, I and II, are shown with their electron fluctuation counterparts as drawn from Figures such as 52, 62, etc. The abscissa has been adjusted to wave number units by essentially removing the scales Λ_e and Λ_T from the abscissas of the cited figures. Note that for each eddy size the electron density fluctuation also predominates over the corresponding temperature fluctuation. The ratio of the two is plotted at the bottom of each Figure. The ratio of the relevant fluctuations $\Delta n/n$ and $\Delta T/T$ can then be obtained from the following formulas:

$$\left(\frac{\Delta T(f)}{T}\right)^2 = \left(\frac{\Delta T(f)}{\Delta T(o)}\right)^2 \left(\frac{\Delta T(o)}{\Delta T}\right)^2 \left(\frac{\Delta T}{T}\right)^2 \tag{70}$$

$$\left(\frac{\Delta n(f)}{n}\right)^2 = \left(\frac{\Delta n(f)}{\Delta n(o)}\right)^2 \left(\frac{\Delta n(o)}{\Delta n}\right)^2 \left(\frac{\Delta n}{n}\right)^2 \tag{71}$$

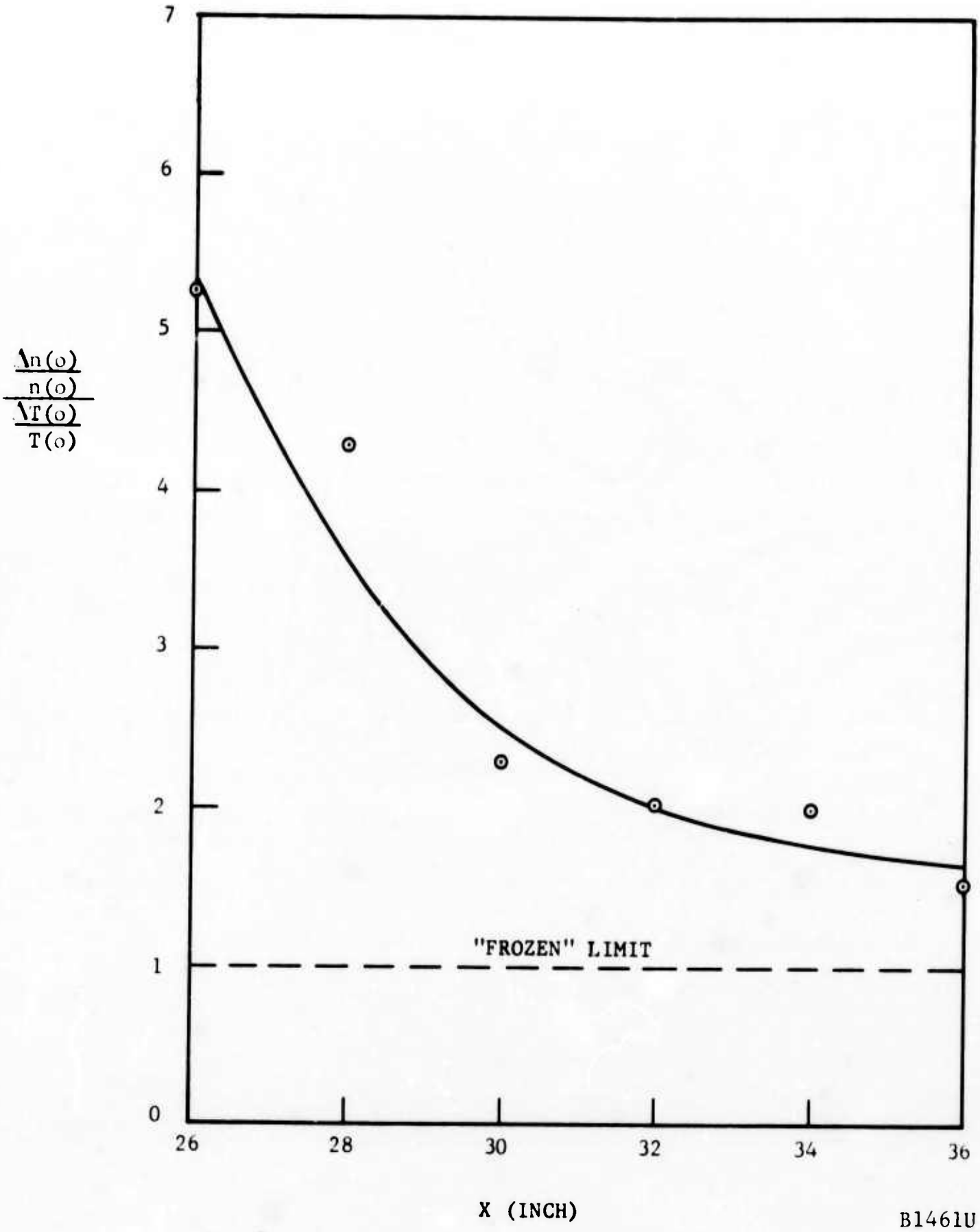

FIGURE 69. AXIAL VARIATION OF THE RATIO OF TOTAL NORMALIZED ELECTRON DENSITY FLUCTUATION TO THE TOTAL NORMALIZED GAS TEMPERATURE FLUCTUATION

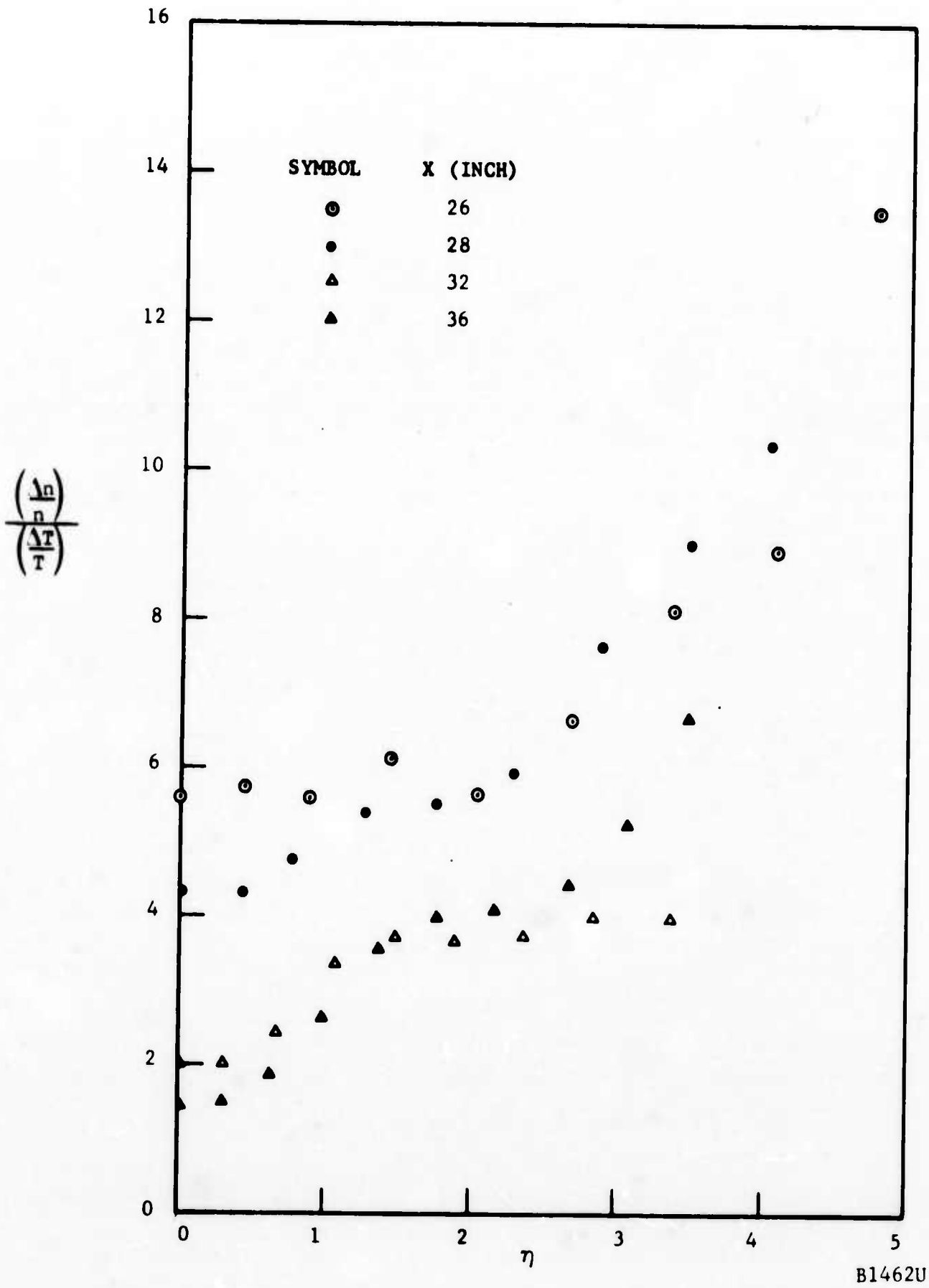

FIGURE 70. RADIAL VARIATION OF THE RATIO OF TOTAL NORMALIZED ELECTRON DENSITY FLUCTUATION TO THE TOTAL NORMALIZED GAS TEMPERATURE FLUCTUATION

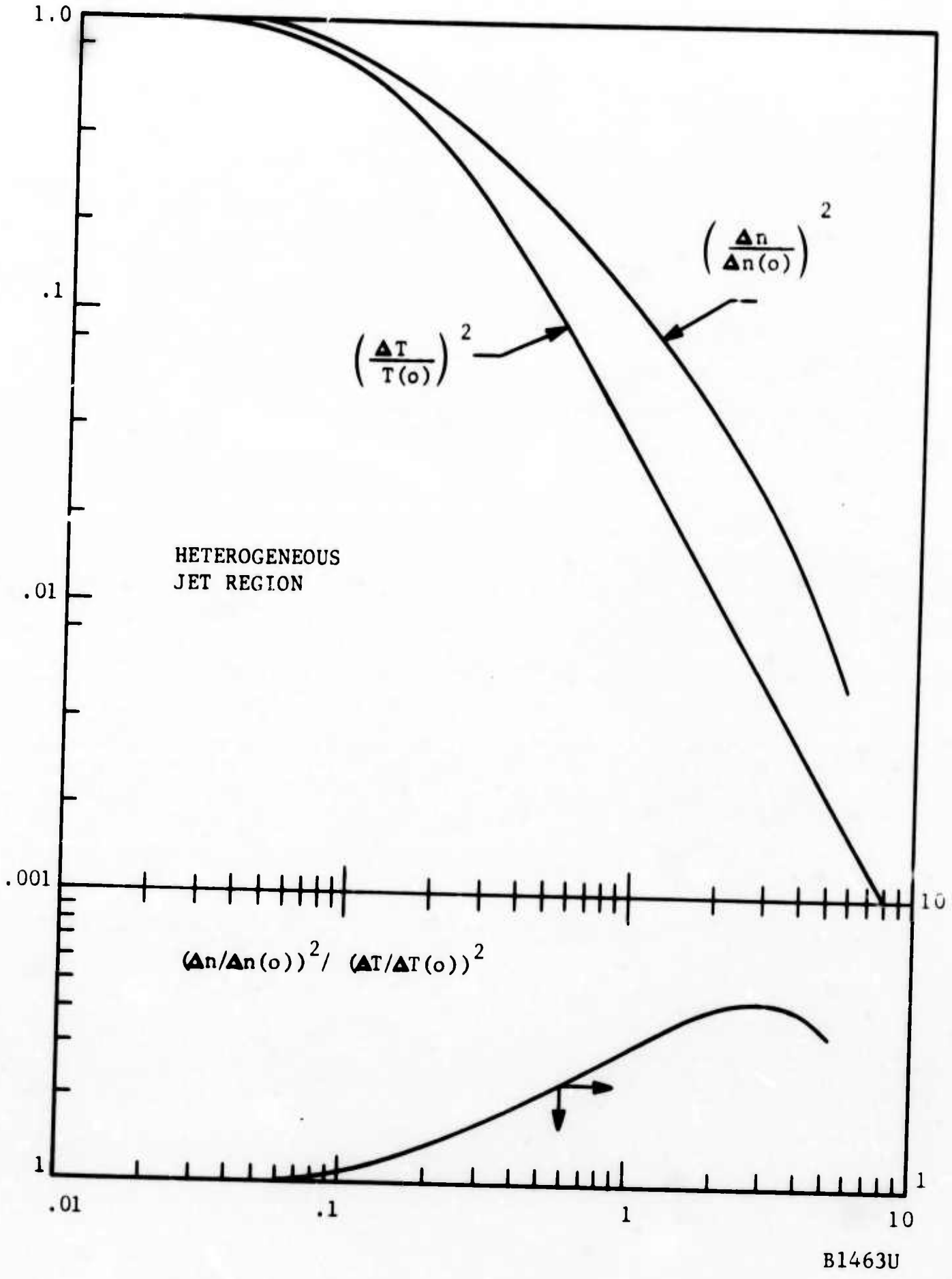

FIGURE 71. RELATIVE IMPORTANCE OF ELECTRON AND TEMPERATURE SPECTRAL DENSITIES IN THE "HETEROGENEOUS" PORTION OF THE JET (ABSCISSA IN ARBITRARY).

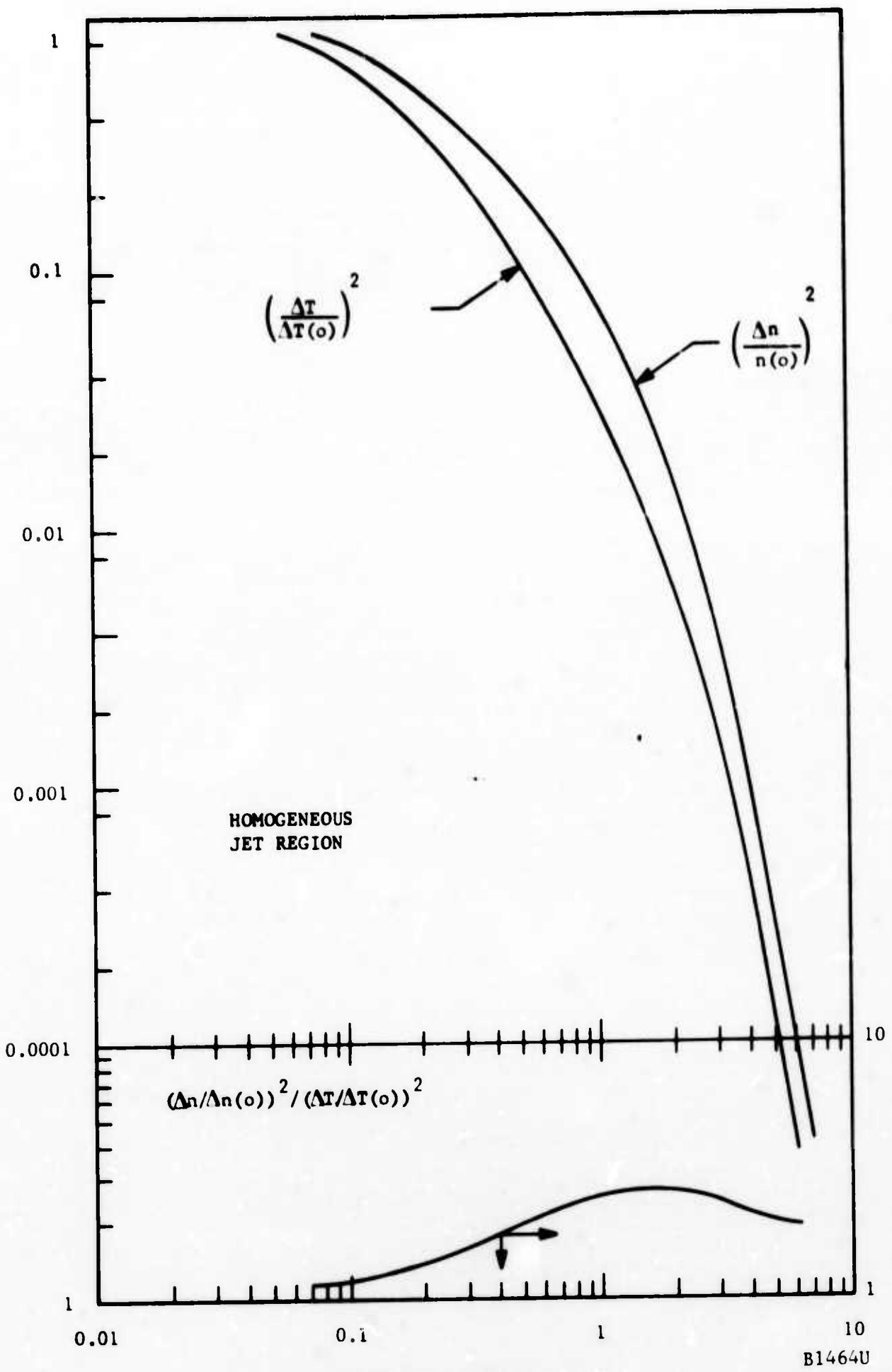

FIGURE 72. RELATIVE IMPORTANCE OF ELECTRON AND TEMPERATURE SPECTRAL DENSITIES IN THE "HOMOGENEOUS" PORTION OF THE JET

Here the nomenclature is as follows:

$\Lambda Q(f)$ Spectral density of Q at frequency f

$\Lambda Q(o)$ Spectral density of Q at zero frequency

ΛQ Frequency-integrated (total) fluctuation of Q

$\overline{Q}$ Mean value of Q.

From the definition of the integral scale

$$\Lambda_Q = \frac{u}{4}\left(\frac{\Lambda Q(o)}{\Lambda Q}\right)^2 \tag{72}$$

we obtain

$$\frac{(\Lambda n(f)/n)^2}{(\Lambda T(f)/T)^2} = \frac{\Lambda e}{\Lambda_T}\left[\frac{\Lambda n(f)/\Lambda n(o)}{\Lambda T(f)/\Lambda T(o)}\ \frac{\Lambda n/n}{\Lambda T/T}\right]^2 \tag{73}$$

The first ratio in the bracket is the one given in Figures 71 and 72, while the second ratio is typically given in Figure 69 on the jet axis. The ratio Λ_e/Λ_T also varies from point to point in the jet, but on the axis it can be given to the degree of accuracy with which Equation (63) and Equation (65) are obtained:

$$\frac{\Lambda_e}{\Lambda_T} = \frac{0.47L}{0.79L} = 0.60 \tag{74}$$

Although this ratio is smaller than unit y, the squared bracket in Equation (73) is considerably higher than unit y under the present flow conditions. Therefore, the electron density fluctuations across the spectrum are numerically larger (occasionally very much so) than the gas temperature fluctuations. Details of these numerical variations with wavenumber and from point in the jet are not yet available.

SECTION V

SUPERSONIC WAKES AT ANGLE OF ATTACK

5.1 INTRODUCTION

Drastic changes are introduced in the wake of a body flying at supersonic speeds when the body is inclined at some incidence (angle of attack) with respect to the flight vector: first, the increased total drag generates an intense inviscid wake, i.e., large gradients appear in the flow surrounding the inner, or turbulent wake. Secondly, these gradients are generally asymmetric about the wake axis. Thirdly, changes in the viscous drag change the characteristics of the viscous wake. Finally, with the generation of lifting forces vortical flows might also appear, causing added complexities to the flow field.

Although the new character of the turbulent wake is hard to assess in these circumstances, its role in the mixing process can be predicted along general lines. Its main complexity should be its growth in and interaction with the asymmetric inviscid wake. The flow thus consists of a "shear layer" contributed to by the inviscid wake, with a superposed wake flow. It is quite clear that the behavior of this composite flow cannot always follow simple wake rules of lateral growth, for example, or of velocity decay, since shear layers and wakes are generally governed by different rules. Thus, a pure shear layer supplies a constant reference velocity scale by definition, while the corresponding velocity scale of the wake decreases with distance. In limiting cases, the competition between the shear-layer-like and wake-like behavior can be foreseen: for small angles of attack and large shear drag, the wake-like behavior should dominate early, while for inclination angles large enough to cause very persistent inviscid asymmetries the flow is probably shear-layer-like for large distances.

The present experiment was designed mainly in a way so as to accentuate this competition between the inviscid and the viscous (turbulent) wake. Calculations of the supersonic inviscid flow behind a two-dimensional slender body at incidence, verified experimentally, showed a considerable persistence of asymmetries in a pattern approaching an ideal shear layer. Thus, the problem is not only relevant, but was done in a way capable of fundamental conclusions on the basic behavior of fluids.

5.2 MODEL AND FACILITIES

This work is performed in the supersonic wind-tunnel at a continuous air flow at Mach 3.0, a stagnation pressure of 730 mm Hg absolute and a total temperature of 39°C. The model consisted of a 0.[illegible]-inch thick, 0.116-inch wide stainless-steel ribbon stretched across the tunnel test-section, identical to that used in the WED experiment (two-dimensional adiabatic wake at zero incidence). A major modification to the model support consisted of the addition of a fixed steel protractor and pointer by which incidence angle could be set and resolved to better than 0.25 degree. Twist-angle resolution is about 0.1 degree. The protractor is shown on Figure 73.

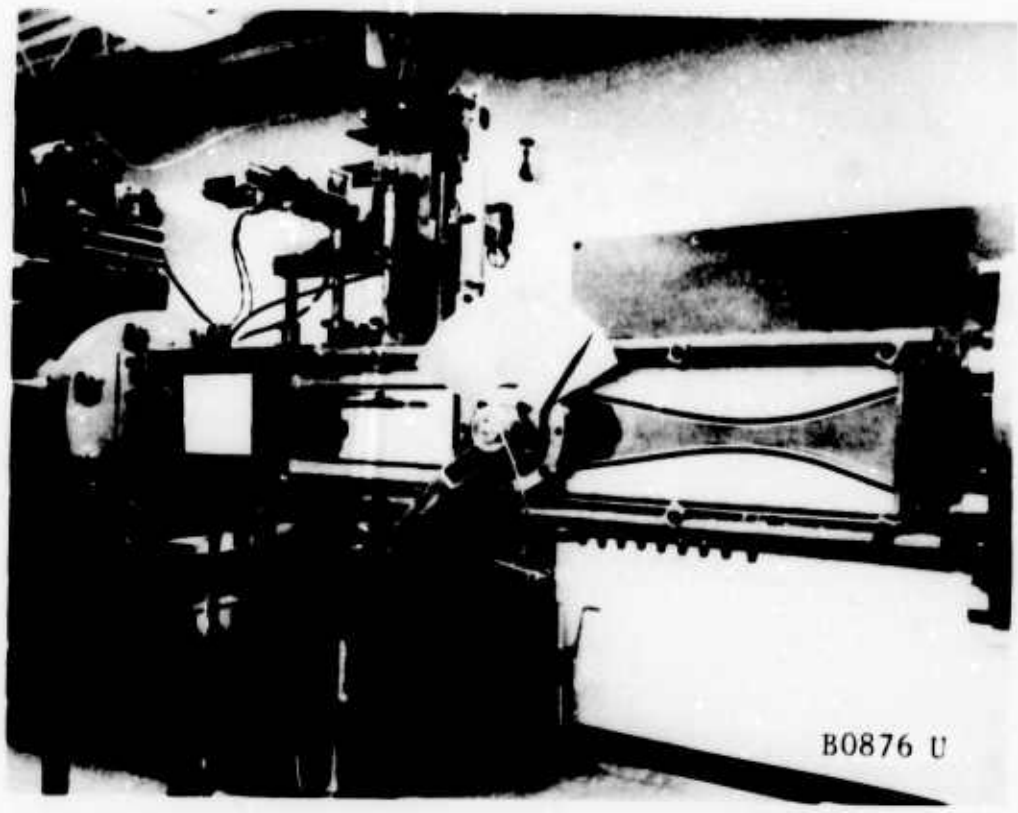

FIGURE 73. EXPERIMENTAL ARRANGEMENT FOR ANGLE-OF-ATTACK STUDIES SHOWING THE PROTRACTOR IN THE TEST SECTION.

Figure 74 shows the arrangement of the model and the nomenclature of the flow phenomena and coordinate axes.

5.3 EXPERIMENT DESIGN

5.3.1 INVISCID WAKE

Detailed calculations of the inviscid wake of the flat plate were made using the method of two-dimensional characteristics at an angle of attack of 20 degrees; for different angles, the flow field should not alter qualitatively from this calculation, provided that the incidence angle for shock detachment at the leading edge (about 34 degrees at this Mach number) is not exceeded. In this calculation the upstream boundary conditions on the windward side were the oblique shock at the leading edge; for the leeward side, the trailing edge shock as modified by the leading-edge expansion fan. Figure 75 shows graphically the result. Attention should be drawn to the two nearly parallel streamlines showning on either side of the wake axis. It turns out that these demark abruptly changing conditions in the sense of flow gradients (not in the sense of flow discontinuities). The net result is that between each of these two streamlines and the axis there appears a uniform "plateau" in flow conditions; the two adjacent "plateau" constitute, then, a shear-layer situation which apparently does not decay much, either in extent or intensity, as one moves downstream. Typical such plateaus are seen in cross-sectional views of Figure 75 shown in Figure 76.

The calculations outlined above demonstrate that, although quantitatively different for the axisymmetric hypersonic wake, an essential feature of the wake-at-incidence problem could indeed be obtained in our wind-tunnel. As described in the following paragraphs, the shear-layer feature was clearly evident from the data collected so far.

5.3.2 CHOICE OF INCIDENCE SETTINGS

To study the effect of incidence, more than one incidence angle should be chosen, if possible; a judicious choice of angles is needed in order to illuminate the effect without undue labor. It is known on theoretical grounds that beyond the detachment angle (34 degrees) the inviscid wake "freezes" to a configuration not very sensitive to angle of incidence. Tests verified this effect, and in the detached case it was decided to work only with $\alpha = 90^{o}$ (plate normal to the stream) so that the blunt-body turbulent wake could at least be probed.

In the pre-detachment range of α wake "pitot maps", such as shown for $\alpha = 0^{o}$ on Figure 30 of Reference 1, were taken at $\alpha = 10^{o}$, 15^{o}, 20^{o} and 30^{o}. Such maps are easy to construct and are invaluable in giving an overall picture of the flow field. Since the shear-layer-like behavior was present in each case, the angles $\alpha = 10^{o}$ and 20^{o} were chosen for further study. In designing the experiment, the farthest downstream distance where measurements can be made is important to know. In the wind-tunnel this distance is shortened when the model is pitched because of the earlier reflection of the strengthened shocks from the tunnel wall. In the present set-up the farthest downstream distance for $\alpha = 0^{o}$, 10^{o}, 20^{o} and 90^{o} is 7.8 inches,

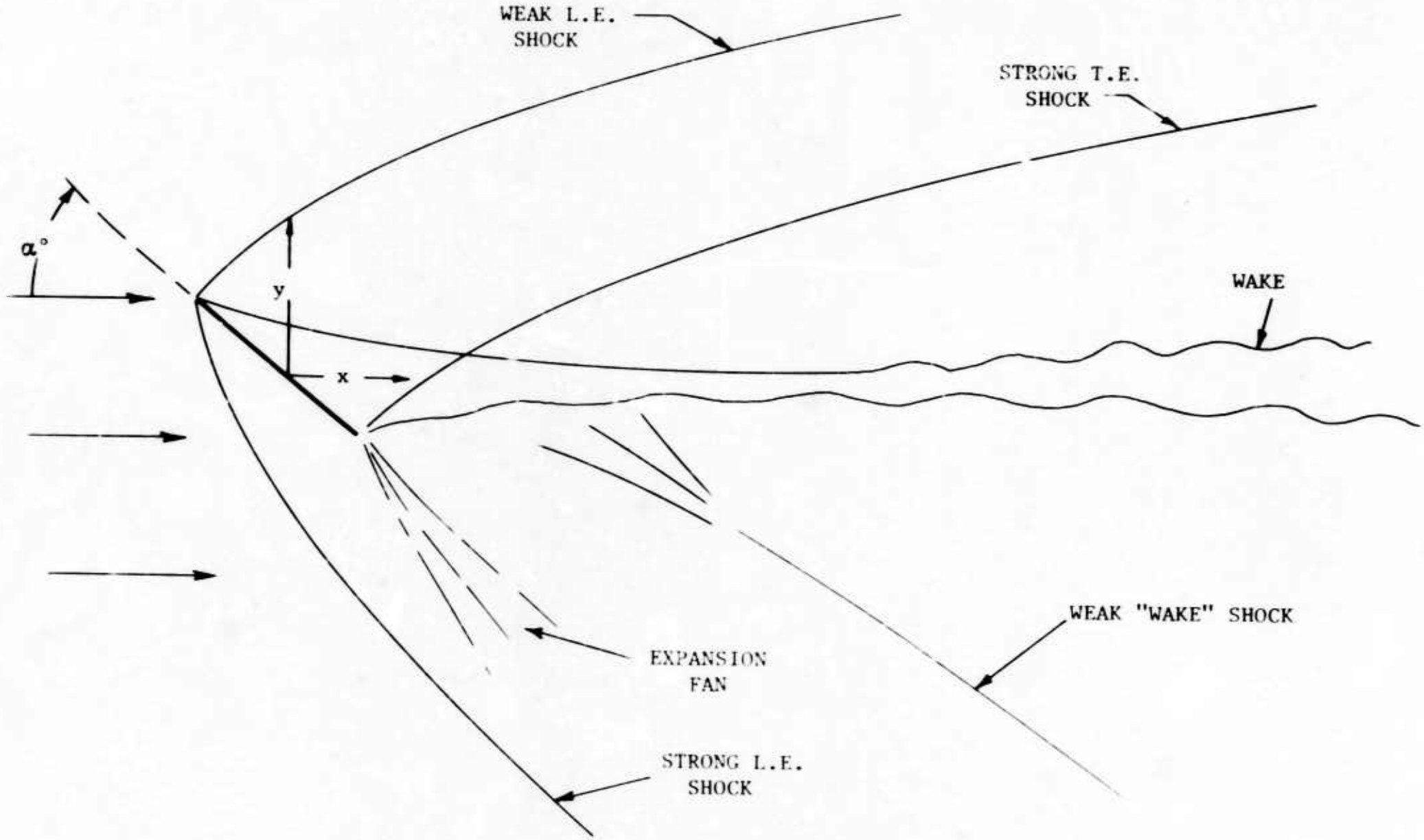

B0877 U

FIGURE 74. NOMENCLATURE AND FLOW FIELD FOR ANGLE-OF-ATTACK EXPERIMENTS (WEF)

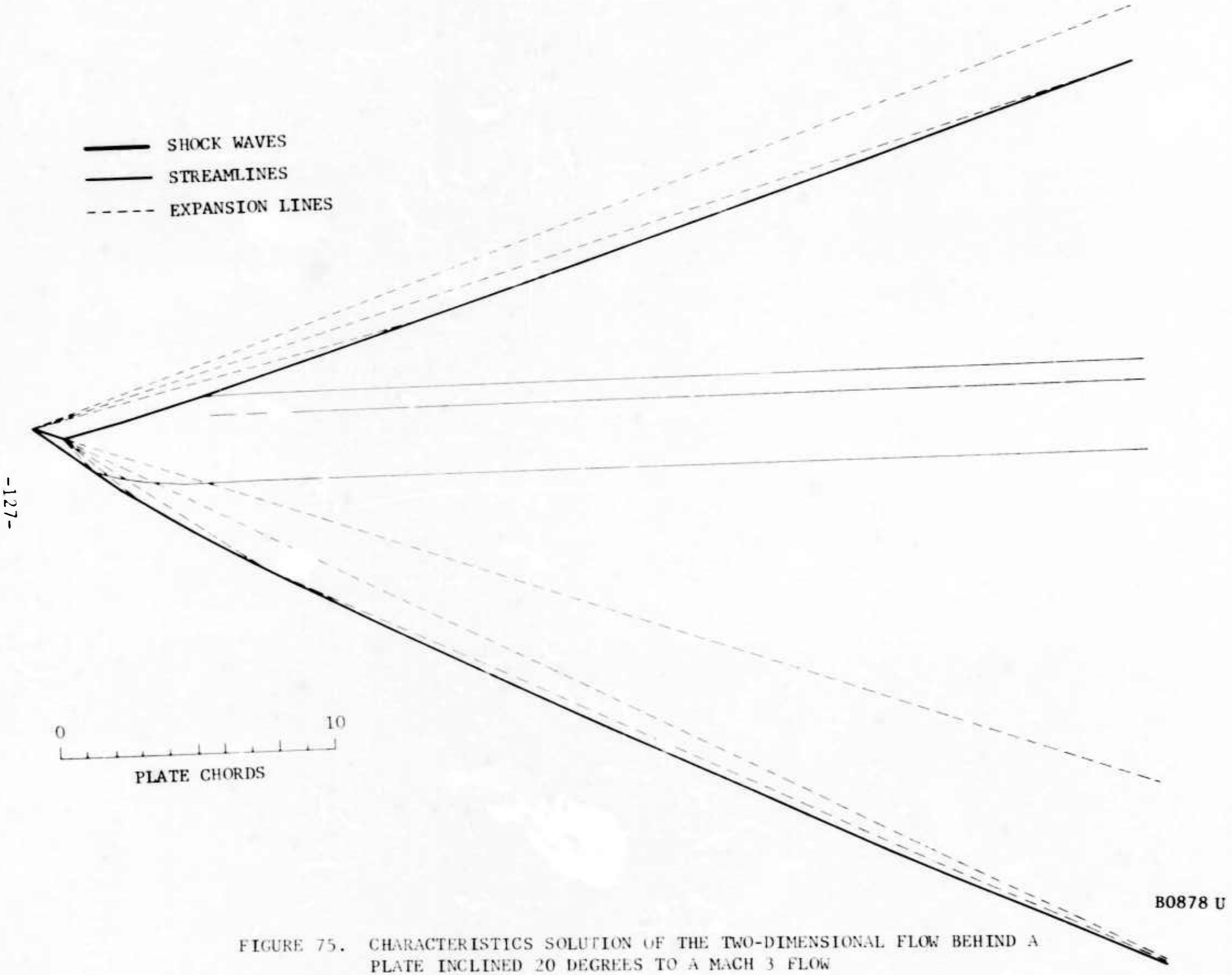

FIGURE 75. CHARACTERISTICS SOLUTION OF THE TWO-DIMENSIONAL FLOW BEHIND A PLATE INCLINED 20 DEGREES TO A MACH 3 FLOW

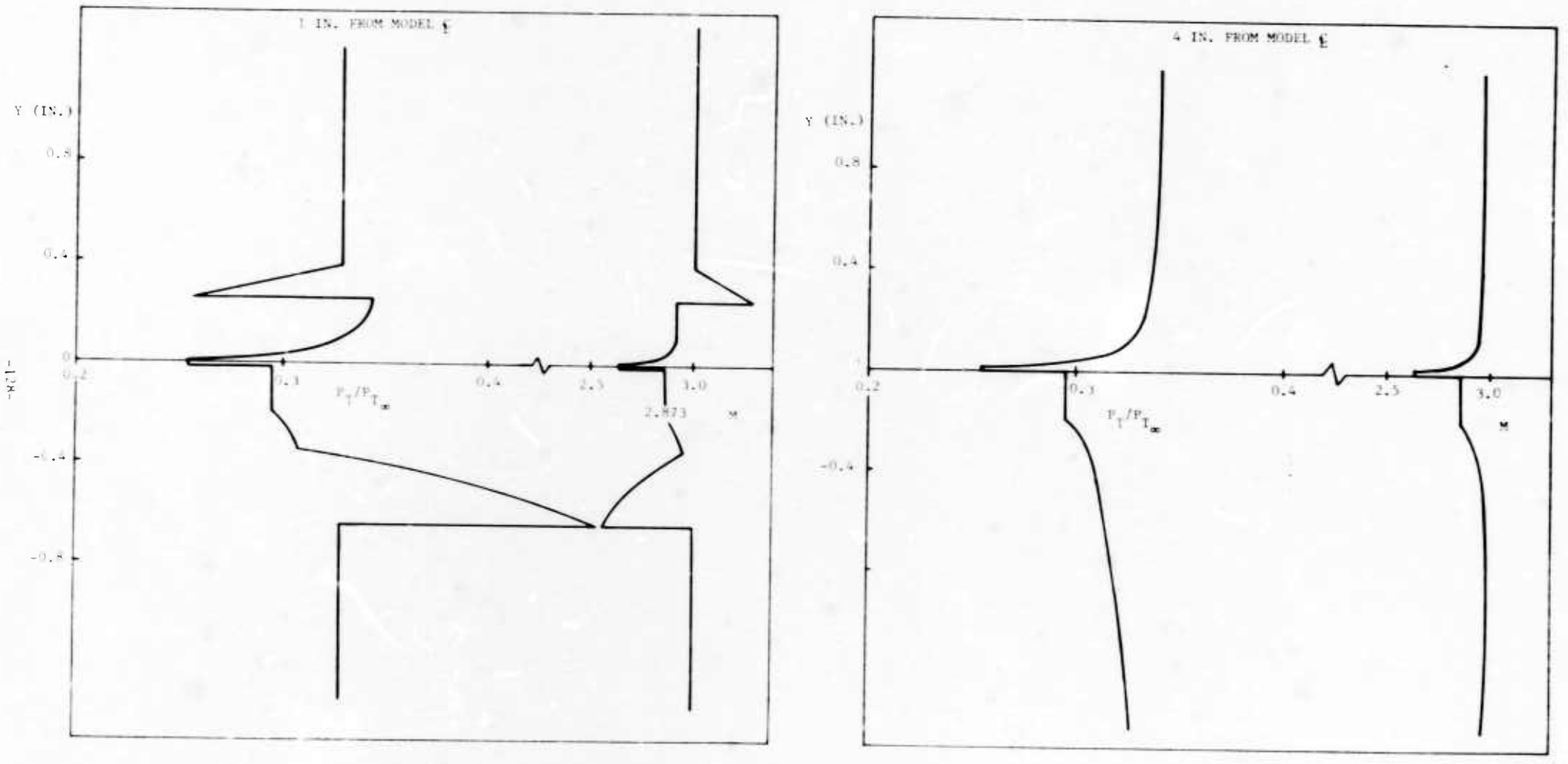

B0879U

FIGURE 76. PREDICTED FLOW PROPERTIES AT SELECTED DISTANCES BEHIND THE MODEL AT 20-DEGREE INCIDENCE.

7 inches, 6.2 inches and 4.7 inches, respectively. Note that for $\alpha = 0^{o}$, a distance of 7.8 inches implies a distance of about 1,800 virtual body diameters.

5.4 DIAGNOSTIC INSTRUMENTATION

The diagnostic tools used for this experiment were identical to those employed for the WED (see Reference 1). The 0.00005 inch diameter Pt 10 percent Rh hot-wire used for this work managed to stay intact through the mean-flow and turbulence measurements and through most of the spectral measurements. This remarkable wire survived 45 calendar days of use, during which time it was operated for about 70 hours in supersonic flow. Through frequent oven- and flow-calibrations small changes in its characteristics could be monitored and accounted for.

5.5 PROCEDURE

This experiment was designated WEF (Wake Experiment F) and the $\alpha = 10^{o}$, 20^{o}, and 90^{o} sub-experiments were designated WEF-10, WEF-20, and WEF-90, respectively. As done with the WED experiment, the distance between the model mid-chord and the end (farthest downstream) point was marked by X-stations spaced by 0.300 inch increments. Continuous analog traverses were taken at each X-Station with the pitot and static probes and the hot-wire anemometer, the latter operated either in the mean-flow or the turbulent mode. From these data the mean and turbulent properties can be extracted.

5.6 RESULTS OF MEASUREMENTS

As already mentioned, the actual viscous wake measurements were preceded by tracing the inviscid wake in order to observe the overall flow field and to examine the existence of the "shear-layer" effect. Figure 77 compares a typical pitot traverse with the pitot pressure expected from the characteristics computation shown on Figures 75 and 76 for $\alpha = 20^{o}$. It is obvious from the measurement that two shocks appear on each side of the inviscid wake, instead of one as given by the characteristics method. On the windward side, aside in addition to the bow shock at the leading edge, a second shock is thought to originate in the recompression region of the wake "neck", as illustrated tentatively on Figure 74. In the leeward side a shock appears, of course, at the model leading edge in addition to the expansion fan.* Nevertheless the agreement shown on Figure 76 between the calculated and measured pitot pressures is adequate; both demonstrate, in fact, the "plateaus" on either side of the turbulent wake.

A second preliminary measurement made before detailed studies were attempted concerned the existence of turbulence. Qualitative traverses with the hot-wire showed that angle of attack did not inhibit the appearance of turbulence in the inner wake. Proceeding to the latter, Figure 78 shows pitot-pressure traces at typical X-Stations for all three experiments, i.e.,

*Photography of the two-dimensional model itself is impossible because of obstructions. The identification of the additional two shocks is left to reasonable conjecture.

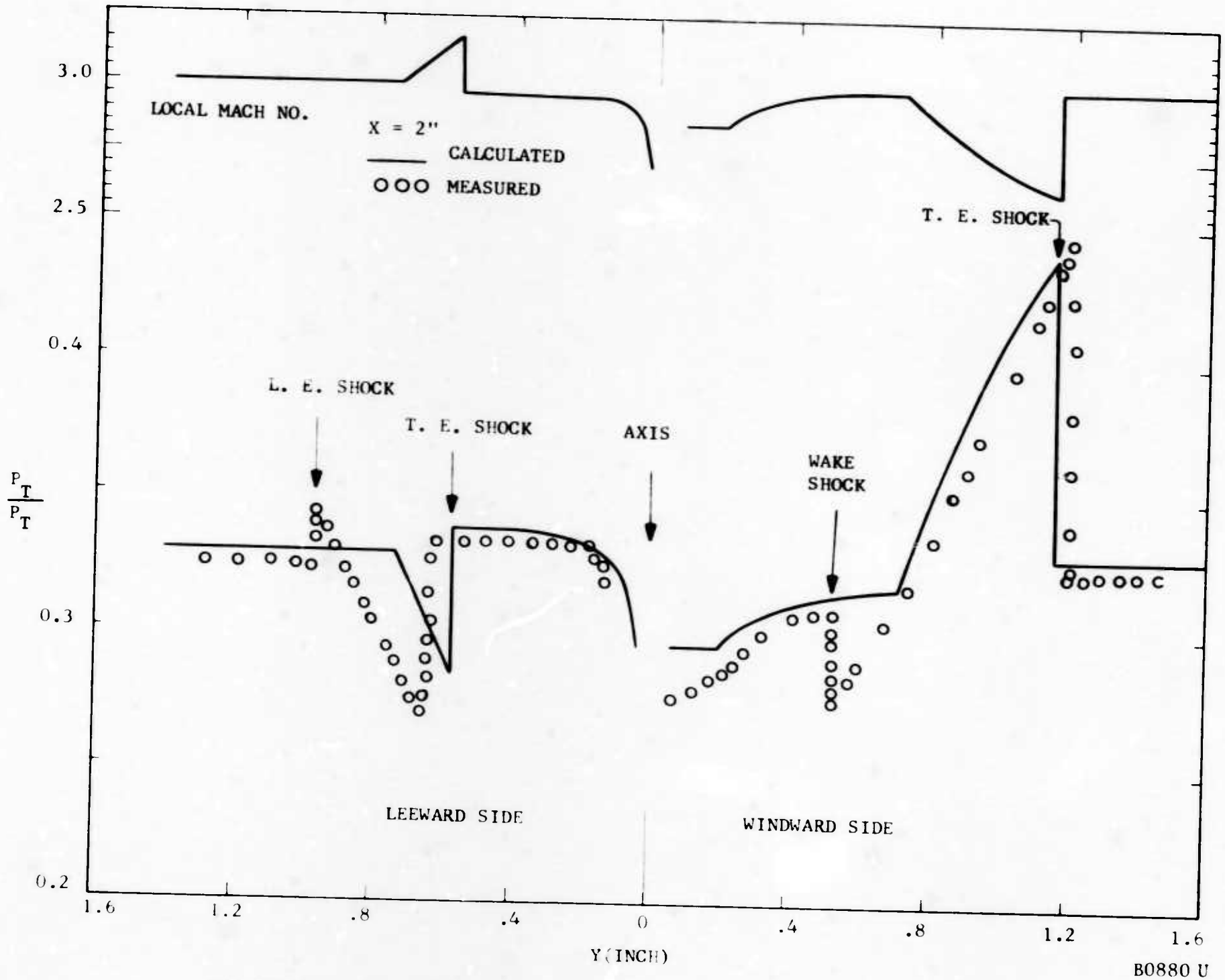

FIGURE 77. COMPARISON OF PREDICTED AND MEASURED PITOT-TUBE "PROFILE" AT 20-DEGREE INCIDENCE

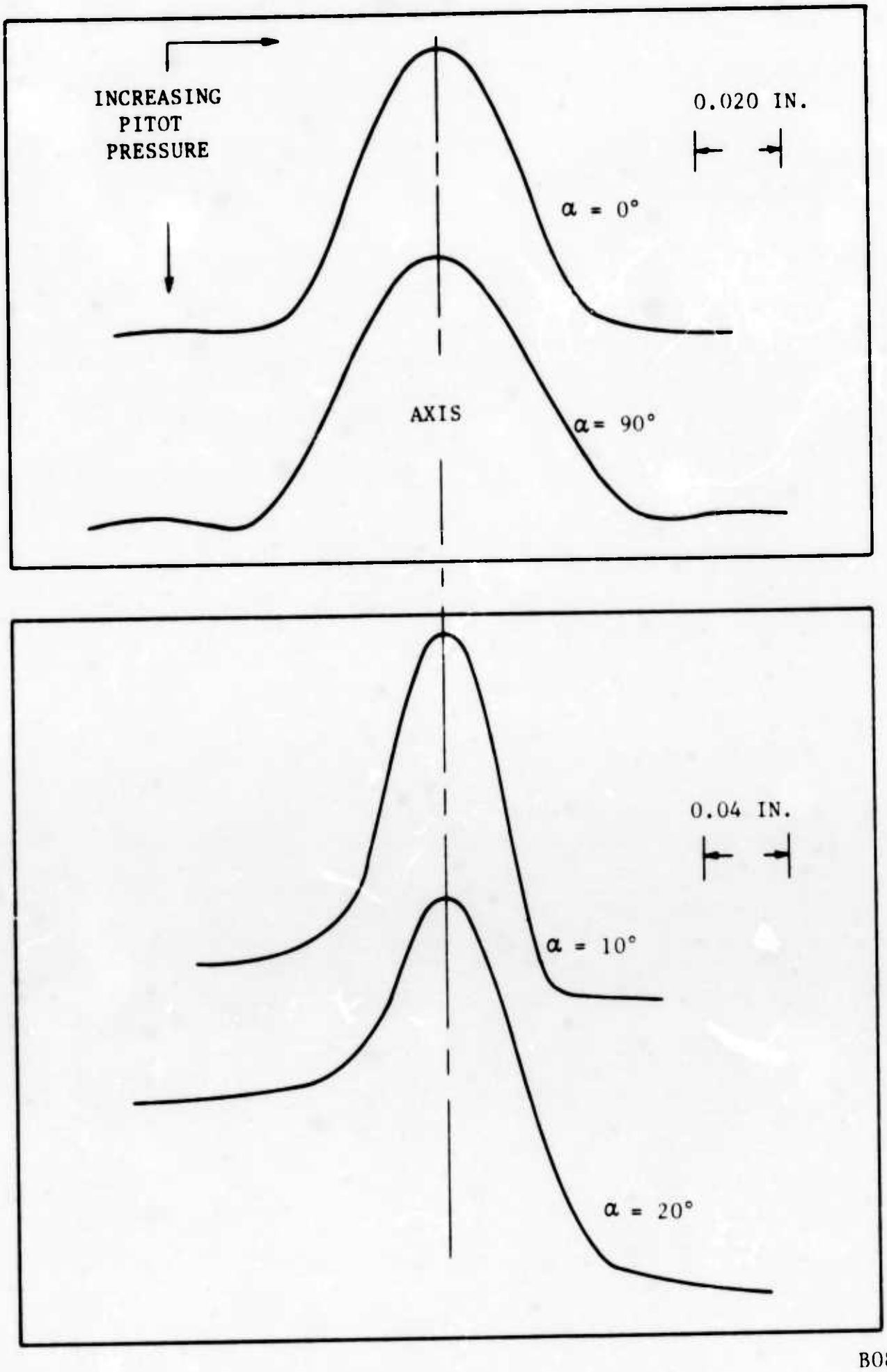

B0881U

FIGURE 78. COMPARISON OF MEASURED PITOT PROFILES (AT FIXED X) FOR DIFFERENT INCIDENCE ANGLES

WEF-10, WEF-20, and WEF-90. A trace for WED (corresponding to WEF-0) is also shown. The object of this figure is to demonstrate the wake symmetry which understandably obtains for the symmetric body configurations, namely for WED and WEF-90. Note, also, the expected change in "free-stream" pitot level for the WEF-10 and WEF-20 traces, illustrating the "shear-layer" effect.

Typical static pressure traverses are shown on Figure 79. Although these traces appear reasonably smooth, it should be recalled that the static-probe resolution is quite poor, since the diameter of the probe was never smaller than five times or so the wake thickness. On the other hand there is strong belief that the mixing in the far wake occurs at constant pressure, or else the whole flow system should shift progressively in the direction of decreasing pressure. In fact, this probe gave seemingly good resolution in regions of sensible pressure gradients, such as at or near shock waves.

Hot-wire measurements consist of the usual three sets: one set consists of five curves at each X-Station, necessary to complete the inputs for the mean flow measurements. A second set, with 15 curves (each at different current) traces the variation of mean voltage across the wake; a companion set of 15 curves plots the mean-square of the wire ac (turbulent) component. Here one should note that the turbulent fluctuations are highest on the side of the wake where the velocity gradients are the highest. Spectral measurements have not been taken as yet.

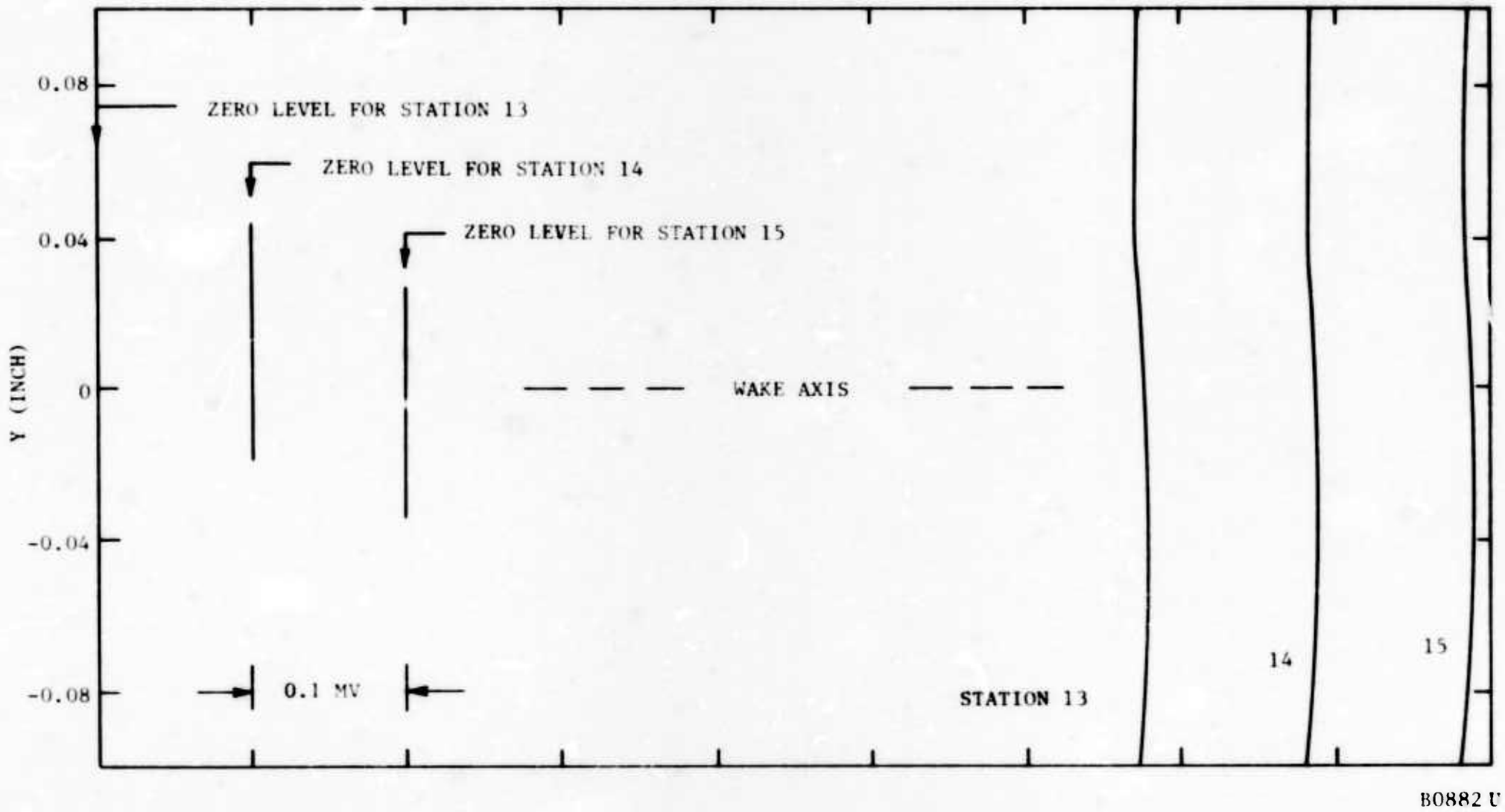

FIGURE 79. STATIC-PRESSURE-PROBE TRACES IN THE WAKE AT 20-DEGREE INCIDENCE.

PRECEDING PAGE BLANK-NOT FILMED

SECTION VI

SUPERSONIC WAKE WITH HEAT TRANSFER

6.1 INTRODUCTION

There are several distinct reasons why the presence of heat transfer is important to understanding the fluid mechanics of the high-speed wakes. In the first place, it is well known from stability arguments (Reference 7) that the location of wake transition to turbulence is sensitive to heat exchanged between the body and the flow. Secondly, the extent to which heat transfer changes the self-preservation behavior is not well understood. Third, the fluctuations in the wake are much more complex with heat-transfer; for example, the simple relationship between velocity and density fluctuations valid for the isoenergetic wake does not apply.

In the present series of experiments, it is planned to study the mean, intermittent and turbulent flow component behind an axisymmetric cooled model and a two-dimensional heated model. The latter experiment has been initiated and most of the tests have actually been completed. It will be described in this section.

6.2 MODEL AND FACILITIES

This experiment is performed in the same wind-tunnel, at the same conditions, with the same model and concurrently as the angle-of-attack experiment discussed in Section V. Provisions to the model support, additional to those described in the latter section as necessary for the angle-of-attack measurement, were incorporated specifically for the heat-transfer measurement.

The steel ribbon is heated electrically by a Harrison Laboratories Model No. 814A regulated dc power supply. Load regulation is held to below 0.05 percent, and power-line ripple, already low, is made effectively imperceptible because of high thermal inertia of the heated ribbon. The ribbon current can be adjusted from 0 to 25 amperes dc and is continuously displayed on a Speedomax-W strip-chart recorder running at a speed of 1 inch of paper per minute. Aided by the chart resolution and a fine variable resistor added externally to the circuit, the operator can thus readjust and control the ribbon current to about 0.015 percent of the desired value, an error lying much below the current change needed for perceptible changes in the heated wake characteristics. The power settled upon for this measurement will be given farther below.

Expansion of the model by thermal relaxation necessitated a scheme by which the ribbon tension could be adjusted automatically. This was done by spring-loading one end of the ribbon so that the model could expand when heated and retract to a stretched position when the electrical power was turned off.

6.3 ADJUSTMENT OF OPERATING CONDITIONS

To bring about easily observable heat-transfer effects, it was desired to dissipate the highest possible amount of power in the ribbon. Several other conditions should be satisfied simultaneously; the ribbon should not weaken structurally or deform, the turbulence should not be inhibited to the point where the wake became wholly laminar, and the ribbon temperature non-uniformity because of heat conduction into the supports should be kept minimal. There was furthermore some fear that the increased wake temperatures could restrict the operating temperature of the hot-wire or even destroy it when both the model and the hot-wire operating temperatures were high. As it developed, all these criteria were satisfied once the ribbon maximum power was set.

This was accomplished by gradually increasing the ribbon current until the model glowed faintly in the supersonic flow. The current was then reduced until the glow disappeared. At this point the ribbon current was set at 19.90 amperes giving a voltage drop across it of 4.344 volts dc, for a total power dissipation of W = 86.8 watts. It is interesting to compare this power to the "Kinetic" power of the flow P = (drag) × (flow velocity). Utilizing the viscous drag coefficient of the ribbon from the zero-incidence WED experiment (Section II) a ratio of W/P = 1.2 is obtained.

After the necessary tests for finding the true zero-twist and zero-incidence angles (see Reference 1), the hot-wire was employed qualitatively for studying the transition to turbulence with and the transverse (span-wise) uniformity of the heating process. Transition was detected by the usual method of noting the point of maximum turbulence intensity along the center line (Reference 28). Figure 80 shows the remarkable differences in transition distance observed with heating* this distance, located about 100 virtual diameters (momentum thicknesses) behind the adiabatic body, moved to about 800 diameters when heating was applied. This phenomenon is consistent with the predictions of stability theory by which the laminar wake is stabilized if the model or vehicle producing it is heated (Reference 7). One result of this transition delay was that the available range in the axial direction over which diagnostics could be made was only about half the range available for wake studies with the adiabatic body. In exchange, however, one obtains a long transitional wake from which information important to the transition process could be extracted. For this reason probings began again, as in WED, shortly downstream of the body rather than at the transition distance.

Visual observation of the ribbon following its overheating to the glowing point showed that its rear half (from about mid-chord to the trailing edge) had been discolored in the way typical of metals after exposure to high temperatures. That the ribbon temperature increases along its chord toward the trailing edge is fully expected because of the more efficient heat transfer for the thinner boundary layer. The discolored region extended uniformly along the span, but it was observed to stop abruptly about one

*Henceforth "heating" refers to the 86.8 watts settled upon as noted previously.

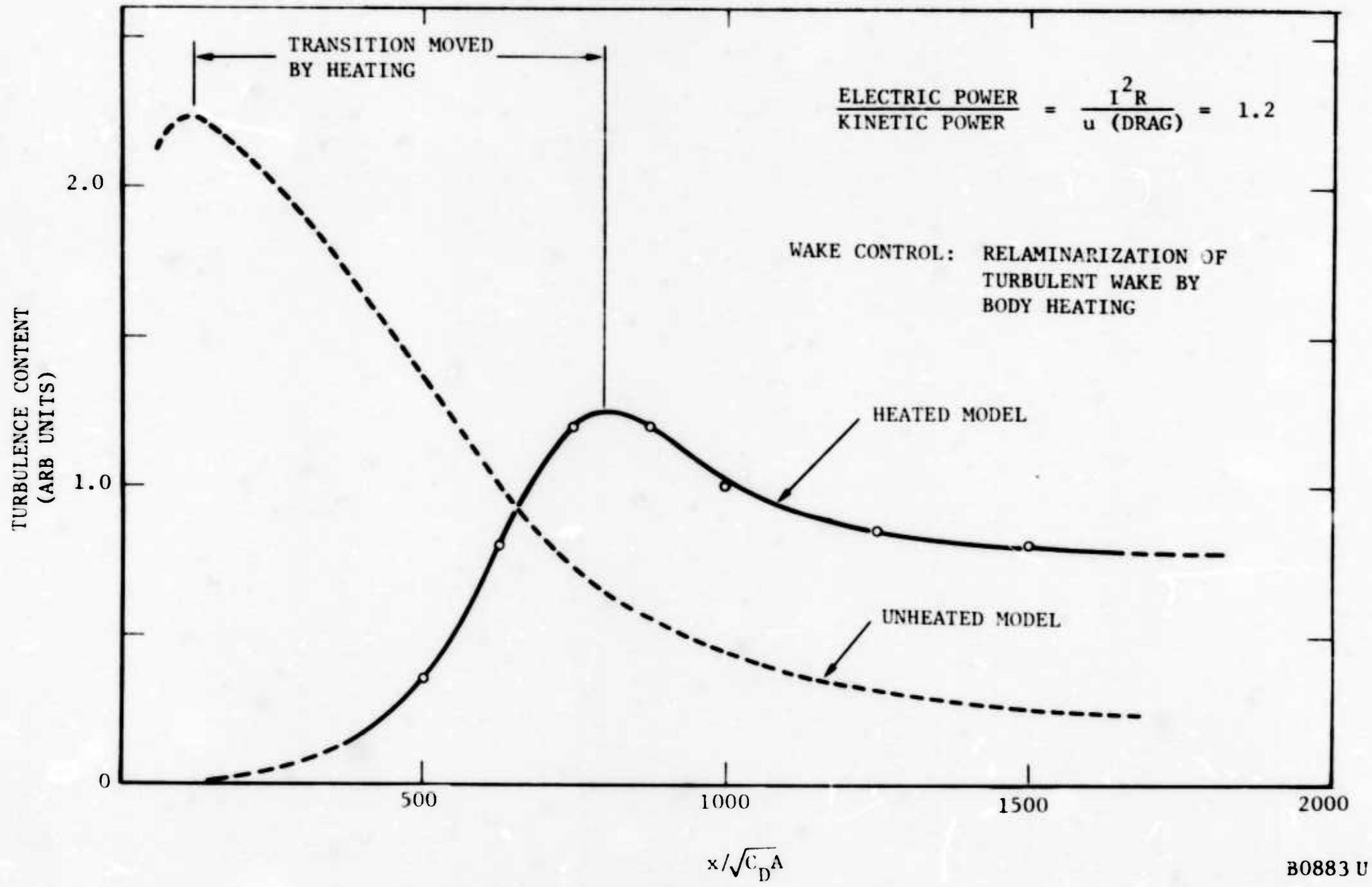

FIGURE 80. EFFECT OF BODY HEATING ON TRANSITION DISTANCE (WEG)

ribbon chord before it reached the tunnel sidewalls. The ends of the ribbon were therefore cooler since, of course, heat conduction to the solid supports increased at those points.

The observations described above are crucial to the span-wise uniformity of heat transfer from the ribbon to its wake, that is, the question of true two-dimensionality of the experiment. This question was further examined by taking hot-wire profile of the local total wake temperature at fixed distances behind the model and difference spanwise stations. Within an inch of the spanwise direction around the center-span position (covering about 35 percent of the total span), the wake axis temperature varied by about 10 percent; at least part of this variation is attributable to slight flow non-uniformities. The two-dimensionality was thus judged to be adequate.

6.4 PROCEDURES AND INSTRUMENTATION

The instrumentation used for this work was identical to that used for the WED and WEF experiments. Although the ribbon itself was heated highly, turbulent diffusion reduced the local stagnation temperatures to the point where no question of damage to the probes by high temperatures ever arose. In fact the 0.00005 inch diameter wire was operated in the same full range of heating currents (maximum of about 7.5 milliamperes) without ever failing by causes attributable to high wake temperatures.

The present experiment, done with the heated two-dimensional body at zero incidence, is designated WEG (Wake Experiment G). The measurements were performed at each of 23 axial positions along the wake. (X STATIONS 1 through 23) beginning at 0.658 inch from the ribbon mid-chord point. At each station one pitot-pressure transverse, one static-probe transverse, and five hot-wire traverses were performed to collect data sufficient to describe fully the mean flow field. Each wire traverse was of course performed at different heating currents. For the turbulence, 15 traces of mean wire voltage and rms voltage were collected at each station. For the spectra, ten distinct radial locations were chosen at which spectra were recorded at each of six different heating currents. Since the acquisition and reduction of the spectral data is extremely time-consuming, data were taken only at alternate X STATIONS (the odd-numbered stations 1, 3, 5,.... 23). Thus a total of $10 \times 6 \times 12 = 720$ spectra were recorded.

It is perhaps advisable to reiterate here the data reduction process through which the WEG data are now progressing. The mean-flow data have been digitized and put into the WEB-V and WEB-VIII computer programs which have for some time been prepared for the Philco-2000 digital computer. The spectral data are first used into the WEB-II program from which one extracts the so-called error ratios, that is, a correction factor necessary to use in correcting the system frequency response. The output of this program and the turbulence data are then used into the WEB-III and WEB-IV programs to deduce the turbulence properties and further into the WEB-VII program from which turbulence properties in scaled form are obtained.

SECTION VII

PROJECT LOGISTICS

7.1 PERSONNEL

This work is performed for the Space and Re-entry Systems Division under the general supervision of John Knudsen. The technical work is done at the Fluid Mechanics Department of the Aeronutronic Advanced Development Operation by A. Demetriades, Supervisor of the Experimental Aerodynamics Section, assisted by Ernest L. Doughman, Research and Development Engineer and Lee Von Seggern, Engineer. Computation services are rendered by the SRS Computation Department under N. Habibe, Supervisor.

7.2 DEVELOPMENT OF FACILITIES, INSTRUMENTS AND TECHNIQUE

7.2.1 FLOW FACILITIES

The work described in this report is performed in the supersonic wind tunnel and plasma wind tunnel constructed and maintained by Philco-Ford. In the present period, improvements have been made by the Corporation to these facilities for the purpose of enhancing the efficiency of the work and the quality of data. An automatic current control has been installed in the plasma wind tunnel for the purpose of avoiding excursions in the arc current of the plasma generator and the resulting changes in the turbulent jet characteristics. An improved plasma generator has also been purchased with which improvements in the precision and repeatability of the measurements will be sought.

7.2.2 INSTRUMENTATION

The following specialized instrumentation has been added by the company in the current period for the purpose of facilitating and improving current and projected work:

a. Heat-Flux Probe. A heat flux probe has been constructed for cross-checking mean-flow data acquired in the plasma jet by measuring the local heat flux. The sensor has a flat circular face 0.25-inch diameter and a calibrated range of 500 Btu/ft^2/sec. Its output is 1 mv per 50 Btu/ft^2/sec. This is shown in Figure 81.

b. Ultra-Small Hot-Wire Probes. The smallest hot-wire probes used in the supersonic wind tunnel to date have been 0.01-inch long and 0.00005-inch diameter, and have a limiting (zero-current) time constant of 0.100 msec. Although the frequency response of these wires is greatly augmented by electronic and computational methods, there is continuing need, in this work, for higher response instruments. Attempts were made in the current period to mount wires of 0.00002 and 0.00001 inch diameter (20 and 10 microinches, respectively) which potentially have time constants of 25 and 10 microseconds. Reportedly, such wires have been mounted elsewhere only rarely and have never been before used in supersonic flow. So far,

FIGURE 81. TOTAL-ENTHALPY PROBE SHOWN PRIOR TO ASSEMBLY.

0.00002-inch diameter Pt 10 percent rh wires have been successfully mounted in lengths of 0.004 inch, annealed and calibrated in the controlled oven. They have also been immersed in the supersonic flow without breakage and there heat-transfer characteristics in that flow have been measured. These are pictured in Figures 82 and 83.

c. Wire Conditioning Circuit. A hot-wire conditioning circuit for mounting, annealing and calibrating hot-wire probes has been designed and built by Philco-Ford personnel. It has greatly facilitated the hot-wire work reported herein.

d. High-Frequency Amplifier. The need to cover the frequency range of turbulence extant in present and projected experiments without overtaxing present techniques of electronic and computer compensation, has been frustrated by the lack of commercially available hot-wire amplifiers "flat" to 2 MHz. A new amplifier has therefore been designed and is now being built at the Company. Frequency response is designed to 2 MHz at a gain of 1,000. Compensation to 10 microseconds will be available, as well as innovations such as pushbutton wire current selection. Two such amplifiers are being built since two-point correlation measurements in the wake are being planned.

e. Correlation Probes. For two-point correlation work, two novel probes are being readied. For the supersonic wind tunnel a two-degree-of-freedom (five degree if the translation of the entire probe is included) two-wire probe will be used: for the plasma wind tunnel a six-degree-of-freedom, two-wire (or langmuir) probe is being adapted from an earlier design. These probes pictured in Figures 84 and 85 will be actuated remotely so that the operator will be able to change the spacing of the two sensors rapidly and at will along any of two (or three) Cartesian axes.

f. Processing Electronics. Other electronic circuits now planned include a constant-temperature anemometer amplifier and a circuit for performing one or more of the following operations on two separate signals: addition, subtraction, multiplication, division, averaging, and integration.

7.2.3 ADDITIONS TO COMPUTATIONAL FACILITIES

In addition to the regular computing facilities available from the Aeronutronic Computing Services Center, Time-Sharing services are now conveniently available for this work. A terminal to the Los Angeles General Electric 235 System is available on full-time basis. The most common language is BASIC and FORTRAN II. In addition to the SPECTR program shown in Appendix B, two BASIC language programs (LINFIT and NUSELT) have been written for calibrating the hot-wire in the controlled oven and in the supersonic flow. These are shown in Figures 86 and 87.

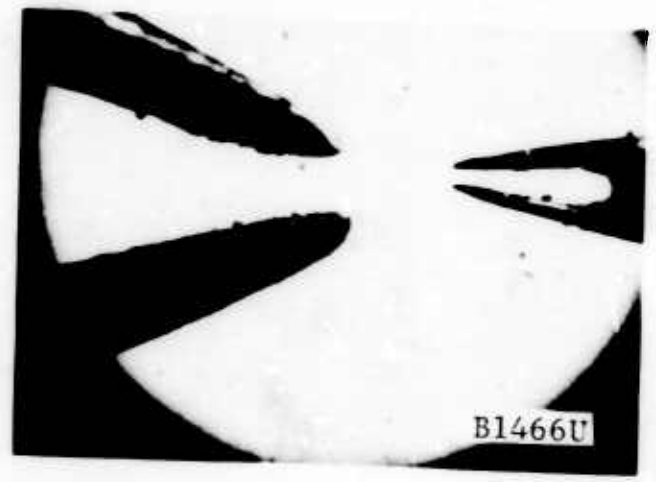

FIGURE 82. COMPARISON OF "SMALL" AND "LARGE" HOT-WIRE PROBES

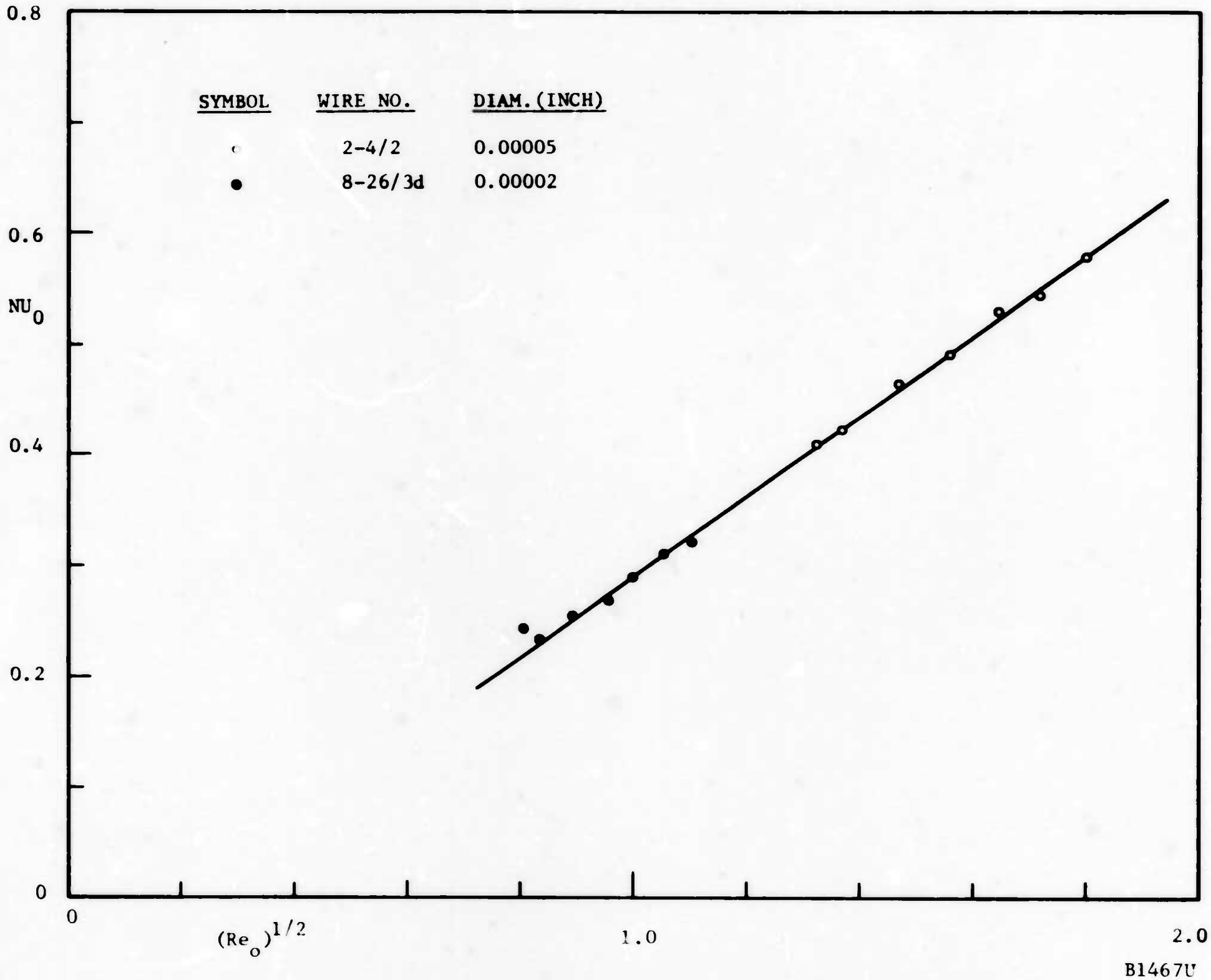

FIGURE 83. HEAT TRANSFER CHARACTERISTICS OF TYPICAL 0.00002-INCH WIRE OF SAME ASPECT RATIO AS 0.00005-INCH WIRE

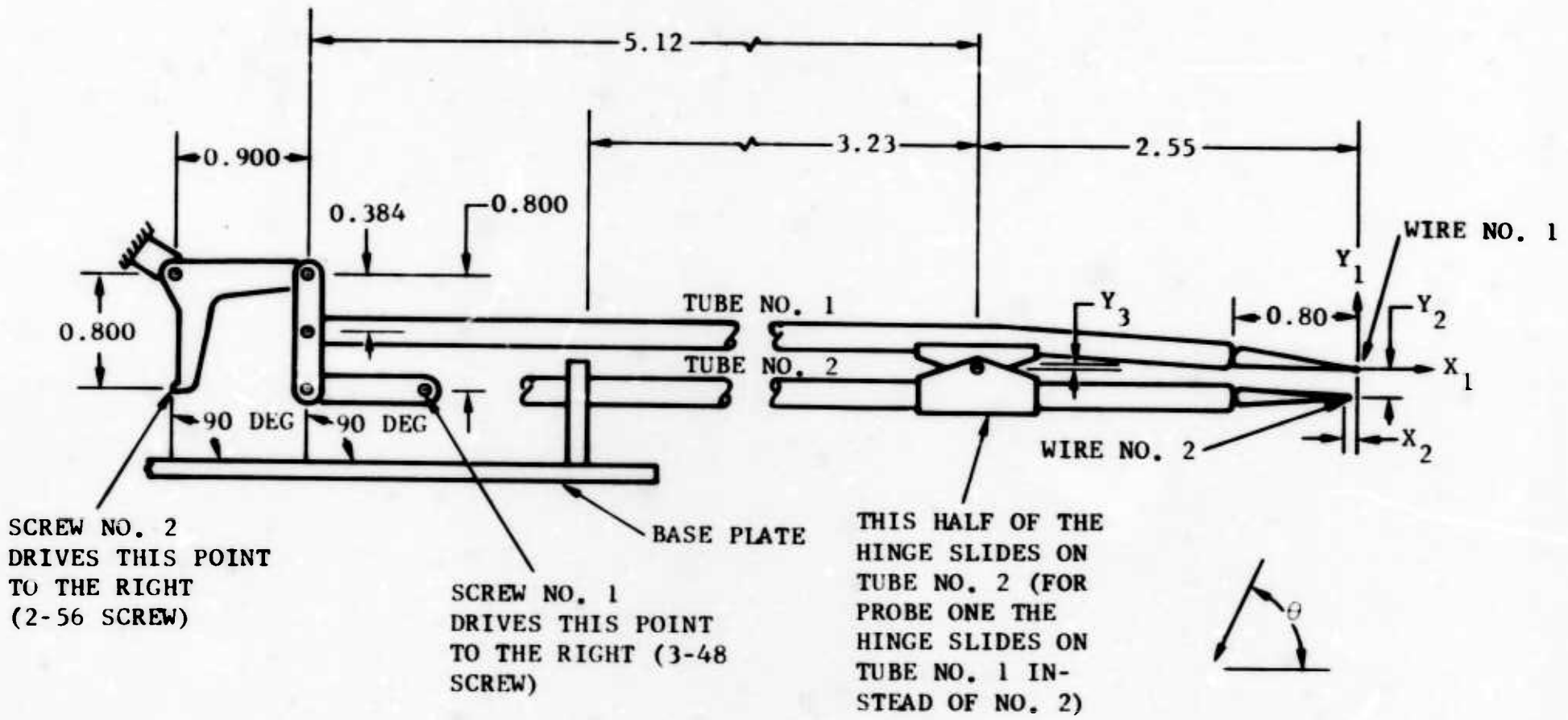

FO4921 U

FIGURE 84. TWO-WIRE CORRELATION PROBE FOR WORK IN THE SUPERSONIC WIND-TUNNEL

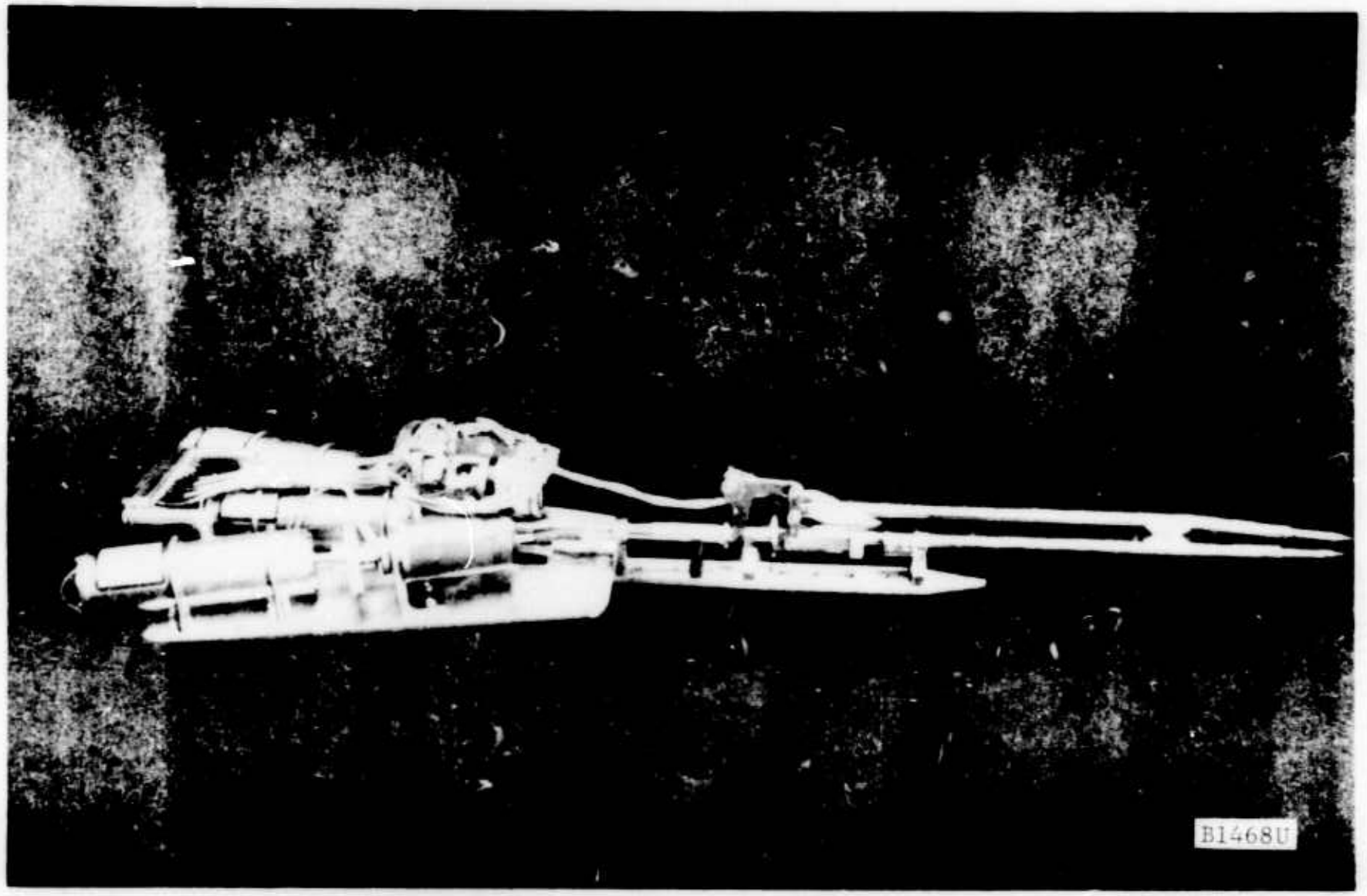

FIGURE 85. TWO-WIRE CORRELATION PROBE FOR WORK IN THE PLASMA TUNNEL

```
   1 P(20),T(20),R(20),C(20),A(20),W(20)
 110 READ C1,C2,C3,C4,C5,N
 120 PRINT
 130 PRINT
 140 PRINT "SET NØ.","  P","  T","  R(0)","DR/DI2"
 150 PRINT
 160 FØR K=1 TØ N
 170 LET S1=0
 180 LET S2=0
 190 LET S3=0
 200 LET S4=0
 210 READ P(K),T(K)
 220 FØR J=1 TØ 5
 230 READ I,V
 240 LET R1=V/I
 250 LET I2=I*I
 260 LET S1=S1+R1
 270 LET S2=S2+I2
 280 LET S3=S3+R1*I2
 290 LET S4=S4+I2*I2
 300 NEXT J
 310 GØSUBØ600
 320 LET A(K)=A1
 330 LET R(K)=A0 - C2
 340 PRINT K,P(K),T(K),R(K),A(K)
 350 NEXT K
 360 PRINT
 370 PRINT
 380 PRINT
 390 PRINT "SET NO.","  RE","  SQ
 400 PRINT "SET N2.","  IW1","  IN2","  K"
 410 FØR K=1 TØ N
 420 LET T1 = 1/C3*(R(K)/C1 - 1)
 430 LET W(K) = 273.13 + T1
 440 LET C(K)=.00000939*W(K) + .0000693
 450 PRINT K,T1,W(K),C(K)
 460 NEXT K
 470 PRINT
 480 PRINT
 490 PRINT
 500 PRINT "SET NO.","  RE","SQRE","  ETA","  NU"
 510 PRINT
 520 FØR K=1 TØ N
 530 LET T1=P(K)*C5*(117.5-0.5*T(K))
 540 LET T2=C3*C1/3.1419/C4
 550 LET T2=T2*0.000001*R(K)/C(K)/A(K)
 555 LET T3=W(K)/(273.13 + T(K))
 560 PRINT K, T1,SQR(T1),T3,T2
 570 NEXT K
 580 STØP
 600 LET A1=(S2*S1-5*S3)/(S2*S2-5*S4)
 610 LET A0=(S1-S2*A1)/5
 620 RETURN
9999 END
```

FIGURE 86. THE LINFIT COMPUTER PROGRAM

```
100 DIM T(5),I(8),V(8),R(8),S(8),N(5),M(5)
110  READ N1
120  FOR J=1 TO N1
130  READ T(J),N(J)
140  NEXT J
150 PRINT
155 PRINT
160  FOR L1=1 TO N1
170 LET S1=0
180 LET S2=0
190 LET S3=0
200 LET S4=0
210 LET N0=N(L1)
230  FOR L2=1 TO N(L1)
240  READ I(L2),V(L2)
250 LET S(L2)=I(L2)*I(L2)
260 LET R(L2)=V(L2)/I(L2)
270 LET S1=S1+R(L2)
280 LET S2=S2+S(L2)
290 LET S3=S3+R(L2)*S(L2)
300 LET S4=S4+S(L2)*S(L2)
310  NEXT L2
320  GOSUB 900
330  PRINT "GROUP ";L1," T = ";T(L1)
335 PRINT "--------"
340  PRINT
350 PRINT "    TERM","COEFFICIENT"
360 PRINT "       0",A0
370 PRINT "       1",A1
380  PRINT
390 PRINT "   I","   V","   I*V","  R-ACTUAL","  R-CALC"
400  PRINT
410  FOR L2=1 TO N(L1)
420 LET C=A0 + A1*S(L2)
430  PRINT I(L2),V(L2),S(L2),R(L2),C
440  NEXT L2
450  PRINT
460  PRINT
470 LET M(L1)=A0-0.95
480  NEXT L1
490 LET S1=0
500 LET S2=0
510 LET S3=0
520 LET S4=0
530 LET N0=N1
540  FOR L1=1 TO N1
550 LET S1=S1+M(L1)
560 LET S2=S2+T(L1)
570 LET S3=S3+T(L1)*T(L1)
580 LET S4=S4+T(L1)*T(L1)
590  NEXT L1
600  GOSUB 900
610  PRINT
611 PRINT "SUMMARY"
612 PRINT "-------"
613 PRINT
614 PRINT "    TERM","COEFFICIENT"
615 PRINT "       0",A0
616 PRINT "       1",A1
620  PRINT
630 PRINT "   T","RM-ACTUAL","  RM-CALC"
640  PRINT
650  FOR L1=1 TO N1
660 LET C=A0 + A1*T(L1)
670  PRINT T(L1),M(L1),C
680  NEXT L1
690  PRINT
700  PRINT
710 LET R2=A0 + A1*20
720 LET A=A1/A0
730 LET L=12*R2/44205
740 LET D=L/0.00005
750  PRINT "R40 = ",A0
760  PRINT "R20 = ",R2
770  PRINT "AR  = ",A1
780  PRINT "A   = ",A
790  PRINT "L   = ",L
800  PRINT "L/D = ",D
810 PRINT
820 PRINT
830 PRINT
840 STOP
900 LET A1=(S2*S1-N0*S3)/(S2*S2-N0*S4)
910 LET A0=(S1-S2*A1)/N0
920  RETURN
9999 END
```

FIGURE 87. THE NUSELT COMPUTER PROGRAM

7.2.4 THE NEW DATA ACQUISITION AND A/D CONVERSION SYSTEM

In the present period a review was made of needs to improve the flow of work from the data acquisition to the data analysis stage. Four major needs were delineated:

(1) Accelerate the analog-to-digital conversion process.

(2) Accelerate certain steps in data acquisition such as recording the spectra.

(3) Store the raw signals of a complete experiment.

(4) Enable certain measurements such as two-point correlations.

The main criteria for the A/D conversion scheme were (1) continuous monitoring in the analog and/or digital stage, and (2) compatibility with the Philco-2000 digital computer. Candidates for conversion were, first, dc bivariate signals (e.g., mean-square wire voltage versus probe position voltage) and secondly, the high-frequency time-dependent raw hot-wire signal containing frequencies up to 2 to 3 MHz. The conversion of each dc signal is accomplished by channeling the analog voltage through a digital voltmeter (Hewlett-Packard Model No. 3440A) to a coupler and then to an IBM Model No. 526 card-puncher which is continuously monitored by a digital recorder (Hewlett-Packard Model No. 5050A). The output of the latter also gives the option of manual keypunch if desired. Finally, a Mosely Model No. F-3B Line Follower System will be available for non-real-time A/D conversion of data already accumulated in analog form.

Spectra have been hitherto recorded in analog form at five-minute intervals. In the supersonic tunnel as many as 1000 spectra per experiment are needed, resulting in a great deal of effort. In the new system, the sweep with frequency is done electronically in real time, so that an acceleration of the spectral measurements by a factor of 3 to 5 is thought possible.

A Honeywell Model No. 7600 seven-channel magnetic tape recorder has been acquired mainly for the purpose of storing the raw signals for future processing as the need arises and as techniques become available. A second important use of the playback will be to "splice-off" the tape electronically for measurement of the eddy properties. A third function will be to bring the signals within the frequency range of processing electronics having state-of-the-art bandwidth limitations. For example, the state-of-the-art bandwidth for variable-delay cross-correlators currently is 250 kHz, much below the 2,000 kHz range of turbulence. By recording the latter signal at 120 ips and playing back at 15 ips the signal comes within the 250 kHz range.

7.3 INFORMATION EXCHANGE

Contact with other ARPA contractors has been maintained and accelerated in the current period through personal exchanges (visits, telephone conferences etc.) and technical reports issued by Philco-Ford and distributed via SAMSO channels. Especially useful have been the exchanges with the following:

(1) Cal Tech Hypersonic Group (Lees, Kubota, Behrens).

(2) University of Southern California (Laufer).

(3) Jet Propulsion Laboratory (Kendall).

(4) University of California, La Jolla (Lin, Gibson).

(5) University of Colorado (Sanborn).

(6) Bell Telephone Laboratories (Granatstein).

(7) TRW Systems (Webb, Lewis).

(8) RCA Montreal (Johnson).

(9) Stanford Research Institute (Guthart).

(10) Aerospace/El Segundo (Ross).

(11) Aerospace/SBO (Renau).

The three Technical Reports issued in the current period are:

(1) "Turbulent Front Structure of An Axisymmetric Compressible Wake", Philco-Ford Publication No. UG-4259, SAMSO TR 68-44, 15 November 1967.

(2) "Mean Flow Measurements In A Self-Preserving Turbulent Plasma Jet", SAMSO TR 68-166, February 1968.

(3) "Turbulent Mean-Flow Measurements In A Two-Dimensional Compressible Wake", SAMSO TR 68-369, July 1968.

Publication in the technical literature of selected portion of this work, as approved by SAMSO, has stimulated valuable feedback from the technical community. In the current period publication activity was as follows:

(1) "Mean Flow Measurements in An Axisymmetric Compressible Turbulent Wake", AIAA J., Vol. 6, No. 3, p. 432, March 1968.

(2) "Turbulence Measurements In An Axisymmetric Compressible Wake", Physics of Fluids, Vol. 11, No. 9, p. 1841, September 1968.

(3) "Turbulent Front Structure of An Axisymmetric Compressible Wake", to be published in the Journal of Fluid Mechanics, 1968.

(4) "The Mean and Intermittent Flow of A Self-Preserving Plasma Jet", accepted for publication in the AIAA Journal.

(5) "Turbulent Mean-Flow Measurements In A Two-Dimensional Supersonic Wake", accepted for publication in the Physics of Fluids.

(6) "Structure of Compressible Turbulent Wakes", Proceedings of the 25th AMRAC Meeting, Washington, D.C., 24-26 April 1968, p. 327.

APPENDIX A

THE JEA-II COMPUTER PROGRAM

The purpose of the JEA-II program was to reduce the raw data of the electron density spectra measurements taken in the turbulent plasma jet. The program also calculates the total mean square values and the longitudinal integral scale. Inputs to this program were the wave analyzer center frequency, F, signal level, V_s, noise level V_n per 200 Hz bandwidth, the mean current E_{mean}, directly from the Langmuir probe and the mean velocity U taken from the JEA-I computer program. Input consisted of data at zero Hz, 500 Hz, 1000 Hz, and then in steps of 1000 Hz up to frequencies where the signal and noise levels were the same. The highest frequency was 26 kHz. Therefore the input consisted of less than 30 input frequencies per spectrum.

The program output listed the following data: the probe position, x in inches from the jet nozzle, Y in volts (1 volt = 1/4 inch), the total mean square value equal to the area under each spectrum curve E INT, the ratio of the mean square spectal density at zero frequency to the total mean square value under the spectra curve E(0)2/E2, and the longitudinal integral scale LAMDAF. Listed as a function of frequency are the following: rms signal value per 200 Hz passband E(F)S, rms noise value per 200 Hz passband E(F)N, mean square value per 200 Hz passband of the true signal (signal-noise) E(F)2, the ratio of the true rms per 200 Hz to the total mean value for all frequencies, A1, the ratio of the mean square per cycle to the total mean square for all frequencies A2, ratio of the mean square per cycle to the normalized mean square at zero frequency A3, and finally the normalized wave number, FN. The program computational procedure appears on Figure A-1, its listing on Figure A-2 and a typical output page on Figure A-3.

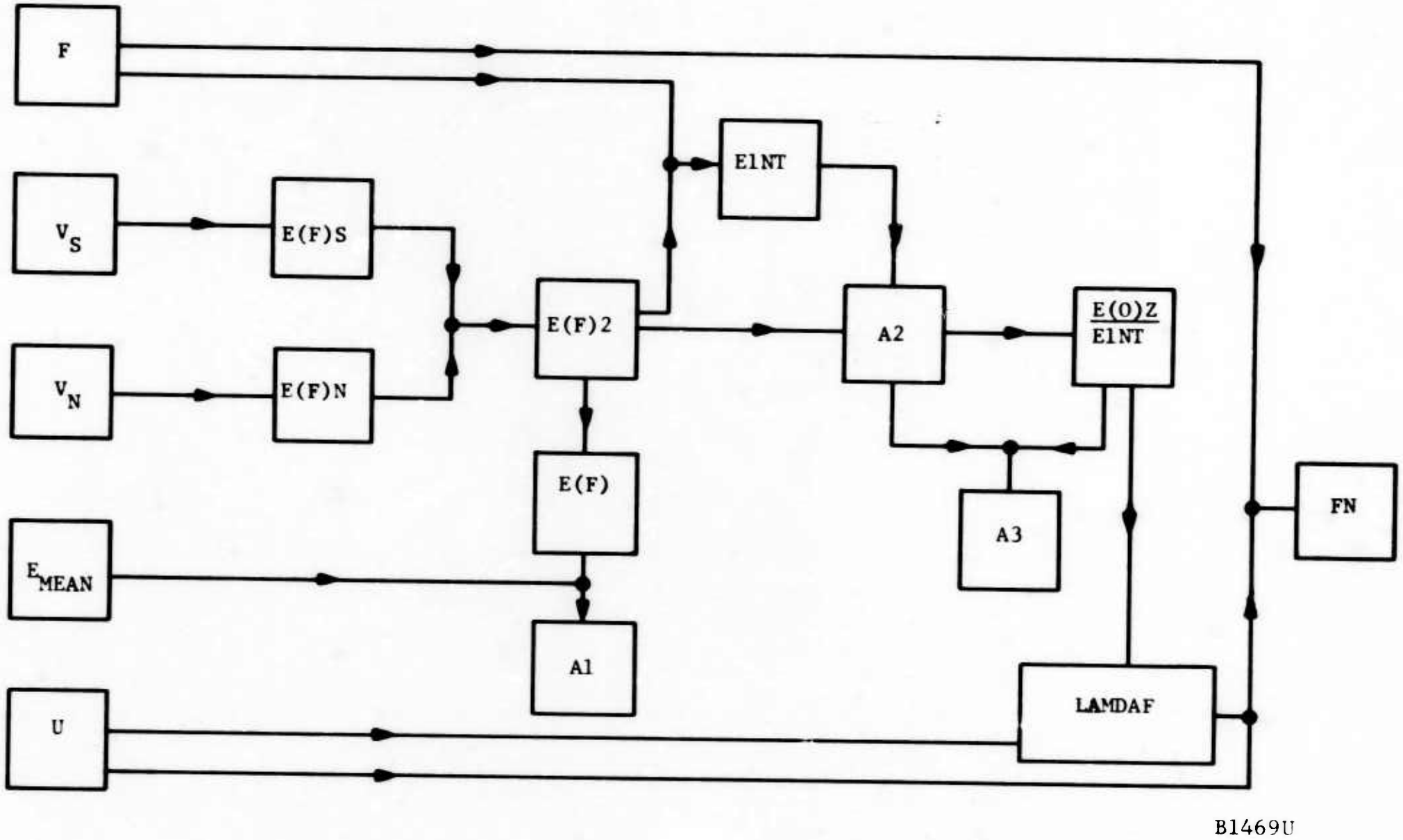

FIGURE A-1. PROCEDURAL DIAGRAM OF THE JEA PROGRAM

FORTRAN 4 PROGRAM ELECTRON DENSITY

```
0001          C ELECTRON DENSITY FLUCTUATIONS
0002          C E. DOUGHMAN ,  A. DEMETRIADES
0003                EQUIVALENCE (NT, D(6))
0004                COMMON /FUNC/ESQ,NF,FREQ
0005                DIMENSION   D(100)
0006                DIMENSION   FREQ (30)
0007                DIMENSION   VS   (30)
0008                DIMENSION   VN   (30)
0009                DIMENSION   ES   (30)
0010                DIMENSION   EN   (30)
0011                DIMENSION   ESQ  (30)
0012                DIMENSION   A1   (30)
0013                DIMENSION   A2   (30)
0014                DIMENSION   A3   (30)
0015                DIMENSION   FN   (30)
0016                REAL LAMDAF
0017                EXTERNAL    FUNCXY
0018                N= 0
0019          10    CALL  GOGO  (D, KSTOP)
0020                N = N +1
0021                X = D(1)
0022                Y = D(2)
0023                C = D(3)
0024                U = D(4)
0025                EMEAN = D(5)
0026                J = 0
0027                INDEX = NT - 4
0028                DO 50  I = 7, INDEX, 3
0029                J = J+ 1
0030                FREQ (J) =  D(I)
0031                VS(J) =     D(I+1)
0032                VN(J) =     D(I+2)
0033          50    CONTINUE
0034                EINT = 0.0
0035                NF   = NT/ 3
0036                DO 100  I = 1, NF
0037                ES(I) = C * VS(I)**.9
0038                EN(I) = C*VN(I) **.9
0039                ESQ(I)=  ES(I)**2 - EN(I)**2
0040                IF (I .EQ. 1) ESQ0 = ESQ(I)
0041                IF (FREQ(I) .EQ. 0.0) ESQ0 = ESQ(I)
0042          100   CONTINUE
0043                F1=FREQ(1)
0044                F2=FREQ(NF)
0045                DY=100.
0046                EINT=RINT(F1,F2,DY,FUNCXY)/200.
0047                DO 150 I = 1, NF
0048                A1(I) = SQRT(ESQ(I))/ EMEAN
0049                A2(I) = ESQ(I) /(EINT * 200.)
0050                EQUOT = ESQ0 /(EINT *200.)
0051                A3(I) = A2(I) /EQUOT
0052                LAMDAF = U/4. * EQUOT
0053                FN(I) = FREQ(I)/ 4. * EQUOT
0054          150   CONTINUE
0055                WRITE (5, 55)  X, Y, EINT,  EQUOT,  LAMDAF
0056                DO 200 I = 1, NF
0057                WRITE (5, 60) ES(I), EN(I), ESQ(I), A1(I), A2(I), A3(I), FN(I)
0058          200   CONTINUE
0059                GO TO 10
0060          55    FORMAT (1H1, 4H X= F7.2, 5X,4H Y= F7.2,5X,5HEINT=F12.6, 5X,
0061               X 5HE(0)2/E2=    F12.6, 5X, 7HLAMDAF=F12.4//     3X, 4HF(I), 9X,
0062               X 6HE(I)N, 8X, 5HE(I)2 , 9X, 2HA1,  8X, 2HA2, 10X, 2HA3, 9X, 2HFN)
0063          60    FORMAT (1H0,7F12.5)
0064                END
```

FIGURE A-2. THE JEA PROGRAM

```
FORTRAN 4 PROGRAM                                          00-00 00-00.0    PAGE    1

0001            FUNCTION FUNCXY(DUM)
0002            COMMON /FUNC/ESO,NF,FREQ
0003            DIMENSION FREQ(30)
0004            DIMENSION ESO(30)
0005            CALL CLINT(DUM,FREQ,ESO,NF,ANS)
0006            FUNCXY=ANS
0007            RETURN
0008             END
```

```
FORTRAN 4 PROGRAM    TRAPEZ                                00-00 00-00.0    PAGE    1

0001        CTRAPEZ
0002                SUBROUTINE TRAPEZ(F1,F2,F3,DF,ANS)
0003                ANS=(.5*F1 +F2+.5*F3)*DF
0004                RETURN
0005                END
```

```
FORTRAN 4 PROGRAM    RINT                                  00-00 00-00.0    PAGE    1

0001        CRINT
0002                FUNCTION RINT(C, D, DY, FUNCXY)
0003                EXTERNAL FUNCXY
0004                SIM = 0.0                                          SIM    50
0005              10 IF (D-C) 11,99,20                                 SIM    60
0006              11 DELTAY = -ABS (DY)                                SIM    70
0007                 GO TO 30                                          SIM    80
0008              20 DELTAY = ABS (DY)                                 SIM    90
0009              30 NY = (D-C)/ ( 2.0 * DELTAY)                       SIM   100
0010                 IHEM = 0                                          SIM   110
0011                 Y1 = C                                            SIM   120
0012                 SUM = FUNCXY(C)                                   SIM   130
0013                 IF (NY) 45,70,45                                  SIM   140
0014              45 N = 2*NY                                          SIM   150
0015              50 DO 60 J=1,N,2                                     SIM   160
0016                 Y1 = Y1 + DELTAY                                  SIM   170
0017                 Y2 = Y1 + DELTAY                                  SIM   180
0018                 F1 = FUNCXY(Y1)                                   SIM   190
0019                 F2 = FUNCXY(Y2)                                   SIM   200
0020                 SUM = SUM + 4.0*F1 + 2.0*F2                       SIM   210
0021                 Y1 = Y2                                           SIM   220
0022              60 CONTINUE                                          SIM   230
0023                 SUM = SUM - F2                                    SIM   240
0024                 SIM = SIM +  SUM * ABS (DELTAY) / 3.0             SIM   250
0025                 SUM = F2                                          SIM   260
0026                 IF (ABS (Y1-D)-1.E-10) 99,99,70                   SIM   270
0027              70 IF(IHEM) 99,75,99                                 SIM   280
0028              75 DELTAY = (D-Y1) * 0.25                            SIM   290
0029                 N= 3                                              SIM   300
0030                 IHEM = 1                                          SIM   310
0031                 GO TO 50                                          SIM   320
0032              99 RINT = SIM                                        SIM   330
0033                 RETURN                                            SIM   340
0034                 END                                               SIM   350
```

FIGURE A-2. (Continued)

E(F)S.	E(F)V.	E(F)2	A1	A2	A3	A4
0.01390	0.00697	0.00357	[illegible]	0.00045	[illegible]	[illegible]
0.79587	0.00697	0.03335	[illegible]	[illegible]	0.04673	1.42456
0.54395	0.00697	0.29583	0.10300	0.00003	0.03257	0.63084
0.38657	0.00697	0.14939	0.07302	0.00001	0.01645	0.84917
0.29609	0.00697	0.08762	0.05458	0.00001	0.00965	1.06140
0.22145	0.00697	0.04899	0.04216	0.00000	0.00539	1.27368
0.17337	0.00697	0.03001	0.03300	0.00000	0.00330	1.48596
0.13983	0.00697	0.01923	0.02641	0.00000	0.00212	1.69824
0.10845	0.00697	0.01171	0.02061	0.00000	0.00129	1.91052
0.08239	0.00697	0.00674	0.01564	0.00000	0.00074	2.12281
0.06631	0.00697	0.00435	0.01256	0.00000	0.00048	2.33509
0.05977	0.00697	0.00352	0.01131	0.00000	0.00039	2.54737
0.04441	0.00697	0.00211	0.00874	0.00000	0.00023	2.75965
0.03728	0.00697	0.00134	0.00678	0.00000	0.00015	2.97193
0.03026	0.00697	0.00087	0.00561	0.00000	0.00010	3.18421
0.02548	0.00697	0.00060	0.00467	0.00000	0.00007	3.39649
0.02123	0.00697	0.00043	0.00394	0.00000	0.00005	3.60877
0.01935	0.00697	0.00033	0.00344	0.00000	0.00004	3.82105
0.01748	0.00697	0.00026	0.00305	0.00000	0.00003	4.03333
0.01558	0.00697	0.00019	0.00265	0.00000	0.00002	4.24561
0.01404	0.00697	0.00015	0.00242	0.00000	0.00002	4.45789
0.01324	0.00697	0.00013	0.00215	0.00000	0.00001	4.67017
0.01222	0.00697	0.00010	0.00191	0.00000	0.00001	4.88245
0.01133	0.00697	0.00008	0.00169	0.00000	0.00001	5.09473
0.01077	0.00697	0.00006	0.00156	0.00000	0.00001	5.30701

FIGURE A-3. TYPICAL OUTPUT OF THE JEA PROGRAM.

APPENDIX B

THE SPECTR COMPUTER PROGRAM

The SPECTR computer program was written for the GE Time Sharing computer to reduce the hot wire anemometer temperature spectra data taken in the turbulent plasma jet. Inputs to the program as a function of every 333.3 Hz were signal, S, and noise, N, levels. The program was limited to 41 sets. FORTRAN II language was used. Other input for each spectra consisted of mean velocity, u, from the JEA-1 program, and hot wire time constant, TW. A number of other inputs were initially integrated into the program such as wave analyzer bandwidth, compensated time constant setting, amplifier gain, and the equations describing the hot wire response curve and the characteristic roll-off curve of the hot wire amplifier, as well as the conversion factor for changing inch readings of data measurements into millivolts.

The program listed the following outputs as a function of frequency: The signal V_1 and noise D_1 levels; true signal H, (signal-noise); correction factor, OT, to adjust for drop-off of hot wire response and amplifier with frequency; corrected mean square of the true signal, E2; normalized corrected mean square of the true signal DN; and finally the nondimensionalized wave number FL. Also included is the total mean square value under the spectral curve before using the correction factor I1, and after using the correction factor I2; the ratio of the two is given as J; and the longitudinal temperature integral scale is given as LT. The computational procedure of this program appears on Figure B-1, the program appears on Figure B-2, and a typical output (at a point in the jet) on Figure B-3.

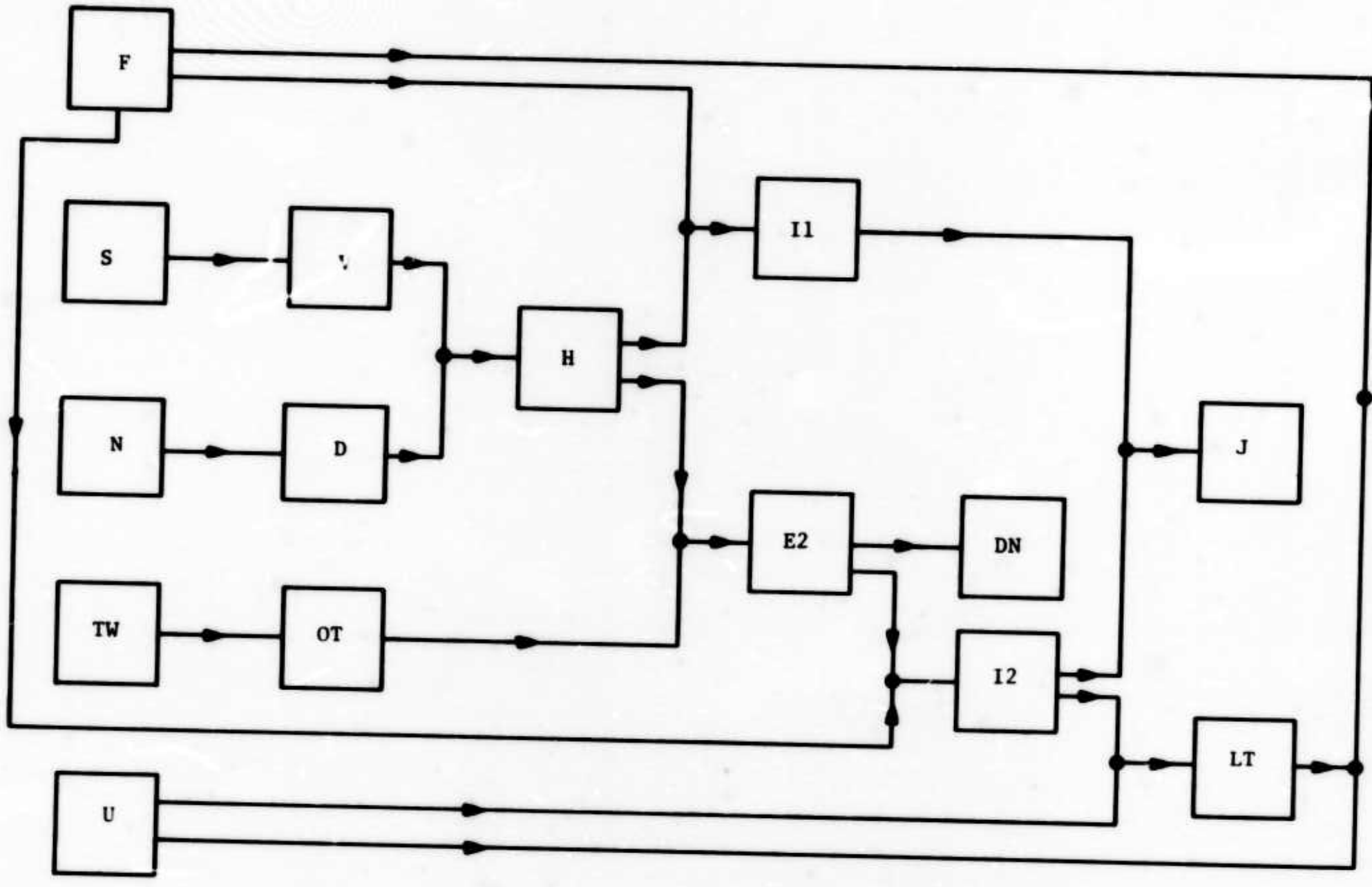

FIGURE B-1. PROCEDURAL DIAGRAM OF THE SPECTR PROGRAM

```
SPECTR     13:24    LA "M" 10/14/68

0010  DIMENSION F(42),S(41),W(41),V(41),D(41),ØT(41),E2(41),DN(41),H(41)
0080  & FL(Ø(),ØC(10),GG(10)
0030  REAL M,N,K,I1,I2,J,LT
0040  F(1)=0.
0050  F(2)=333.
0060  F(3)=666.
0070  DØ 100 I=4,40,3
0080  F(I)=F(I-3)+1000.
0090  F(I+1)=F(I-2)+1000.
0100  F(I+2)=F(I-1)+1000.
0110  100 CONTINUE
0115  READ, NUMBER
0120  200 READ, NF
0130  READ, (S(I),W(I),I=1,NF)
0140  READ,M,U,FB,TW,TI,GØ,DEGC,DEGG
0150  DC1 = DEGC + 1.0
0155 DG1 = DEGG + 1.0
0160  READ, (C(I),I=1,DC1)
0170  READ, (GG(I),I=1,DG1)
0180  DØ 300 I=1,NF
0190  V(I)=M*S(I)
0200  D(I)=M*W(I)
0210  EV = V(I)/28.6
0220  ED = D(I)/28.6
0230  H(I) = EV*EV-ED*ED
0240  300 CONTINUE
0250  AREA=(H(1)+H(NF))/2.
0260  NFM1=NF-1
0270  DØ 400 I=2,NFM1
0280  400 AREA = AREA+H(I)
0290  I1=AREA*333.333333/(FB*GØ*GØ)
0300  DØ 600 I=1,NF
0310  K=F(I)/1000.
0320  C(10)=C(1); GG(10)=GG(1)
0330 DØ 510 L=1,DEGC
0340  510 C(10)=C(10)+C(L+1)*K**L
0350  DØ 520 L=1,DEGG
0360  520 GG(10)=GG(10)+GG(L+1)*K**L
0370  W=SQRT(1.+39.44*F(I)*F(I)*TW*TW)
0380  ØT(I)=(W/C(10)/GG(10))**2
0390  E2(I)=H(I)*ØT(I)/FB
0400  DN(I)=E2(I)/E2(1)
0410  H(I)=SQRT(H(I))
0420  500 CONTINUE
0430  AREA=(E2(1)+E2(NF))/2.
0440  DØ 650 I=2,NFM1
0450  650 AREA=AREA+E2(I)
0460  I2=AREA*333.333333/GØ/GØ
0470  J=I2/I1
0480  LT=U*E2(1)/(4.*I2*GØ*GØ)
0490  DØ 700 I=1,NF
0500  700 FL(I)=F(I)*LT/U
0510  PRINT,"""INPUTS
0520  PRINT,"    M IN MILLIVOLTS IS                    ",M
0530  PRINT,"    U IN CM/SEC IS                        ",U
0540  PRINT,"    BANDWIDTH CONSTANT FB IN CPS IS       ",FB
0550  PRINT,"    WIRE TIME CONSTANT TW IN SECONDS IS   ",TW
0560  PRINT,"    INSTRUMENT TIME CONSTANT IN SECONDS IS ",TI
0570  PRINT,"    STRAIGHT AMPLIFIER GAIN IS            ",GØ
```

FIGURE B-2. THE SPECTR PROGRAM

```
0530  PRINT,"^^^ØUTPUTS"
0590  PRINT,"          F                V                D                H                T
0600  PRINT," F(1),V(1),D(1),H(1),ØT(1)
0610  DØ 300 I=2,NF
0620  PRINT, F(I),V(I),D(I),H(I),ØT(I)
0630  300 CONTINUE
0640  PRINT,"^^^          F               E2               DN               FL"
0650  PRINT," F(1),E2(1),DN(1),FL(1)
0660  DØ 900 I=2,NF
0670  PRINT, F(I),E2(I),DN(I),FL(I)
0675  900 CØNTINUE
0680  PRINT,"^^^SUMMARY"
0690  PRINT,"    II = ",II
0700  PRINT,"    I2 = ",I2
0710  PRINT,"    J  = ",J
0720  PRINT,"    LT = ", LT
0725  NCASE = NCASE+1
0730  IF (NCASE-NUMBER) 200
0735  STOP
0740  END
0800  $DATA


BYE

*** OFF AT 13:29   ELAPSED TERMINAL TIME =      5 MIN.
```

FIGURE B-2. (Continued)

```
1000 1,30,1050,45,835,30,487,15,390,15,330,18,280,19,240,22
1010 210,26,180,30,160,32,140,35,125,35,110,37,100,38,90,40
1020 82,41,78,42,71,43,67,44,64,46,61,47,60,48,59,50,58,51
1030 58,52,58,53,59,54,59,55,59,56,59,57
1040 1,7500,200,.0048,.0045,47
1060 5,5,1.000,24.0066,1.94686,-.426688,2.86034E-2,-6.33665E-4
1070 1.000,2.4192E-3,-4.11312E-3,2.0172E-4,-3.97329E-6,2.84577E-8
RUN

SPECTR    13:22    LA SYSM 6/28/68
```

INPUTS

M IN MILLIVOLTS IS	1.00
U IN CM/SEC IS	7500.00
BANDWIDTH CONSTANT FB IN CPS IS	200.00
WIRE TIME CONSTANT TW IN SECONDS IS	.0048
INSTRUMENT TIME CONSTANT IN SECONDS IS	.0045
STRAIGHT AMPLIFIER GAIN IS	47.00

OUTPUTS

F	V	D	H	GT
.00	1050.00	45.00	36.6796	1.00
333.00	835.00	30.00	29.177	1.2029
666.00	487.00	15.00	17.0199	1.2856
1000.00	390.00	15.00	13.6263	1.2939
1333.00	330.00	18.00	11.5213	1.2887
1666.00	280.00	19.00	9.7676	1.2829
2000.00	240.00	22.00	8.3563	1.2807
2333.00	210.00	26.00	7.2862	1.2834
2666.00	180.00	30.00	6.2057	1.2914
3000.00	160.00	32.00	5.4814	1.3049
3333.00	140.00	33.00	4.7572	1.3237
3666.00	125.00	35.00	4.1955	1.3479
4000.00	110.00	37.00	3.622	1.3775
4333.00	100.00	38.00	3.2342	1.4124
4666.00	90.00	40.00	2.819	1.4526
5000.00	82.00	41.00	2.483	1.4983
5333.00	78.00	42.00	2.2981	1.5493
5666.00	71.00	43.00	1.9754	1.6059
6000.00	67.00	44.00	1.7667	1.6683
6333.00	64.00	46.00	1.5558	1.7364
6666.00	61.00	47.00	1.3596	1.8104
7000.00	60.00	48.00	1.2587	1.8908
7333.00	59.00	50.00	1.0951	1.9773
7666.00	58.00	51.00	.9553	2.0703
8000.00	58.00	52.00	.8983	2.1703
8333.00	58.00	53.00	.8237	2.2769
8666.00	59.00	54.00	.8311	2.3906
9000.00	59.00	55.00	.7456	2.512
9333.00	59.00	56.00	.6494	2.6407
9666.00	59.00	57.00	.5326	2.7773

F	E2	DN	FL

FIGURE B-3. TYPICAL OUTPUT OF THE SPECTR PROGRAM.

```
      .00        6.7269        1.00          .00
   333.00        5.1199         .7611        .112
   666.00        1.862          .2768        .2241
  1000.00        1.2013         .1786        .3365
  1333.00         .8553         .1271        .4485
  1666.00         .612          .091         .5605
  2000.00         .4471         .0665        .6729
  2333.00         .3407         .0506        .785
  2666.00         .2687         .037         .897
  3000.00         .196          .0291       1.0094
  3333.00         .1498         .0223       1.1214
  3666.00         .1186         .0176       1.2335
  4000.00         .0904         .0134       1.3459
  4333.00         .0739         .011        1.4579
  4666.00         .0577         .0086       1.5699
  5000.00         .0462         .0069       1.6823
  5333.00         .0409         .0061       1.7944
  5666.00         .0313         .0047       1.9064
  6000.00         .026          .0039       2.0188
  6333.00         .021          .0031       2.1306
  6666.00         .0167         .0025       2.2429
  7000.00         .015          .0022       2.3553
  7333.00         .0119         .0018       2.4673
  7666.00         .0097         .0014       2.5793
  8000.00         .0088         .0013       2.6917
  8333.00         .0077         .0011       2.8038
  8666.00         .0083         .0012       2.9158
  9000.00         .007          .001        3.0282
  9333.00         .0056        8.27869E-04  3.1402
  9666.00         .0039        5.85509E-04  3.2523

SUMMARY
   I1 =          1.9017
   I2 =          2.2627
   J  =          1.1898
   LT =          2.5235

AI LINE NØ. 735: STØP


RAN      19.33 SEC.
READY.

BYE

*** ØFF AT 13:30    ELAPSED TERMINAL TIME =      10 MIN.
```

FIGURE B-3. (Continued)

REFERENCES

1. Demetriades, A., "Turbulent Mean-Flow Measurements in a Two-Dimensional Wake," Philco-Ford Publication No. UG-4431, SAMSO TR 68-369 (October 1968).

2. Demetriades, A. and Doughman, E., "Mean-Flow Measurements in a Self-Preserving Turbulent Plasma Jet," SAMSO TR 68-166 (February 1968).

3. Demetriades, A., "Mean-Flow Measurements in an Axisymmetric Compressible Turbulent Wake," Philco-Ford Corporation Report U-3978, Newport Beach, California (March 1967). Also, AIAA Journal, Vol. 6, No. 3 (March 1968), p. 432.

4. Demetriades, A. "Turbulent Front Structure of an Axisymmetric Compressible Wake," Philco-Ford Publication No. UG-4259, SAMSO TR 68-44 (15 November 1967).

5. Demetriades, A., "Turbulence Measurements in an Axisymmetric Compressible Wake," Philco-Ford Report No. UG-4119, Newport Beach, California (August 1967). Also, Physics of Fluids, Vol. 11, No. 9 (September 1968), p. 1841.

6. "Advanced Penetration Problems, Wake Structure Measurements," Final Report, Contract AF 04(694)-994, Philco-Ford Publication No. UG-4201 (15 October 1967).

7. Lees, L. and Gold, H., "Stability of Laminar Boundary Layers and Wakes at Hypersonic Speeds," Proceedings of International Symposium on Fundamental Phenoma in Hypersonic Flow, Cornell University Press (1966).

8. Townsend, A. A., "The Structure of Turbulent Shear Flow," Cambridge University Press (1956).

9. Kovasznay, L. S. G., "Turbulence in Supersonic Flow," Journal of Aeronautical Science, Vol. 20, No. 10 (October 1953), p.657.

10. Morkovin, M. V., "Effects of Compressibility on Turbulent Flows," Coll. International Du Centre Nationale de la Recherche Scientifique, No. 108: Mecanique de la Turbulence, Editions Du Centre Nationale de la Recherche Scientifique, 15 Quai Anatole, Paris, France (1962), p. 367.

11. Corrsin, S. and Kistler, A. L., "Free-Stream Boundaries of Turbulent Flows," NACA TR 1244, Washington, D.C. (1953).

12. Guthart, H., Weissman, D. E. and Morita, T., "Measurements of the Charged Particles of an Equilibrium Turbulent Plasma," Physics of Fluids, Vol. 9, No. 9 (September 1966), p. 1766.

13. Granatstein, V. L., "Structure of Wind-Driven Plasma Turbulence as Resolved by Continuum Ion Probes," Physics of Fluids, Vol. 10, No. 6 (June 1967), p. 1236.

14. Johnson, T. (Private Communication, RCA, Montreal (1968).

15. Demetriades, A., "Electron Fluctuations in an Equilibrium Turbulent Plasma," AIAA Journal, Vol. 2, No. 7 (July 1964), p. 1347. Also, Demetriades, A., "Reply by Author to F. Lane and S. L. Zeiberg," AIAA Journal (1965).

16. Guthart, H., "Spectrum of Neutral and Ion Density Fluctuations in an Equilibrium Turbulent Plasma," Physics of Fluids, Vol. 8, No. 5 (May 1965), p. 999.

17. Bradbury, L. J. S., "A Simple Circuit for the Measurement of the Intermittency Factor in a Turbulent Flow," Aeronautical Quarterly, Vol. 15 (1965), p. 281.

18. Becker, H. A., Hottel, H. C. and Williams, G. C., "The Nozzle-Fluid Concentration Field of the Round Turbulent Free Jet," Journal of Fluid Mechanics, Vol. 30, Part 2 (1967), p. 285.

19. Bradbury, L. J. S., "The Structure of a Self-Preserving Turbulent Plane Jet," Journal of Fluid Mechanics, Vol. 23, Part 1 (1965), p. 31.

20. Demetriades, A. and Doughman, E. L., "Langmuir Probe Diagnosis of Turbulent Plasmas," AIAA Journal, Vol. 4, No. 3 (March 1966), p. 451.

21. Bettinger, R. T. and Walker, E. H., "Relationship for Plasma Sheaths About Langmuir Probes," Physics of Fluids, Vol. 8, No. 4 (April 1965), p. 748.

22. Sutton, G. W., "On the Feasibility of Using a Langmuir Probe to Measure Electron Densities in Turbulent Hypersonic Wakes," Aveo-Everett, R. R., 276 (June 1967).

23. Proudian, A. P. and Feldman, S., "A New Model for Mixing and Fluctuations in a Turbulent Wake," AIAA Journal, Volume 3, No. 4 (April 1965), p. 602.

24. Lin, S. C. and Hayes, J. E., "A Quasi-One-Dimensional Treatment of Chemical Reactions in Turbulent Wakes of Hypersonic Objects," AIAA Journal, Vol. 2, No. 7 (July 1964), p. 1214.

25. Wygnanski, I. and Fiedler, H., "Some Measurements in the Self-Preserving Jet," Boeing Scientific Research Laboratory Report No. DI-82-0712 (April 1968).

26. Corrsin, S. and Uberoi, M. S., "Further Experiments on the Flow and Heat Transfer in a Heated Turbulent Jet," NACA TR 998, Washington, D. C. (1950).

27. Laufer, J., "On Turbulent Shear Flows of Variable Density," AIAA Paper No. 68-41, 6th Aerospace Sciences Meeting, New York, New York (January 1968).

28. Demetriades, A., "Some Hot-Wire Anemometer Measurements in a Hypersonic Wake," Proceedings of the 1961 HTFMI, Stanford University Press, p.1.

PRECEDING PAGE BLANK-NOT FILMED

Unclassified

Security Classification

DOCUMENT CONTROL DATA - R&D

(Security classification of title, body of abstract and indexing annotation must be entered when the overall report is classified)

1 ORIGINATING ACTIVITY *(Corporate author)*
Philco-Ford Corporation, Space and Re-entry Systems Division, Newport Beach, California

2a REPORT SECURITY CLASSIFICATION
Unclassified

2b GROUP
N/A

3 REPORT TITLE
Advanced Penetration Problems, Wake Structure Measurements

4 DESCRIPTIVE NOTES *(Type of report and inclusive dates)*
Final Report, 15 October 1967 to 15 October 1968

5 AUTHOR(S) *(Last name, first name, initial)*
Demetriades, A.

6 REPORT DATE	7a TOTAL NO OF PAGES	7b NO OF REFS
31 October 1968	182	28

8a CONTRACT OR GRANT NO
F04701-68-C-0032

b PROJECT NO
ARPA Order 888

c

d

9a ORIGINATOR'S REPORT NUMBER(S)

9b OTHER REPORT NO(S) *(Any other numbers that may be assigned this report)*
SAMSO TR 69-13 Volume II

10 AVAILABILITY/LIMITATION NOTICES
This document may be further distributed by any holder only with specific approval of SAMSO (SMSD), ~~Norton AFB, California 92409~~ L.A. AFS, Calif 90045

11 SUPPLEMENTARY NOTES The distribution of this report is limited because it contains technology requiring strict approval of SAMSO.

12 SPONSORING MILITARY ACTIVITY
SAMSO
Norton AFB
California

13 ABSTRACT

This report summarizes experimental work done in the period 15 October 1967 to 15 October 1968 on the structure of compressible turbulent wakes and turbulent plasmas. Detailed point measurements in the two dimensional wake, made very far from the body, have fully confirmed the predictions of the Dynamic Equilibrium Hypothesis regarding the asymptotic values of the velocity and temperature fluctuation and the statistics of the interface. For flight at angle of incidence radical changes in the wake structure have been observed, while heat transferred from the model to the flow was found to delay greatly the onset of transition to turbulence. In the plasma jet transition zone the remnants of the laminar fluid create a turbulent fluid of highly heterogeneous electron density with hitherto unexpected statistics. The longitudinal scales of the electrons are larger than those of the temperature but numerically not much different from low-speed turbulence scales. The electron density fluctuations always predominate the temperature fluctuations especially at the higher frequencies. Spectral decay obtains a (-5/3) range for the temperature but this behavior is not observed for the electrons.

DD FORM 1 JAN 64 1473

Unclassified

Security Classification

14 KEY WORDS	LINK A		LINK B		LINK C	
	ROLE	WT	ROLE	WT	ROLE	WT
Compressible turbulent wakes Compressible turbulent plasmas Plasma jet transition Electron density Spectral decay Laminar fluid						

INSTRUCTIONS

1. ORIGINATING ACTIVITY: Enter the name and address of the contractor, subcontractor, grantee, Department of Defense activity or other organization *(corporate author)* issuing the report.

2a. REPORT SECURITY CLASSIFICATION: Enter the overall security classification of the report. Indicate whether "Restricted Data" is included. Marking is to be in accordance with appropriate security regulations.

2b. GROUP: Automatic downgrading is specified in DoD Directive 5200.10 and Armed Forces Industrial Manual. Enter the group number. Also, when applicable, show that optional markings have been used for Group 3 and Group 4 as authorized.

3. REPORT TITLE: Enter the complete report title in all capital letters. Titles in all cases should be unclassified. If a meaningful title cannot be selected without classification, show title classification in all capitals in parenthesis immediately following the title.

4. DESCRIPTIVE NOTES: If appropriate, enter the type of report, e.g., interim, progress, summary, annual, or final. Give the inclusive dates when a specific reporting period is covered.

5. AUTHOR(S): Enter the name(s) of author(s) as shown on or in the report. Enter last name, first name, middle initial. If military, show rank and branch of service. The name of the principal author is an absolute minimum requirement.

6. REPORT DATE: Enter the date of the report as day, month, year, or month, year. If more than one date appears on the report, use date of publication.

7a. TOTAL NUMBER OF PAGES: The total page count should follow normal pagination procedures, i.e., enter the number of pages containing information.

7b. NUMBER OF REFERENCES: Enter the total number of references cited in the report.

8a. CONTRACT OR GRANT NUMBER: If appropriate, enter the applicable number of the contract or grant under which the report was written.

8b, 8c, & 8d. PROJECT NUMBER: Enter the appropriate military department identification, such as project number, subproject number, system numbers, task number, etc.

9a. ORIGINATOR'S REPORT NUMBER(S): Enter the official report number by which the document will be identified and controlled by the originating activity. This number must be unique to this report.

9b. OTHER REPORT NUMBER(S): If the report has been assigned any other report numbers *(either by the originator or by the sponsor)*, also enter this number(s).

10. AVAILABILITY/LIMITATION NOTICES: Enter any limitations on further dissemination of the report, other than those imposed by security classification, using standard statements such as:

(1) "Qualified requesters may obtain copies of this report from DDC."

(2) "Foreign announcement and dissemination of this report by DDC is not authorized."

(3) "U. S. Government agencies may obtain copies of this report directly from DDC. Other qualified DDC users shall request through

_____."

(4) "U. S. military agencies may obtain copies of this report directly from DDC. Other qualified users shall request through

_____."

(5) "All distribution of this report is controlled. Qualified DDC users shall request through

_____."

If the report has been furnished to the Office of Technical Services, Department of Commerce, for sale to the public, indicate this fact and enter the price, if known.

11. SUPPLEMENTARY NOTES: Use for additional explanatory notes.

12. SPONSORING MILITARY ACTIVITY: Enter the name of the departmental project office or laboratory sponsoring *(paying for)* the research and development. Include address.

13. ABSTRACT: Enter an abstract giving a brief and factual summary of the document indicative of the report, even though it may also appear elsewhere in the body of the technical report. If additional space is required, a continuation sheet shall be attached.

It is highly desirable that the abstract of classified reports be unclassified. Each paragraph of the abstract shall end with an indication of the military security classification of the information in the paragraph, represented as *(TS)*, *(S)*, *(C)*, or *(U)*.

There is no limitation on the length of the abstract. However, the suggested length is from 150 to 225 words.

14. KEY WORDS: Key words are technically meaningful terms or short phrases that characterize a report and may be used as index entries for cataloging the report. Key words must be selected so that no security classification is required. Identifiers, such as equipment model designation, trade name, military project code name, geographic location, may be used as key words but will be followed by an indication of technical context. The assignment of links, rules, and weights is optional.

GPO 886-551